INSTYTUT BIOCYBERNETYKI
I INŻYNIERII BIOMEDYCZNEJ
IM. MACIEJA NAŁĘCZA
POLSKIEJ AKADEMII NAUK

DOCTORAL THESIS

Application of personalized pulse wave propagation modeling for estimating selected cardiovascular parameters

Zastosowanie spersonalizowanego modelowania propagacji fali pulsu do szacowania wybranych parametrów układu sercowo-naczyniowego

Author:
mgr Kamil WOŁOS

Advisor:
Dr hab. Jan POLESZCZUK
Auxiliary Advisor:
Dr inż. Leszek PSTRAŚ

September, 2025

Fundusze Europejskie Wiedza Edukacja Rozwój
Rzeczpospolita Polska
Unia Europejska Europejski Fundusz Społeczny

Declaration of Authorship

I, Kamil Wołos, declare that this thesis titled, "Application of personalized pulse wave propagation modeling for estimating selected cardiovascular parameters" and the work presented in it are my own. I confirm that:

- This work was done wholly or mainly while in candidature for a research degree at the Doctoral School of Information and Biomedical Technologies at the Polish Academy of Sciences.
- Where I have consulted the published work of others, this is always clearly attributed.
- Where I have quoted from the work of others, the source is always given. With the exception of such quotations, this thesis is entirely my own work.
- I have acknowledged all main sources of help.
- Where the thesis is based on work done by myself jointly with others, I have made clear exactly what was done by others and what I have contributed myself.

Signed:

Date:

Acknowledgements

This dissertation would not have been possible without the support of many people, to whom I wish to express my deepest gratitude.

First and foremost, I would like to thank my Advisor, Prof. Jan Poleszczuk, for his invaluable support throughout every stage of my doctoral work, as well as in matters beyond science. Thank you for believing in my abilities, introducing me to the world of research, and inspiring me with your curiosity and passion.

I am also grateful to my Auxiliary Advisor, Dr. Leszek Pstraś, for his careful reading of my manuscripts, insightful comments, and thought-provoking questions, all of which significantly improved the quality of my work. I also extend my thanks to Prof. Małgorzata Debowska for her collaboration and support in my research.

Special thanks go to Julia and Ula, with whom I shared the challenges of doctoral studies (and the same Advisor).

I would also like to thank my loved ones, family, and friends for their unwavering support and understanding throughout my doctoral journey.

Above all, I am deeply grateful to my wife, Kasia. Your support has been my greatest strength.

Contents

Declaration of Authorship iii

Acknowledgements v

Summary 1

Streszczenie 3

List of Publications 5

1 Introduction 7
- 1.1 Motivation . . . 7
- 1.2 What parameters are routinely measured to monitor cardiovascular function? . . . 8
- 1.3 Information about the cardiovascular system status contained in the arterial pressure waveform . . . 10
- 1.4 How to measure and decipher pulse waves? . . . 12
- 1.5 Pulse wave propagation modeling as a tool to decipher pulse waveforms 15
  - 1.5.1 What is 0-1D pulse wave propagation modeling? . . . 15
  - 1.5.2 Personalization of the models . . . 16
  - 1.5.3 Previous studies on fitting the models to measured pulse waveforms . . . 18
- 1.6 Aim of this study and research hypotheses . . . 19
  - 1.6.1 Hypotheses . . . 20
  - 1.6.2 Research questions . . . 20

2 Publication [A1]: Non-invasive assessment of stroke volume and cardiovascular parameters based on peripheral pressure waveform 23
- 2.1 Summary of the study . . . 23
- 2.2 My contributions . . . 25
- 2.3 Author contributions . . . 25
- 2.4 Publication . . . 25

3 Publication [A2]: Personalized Pulse Wave Propagation Modeling to Improve Vasopressor Dosing Management in Patients with Severe Traumatic Brain Injury 65
- 3.1 Summary of the study . . . 65
- 3.2 My contributions . . . 67
- 3.3 Author contributions . . . 67
- 3.4 Publication . . . 67

4 Publication [A3]: Impact of Multi-Limb Oscillometric Cuff Measurements on Hemodynamics: Insights from Pulse Wave Propagation Modeling **119**
4.1 Summary of the study 119
4.2 My contributions 121
4.3 Author contributions 121
4.4 Publication 121

5 General Discussion and Conclusions **147**
5.1 Summary of Key Findings 147
5.2 Limitations and Future Perspectives 148
5.3 Concluding Remarks 149

A Curriculum Vitae **151**

B Declarations of the Authorship **155**

Bibliography **165**

Summary

Cardiovascular diseases remain a major global health challenge, affecting a growing number of individuals and contributing significantly to mortality. This highlights the need for non-invasive, widely accessible diagnostic and monitoring tools to better assess cardiovascular function. In my dissertation, I explore the potential of personalized pulse wave propagation modeling – a mathematical approach that simulates blood flow and pressure waveforms in the arterial system – to estimate clinically relevant cardiovascular parameters based on non-invasively recorded peripheral pulse waveforms. I present three studies that apply this modeling framework in different clinical contexts, demonstrating its versatility and potential utility.

In the first study, I developed a personalized pulse wave propagation model to estimate stroke volume (SV) and other cardiovascular parameters, and performed its initial validation in 14 healthy subjects and 35 patients with chronic kidney disease (CKD). Using radial artery pressure waveforms recorded non-invasively via applanation tonometry, I fitted a 0-1D pulse wave propagation model to each individual's data. The model-derived SV estimates demonstrated good correlation with the results obtained from bioimpedance cardiography, indicating that this approach may enable non-invasive assessment of cardiac function in CKD patients. This study addresses the challenge of routine monitoring of cardiovascular status in this high-risk population.

The second study focused on patients with severe traumatic brain injury (sTBI), a population that often requires vasopressor therapy to maintain adequate organ perfusion. In this study, I explored whether the values of cardiovascular parameters derived from a personalized pulse wave propagation model could predict adjustments in vasopressor (norepinephrine) dosing in sTBI patients. Using non-invasive pulse wave recordings from multiple peripheral sites (wrists and ankles) obtained via an oscillometric device in 25 patients, I fitted a detailed 0-1D cardiovascular model to each patient's data. The personalized parameters were then incorporated into machine learning models to predict changes in norepinephrine dosing over the next 24 hours after the measurement. The results demonstrated that including the parameters derived from pulse wave propagation model improved prediction accuracy compared to using standard clinical variables alone. This highlights the potential of personalized modeling to inform individualized treatment strategies for critically ill patients.

The oscillometric measurements used in the second study involved inflating cuffs on multiple limbs to suprasystolic pressure, which can influence hemodynamics, particularly in patients with impaired cardiovascular regulation. This observation led to the third study, where I investigated the hemodynamic effects of simultaneous multi-limb oscillometric cuff inflation using a pulse wave propagation model. By extending the 0-1D model to account for peripheral arterial occlusion caused by cuff inflation, I simulated the impact of single- and multi-limb cuff inflation on central and peripheral hemodynamics. The simulations showed that while single-limb cuff occlusion had minimal effects on central hemodynamics, four-limb cuff occlusion significantly increased mean arterial pressure and blood flow in the carotid artery. Sensitivity analyses identified key cardiovascular parameters that influenced these responses,

and simulations incorporating inter-patient variability demonstrated that the magnitude of hemodynamic changes depends on baseline cardiovascular properties. This study provides valuable insights into the systemic effects of simultaneous multi-cuff measurements, particularly in patients with impaired cardiovascular regulation.

Together, these studies demonstrate the potential of personalized pulse wave propagation modeling as a non-invasive tool for estimating cardiovascular parameters in diverse clinical contexts. The findings suggest that this approach can potentially enhance cardiovascular assessment in CKD patients, guide vasopressor dosing in sTBI patients, and provide insights into the hemodynamic effects of multi-limb cuff inflation. While further validation of the proposed models in larger cohorts is necessary, this dissertation establishes a foundation for integrating personalized pulse wave propagation modeling into clinical practice, with the ultimate goal of improving patient outcomes through enhanced cardiovascular monitoring and management.

Streszczenie

Choroby sercowo-naczyniowe stanowią poważne globalne wyzwanie zdrowotne, dotykające coraz większą liczbę osób i powodujące znaczną śmiertelność. Istnieje zatem potrzeba opracowania nowych, nieinwazyjnych, łatwo dostępnych narzędzi diagnostycznych i monitorujących, które pozwoliłyby lepiej oceniać funkcjonowanie układu sercowo-naczyniowego. W mojej rozprawie doktorskiej badam potencjał modelowania propagacji fali pulsu – podejścia matematycznego, umożliwiającego symulację przepływu krwi i przebiegu fal ciśnienia w układzie tętniczym – do szacowania klinicznie istotnych parametrów sercowo-naczyniowych na podstawie obwodowych fal pulsu rejestrowanych w sposób nieinwazyjny. Przedstawiam trzy publikacje, w których zastosowałem tę metodę modelowania w różnych kontekstach klinicznych, wykazując jej wszechstronność i potencjalną użyteczność.

W pierwszym badaniu opracowałem spersonalizowany model propagacji fali pulsu pozwalający na oszacowanie objętości wyrzutowej serca (ang. *stroke volume*, SV) i innych parametrów sercowo-naczyniowych, który został przetestowany u 14 zdrowych osób i 35 pacjentów z przewlekłą chorobą nerek (PChN). Dla każdej osoby dopasowałem hemodynamiczny model 0-1D, wykorzystując nieinwazyjne przebiegi fal ciśnienia tętniczego zarejestrowane na tętnicy promieniowej za pomocą tonometru aplanacyjnego. Oszacowania SV otrzymane na podstawie modelu wykazały dobrą korelację z pomiarami referencyjnymi uzyskanymi za pomocą kardiografii bioimpedancyjnej, co wskazuje, że podejście to może umożliwić nieinwazyjną ocenę funkcji serca u pacjentów z PChN. Prezentowane badanie może stanowić odpowiedź na wyzwanie związane z rutynowym monitorowaniem zdrowia układu sercowo-naczyniowego w tej populacji wysokiego ryzyka.

Drugie badanie skupiało się na pacjentach z ciężkim urazowym uszkodzeniem mózgu (ang. *severe traumatic brain injury*, sTBI), populacji, która często wymaga terapii lekami wazopresyjnymi (zwiększającymi ciśnienie krwi) w celu utrzymania odpowiedniego ukrwienia organów. W badaniu tym analizowałem, czy wartości parametrów sercowo-naczyniowych uzyskane za pomocą spersonalizowanego modelu propagacji fali pulsu mogą posłużyć do przewidywania zmian dawkowania wazopresora (norepinefryny) u pacjentów z sTBI. Na podstawie zapisów fal tętna zarejestrowanych oscylometrycznie u 25 pacjentów w czterech miejscach (na nadgarstkach i kostkach) dopasowałem szczegółowy model układu sercowo-naczyniowego 0-1D do danych pochodzących od poszczególnych pacjentów. Spersonalizowane parametry sercowo-naczyniowe zostały następnie wykorzystane w modelach uczenia maszynowego w celu przewidywania zmian dawkowania norepinefryny w ciągu następnych 24 godzin po pomiarze. Wyniki wykazały, że uwzględnienie parametrów oszacowanych za pomocą modelu propagacji fali pulsu poprawiło dokładność przewidywań w porównaniu z wykorzystaniem wyłącznie standardowych zmiennych klinicznych. Wskazuje to na potencjał wykorzystania spersonalizowanego modelowania propagacji fali pulsu do opracowywania zindywidualizowanych strategii leczenia pacjentów w stanie krytycznym.

Pomiary oscylometryczne zastosowane w drugim badaniu obejmowały pompowanie mankietów oscylometrycznych na czterech kończynach do poziomu ciśnienia przekraczającego ciśnienie skurczowe krwi. Taki zabieg może wpływać na hemodynamikę,

szczególnie u pacjentów z zaburzeniami regulacji sercowo-naczyniowej. Stanowiło to motywację do mojego trzeciego badania, w którym ekspolorowałem skutki hemodynamiczne jednoczesnego napompowania mankietów oscylometrycznych na kilku kończynach. Aby uwzględnić niedrożność tętnic obwodowych spowodowaną zaciśnięciem mankietów, rozszerzyłem odpowiednio rozważany wcześniej model układu sercowo-naczyniowego 0-1D. Następnie przeprowadziłem symulację wpływu napompowania mankietów (na jednej lub wielu kończynach) na hemodynamikę centralną i obwodową. Symulacje wykazały, że podczas gdy okluzja tętnic pod mankietem na jednej kończynie ma niewielki wpływ na hemodynamikę centralną, jednoczesna okluzja tętnic pod mankietami na czterech kończynach znacznie zwiększyła średnie ciśnienie tętnicze i przepływ krwi w tętnicy szyjnej. Ponadto analiza wrażliwości pozwoliła zidentyfikować parametry sercowo-naczyniowe, które miały kluczowy wpływ na takie zmiany. Co więcej, symulacje uwzględniające zmienność międzyosobniczą wykazały, że wielkość zmian hemodynamicznych wywołanych napompowaniem mankietów zależy od wyjściowych wartości parametrów sercowo-naczyniowych. Badanie to dostarcza cennych informacji na temat ogólnoustrojowych skutków jednoczesnych pomiarów wielo-mankietowych, zwłaszcza w populacjach szczególnie z upośledzonymi mechanizmami regulacji sercowo-naczyniowej.

Podsumowując, przedstawione badania pokazują potencjał spersonalizowanego modelowania propagacji fali pulsu jako nieinwazyjnego narzędzia do szacowania parametrów sercowo-naczyniowych w różnych kontekstach klinicznych. Wyniki badań sugerują, że podejście to może usprawnić ocenę układu sercowo-naczyniowego u pacjentów z PChN, pomóc w doborze dawki leków wazopresyjnych u pacjentów z sTBI oraz dostarczyć informacji na temat hemodynamicznego wpływu jednoczesnego napompowania mankietów na wielu kończynach. Chociaż konieczna jest dalsza walidacja zaproponowanych modeli na większych grupach pacjentów, niniejsza rozprawa stanowi podstawę do prowadzenia dalszych badań nad spersonalizowanym modelowaniem propagacji fali pulsu w celu poprawy wyników leczenia pacjentów poprzez udoskonalone monitorowanie układu sercowo-naczyniowego.

List of Publications

Publications included in the dissertation

[A1] **Wołos K.**, Pstras L., Debowska M., Dabrowski W., Siwicka-Gieroba D., & Poleszczuk, J. (2024). Non-invasive assessment of stroke volume and cardiovascular parameters based on peripheral pressure waveform. PLOS Computational Biology, 20(4), e1012013, doi: 10.1371/journal.pcbi.1012013.
Ministerial Points: 140 pts, **IF:** 3.6 (2024).

[A2] **Wolos K.**, Pstras L., Bialonczyk U., Debowska M., Dabrowski W., Siwicka-Gieroba D., & Poleszczuk J. (2025). Personalized pulse wave propagation modeling to improve vasopressor dosing management in patients with severe traumatic brain injury. PLOS Computational Biology, 21(9), e1013501, doi: 10.1371/journal.pcbi.1013501.
Ministerial Points: 140 pts, **IF:** 3.6 (2024).

[A3] **Wolos K.**, Pstras L., Debowska M., & Poleszczuk J. (2025). Impact of multi-limb oscillometric cuff measurements on hemodynamics: Insights from pulse wave propagation modeling. Frontiers in Physiology, 16,
doi: 10.3389/fphys.2025.1642645.
Ministerial Points: 100 pts, **IF:** 3.4 (2024).

Summary of the publications included in the dissertation:

Total Ministerial Points: **380 pts**, Total IF: **10.6 (2024).**

Publications not included in the dissertation

[N1] Kosewski P., & **Wołos K.** (2021). Existence and regularity result for Stokes system with special inlet/outlet condition. Mathematical Methods in the Applied Sciences, 44(17), 12797–12809, doi: 10.1002/mma.7580.
Ministerial Points: 100 pts, **IF:** 1.8 (2024)

Summary of the all publications:

Total Ministerial Points: **480 pts**, Total IF: **12.4 (2024).**

Chapter 1

Introduction

1.1 Motivation

According to the World Health Organization, cardiovascular diseases (CVDs) are the leading cause of death worldwide, accounting for approximately 20 million deaths annually and representing nearly one-third of all global deaths [1]. Common CVDs include coronary artery disease, heart failure, arrhythmias, and peripheral artery disease [1]; Figure 1.1 illustrates global causes of death in 2019, highlighting the contribution of CVDs [2]. It is predicted that in the coming decades, the incidence of CVDs will rise [3]. The main factors responsible for this phenomenon are: changes in the age structure of the population, unhealthy lifestyle choices and persistent inequalities in access to healthcare [3, 4]. Without significant advances in prevention, diagnosis, and treatment, the growing burden of CVDs could overwhelm healthcare systems [3].

Patients with chronic kidney disease (CKD) are at particularly high risk for developing CVD [5, 6]. CKD is characterized by a gradual loss of kidney function, leading to the accumulation of waste products of metabolism and fluid in the body [7]. Globally, CKD affects more than 850 million people (about 11% of the population) and its prevalence increased by 33% between 1990 and 2017 [5, 8]. The elevated risk of CVD in CKD patients arises from both traditional risk factors (such as hypertension and diabetes) and non-traditional factors (including inflammation and vascular calcification) [5]. In advanced stages of CKD, cardiovascular complications, including heart failure, arrhythmias, and sudden cardiac death, account for approximately 40-50% of all deaths [9]. Thus, the high prevalence of CVDs in patients with CKD, especially in later stages of the disease, is a major contributor to increased mortality in this population [10, 5].

Of particular concern during treatment of CKD patients who require hemodialysis (HD) is that during HD, the rapid removal of fluid may overburden the body's compensatory mechanisms, leading to significant hemodynamic changes, such as intradialytic hypotension [11]. Therefore, continuous non-invasive monitoring of cardiovascular function during HD may help prevent complications and improve patient outcomes.

While continuous monitoring of cardiovascular function is not yet routinely used during HD, it is the standard of care in other settings, particularly in patients in intensive care units, such as those with severe traumatic brain injury (sTBI). Generally, traumatic brain injury (TBI) is defined as damage to brain function due to external forces [12] and is one of the leading causes of death and disability worldwide [13, 14]. TBI affects an estimated 50–60 million people annually [14], with an increasing trend [15]. Severe TBI represents a subset of TBI cases, characterized by more significant brain damage, requiring intensive medical intervention and long-term rehabilitation [16]. In order to prevent secondary brain injury, maintaining adequate

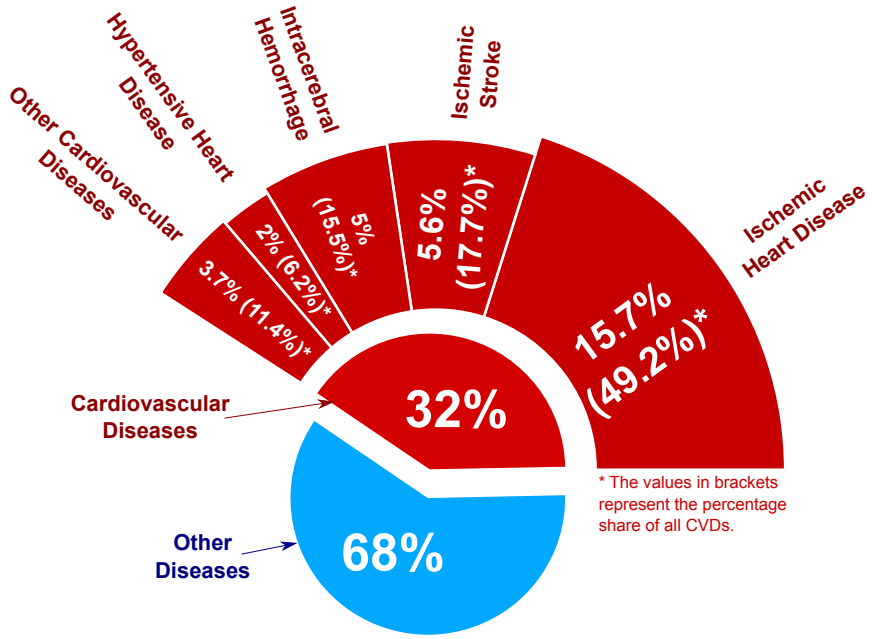

FIGURE 1.1: Global causes of death in 2019. Data extracted from [1] and [2].

cerebral perfusion in sTBI patients is of utmost importance [17, 18]. This requires precise regulation of systemic blood pressure, typically achieved through administration of vasoactive drugs (mainly vasopressors) that alter the tone of small arteries and arterioles by constricting or dilating them [19]. Proper dosing of these drugs requires monitoring of the patient's cardiovascular state and is usually challenging due to the variability in individual responses to various drugs and the complexity of the underlying pathophysiologies [20, 21, 22].

While sTBI represents an acute, rapidly evolving condition [17], CKD and CVD exemplify chronic, progressive changes in cardiovascular properties. In all these scenarios, thorough cardiovascular assessment is important but remains difficult to achieve. Understanding the patient's cardiovascular state in quantitative terms enables clinicians to make more informed decisions. Interventions such as fluid resuscitation, vasopressor administration, or mechanical support depend critically on dynamically changing cardiovascular parameters. Some of them are routinely measured in clinical practice, especially in intensive care units.

1.2 What parameters are routinely measured to monitor cardiovascular function?

A variety of hemodynamic parameters are routinely used to monitor the cardiovascular status of patients. One of the most commonly assessed parameters is the heart rate (HR) [23, 24], which reflects the number of heartbeats per minute. HR is a simple yet informative cardiovascular risk factor in both the general population and specific groups, such as patients with hypertension [25], chronic heart failure [23], or arrhythmias [26]. It is typically measured non-invasively using manual measurements, oscillometric devices, or electrocardiography (ECG) [27].

Another fundamental cardiovascular parameter is arterial blood pressure (BP), which quantifies the force of blood exerted on the arterial walls [28]. It is typically reported as two values: the systolic blood pressure (SBP), representing the pressure

during cardiac contraction, and diastolic blood pressure (DBP), indicating the pressure during cardiac relaxation [27]. Elevated BP, particularly sustained hypertension, is a major risk factor for the development and progression of CVD [29, 30]. BP is also essential for identifying hypotension – one of the major complications in patients undergoing hemodialysis (HD) [31], those with severe traumatic brain injury (sTBI) [32, 33], and septic patients [34].

Other measures of blood pressure are pulse pressure (PP) and mean arterial pressure (MAP). PP is defined as the difference between systolic blood pressure (SBP) and diastolic blood pressure (DBP), and can predict the risk of cardiovascular events such as stroke or myocardial infarction [35, 36]. MAP is particularly important in intensive care settings, as it represents the average pressure in the arteries throughout the cardiac cycle and is a critical determinant of tissue and organ perfusion [34, 37]. MAP is often estimated using the empirical formula $DBP + \frac{1}{3}(SBP - DBP)$ [38], although its accuracy is debated [39, 40]. Blood pressure is usually measured non-invasively with a sphygmomanometer or an automated oscillometric device [27] and is expressed relative to ambient atmospheric pressure [28]. When continuous measurements are needed (as in patients with sTBI), it can be measured invasively via an arterial catheter [27] or, when high accuracy is not crucial, using various non-invasive continuous measurements techniques [41].

Beyond HR, and BP measurements, several additional hemodynamic parameters are important for monitoring and assessing the patient's cardiovascular status. Although clinically significant, many of these require advanced or expensive measurement techniques. Notable examples include stroke volume (SV) and cardiac output (CO). SV quantifies the amount of blood ejected by the left ventricle with a single heartbeat, reflecting the heart's pumping efficiency. CO represents the total volume of blood pumped by the heart per minute and is typically approximated as the product of SV and HR. For a more objective assessment of cardiovascular function, the cardiac index (CI) is frequently used; CI normalizes CO to body surface area [27, 42]. The stroke volume index is defined analogously [42]. Unfortunately, the most accurate methods for measuring SV and CO are either invasive (e.g., thermodilution via a pulmonary artery catheter [43]) or require expensive equipment (e.g., cardiac magnetic resonance imaging) or qualified personnel (e.g., for echocardiography). Although bioimpedance cardiography offers a non-invasive and relatively affordable alternative, its accuracy remains a subject of ongoing research [43, 44].

Another clinically relevant parameter is systemic vascular resistance (SVR), also known as total peripheral resistance (TPR), which quantifies the resistance that the heart must overcome to pump blood through the circulatory system [45]. Its value may be estimated by dividing the difference between MAP and central venous pressure (CVP) by CO [46]. SVR provides insight into vascular tone and the overall state of the cardiovascular system. For instance, SVR is crucial for assessing blood vessel narrowing (vasoconstriction) and widening (vasodilation), and thus, it may guide vasopressor therapy [45]. On the other hand, CVP plays an important role in assessing right ventricular function and is typically measured invasively via a central venous catheter [47, 48].

Ejection fraction (EF) is another key indicator of cardiac function, representing the percentage of blood ejected from a ventricle during contraction [49]. The left ventricular ejection fraction (LVEF) is especially important, as it is used to classify and assess the severity of heart failure [50, 51]. The most common method for measuring LVEF is echocardiography [52, 53], although cardiac magnetic resonance imaging also provides an accurate and non-invasive assessment. Invasive cardiac catheterization can be used in selected cases [54, 55].

Many of the parameters discussed above require measurement using invasive procedures, expensive imaging equipment, and well-qualified personnel, and are therefore typically available only in intensive care units or specialized cardiology centers. These limitations motivate the development of non-invasive, assessment methods. Pulse wave recordings are particularly attractive in this context: they are relatively easy to acquire and contain rich information about arterial and cardiac function. This information can be leveraged to estimate cardiovascular parameters that would otherwise be inaccessible at the bedside.

1.3 Information about the cardiovascular system status contained in the arterial pressure waveform

The human cardiovascular system is a closed network of blood vessels comprising two interconnected circuits: the systemic circulation, which delivers oxygenated blood from the heart to organs and tissues, and the pulmonary circulation, which directs deoxygenated blood to the lungs for gas exchange. Periodic ejection of blood from the left ventricle into the systemic circulation (with period $T = 1/\mathrm{HR}$) generates arterial flow, characterized by the propagation of pressure waves (and associated changes in vessel volume and diameter), commonly referred to as pulse waves. These waves travel along the arterial tree, which is composed of tapered vessels and multiple bifurcations [56]. The shape and characteristics of pulse waves is complex, influenced by various physiological and pathological factors within the cardiovascular system [57]. A thorough analysis of the pulse waveform (i.e., a graphical representation of the pulse wave over time) holds significant promise for improving the diagnosis and monitoring of CVDs [57, 58].

At a very basic level, the pulse waveform $P(t)$, representing pressure as a function of time, can be characterized by its maximum and minimum values, which correspond to SBP during ventricular ejection and DBP at the end of diastole, immediately before the next ventricular contraction. The PP reflects the amplitude of the pulse wave. Additionally, the shape of the pulse waveform allows for determination of MAP, which can be calculated as the time-averaged integral $\frac{1}{T}\int_0^T P(t)\,dt$ [59]; see Figure 1.2 for more details.

One of the key factors influencing the propagation of the pulse wave is the elasticity of the vessel walls [60]. Arteries vary significantly in both wall properties and size. Large arteries, such as the ascending aorta or common carotid arteries, typically have diameters ranging from 10 to 25 mm [56]. These vessels are highly elastic, allowing for a large stretch during systole and subsequent recoil during diastole [61]. Smaller arteries, with diameters between 0.1 and 10 mm, and arterioles, with diameters less than 0.1 mm, exhibit reduced elasticity and increased resistance to blood flow [61, 56].

Large elastic arteries play a crucial role in dampening the pulsatile output generated by the heart, allowing for continuous blood flow even during diastole, when the heart is not actively pumping. The increase in pulse pressure observed toward the peripheral arteries (see Figure 1.3A) results from changes in arterial compliance (a measure of vessel elasticity). As a consequence, peripheral systolic and pulse pressures are usually higher than central aortic values [62]. The elastic properties of arteries also determine the speed at which the pulse wave propagates, known as pulse wave velocity (PWV) [60, 63]. In healthy individuals, PWV typically ranges from 4 to 10 m/s in the aorta and large arteries, but it can be significantly higher in cases of increased arterial stiffness (i.e., reduced elasticity) [63, 64]. The carotid–femoral pulse

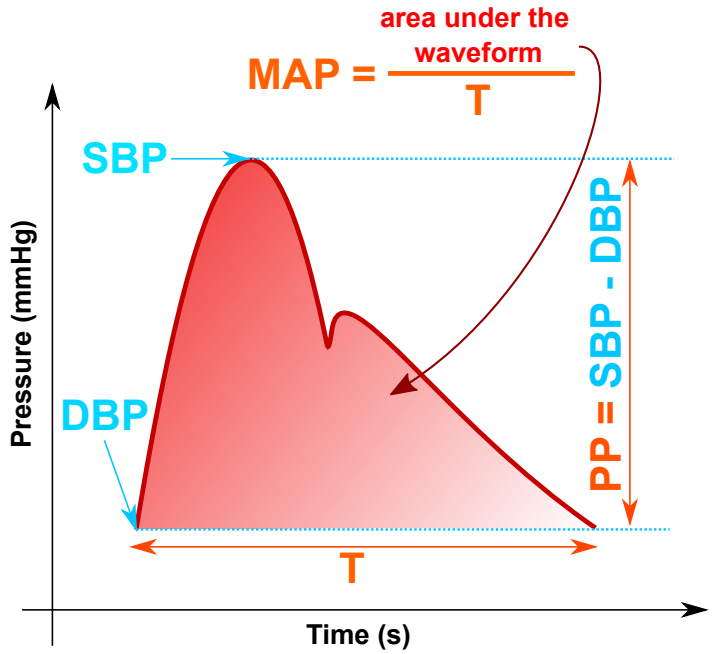

FIGURE 1.2: Schematic representation of a typical peripheral arterial pressure waveform, illustrating key features such as systolic blood pressure (SBP), diastolic blood pressure (DBP), pulse pressure (PP) and mean arterial pressure (MAP).

wave velocity (cfPWV) is considered the gold standard for assessing arterial stiffness [65] and serves as an independent predictor of cardiovascular risk [66]. cfPWV is calculated by dividing the distance between the carotid and femoral measurement sites by the transit time of the pressure wave between them [63]. Figure 1.3 provides a schematic overview of pulse wave propagation in the arterial tree and illustrates the cfPWV measurement.

As pulse waves propagate through the arterial tree, they encounter changes in vessel geometry and mechanical properties that generate wave reflections and backward-traveling waves. These reflections occur at sites of abrupt changes, such as bifurcations, sudden diameter variations, or transitions between arterial segments with differing wall stiffness. Consequently, the recorded pulse waveform represents a complex superposition of the forward-traveling wave and multiple reflected waves [60, 69].

Importantly, the reflected waves depend on the downstream vascular tone: their timing and amplitude depend not only on geometric discontinuities but also on distal vascular properties such as systemic vascular resistance (SVR) and arterial compliance. Arteriolar beds determine SVR and thus influence MAP. Changes in MAP affect arterial wall distension and effective stiffness (arteries stiffen when stretched), which in turn modify PWV and the pattern of wave reflections. As a result, shifts in peripheral resistance or arterial stiffness produce immediate, coupled changes in waveform morphology and timing [70, 63]. Clinically relevant interventions that alter vascular tone (such as vasopressor administration) have both direct effects on MAP and indirect effects on reflected waves and PWV, together shaping the observed peripheral pulse waveforms [71, 63, 72].

In summary, the pulse wave is much more than a simple indicator of heart rate; it is a rich physiological signal that may provide a comprehensive view of cardiovascular health. Subtle changes in pulse wave morphology, including the timing of the reflected waves, can be crucial for both diagnosing and monitoring cardiovascular conditions.

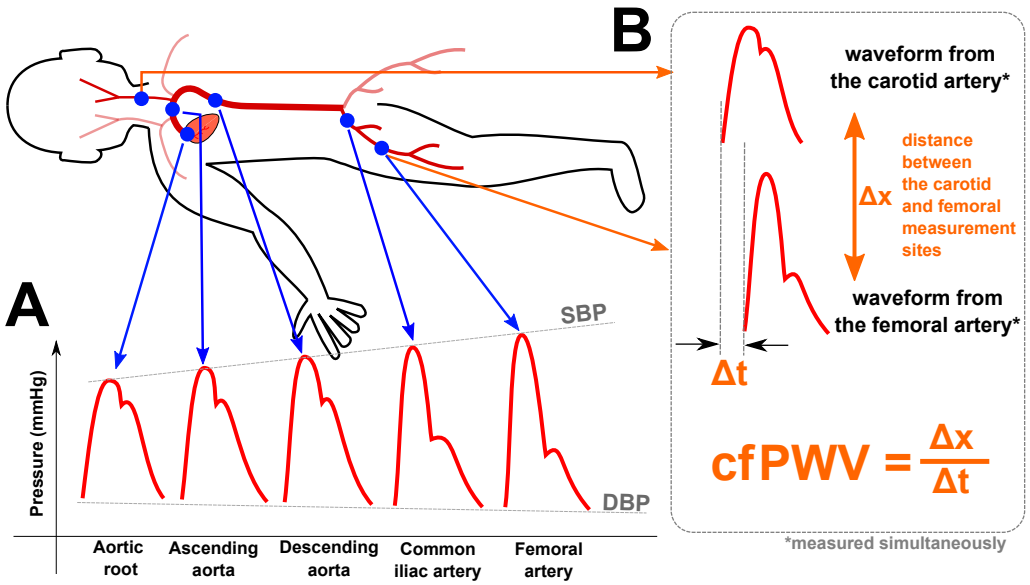

FIGURE 1.3: Schematic representation of pulse wave propagation in the arterial tree. (A) A pressure wave generated by the heart travels through the arterial tree and changes its shape and amplitude as it encounters vessels with different geometry and wall properties. (B) Carotid–femoral pulse wave velocity (cfPWV) is estimated by measuring the transit time of the pulse wave between the carotid and femoral arteries and dividing the distance by this time. Figure based on [67, 68].

Accurate recognition of these characteristic waveform alterations requires reliable and precise measurement techniques.

1.4 How to measure and decipher pulse waves?

Pulse wave measurement methods range from highly invasive to fully non-invasive techniques, with varying degrees of accuracy and clinical applicability. The gold standard remains the direct intra-arterial catheterization, which provides high-fidelity recordings through insertion of a pressure transducer into an artery [73, 74]. The transducer converts the blood motion into electrical signals, which are then sent to a monitor [75]. This method allows also for continuous pressure monitoring [76], but is relatively expensive and carries risks such as thrombosis (blood clot formation) and infection [77].

One of the most widely used non-invasive techniques of pulse wave recording is applanation tonometry. This technique involves a pressure sensor (a tonometer), which is applied externally to superficial arteries (such as the radial or carotid artery). During the measurement, the pressure sensor is gently pressed against a superficial artery to flatten ("applanate") the vessel wall. The tonometer then records the pressure transmitted through the flattened arterial wall, reconstructing the arterial pressure waveform [58]. The accuracy of applanation tonometry depends on proper sensor placement and adequate contact pressure [78]. When performed correctly, it can provide high-fidelity waveforms that closely approximate intra-arterial pressure [79]. However, it requires operator skill and experience to ensure reliable results. Figure 1.4A shows an example of a commercially available applanation tonometer device (SphygmoCor, AtCor Medical, Australia).

An oscillometric method is another non-invasive technique for recording pulse waves. This method employs a blood pressure cuff to record pulse waveforms at

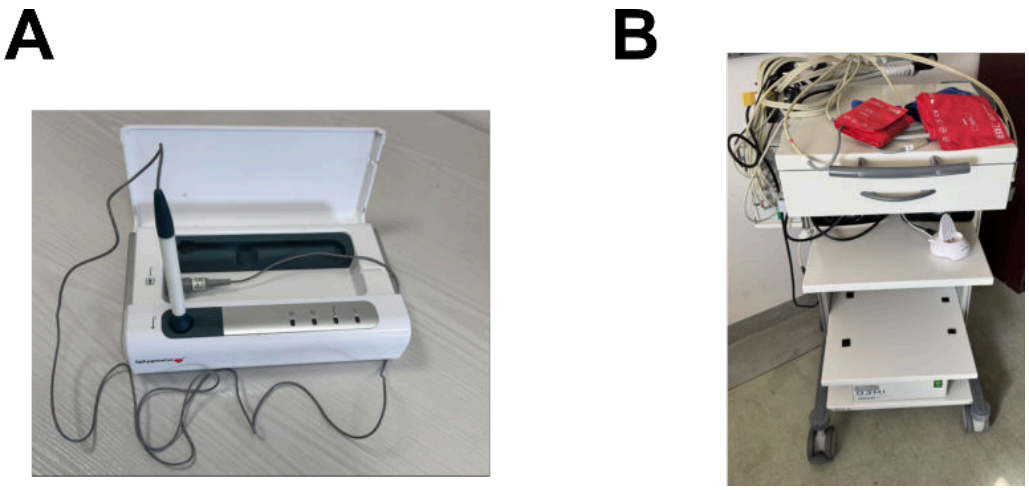

FIGURE 1.4: Exemplary devices for non-invasive pulse wave measurements (recordings): (A) an applanation tonometer device (SphygmoCor, AtCor Medical, Australia), (B) an oscillometric cuff-based device (AngE, SoT Medical, Austria).

specific cuff pressures. The measured oscillations correspond to variations in cuff pressure caused by pulsatile changes in arterial volume beneath the cuff (partially attenuated). When the cuff pressure is close to diastolic BP level, the recorded waveform provides a reasonable approximation of the shape of the arterial volume pulse wave [80, 81]. An example of device employing this method is the AngE system (SoT Medical, Austria), shown in Figure 1.4B.

Another non-invasive method of recording pulse waves is photoplethysmography (PPG). In this technique, a light-emitting diode (typically infrared or green light) illuminates the skin (e.g., on a fingertip), and a photodetector measures changes in blood volume by detecting variations in light absorption by blood in the skin vessels. The pulsatile component of the PPG waveform reflects the peripheral pulse (volume) waveform morphology, enabling analysis of features such as pulse width, pulse area, and dicrotic notch [82]. PPG is inexpensive and convenient but susceptible to motion artifacts, filtering effects, and influences of tissue optical properties [82]. Interestingly, more and more research is focusing on advanced signal processing and machine learning techniques to enhance PPG-based measurements [83, 84, 85].

The volume-clamp method is also a non-invasive, continuous monitoring technique that uses an inflatable finger cuff with infrared PPG to estimate arterial volume changes. The cuff applies variable pressure to maintain a constant arterial volume under the cuff, allowing for continuous reconstruction of the arterial pressure waveform [86, 87]. However, this method is sensitive to patient movement. It can also be difficult to obtain an accurate reading in patients with severe vasoconstriction, peripheral vascular disease or distorted fingers due to arthritis [88].

To extract clinically relevant information from the recorded pulse waveform, a special analysis is required. One of such analytical methods is Pulse Wave Analysis (PWA) [89]. PWA leverages peripheral pulse waveforms to estimate central blood pressure (cBP), i.e. the pressure in the aorta, via generalized transfer functions (GTF) [89, 90]. A GTF is a mathematical model that characterizes the relationship between the shape of the peripheral pressure wave and the central pressure wave [91]. Figure 1.5 illustrates the schematic of analysis of the aortic pressure waveform from the radial artery waveform using a GTF.

Assessing cBP is clinically important, as multiple studies suggest it is a superior predictor of cardiac morbidity and mortality compared to peripheral BP [92,

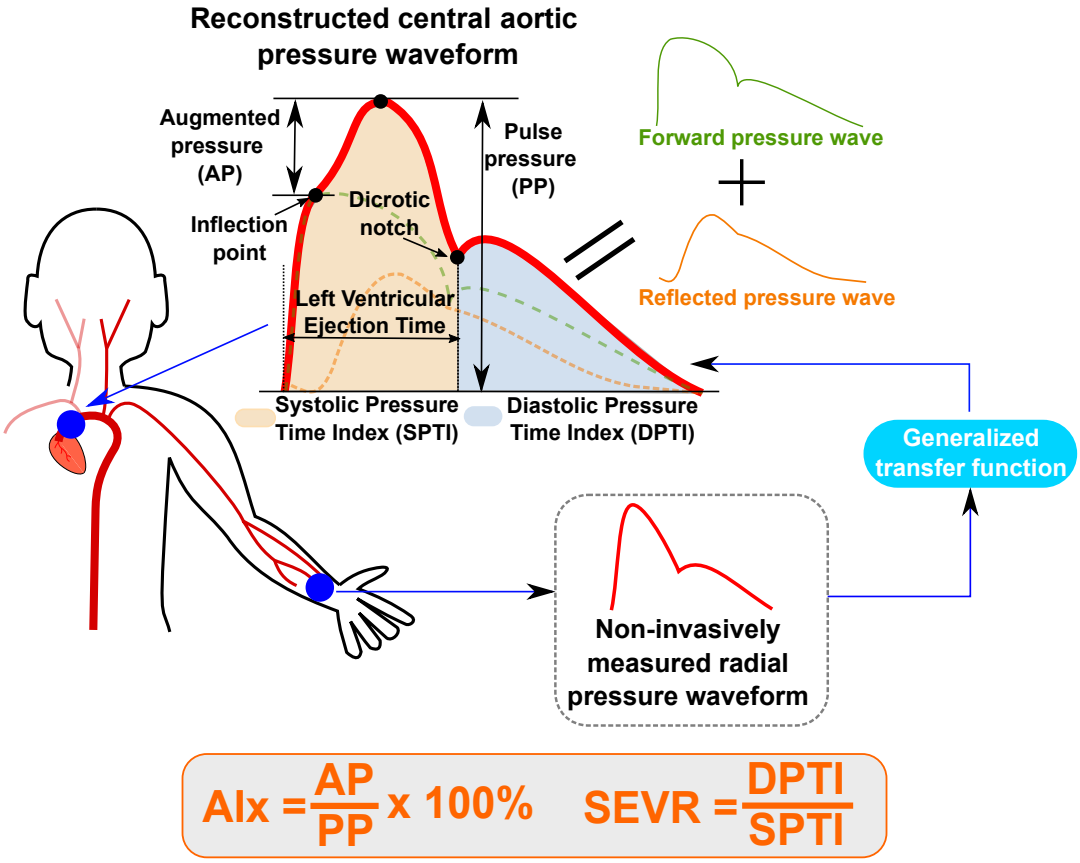

FIGURE 1.5: Schematic representation of analysis of aortic pressure waveform from radial artery waveform, illustrating key features such as augmentation pressure (AP), pulse pressure (PP), central augmentation index (AIx), subendocardial viability ratio (SEVR) and left ventricular ejection time (LVET).

93]. However, the use of GTFs has limitations, particularly in certain populations, such as patients with chronic kidney disease (CKD), in whom their accuracy may be reduced [94].

One commonly derived parameter of the aortic waveform is augmentation pressure (AP), which quantifies the increase in central blood pressure (cBP) caused by the reflected pressure waves. Closely related to AP is the central augmentation index (AIx), a normalized measure that expresses AP as a percentage of pulse pressure. Elevated AP and AIx generally indicate increased arterial stiffness and a higher risk of CVD [95, 96, 97].

Another clinically relevant metric is the subendocardial viability ratio (SEVR), which is defined as the ratio of the area under the central pressure waveform during diastole (Diastolic Pressure Time Index; DPTI) to the area under the waveform during systole (Systolic Pressure Time Index; SPTI) [98], see Figure 1.5 for more details. Higher SEVR values indicate better myocardial perfusion and a more favorable cardiac oxygen supply-demand balance, while lower SEVR values suggest a mismatch between supply and demand, which can serve as an early indicator of myocardial ischemia (insufficient blood flow to the heart muscle) [99].

From the aortic waveform we are also able to estimate the left ventricular ejection time (LVET) – the duration of the systolic ejection phase, i.e., the time interval between the opening of the aortic valve (characterized as the onset of the rapid upstroke of pressure in the aorta) and its closing (characterized by the dicrotic notch

in the pressure waveform) [100]. Prolonged LVET are observed in patients with significant aortic stenosis, whereas shortened LVET may be seen in conditions such as non-treated hypertension [101]. This parameter has also utility as an independent predictor of heart failure [102]. For a visual summary of the aortic waveform-derived parameters see Figure 1.5.

Overall, based on its shape and propagation characteristics, the pulse wave may allow for the monitoring of physiological and pathological changes in the cardiovascular system. Currently, there are many methods for non-invasive pulse wave measurement, which offer the possibility of an accessible but also advanced analysis of the pulse waveform. Is it possible, then, to extract additional clinically relevant information from the pulse wave? Given the complexity and physiological importance of pulse wave dynamics, mathematical modeling of pulse wave propagation has emerged as a powerful tool to deepen our understanding of cardiovascular function, interpret measurements cardiovascular parameters that are difficult to measure directly.

1.5 Pulse wave propagation modeling as a tool to decipher pulse waveforms

1.5.1 What is 0-1D pulse wave propagation modeling?

Before delving into the specifics, it is important to understand the concept of pulse wave propagation modeling. This approach aims to represent the vascular system as a network of arterial vessels and use differential equations to simulate how the pulse waves propagate, reflect, and change their shape as they travel through the arterial network. These models are typically based on one-dimensional (1D) formulations of mass, momentum and energy conservation in large and medium arteries, coupled with lumped-parameter models that characterize small arteries and arterioles. This enables realistic modeling of wave propagation dynamics with relatively low computational requirements. Historically, the first one-dimensional models were developed in parallel with early lumped-parameter models [103, 104], but their practical application became feasible only with the advent of digital computing. As computational resources became more accessible, the use of 1D models in cardiovascular research increased significantly.

Pulse wave propagation models are based on several assumptions that simplify the complex nature of the circulatory system. The arterial network is usually depicted as a tree of branching arteries, with each branch representing a large artery (segments of aorta or conduit arteries), with two or three levels of bifurcation, while excluding small arteries and arterioles [105, 106, 107, 108]. Vessels are assumed to be slightly tapered, distensible tubes with axisymmetric, circular cross-sections.

Blood is a non-Newtonian fluid, meaning its viscosity is not constant but depends on the shear rate (the shear-thinning property). This behavior is particularly important in very small vessels ($< 200\mu$m) and under conditions of low shear stress [109]. However, in large arteries, where shear rates are typically high, blood can be approximated as a Newtonian fluid with constant viscosity [110]. Therefore, in 1D models, blood is often modeled as an incompressible, Newtonian fluid with constant density and viscosity.

To further simplify the mathematical formulation, it is necessary to assume a specific blood velocity profile. The most commonly used profiles are parabolic (Poiseuille) and flat [60, 106].

A comprehensive description of blood flow relies on the set of three main equations:

- governing equation for blood motion, typically derived from a reduced form of the Navier–Stokes equations;
- the continuity equation, which arises from the incompressibility of blood and ensures mass conservation within each arterial segment;
- an equation describing the interaction between blood pressure and vessel wall deformation.

Proper boundary conditions are essential for accurate pulse wave propagation modeling. At vascular bifurcations, most models enforce continuity of pressure and conservation of mass, ensuring physically consistent wave transmission and reflection [111, 107]. In addition, some approaches incorporate energy losses resulting from vortex formation at these vessel junctions [106, 111, 112].

Several approaches are used for the outflow boundaries (i.e., the terminal ends of the vascular tree), including pure resistance models [113, 114], 3-element Windkessel models [105, 115], and structured tree models that approximate the impedance of the downstream vasculature [106, 116]. These models are intended to represent small arteries and arterioles, which are normally not included in the 1D model of the arterial tree [117].

Inflow boundary conditions, (i.e., conditions describing the blood flow from the left ventricle to the arterial system), are often defined using phenomenological functions independent of downstream conditions [118, 119, 120]. Alternatively, more advanced approaches use time-varying elastance models based on Suga's and Sagawa's work from the 1970s [121, 122], which account for the left ventricular contraction dynamics [108, 123, 124].

For simplicity, venous return and pulmonary circulation are generally omitted, although models that include them also exist in the literature [125, 126].

Figure 1.6 presents a schematic representation of an exemplary 0-1D pulse wave propagation model, illustrating the key components within the cardiovascular system.

1.5.2 Personalization of the models

One of the key strengths of 0–1D pulse wave propagation models is their ability to be relatively quickly personalized for individual patients, in contrast to more complex higher-dimensional models. By adjusting selected model inputs such as vascular geometry, HR, or inflow boundary condition, these models can account for inter-individual variability. Such personalization increases the clinical relevance of the models, enabling more precise cardiovascular assessment and tailored therapeutic guidance for diverse patient populations.

The equations describing pulse wave propagation models are governed by a range of parameters, including those characterizing the elastic properties of arterial walls, the resistance and compliance of peripheral vascular beds, and cardiac function. To tailor a model to a specific patient, some authors scale the dimensions of the entire vascular tree or adjust the length of the ascending aorta according to the patient's height [127, 128, 119, 129]. However, such adjustments are often insufficient for full personalization, particularly in the presence of cardiovascular pathologies. To estimate the values of model (patient) parameters that are unavailable or impossible to measure, one can formulate an inverse problem: given the measured data (corresponding to a certain model output, such as a pressure or flow waveform), the objective is to identify the set of model parameters that best reproduce the observed data.

To achieve personalization of a pulse wave propagation model, some researchers use pulse waveform measurements [127, 128, 119]. An objective function is defined,

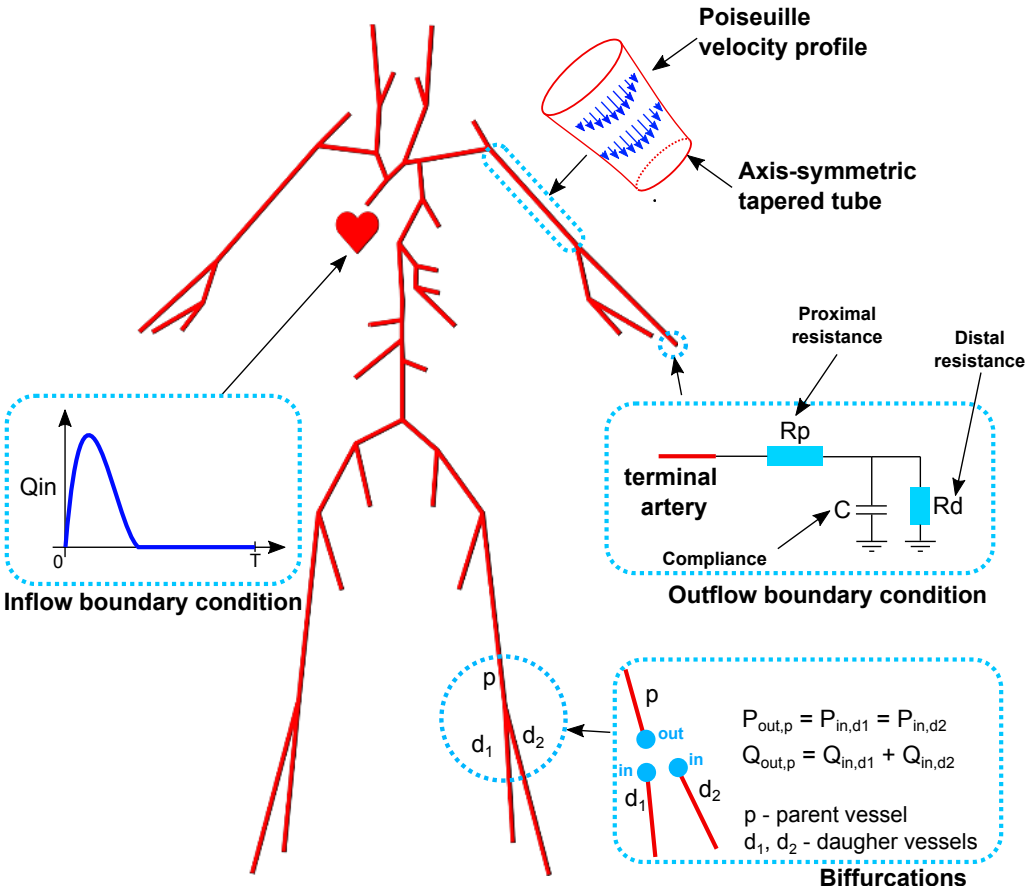

FIGURE 1.6: Schematic representation of an exemplary 0-1D pulse wave propagation model. The cardiovascular system is represented as a network of one-dimensional arterial segments (large arteries) connected to the inflow boundary condition (e.g., a phenomenological function describing the blood outflow from the left cardiac ventricle) and outflow boundary conditions (e.g., 3-element Windkessel models connected to the end of the modelled arteries). P denotes pressure and Q denotes flow.

and optimization methods are applied to minimize the error between the measured and model-predicted waveforms. The optimization process iteratively adjusts the non-fixed model parameters to reduce the discrepancy between the simulation output and the data. As a result, personalized parameter values are obtained, enabling more accurate model-based hemodynamic assessments and estimation of physiological quantities that are not directly accessible through standard clinical measurements. These may include vessel wall stiffness, peripheral resistance, compliance, or cardiac-related parameters such end-systolic left ventricular elastance. However, the success of this approach depends on data quality, parameter identifiability, and the choice of optimization algorithm, all of which must be carefully considered in clinical applications. Conducting a sensitivity analysis is considered good practice, as it helps identify the model parameters with the most significant influence on the given model outputs.

An important aspect of 0–1D modeling is its modularity, which allows for integration of additional compartments into the cardiovascular system representation or additional model features, for example, modeling the venous return system [125], the cerebral autoregulation [130], or even the impact of external devices such as pressure cuffs [131]. Such model extensions may enhance the model's ability to simulate complex physiological and clinical scenarios.

1.5.3 Previous studies on fitting the models to measured pulse waveforms

Personalized pulse wave propagation models are increasingly recognized as powerful tools for simulating and understanding cardiovascular dynamics. Traditionally, model personalization has relied on manual adjustment of selected model parameters, such as parameters describing vessel geometry as well as inflow boundary conditions based on measured physiological data [108, 129]. However, only a limited number of studies (typically involving small groups of volunteers) have directly fitted pulse wave propagation models to recorded pressure or flow waveforms.

Poleszczuk et al. developed a subject-specific one-dimensional pulse wave propagation model, personalized by adjusting six key parameters, including wall stiffness coefficients, cardiac output, time of peak blood ejection, and terminal resistance/compliance scaling factors, to fit radial pressure waveforms recorded via applanation tonometry in 20 healthy volunteers [128]. A two-stage optimization process was used to find optimal values of the aforementioned parameters, combining particle swarm optimization with a gradient-based method. This framework enables enhanced cardiovascular assessment and simulation of virtual patient scenarios [128].

Zhang et al. introduced a personalized hemodynamic modeling framework that combines a 0-1D cardiovascular model with the Levenberg–Marquardt optimization algorithm to estimate individual pressure and flow waveforms in the brachial and carotid common arteries [119]. The study involved 62 healthy volunteers aged 20–70 years, in whom brachial arterial pressure waveforms were measured using the volume-clamp method, and stroke volumes and artery diameters were measured using ultrasound. Subject-specific arterial stiffness parameters were estimated using inverse optimization. Validation demonstrated that the model accurately estimates individual pulse waveforms.

Hao et al. proposed a subject-specific approach for estimating central hemodynamics by combining a generalized transfer function (GTF) with a 0-1D cardiovascular model [132]. To address the large number of uncertain arterial parameters, a two-step sensitivity analysis was performed: first, the Morris method identified the parameters with the highest impact on the shape of the peripheral (brachial and radial) pressure waveforms, followed by the adaptive sparse generalized polynomial chaos expansion (agPCE) for uncertainty quantification. Model personalization was achieved using simulated annealing to minimize the error between the measured and estimated peripheral aortic pressure waveforms. The method was validated in 26 patients who underwent cardiac catheterization, and its performance was compared with conventional GTF approach. The proposed method reliably estimated central aortic waveforms and pressures, outperforming standard GTF method.

Liu et al. developed a non-invasive method for estimating left ventricular pressure waveforms in patients with coronary artery disease by integrating a single-fiber ventricular model, diode-like heart valves, and a 0-1D arterial tree model [133]. Model personalization was achieved through a two-step process: first, the Morris sensitivity analysis identified a crucial subset of 16 model parameters - including ventricular activation and contractile element properties, valve resistances, arterial diameters, wall stiffnesses, and peripheral Windkessel resistances/compliances. Next, differential evolution optimization was applied to fit the model to patient data. Validation was performed using aortic pressure waveforms recorded invasively (via cardiac catheterization) in 32 patients with suspected coronary artery disease [133].

In another patient-specific study, Poleszczuk et al. applied pulse wave propagation modeling to identify cardiovascular risk characteristics in hemodialysis patients,

aiming to address the limitations of traditional pulse wave analysis [127]. Model personalization was achieved similarly as in their previously discussed study [128]. The model was validated in a cohort of 35 anuric prevalent hemodialysis patients and 32 healthy volunteers.

Pulse wave propagation models also enable the estimation of waveforms other than pressure, such as flow waveforms. In some studies, mathematical models are personalized using flow waveforms measured by Doppler ultrasound.

For example, in the study by Zhang et al. [134], a personalized 0–1D cardiovascular model was developed to simulate the hemodynamic effects of enhanced external counterpulsation (EECP). The model integrates a 1D pulse wave propagation through arteries, a 0D lumped-parameter representation of veins and capillaries, and a single-fiber heart model, further coupled with an EECP module. Clinical ultrasound data, including flow waveforms from the carotid, femoral, and brachial arteries, were collected from 22 volunteers both at rest and during EECP. A two-step sensitivity analysis was performed to identify key model parameters, which were then optimized using simulated annealing to construct subject-specific models. Validation demonstrated high agreement between the simulated and measured flow waveforms.

In another study [135], researchers applied one-dimensional hemodynamic modeling to investigate the effects of intracranial internal carotid artery stenosis on extracranial blood flow patterns, aiming to develop a non-invasive diagnostic approach for early stenosis detection. Personalization was initially achieved by adjusting multiple patient-specific parameters, including stroke volume, heart rate, and arterial diameters at key locations (carotid, vertebral, and aortic segments), as well as stenosis geometry derived from magnetic resonance angiography images. Subsequently, three cardiovascular parameters (elastic modulus, peripheral resistance, and peripheral compliance) were optimized using the Levenberg–Marquardt algorithm to fit the model's predicted internal carotid artery flow velocity waveforms to the actual Doppler ultrasound measurements for each patient. Validation was performed in a cohort of 52 patients with varying degrees of intracranial internal carotid artery stenosis and 24 control subjects.

Despite the aforementioned studies, integrating personalized hemodynamic modeling into routine clinical practice remains challenging. Nevertheless, there is growing recognition of the potential clinical benefits these models may offer. Further research is needed to validate pulse wave propagation models across diverse populations and clinical scenarios, ensuring their reliability and utility in real-world settings.

1.6 Aim of this study and research hypotheses

Pulse wave propagation modeling has emerged as a promising tool for extracting cardiovascular information from non-invasive measurements. Recent approaches, particularly those involving personalized pulse wave propagation modeling and direct fitting of pulse waveforms, aim to improve the accuracy and reliability of cardiovascular assessments. These methods also enable the estimation of key hemodynamic parameters, such as arterial stiffness and vascular resistance, using data collected non-invasively. However, only a limited number of studies have applied these models to specific patient populations, and the topic remains insufficiently explored.

My dissertation aims to address this gap by developing personalized pulse wave propagation modeling approaches that leverage non-invasive measurements to enhance cardiovascular assessment and guide therapy. I focus on two underrepresented patient populations in pulse wave research: patients with chronic kidney disease

(CKD) and those with severe traumatic brain injury (sTBI). By applying and validating these models in these patient groups, my work seeks to provide new insights into patient-specific hemodynamics and support more individualized clinical decision-making.

1.6.1 Hypotheses

Based on the characteristics of my research, I formulated the following hypotheses:

(H1) A pulse wave propagation model, after calibration with peripheral pressure waveforms recorded non-invasively using applanation tonometry, can be used to estimate heart function parameters in both healthy individuals and patients with altered cardiovascular status.

(H2) A pulse wave propagation model can approximate arterial pulse waveforms recorded simultaneously at multiple locations using the oscillometric technique.

(H3) Cardiovascular parameters estimated through personalization of a pulse wave propagation model may be used for prediction of vasopressor dosage adjustments in patients with severe traumatic brain injury.

(H4) A pulse wave propagation model can be used to assess the hemodynamic effects of peripheral arterial occlusions due to oscillometric cuff measurements.

1.6.2 Research questions

To address the research aims and test the hypotheses, I formulated the following research questions:

(H1Q1) How can a pulse wave propagation model be efficiently coupled with a time-varying left ventricle elastance function model?

(H1Q2) How do the values of stroke volume estimated based on pulse wave propagation modelling compare with the values obtained using bioimpedance cardiography?

(H2Q1) Which parameters of a pulse wave propagation model should be adjusted to fit the model to four peripheral pulse waveforms (recorded on wrists and ankles)?

(H2Q2) Can a pulse wave propagation model approximate pulse waveforms recorded oscillometrically from four peripheral sites (wrists and ankles)?

(H3Q1) Do the values of cardiovascular parameters estimated from pulse wave propagation modeling allow for predictions of vasopressor dosing adjustments in patients with severe traumatic brain injury?

(H3Q2) Are the above-mentioned predictions better compared to predictions based on standard hemodynamic parameters and patient characteristics?

(H4Q1) How can a pulse wave propagation model be adapted to simulate peripheral arterial occlusion due to oscillometric cuff measurements?

(H4Q2) What are the local and central hemodynamic consequences of a single-limb oscillometric cuff measurement?

(H4Q3) What are the local and central hemodynamic consequences of multi-limb oscillometric cuff measurements?

(H4Q4) Are the central hemodynamic consequences of multi-limb oscillometric cuff measurements similar in different subjects?

In Chapters 2–4, I refer to specific hypotheses and research questions while discussing three publications attached to the dissertation: [A1], [A2], and [A3]. The Chapters are titled after the respective publications.

Chapter 2

Publication [A1]: Non-invasive assessment of stroke volume and cardiovascular parameters based on peripheral pressure waveform

2.1 Summary of the study

In the clinical setting, cardiac stroke volume (SV) is commonly estimated using echocardiography or invasive methods such as thermodilution during cardiac catheterization [43]. However, these techniques can be costly and require special equipment and trained personnel, and therefore are not suitable for routine use. Less invasive approaches, such as non-invasive bioimpedance cardiography, also require dedicated devices and skilled operators, but their accuracy can be limited [136, 137]. Therefore, there is growing interest in developing new non-invasive methods for estimating SV and other parameters of cardiac function. One promising approach uses pulse wave propagation models that simulate blood flow and pressure dynamics in the arterial system. By calibrating such models with non-invasively recorded peripheral pressure waveforms, it is possible to infer central hemodynamics, including left ventricular outflow and parameters describing cardiac function. Recently, Bikia et al. personalized a pulse wave propagation model using the measured pulse wave velocity, and brachial systolic and diastolic blood pressures, reporting promising results in estimating cardiac output and central systolic pressure [138]. To our knowledge, no previous studies have validated model personalization for SV estimation in patients with altered cardiovascular status, using the peripheral pulse waveform to inform the model.

In the first publication included in this dissertation, I present a non-invasive method to estimate SV and other cardiovascular parameters from peripheral pressure waveforms recorded by applanation tonometry (SphygmoCor, AtCor Medical, Australia); see also Figure 1.4 in Chapter 1.4. With this study, I aimed to address the first research hypothesis (H1) outlined in Chapter 1.6:

(H1) *A pulse wave propagation model, after calibration with peripheral pressure waveforms recorded non-invasively using applanation tonometry, can be used to estimate heart function parameters in both healthy individuals and patients with altered cardiovascular status.*

In my research, I built upon a 0-1D cardiovascular model previously applied by Poleszczuk et al. [127, 128]. To address the above hypothesis, I needed to develop a more advanced representation of left ventricular function and perform a detailed

comparison of SV estimates derived from the model with those obtained via another method. Therefore, I formulated two specific research questions (H1Q1, H1Q2), as outlined in Chapter 1.6:

(H1Q1) *How can a pulse wave propagation model be efficiently coupled with a time-varying left ventricle elastance function model?*

(H1Q2) *How do the values of stroke volume estimated based on pulse wave propagation modelling compare with the values obtained using bioimpedance cardiography?*

To address these questions, I first integrated a time-varying elastance representation of left ventricular function into the one-dimensional pulse wave propagation model previously developed by my Advisor [127, 128] (H1Q1). The used left ventricle model, originally part of a lumped cardiovascular system model, is based on the work of Ottesen et al. [124]. My objective was to implement this formulation within the 0-1D pulse wave propagation model, replacing the earlier phenomenological formulation derived from another study by Olufsen [118]. Unlike simpler cardiac ejection models [119, 118], this model provides a more physiologically accurate representation of ventricular contraction as a time-dependent process. It achieves this by coupling the left ventricular elastance function with the aortic root pressure computed within the 0-1D pulse wave propagation model. This integration enables simulation of the interaction between cardiac function and arterial hemodynamics. Additionally, the lumped-parameter formulation of the left ventricle model offers a computationally efficient way to represent the complex dynamics of the left ventricle, making it well-suited for parameter estimation based on non-invasive measurements (H1Q1).

Next, I personalized the model using radial artery pressure waveforms recorded with an applanation tonometer from 14 healthy volunteers and 35 anuric, maintenance hemodialysis (HD) patients. For each HD patient, the waveforms were recorded four times per dialysis session: approximately 15 minutes before the start, after the start, before the end, and after the end of the session. These recordings were conducted during two HD sessions following both longer and shorter interdialytic breaks, resulting in a total of 280 measurements. Selected cardiovascular parameters, including the maximal left ventricular elastance ($E_{\max}$) and peripheral vascular resistance, were estimated using a two-step parameter optimization procedure that minimized the difference between the measured and simulated radial pressure waveforms.

For each subject, SV was then estimated using the simulated flow in the ascending aorta (addressing H1Q2) and compared to values measured using bioimpedance cardiography (PhysioFlow, Manatec Biomedical, France). The model-derived SVs showed moderate correlation with bioimpedance-based values in both the control group ($r = 0.57$, $p < 0.05$) and the HD cohort ($r = 0.58$, $p < 0.001$), although, on average, the SV values estimated by the model were approximately 34% lower than those measured by bioimpedance cardiography in both groups.

It is important to note that bioimpedance cardiography, while less burdensome than echocardiography for repeated evaluations during HD sessions, may not provide fully accurate measurements [136, 137], and hence the observed bias in the model-estimated SVs may be related to the reference measurements. Additionally, discrepancies between the bioimpedance- and model-estimated SVs could arise from inaccuracies in pulse wave measurements used for model calibration. Although applanation tonometry is considered a relatively reliable method for capturing pressure waveforms, it is highly dependent on the operator technique and is sensitive to movement artifacts, which can compromise signal quality. Indeed, due to the poor quality of some recordings (both SV and pulse waveforms), I had to exclude 136 out of the 280 recordings from the analysis (see Fig. S3 in the Supplementary Materials).

The results of this study highlight the potential of non-invasive pulse wave propagation modeling for assessing SV in HD patients. By calibrating the model to peripheral pressure waveforms, which are relatively easy to obtain, this approach offers a promising alternative for cardiovascular assessment. To the best of my knowledge, this is the first study to utilize the shape of the pulse waveform for model calibration to estimate SV, and to apply this method in both healthy individuals and a specific patient group. Nevertheless, further validation against gold-standard techniques, such as thermodilution, is required to fully establish the accuracy of this methodology.

The mathematical model developed in this work is available in my public GitHub repository: https://github.com/kwolos/PWA_public. The data used for the analysis can be found at https://zenodo.org/record/8131393.

2.2 My contributions

I am the first author of this publication, responsible for the conceptualization, methodology, software implementation, validation, investigation, formal analysis, and first draft writing. I developed the mathematical model by integrating the time-varying elastance function into the existing one-dimensional pulse wave propagation framework. Furthermore, I conducted the simulations and analyses comparing the model-derived stroke volume estimates with bioimpedance cardiography measurements. Additionally, I prepared all figures and tables presented in the article and supplementary materials.

2.3 Author contributions

The conceptualization of the study was discussed collaboratively with my Advisors, Prof. Jan Poleszczuk, and Dr. Leszek Pstraś. Methodological discussions involved Prof. Małgorzata Debowska and Prof. Wojciech Dąbrowski, while Prof. Dąbrowski and Prof. Dorota Siwicka-Gieroba oversaw the collection of medical data used in the study. The manuscript underwent review and revisions by my Advisors and Prof. Debowska.

2.4 Publication

PLOS COMPUTATIONAL BIOLOGY

RESEARCH ARTICLE

Non-invasive assessment of stroke volume and cardiovascular parameters based on peripheral pressure waveform

Kamil Wołos[1]*, Leszek Pstras[1], Malgorzata Debowska[1], Wojciech Dabrowski[2], Dorota Siwicka-Gieroba[2], Jan Poleszczuk[1]

1 Laboratory of Mathematical Modeling of Physiological Processes, Nalecz Institute of Biocybernetics and Biomedical Engineering, Polish Academy of Sciences, Warsaw, Poland, **2** Department of Anesthesiology and Intensive Therapy, Medical University of Lublin, Lublin, Poland

* kwolos@ibib.waw.pl

Citation: Wołos K, Pstras L, Debowska M, Dabrowski W, Siwicka-Gieroba D, Poleszczuk J (2024) Non-invasive assessment of stroke volume and cardiovascular parameters based on peripheral pressure waveform. PLoS Comput Biol 20(4): e1012013. https://doi.org/10.1371/journal.pcbi.1012013

Editor: Mark Alber, University of California Riverside, UNITED STATES

Received: July 26, 2023

Accepted: March 19, 2024

Published: April 18, 2024

Data Availability Statement: The mathematical model developed in this work can be found at https://github.com/kwolos/PWA_public. The data used for the analysis can be found in https://zenodo.org/record/8131393 [45].

Funding: JP, MD, WD, DSG and KW were partly supported by the National Science Centre (Poland), grant No. 2018/31/D/ST7/03472. KW was partly supported by European Social Fund (ESF), POWR.03.02.00-00-I028/17-00. The funders had

Abstract

Cardiovascular diseases are the leading cause of death globally, making the development of non-invasive and simple-to-use tools that bring insights into the state of the cardiovascular system of utmost importance. We investigated the possibility of using peripheral pulse wave recordings to estimate stroke volume (SV) and subject-specific parameters describing the selected properties of the cardiovascular system. Peripheral pressure waveforms were recorded in the radial artery using applanation tonometry (SphygmoCor) in 35 hemodialysis (HD) patients and 14 healthy subjects. The pressure waveforms were then used to estimate subject-specific parameters of a mathematical model of pulse wave propagation coupled with the elastance-based model of the left ventricle. Bioimpedance cardiography measurements (PhysioFlow) were performed to validate the model-estimated SV. Mean absolute percentage error between the simulated and measured pressure waveforms was 4.0% and 2.8% for the HD and control group, respectively. We obtained a moderate correlation between the model-estimated and bioimpedance-based SV ($r = 0.57$, $p<0.05$, and $r = 0.58$, $p<0.001$, for the control group and HD patients, respectively). We also observed a correlation between the estimated end-systolic elastance of the left ventricle and the peripheral systolic pressure in both HD patients ($r = 0.84$, $p<0.001$) and the control group ($r = 0.70$, $p<0.01$). These preliminary results suggest that, after additional validation and possibly further refinement to increase accuracy, the proposed methodology could support non-invasive assessment of stroke volume and selected heart function parameters and vascular properties. Importantly, the proposed method could be potentially implemented in the existing devices measuring peripheral pressure waveforms.

Author summary

With a growing number of people suffering from cardiovascular diseases (CVD), it is extremely important to develop non-invasive methods that could quickly and comprehensively assess the condition of the cardiovascular system. Hemodialysis (HD) patients are

no role in study design, data collection and analysis, decision to publish, or preparation of the manuscript.

Competing interests: The authors have declared that no competing interests exist.

particularly prone to CVD, but studies aimed at developing new techniques for non-invasive assessment of cardiovascular parameters are typically based on healthy subjects. We set out to investigate the possibility of using peripheral pressure waveforms to estimate stroke volume (SV) and selected parameters of the cardiovascular system in both healthy subjects and HD patients. To that aim, we developed a mathematical model of pulse wave propagation coupled with an elastance-based model of the left-ventricular function. The validity of the model has been assessed using bioimpedance-based SV estimates from both healthy subjects and HD patients. We believe that the proposed model-based procedure, subject to further validation and improvements, could serve as an auxiliary tool for evaluating SV. In addition, it enables estimation of selected cardiovascular parameters, some of which, as we have shown, appear to be related to known pulse wave-derived parameters.

Introduction

Chronic kidney disease (CKD) is a long-term decrease in kidney function characterized by its progressive nature, lack of a definitive cure, and high morbidity and mortality. It is relatively common in the general adult population, particularly among individuals affected by diabetes and hypertension [1]. Prevalence of CKD is estimated at 13.4% globally and its incidence is expected to rise in the future [2,3]. About 50% of patients with CKD stage 4 or 5 have a cardiovascular disease (CVD), with approximately 40% to 50% of all deaths in this group being attributed to CVD [2]. CVD risk factors in patients with CKD include, among others, vascular calcification, inflammation, hypertension, or diabetes [2]. Furthermore, nearly half of patients with heart failure suffer from CKD [4] and a long-term decrease in cardiac output or stroke volume may indicate progression of heart failure, which can decrease kidney perfusion and lead to kidney failure [5,6]. Non-invasive methods of assessing the patient's cardiovascular health can be an important aid in understanding the CKD-related mechanisms behind CVD, predicting hemodynamic response to various treatments, or creating personalized treatment plans. Moreover, non-invasive assessment of stroke volume in end-stage CKD patients receiving dialysis treatment could potentially help in assessing the fluid overload in such patients and prescribing an adequate and safe dialysis treatment. It could also be used for categorizing dialysis patients based on their intradialytic hemodynamic changes [7]. For these reasons, it is critically important to develop easy-to-use and non-invasive methods of assessing the patient's cardiovascular condition.

In recent years, personalized cardiovascular mathematical models of various complexity have begun to play an increasingly important role in the assessment of the state of the patient's cardiovascular system [8–13]. Coupled 0-1D models are a good compromise between the simplicity of lumped models and the complexity of multidimensional models in the case when one is interested in describing the whole-body circulation. In this type of reduced-order modeling, the pulse and flow wave propagation are described using a one-dimensional bifurcation tree reflecting the largest arteries in the body, on which the flow equations are imposed. In such models, the lumped parts typically explain the behavior of the peripheral arteries and the work of the heart. The size of the modeled system, as well as the parameters describing the heart and the vasculature (i.e. peripheral compliance, resistance, etc.) are subject-specific and should be estimated for a given patient. To personalize a model, one needs to collect (preferably non-invasively) patient data corresponding to the model outputs and then to adjust the model (i.e. optimize the model parameters), so that its outputs match gathered data as closely as possible. A proper optimization method, combined with appropriately assigned initial values of the parameters to be

optimized (e.g. based on patient size, age, gender, etc.), should minimize the difference between the model outputs and patient data, providing the final estimates of patient-specific values of those parameters, thus making the model personalized. Depending on the application and the details of the model, various approaches to model personalization may be used.

For instance, in the study by Zang et al [14] a 0-1D model describing 55 main arteries (defined previously in the works of Stergiopulos et al. [15] and Olufsen et al. [16]) was personalized by scaling the artery lengths and diameters according to subject height and a cluster-dependent scaling factor, followed by minimizing the error between the measured and simulated peripheral pressure waveforms using the gradient-based optimization algorithm. In the study by Bikia et al. [11] a model based on a more detailed bifurcation tree with 103 arteries (defined previously by Reymond et al. [17]), was personalized by: 1) adjustments of the arterial tree based on age, gender, height, and body surface area; 2) using a gradient-based optimization procedure to minimize the error between the measured and computed cardiovascular variables such as systolic and diastolic blood pressure, and carotid-femoral pulse wave velocity. Carson et al. [18] used a two-tier optimization procedure involving adjustments of parameters such as peripheral resistances, compliances, blood volume, and arterial cross-sectional areas to fit the model to the measured systolic and diastolic blood pressure, pulse wave velocity, as well as peak systolic and end-diastolic blood flow velocity.

Once the model is personalized, the resulting set of subject-specific parameters can provide deeper insight into the patient's condition without the use of invasive measurements [9–11,19]. However, to our knowledge, not many of such studies have been conducted in patients with chronic diseases such as CKD, who, as already mentioned, are particularly prone to CVD.

In our previous papers, we have investigated whether a 0-1D model could reproduce applanation tonometry recordings of pressure waves from the radial artery in healthy subjects and hemodialysis (HD) patients [10,19]. We also performed a detailed study on whether the cardiovascular risk factors for HD patients, such as arterial stiffness, could be derived from the measured pressure waveforms [19]. In the present paper, we extend our previous study by investigating if the measured pressure waveform can be used for a detailed heart function assessment, including stroke volume (SV) estimation. We use a similar 0-1D model as before i.e. the model based on the aforementioned commonly-used 55-element arterial tree and a 3-element Windkessel model at the terminal ends of the arteries. However, we decided to use a different boundary condition describing the inflow of blood to the arterial tree, which in the present study is based on the elastance function of the heart. To validate the model-based estimates of SV, we used bioimpedance cardiography measurements (PhysioFlow, Manatec Biomedical, France) performed simultaneously with peripheral pulse waves recordings.

Results

Reproduction of the measured pressure waveforms

After subject-specific personalization (calibration) of the model (see Fig 1 for a graphical representation of the calibration process), our pulse wave propagation model was able to reproduce the pressure waveforms recorded in the radial arteries with satisfactory accuracy in most cases. Exemplary model simulations after data fitting are presented in Fig 2, whereas all cases are presented in the S1 File. Additionally, S1 Fig shows exemplary model outputs at different locations in the arterial tree (i.e. flow and pressure waveforms). For the control group, the average mean absolute percentage error (MAPE) between the measured and fitted pressure waveforms (for all available data points) was 2.8%, whereas for HD patients it was 4% (see Fig 3 for more details). The average MAPE for the measurements performed during HD after a long interdialytic break (i.e. 3 days) was slightly lower compared with that obtained for the measurements

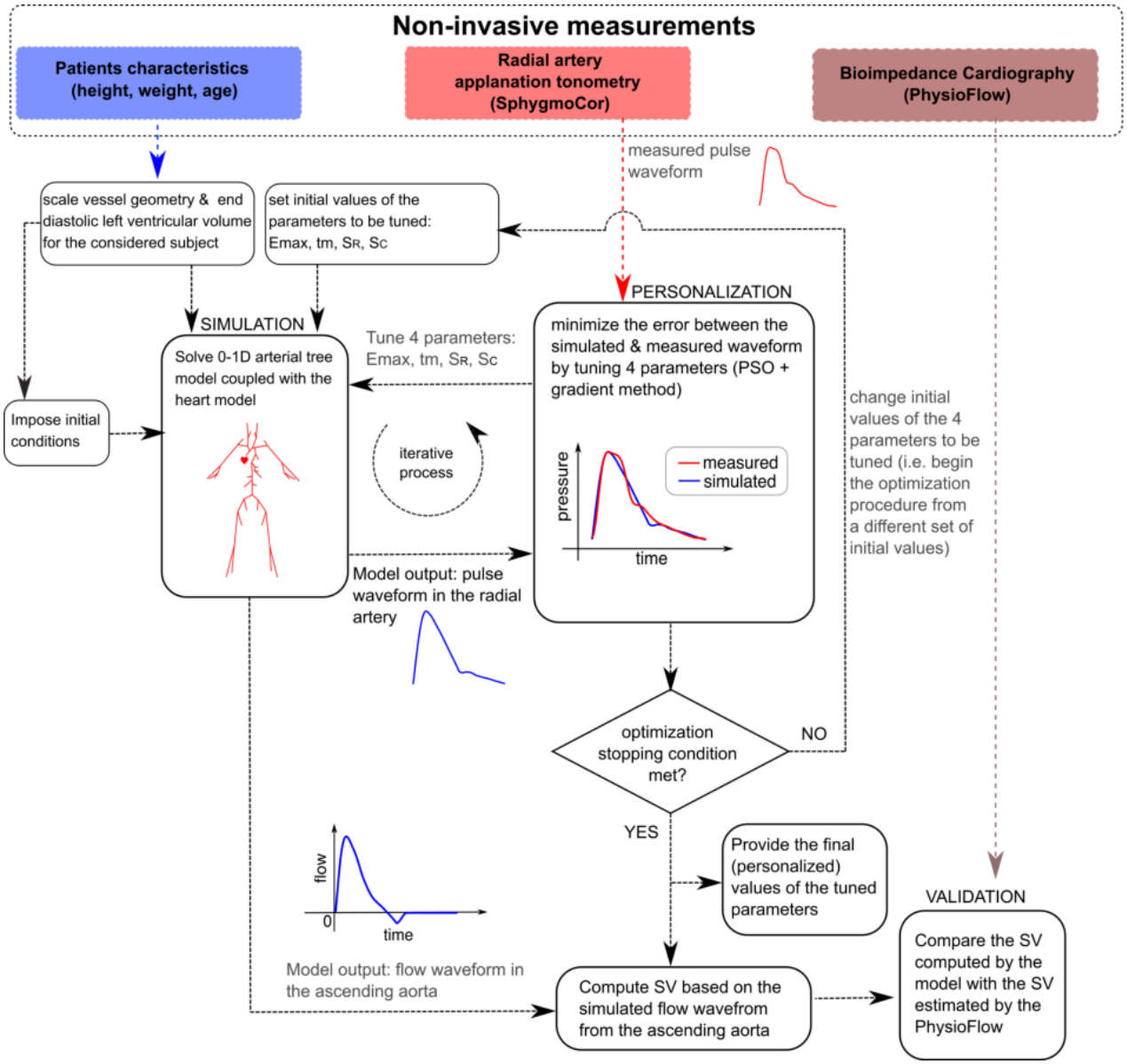

Fig 1. Simplified workflow of the study. For each measured pressure waveform, model personalization (calibration) was performed. An iterative optimization procedure was employed to tune the values of parameters describing the function of the heart (i.e. E_{max}–maximal value of the elastance function, and t_m–time to the onset of constant elastance) as well as terminal compliances and resistances (S_c and S_R, respectively) that would minimize the error between the measured and simulated pressure waveform in the radial artery. After model personalization, the model-simulated blood flow waveform in the ascending aorta was used to estimate stroke volume (SV). Finally, model-estimated and reference SV values have been compared.

https://doi.org/10.1371/journal.pcbi.1012013.g001

performed after a short, 2-day break (3.8% vs. 4.2%; difference not significant), see Fig 3b. The worst (highest) MAPE values were obtained for the measurements conducted after the end of HD (average 4.9% for all HD sessions, 4.4% for the sessions after the long interdialytic break, and 5.5% for the sessions after the short interdialytic break; difference not significant).

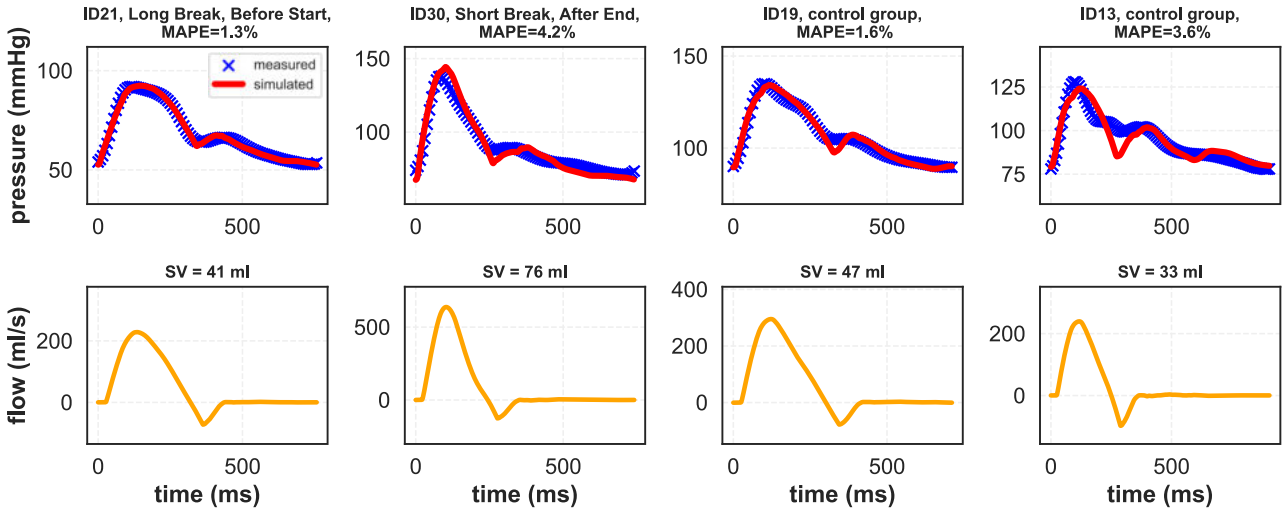

Fig 2. Exemplary model simulations of the pressure waveform in the radial artery (upper panels) and the corresponding blood flow waveform in the ascending aorta (lower panels) in four subjects: Two HD patients and two subjects from the control group.

https://doi.org/10.1371/journal.pcbi.1012013.g002

Stroke volume estimation

For the control group, the Pearson correlation coefficient between SVs estimated by the bioimpedance cardiograph and those estimated using our model was r = 0.57 (p = 0.032), see the scatter plot in Fig 4a. For HD patients, the correlation coefficient for all measurements was

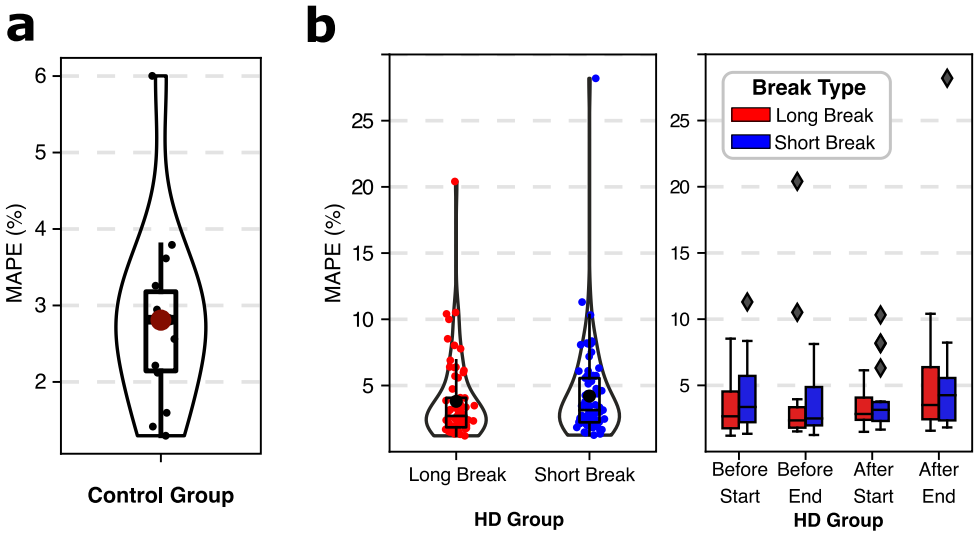

Fig 3. The quality of model fits: Mean absolute percentage error (MAPE) between the measured and model-simulated pressure waveforms in the radial artery for (a) control group and (b) HD patients. For HD patients, the results are divided based on either the length of the interdialytic break before the HD session (a long, 3-day break vs short, 2-day break) or the time of the measurement (before/after the start of the HD session and before/after the end of the session).

https://doi.org/10.1371/journal.pcbi.1012013.g003

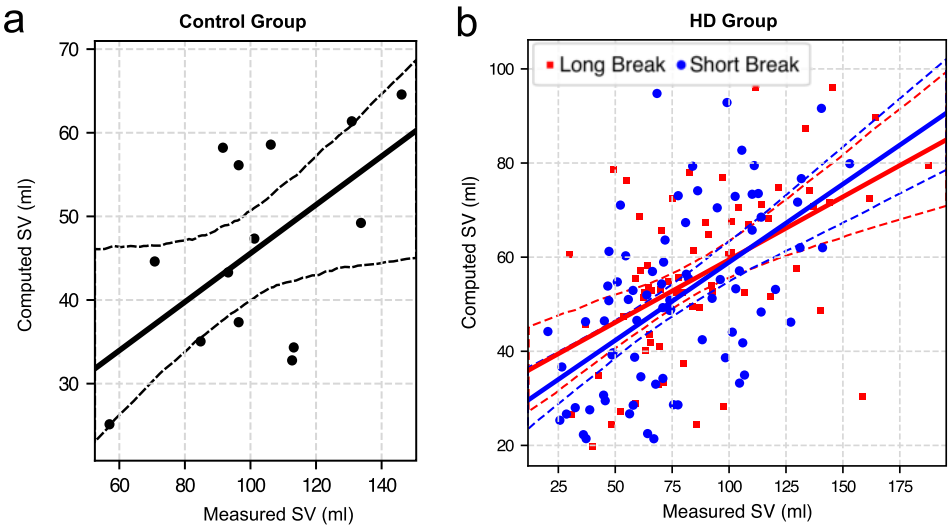

Fig 4. Comparison between the model-estimated (computed) stroke volume (SV) and bioimpedance-based (measured) SV values for (a) control group and (b) HD patients (data shown separately for the HD sessions after a long and short interdialytic break). Solid and dashed lines represent linear regression, and 95% confidence intervals, respectively.

https://doi.org/10.1371/journal.pcbi.1012013.g004

$r = 0.58$ ($p < 0.001$), with $r = 0.56$ and $r = 0.59$ for the measurements performed after the short and long interdialytic break, respectively ($p < 0.001$ in both cases; see Fig 4b for the scatter plots). The correlation coefficients were similar regardless of the time of measurement during the HD session, with the only exception for the measurements performed before the end of HD session after a long interdialytic break, where the correlation was higher ($r = 0.75$, $p < 0.001$), although only after excluding one clear outlier, see S2 Fig.

Fig 5 presents the Bland-Altman plots comparing the model-estimated and bioimpedance-based SV values in both control and HD groups. Since the differences in SV from the two methods were not normally distributed in the HD group (Shapiro-Wilk test statistic: 0.98, $p < 0.05$), a logarithmic transformation of the data was performed [20] (Shapiro-Wilk test statistic: 0.991, $p = 0.52$).

Estimation of cardiovascular parameters

Table 1 presents the average values of the estimated subject-specific parameters and their standard deviations. The first two parameters are related to the elastance heart model of the left ventricle, while the last two describe the properties of the terminal vascular beds, (see also Fig 6 to compare).

Table 2 shows the comparison between the mean values of the cardiovascular parameters estimated in HD patients for the measurements performed after the long vs short interdialytic break. This comparison is shown in two versions: first, for the available data from all four measurement moments during HD, and second, for the measurements taken only before the start of HD (to exclude the impact of the dialysis itself). In both cases, when paired measurements were taken into account, no statistically significant differences were observed with regard to the length of the interdialytic break.

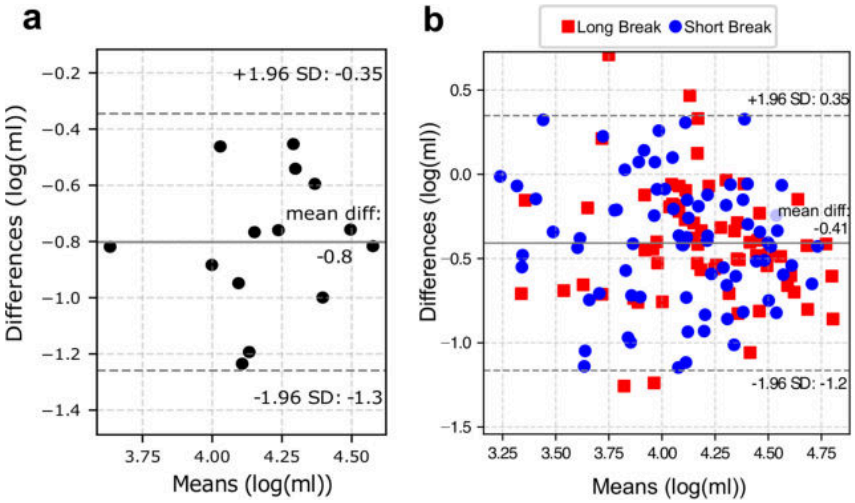

Fig 5. Bland-Altman plots comparing the stroke volume estimated by the model versus estimated using bioimpedance cardiography (PhysioFlow) for (a) control group and (b) hemodialysis patients. Dashed horizontal lines represent the 95% limits of agreement, straight horizontal line represents the mean difference. Before plotting, the data have been logarithmically transformed. SD denotes standard deviation.

https://doi.org/10.1371/journal.pcbi.1012013.g005

Correlations with PWA-derived indices

The SphygmoCor device, which was used for peripheral pressure waveform recordings, performs also the so-called Pulse Wave Analysis (PWA), which is a non-invasive method of assessing the state of the cardiovascular system. The PWA method relies on a generalized transfer function that allows reconstruction of the central pressure waveform from that recorded in the radial artery. Thus, the device also returns parameters characterizing the peripheral and central pressure waveforms, such as the augmentation index. To determine whether the model-estimated SV and the cardiovascular parameters tuned in our model fitting procedure are somehow related to the indices derived by SphygmoCor and the general patient characteristics (age, height, weight), we calculated the Pearson correlation coefficients between those values and presented them in the form of a heatmap, see Fig 7.

Discussion

We presented a model-based methodology for estimating SV based on the pressure waveform recorded in the radial artery. We observed a moderate correlation between the SV estimated by our model and that obtained from bioimpedance cardiography in both healthy subjects and

Table 1. Summary of the estimated patient-specific values of the model parameters for hemodialysis (HD) patients and control group. The data are shown as means and standard deviations (SD).

Parameter		Unit	HD patients		Control group	
			Mean	SD	Mean	SD
E_{max}	Maximal systolic value of elastance function	mmHg/ml	3.13	1.27	2.56	1.06
t_m	Time to the onset of constant elastance	s	0.57	0.09	0.56	0.05
S_R	Scaling factor of terminal resistances	-	1.66	0.71	2.02	0.75
S_c	Scaling factor of terminal compliances	-	10.18	4.34	11.89	4.39

https://doi.org/10.1371/journal.pcbi.1012013.t001

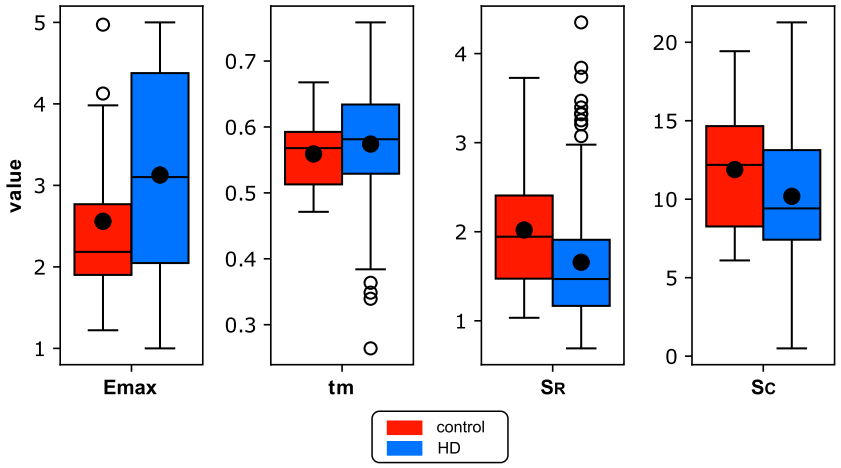

Fig 6. Box-plots for the estimated cardiovascular parameters in the hemodialysis (HD) and control groups. The description of parameters and their units are provided in Table 1.

https://doi.org/10.1371/journal.pcbi.1012013.g006

HD patients (Pearson correlation coefficient of around 0.6). However, our model-based estimates of SV were generally lower than those obtained from bioimpedance cardiography, which may be either due to the limitations of our model or due to imperfectly recorded peripheral pressure waveforms to which our model was fitted, or due to inaccuracy of the reference (bioimpedance-based) SV values (or a combination of the above). For instance, in some cases PhysioFlow provided SV values that could be considered unrealistic (e.g., values over 150 ml, see Fig 4b and S2 Fig). The model, on the other hand, operates on physiological parameters, such as the maximum left-ventricular volume (properly scaled for the given patient), and thus is unable to provide such unrealistically high values of SV. Nevertheless, ignoring the cases with questionable reference data (SV over 150 ml) did not significantly affect the correlation coefficients.

PhysioFlow employs neck and chest electrodes to measure changes of the thorax impedance induced by pulsatile blood flow generated by the heart, thus enabling the estimation of SV. Compared to the well-established echocardiography, bioimpedance cardiography is less

Table 2. Summary of the estimated values of the cardiovascular parameters in hemodialysis (HD) patients depending on the length of the interdialytic break before the studied HD session (a long, 3-day break vs a short, 2-day break). The data are presented as means (± standard deviation).

Parameter	Unit	All measurement moments[1]		Before Start[2]	
		long break	short break	long break	short break
E_{max}	mmHg/ml	2.99±1.13	2.89±1.24	3.43±1.06	3.44±1.24
t_m	s	0.58±0.09	0.58±0.09	0.58±0.06	0.58±0.08
S_R	-	1.57±0.65	1.77±0.75	1.51±0.50	1.71±0.91
S_c	-	10.93±4.70	10.49±3.99	11.82±4.17	11.41±4.66

[1)] the results combine data from all moments of measurements, i.e. before and after the start of the HD session and before and after the end of the session, but limited to cases for which the data for the given patient and the given moment of measurement was available for both HD sessions (i.e. paired data only)

[2)] the results refer to measurements performed before the start of the HD session but limited to cases for which the data for the given patient was available for both HD sessions (i.e. paired data only)

https://doi.org/10.1371/journal.pcbi.1012013.t002

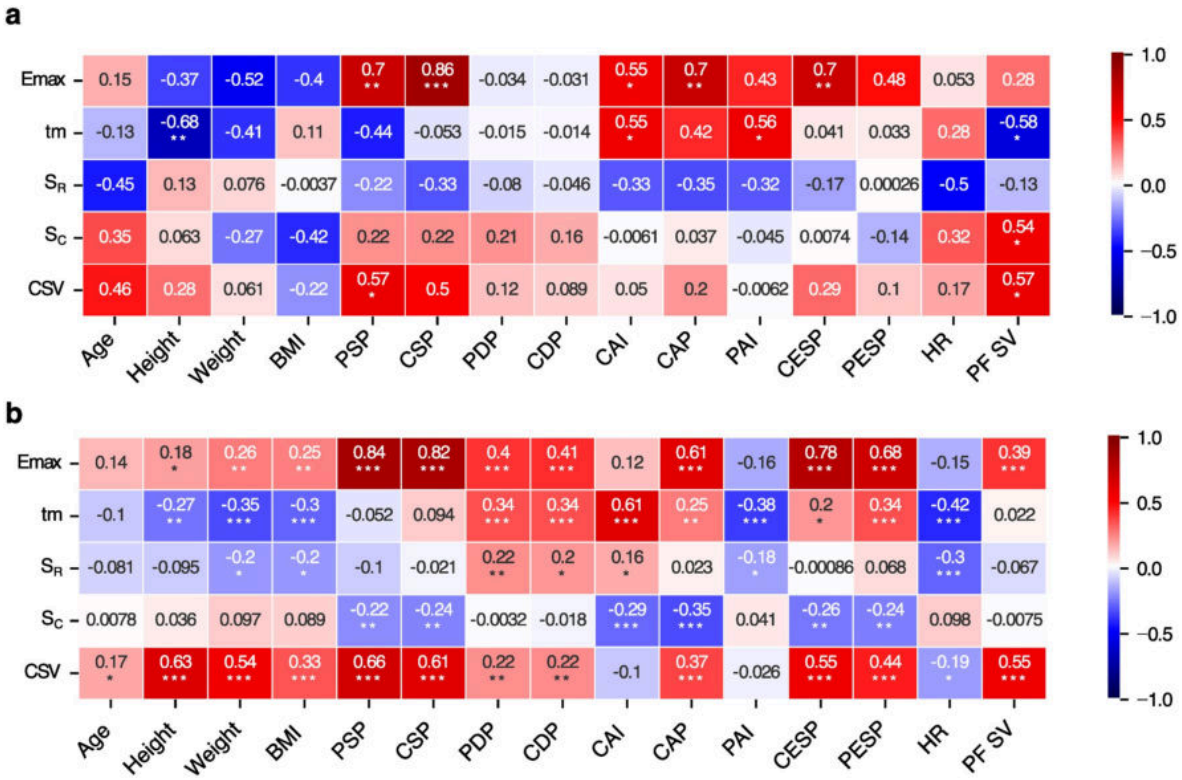

Fig 7. Correlation matrix between the parameters estimated by the model (Y axis) and cardiovascular parameters or indices derived by SphygmoCor (X axis) for (a) control group of healthy subjects and (b) hemodialysis patients, * $p < 0.05$, ** $p < 0.01$, *** $p < 0.001$. CSV–computed stroke volume, BMI–body mass index, PSP–peripheral systolic pressure, CSP–central systolic pressure, PDP–peripheral diastolic pressure, CDP–central diastolic pressure, CAI–central augmentation index, CAP–central augmentation pressure, PAI–peripheral augmentation index, CESP–central end-systolic pressure, PESP–peripheral end-systolic pressure, PF SV–stroke volume estimated by PhysioFlow.

https://doi.org/10.1371/journal.pcbi.1012013.g007

demanding when cardiovascular parameters need to be evaluated multiple times during an HD session [21]. Echocardiography, which uses ultrasound waves to obtain images of the heart structure and function must be operated by a qualified clinician. Given that in our study for each HD session we needed four reference measurements (estimations) of SV performed over the span of approximately 4 hours, we decided, therefore, to use PhysioFlow, which did not require qualified personnel and hence was much easier and cheaper (the electrodes were attached to the patient before the HD session and were kept on for the whole session). A disadvantage of this approach is the aforementioned possible inaccuracy of bioimpedance cardiography in estimating SV–even though some studies report good accuracy of this method, including in HD patients, both at the beginning and at the end of HD [21,22], there are also studies that questioned it in certain groups of patients, such as anemic or pediatric patients [23,24].

The Bland-Altman analysis presented in Fig 5 showed that there was no relation between the differences and the means of the logarithmically transformed SVs obtained from the model and PhysioFlow. For HD patients, the mean difference of the log-transformed SVs was -0.41. The antilog of this difference gives a dimensionless ratio of 0.66, with the relatively wide 95% limits of agreement equal to 0.30 and 1.42. Thus, the model-based estimates of SV were,

on average, 34% lower than the bioimpedance-based values from PhysioFlow, with approximately 95% of results being up to 42% higher and up to 70% lower than the reference values.

Bikia et al. used a similar model but with a more advanced arterial bifurcation tree to estimate the cardiac output (CO) and central systolic blood pressure, based on brachial systolic and diastolic pressure (brSP, brDP) and carotid-to-femoral pulse wave velocity (cf-PWV) [11]. Their approach is based on the assumption that the parameters describing arterial compliance, total peripheral resistance, and maximal blood flow from the left ventricle may be unambiguously estimated from brSP, brDP, and cf-PWV. When they adjusted their model to match brSP, brDP and cf-PWV obtained with SphygmoCor, they achieved a relatively high correlation between the model-estimated CO and the reference CO obtained using 2–D transthoracic echocardiography (r = 0.73), although they studied healthy subjects only (n = 20).

Since HD patients have a very high rate of cardiovascular morbidity and mortality [2,25], similar research in these patients is of utmost importance. Therefore, in our study, we sought to investigate whether a model-based estimation of SV is possible when based on data from HD patients, whose hemodynamics may be impaired due to both CKD and HD treatment. The main difference between our approach and that of Bikia et al. [11], is that we used the entire shape of the peripheral pressure waveform measured by SphygmoCor to inform the model. To our knowledge, no such study has been conducted to date.

The factors leading to the increased incidence of CVD in HD patients are complex and not fully understood [26]. Mathematical models may help explain these relationships. Subject-specific models can allow for an in-depth analysis of the physiological state of the patient using only non-invasive diagnostic tools. In particular, non-invasive estimation of stroke volume or left-ventricular end-systolic elastance, E_{max}, can provide useful information about the condition of the heart. The scaling factor S_R, in turn, may shed some light on the level of peripheral resistance, which is mainly influenced by the resistance of small arteries and arterioles. Tracking changes in the aforementioned parameters for a given patient could help in the early detection of CVD or in the monitoring of CVD progression, and hence it could improve treatment outcomes.

The analysis of correlations between parameters obtained from our model and those derived by SphygmoCor showed that, for both HD and control groups, there was a significant correlation between the maximal (end-systolic) elastance (E_{max}) and systolic pressure (both central and peripheral) and between E_{max} and the end-systolic pressure estimated for the central pressure waveform. E_{max} is generally load-independent (just a little dependent on the arterial load) and is determined by cardiac muscle contractility and ventricular wall mass [27]. It is often approximated by the slope of the line connecting the top-left corners of the cardiac pressure-volume loops [27]. In some studies, the authors underlie that this relation is more curved than straight, which suggests that E_{max} may be dependent on the pressure and volume of the left ventricle [28,29]. This in turn may explain the correlation that we observed between the end-systolic elastance and systolic pressure. Interestingly, in HD patients we observed a moderate correlation between E_{max} and diastolic pressure (both central and peripheral) that was not present in the control group. Moreover, we observed a low positive correlation of E_{max} with weight, height or BMI in HD patients, and no such correlations in the control group.

Limitations

Mathematical modeling of complex systems, such as the cardiovascular system, typically involves many simplifications and thus limitations. In our previous study, we have mentioned the possible limitation related to the fact that our model does not account for the presence of an arteriovenous fistula, which may influence the model-derived parameters [19]. Another

limitation is related to the selection of parameters tuned in the optimization procedure, while leaving other parameters fixed. Moreover, in our model, we consider only the work of the left ventricle, with the pressure in the left atrium fixed at a constant level, which makes it impossible to take into account the Frank-Starling mechanism. Furthermore, an important limitation of our study is the possibly low reliability of some of the reference SV values obtained with PhysioFlow in HD patients. Transthoracic bioimpedance methods are cheap, non-invasive, and relatively easy to use. However, some studies challenge the accuracy of PhysioFlow, e.g., in patients with chronic anemia [23] or pediatric patients [24]. To properly validate our model, future studies should ideally use gold-standard invasive methods for SV estimation, such as the direct Fick method. Also, a more in-depth sensitivity and identifiability analysis should be performed to potentially improve the selection of parameters to estimate.

Materials and methods

Ethics statement

The study was approved by the Bioethical Committee at the Medical University of Lublin (Poland), and informed verbal consent has been obtained from all subjects. Our study was performed in accordance with the Declaration of Helsinki and all applicable regulations.

Study subjects

We studied two groups: 1) the control group consisting of 14 healthy subjects, 2) the HD group, consisting of 35 anuric, prevalent hemodialysis patients, i.e. patients with end-stage renal disease, monitored during two standard HD sessions: after a long (3-day) and a short (2-day) interdialytic break, i.e. the time since the previous HD session. All HD patients had arteriovenous fistulas. None of the patients were diagnosed with CVD at the time of the study. For more detailed information on the studied HD patients, please see our previous work [19] and Table 3.

Measurements

The pressure wave measurements were performed by one trained clinician (on the non-fistula arms in HD patients) using applanation tonometry (SphygmoCor, AtCor Medical, Australia). The results were calibrated with the systolic and diastolic blood pressure measured oscillometrically at the brachial artery (Omron M3, Omron Healthcare, Kyoto, Japan). Based on the "operator index" of the SphygmoCor device, we excluded from the analysis all low-quality recordings (according to the manufacturer's user manual, the results are acceptable when the operator index is ≥ 80).

Table 3. Characteristics of the study subjects. Data are reported as means ± standard deviation. The data reported for hemodialysis (HD) patients were assessed after the mid-week HD hemodialysis session.

	Unit	HD patients	Controls
		N = 35	N = 14
Gender	% (male)	43	43
Age	years	61.2 ± 14.3	45.3 ± 12.0***
Height	cm	167.9 ± 9.4	171.2 ± 6.8
Weight	kg	72.2 ± 19.9	77.4 ± 13.2
Ethnic origin	% (white Caucasian)	100	100

*** $p < 0.001$; Mann-Whitney test

https://doi.org/10.1371/journal.pcbi.1012013.t003

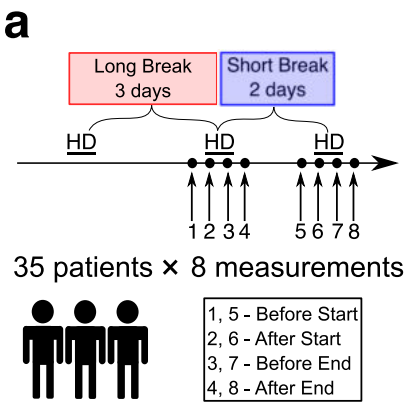

Fig 8. Graphical summary of the timeline of measurements in HD patients. Measurements of the pulse wave in the radial artery were performed in 35 HD patients at 4 time points during two HD sessions (after a long and a short interdialytic break). In the control group the measurements were performed at one time only.

https://doi.org/10.1371/journal.pcbi.1012013.g008

For each subject from the control group, one to three measurements were taken, and the measurement with the best operator index was selected for further analysis. For the HD group, in each patient, 8 recordings of the pressure waveform in the radial artery were performed. The waves were recorded about 15 minutes before the start, after the start, before the end and after the end of two HD sessions, and took about 2 minutes each, see Fig 8. In 18 patients, the measurements were performed in the morning (HD starting around 7 AM), 13 patients had the measurements taken during the midday session (HD starting around 12PM), and the remaining 4 patients were measured in the evening sessions (HD starting around 6 PM). For a given patient, both studied HD sessions (i.e. after the long and the short interdialytic break) were performed at the same time of day.

The measurements of SV were performed using a non-invasive impedance cardiograph (PhysioFlow, Manatec Biomedical, France), according to the manufacturer's protocol. The measurements were taken simultaneously with the pulse wave recordings. The quality of the obtained data was evaluated based on the "signal quality" index recorded by the device during the measurement procedure. Each bioimpedance measurement took about 2 minutes. We averaged the SVs obtained during this time, after excluding all measurements with the signal quality index not exceeding 90 on a scale from 1 to 100. According to the manufacturer, the respiratory component of the chest impedance signal is filtered out and should not affect SV estimation [30]. More detailed description of the measurement methodology can be found in [31] During all measurements the patients were lying motionless in the supine position.

The data for HD patients were divided according to the duration of the interdialytic break (a short vs long break, i.e. a two-day vs three-day break since the previous HD session), and by the moment of measurement (before the start, after the start, before the end, and after the end of the HD session), see S3 Fig.

Analyzing measurements performed at different times during moments of dialysis treatment is justified by hemodynamic changes occurring during HD. Initiating an HD session typically leads to a decrease in arterial blood pressure and workload on the heart. This is attributed to the reduction in the volume of blood in the body, as part of it is redirected to fill the extracorporeal tubing and the dialyzer (assuming that the priming fluid is discarded and not infused to the patient). Typically, all further reductions in blood volume due to removal of

the excess fluid in the dialyzer, result in additional reduction in the ventricular afterload, until a relatively steady state is achieved towards the end of the session (assuming no hypotensive or hypertensive episodes). The final phase of a dialysis session involves the return of blood from the extracorporeal circuit to the body, which increases the intra-body blood volume, having the opposite effects on the heart and pulse wave compared to the pre-dialysis procedure [19].

The duration of the interdialytic break, on the other hand, may be related to the level of cardiovascular risk–the longer the break, the higher the risk, which may be due to greater changes in fluid and electrolyte balance, acidity levels, or arterial wall parameters [32]. Given the ongoing debate on the mechanisms behind increased cardiac mortality rates following a three-day interval break [32], it seems desirable to investigate how cardiovascular parameters correlate with the duration of the interdialytic break.

The cardiovascular model

We propose a one-dimensional bifurcation arterial tree model consisting of 55 compliant arteries coupled with zero-dimensional boundary conditions representing the downstream vessels. The bifurcation tree represents the most important arteries in the human body and has been frequently used to analyze the hemodynamics of the human cardiovascular system [10,14,16,33]. We assumed that blood is an incompressible, Newtonian fluid, flowing with a parabolic velocity profile through axisymmetric elastic cylinders that taper along their length. The equations describing the blood flow and pressure were derived by integrating the incompressible longitudinal components of the Navier-Stokes equations over the vessel cross-sectional area. To close the system and ensure the uniqueness of the solution, we included the following state equation:

$$P(x,t) - P_0 = f(x)\left(1 - \frac{A_0(x,t)}{A(x,t)}\right) \tag{1}$$

which relates the blood pressure P (at distance x and at time t) to the cross-sectional area A of the vessel (A_0 is the cross-sectional area of the vessel at the nominal pressure P_0). In the below equation, we define the elasticity function of the arteries analogously to how it was done by Olufsen et. al. [16],

$$f(x) = \frac{4}{3}(k_1 + exp\,(-k_2 r_0(x)) + k_3), \tag{2}$$

where parameters k_i are global, i.e., the same for each artery and

$$r_0(x) = r_{in}\left(\frac{r_{out}}{r_{in}}\right)^{x/L}, \tag{3}$$

describes the vessel's tapering at the nominal pressure P_0 with r_{in}, r_{out} being the proximal and distal radii of the artery, and L–the length of the artery. At the distal ends, as an outflow boundary condition, we consider the 3-element Windkessel model, which may be expressed by the following formula describing the relation between the terminal flow Q_{end} and pressure P_{end} [34],

$$R_1 R_2 C_T \frac{dQ_{end}(t)}{dt} = R_2 C_T \frac{dP_{end}(t)}{dt} + (P_{end}(t) - P_T) - (R_1 + R_2) Q_{end}(t), \tag{4}$$

where, R_1, R_2 are the proximal and distal resistances, respectively, C_T is the total compliance of the terminal vascular branch, P_T is the reference terminal pressure. It was assumed, that $R_1/R_T = 0.2$ [35], where R_T is the total resistance of the terminal vascular branch ($R_1 + R_2 = R_T$,). The

values of R_T, C_T were taken from [36]. The 3-element Windkessel model is directly connected to the 1D model using the "ghostpoint" method, described in [9,37].

We assume that there are no blood leakages or energy losses at the vessel junctions, which are all characterized by mass conservation and pressure continuity equations:

$$Q_{end,p} = Q_{in,d_1} + Q_{in,d_2}, \text{ and } P_{end,p} = P_{in,d_1} = P_{in,d_2}, \tag{5}$$

where p denotes the parent vessel and d_1, d_2 are the daughter vessels. In reality, there may be some loss of energy at the bifurcations due to the formation of vortices. However, it was shown that assuming pressure continuity is a good approximation for the considered system [15,16,38].

In our previous study, we used a phenomenological inflow boundary condition to describe the work of the heart, as previously proposed by Olufsen [36]. In the present study, to validate the model-based estimations of stroke volume (SV), we decided to use a more accurate description of the aortic inflow based on the elastance function of the left ventricle [39]. For simplicity, we decided not to modify our model of the cardiovascular system by including the arteriovenous (AV) fistula for HD patients. As shown in our previous work, the pulse wave analysis (PWA) is not significantly affected by the presence of an AV fistula, which has only a little effect on the radial-to-aortic transfer function [19].

Because we do not model the venous return to the heart, it is sufficient for the inflow boundary condition to consider only the left-ventricular function. According to the work of Suga et.al. [40] and Danielsen and Ottesen [39], the relation between the pressure in the left ventricle P_{lv} and ventricular volume V_{lv} may be described by the following equation:

$$P_{lv} = E_{lv}(t)(V_{lv} - V_0) \tag{6}$$

where V_0 is the volume of the left ventricle at the zero transmural pressure and $E_{lv}(t)$ is a time-varying elastance function of the left ventricle, which can be approximated by the following formula

$$E_{lv}(t) = E_{min}(1 - \phi(t)) + E_{max}\phi(t) \tag{7}$$

where

$$\phi(t) = \begin{cases} a \sin\left(\frac{\pi t}{t_m}\right) - b \sin\left(\frac{2\pi t}{t_m}\right) & \text{for } 0 \leq t < t_m \\ 0 & \text{for } t_m \leq t < T \end{cases}. \tag{8}$$

The parameters E_{max} and E_{min} are the maximal (systolic) and minimal (diastolic) values of the elastance function, T denotes the heart period, and t_m–the time until the onset of constant (minimal) elastance. The parameters a and b describe the shape of E_{lv} function, see S4 Fig for an exemplary plot of the elastance function.

During the isovolumic relaxation phase, both valves in the left ventricle are closed. The pressure in the left ventricle P_{lv} decreases according to the formula (6), until it is lower than the pressure in the left atrium (P_{la}, constant in our model), that is when the mitral valve opens and the ventricular filling begins. The flow between the left atrium and left ventricle Q_{la} is described as follows:

$$\frac{dQ_{la}}{dt} = \frac{1}{L_{la}}(P_{la} - P_{lv}) - \frac{R_{la}}{L_{la}}Q_{la}, \tag{9}$$

where L_{la} is an inertia term and R_{la} denotes ventricular filling resistance caused mainly by the

viscous properties of the blood. Simultaneously, the volume of the left ventricle increases, according to the formula

$$\frac{dV_{lv}}{dt} = Q_{la}. \tag{10}$$

Once the volume V_{lv} is greater than the maximal volume of the left ventricle, the mitral valve closes (which implies that Q_{la} returns to 0) and the isovolumic contraction begins.

During this phase, both the mitral and aortic valves are closed and the ventricle contracts, which implies that the pressure in the left ventricle increases. When $P_{lv} > P_a$, where P_a is the root aortic pressure, the aortic valve opens, and the heart starts to eject blood into the ascending aorta. The flux between the left ventricle and aorta, Q_{lv}, is given by a formula similar to (9),

$$\frac{dQ_{lv}}{dt} = \frac{1}{L_{lv}}(P_{lv} - P_a) - \frac{R_{lv}}{L_{lv}}Q_{lv}, \tag{11}$$

where P_a is taken directly from the 1D model of the arterial tree. Concurrently, the volume V_{lv} decreases:

$$\frac{dV_{lv}}{dt} = -Q_{lv}. \tag{12}$$

During the aortic valve closure (which begins at time t*), some blood flows back to the left ventricle (negative Q_{lv}). We allow for a certain volume of the backflow $\overline{V_b}$, before the complete closure of the aortic valve. When the backflow volume V_b given by

$$V_b = \int_{t^*}^{t} |Q_{lv}|, \quad t > t^* \tag{13}$$

exceeds $\overline{V_b}$, the aortic valve closes, which implies that $Q_{lv} = 0$, and the cycle repeats.

The above equations and conditions fully describe the blood flow in the modelled system. The governing equations of the blood flow in the 1D domain were solved using the Lax-Wendroff scheme [41]. The inflow and outflow boundary conditions were connected to the 1D model using the "ghost point" method [9,37]. The inflow boundary condition was solved iteratively, i.e. after solving the equations of the 1D model, the elastance model of the left ventricle used the computed pressure, P_a, from the root of the ascending aorta. Then, using the Runge-Kutta scheme, Eqs (6)–(12) were solved. At this point, we had information about the outflow from the left ventricle and the cross-sectional area at the root of the ascending aorta. In the same iterative step, using the explicit Euler method, we solve Eq (4) characterizing the outflow boundary conditions.

Parameter estimation procedure

The bifurcation tree we use describes the vascular system for a 175 cm tall man. To personalize the vascular domain for a given subject, we multiply the lengths of all arteries, along with their proximal and distal lumen radii by the scaling factor S defined as the ratio of the subject height to the default height of 175 cm. Because the values of the resistances and compliances of the terminal branches depend on, among others, the size of the vessels, we also scale their default values by $1/S^3$ and S^3 respectively, similarly as done in our previous studies [10,19]. The parameters k_1, k_2 and k_3, which describe the stiffness of arteries were taken from the work of Olufsen [36]. The distending pressure P_0 from the Eq (1) was set at the level of 97 mmHg [15]. In the elastance model of the left ventricle [23] the initial end-systolic left ventricular volume, V_{lv}, was set to 120 ml and then scaled by S^3. In a similar manner we scaled the volume of the left ventricle at zero pressure, V_o with the default value of 15 ml. The values of the heart

resistances and inertances, (R_{lv}, R_{la}, L_{lv}, L_{la}) as well as the values describing the shape of the elastance function (a, b, E_{min}) and the assumed volume of the backflow, $\bar{V}_b$, were taken from [39] or assumed. All aforementioned parameters remain constant in our model, and their values can be found in the S2 File.

Parameter estimation was carried out in two steps. In the first step, we used the meta-heuristic Particle Swarm Optimization (PSO) method [42]. The optimization started with 15 particles (a swarm), each representing a different combination of the values of the four patient-specific parameters being estimated. Then, these particles iteratively explored the search space to find a near-optimal solution (i.e., to minimize the error function). In our case, we set up 10 iterations, during which, in simple terms, the position of each particle was modified based on its own best previous position and based on the best previous position within the whole swarm, looking for the global minimum of the error function. In the second step, the best set of parameter values obtained with PSO served as the starting point for the gradient-based algorithm (GBA) [43,44], complementing and refining the previous optimization method.

The following parameters were estimated: the scaling factor of terminal resistances S_R, the scaling factor of terminal compliances, S_C, maximal systolic elastance, E_{max}, and t_m denoting the time to the onset of constant elastance. The rationale behind the choice of these parameters is presented in the S2 File.

The model fitting procedure was analogous to the one used in our previous studies [10,19] but with a different error function. We defined the objective function as the sum of squares of differences between the parameters of the Fourier series expansion of the measured and model-simulated pressure waveforms. More precisely, for each measured and simulated pressure waveform in the radial artery, we approximated the first six parameters of the following sine-cosine Fourier series expansion, thus obtaining the following time-dependent signals:

$$signal \approx \frac{a_0}{2} + \sum_{i=1}^{6} \left[a_n \, cos \frac{2\pi t}{T} + b_n \, sin \frac{2\pi t}{T} \right], \tag{14}$$

where T is the heart period, and then for each case we defined the following 13-element vectors:

$$c = [a_0, a_1, \ldots, a_6, b_1, \ldots, b_6]. \tag{15}$$

The error function was defined as follows:

$$err = \sum_{i=1}^{13} \left(c_{s,i} - c_{m,i} \right)^2, \tag{16}$$

where subscripts s and m denote simulation and measurement, respectively. The optimization procedure involved minimizing that error by changing the values of the four selected model parameters. A simplified workflow of the study is presented in Fig 1. The number of analyzed harmonics has been chosen arbitrarily and represents a compromise between the accuracy of the pulse wave representation and the complexity of the objective function; S5 Fig presents some examples of Fourier-transformed pressure waveforms for healthy subjects and HD patients.

Statistical methods

Statistical dependence between *in vivo* data and the model-estimated parameters was measured using Pearson correlation coefficient (r). Statistical differences between the paired data were investigated using the Wilcoxon signed-rank test. Statistical significance was set at the level of p = 0.05. To verify normal distribution of differences between the measured and

estimated SV, the Shapiro-Wilk test was performed. The accuracy of model-simulated pressure waveforms (with respect to the recorded waveforms) was assessed by mean absolute percentage error (MAPE). The regression lines were plotted with 95% confidence intervals.

Conclusions

We investigated the feasibility of using a patient-calibrated 0-1D model of the systemic circulation to estimate SV. The preliminary validation of the model in a group of 35 HD patients and a control group of 14 healthy subjects showed that the model was able to reproduce the pressure waveforms recorded non-invasively in the radial artery with satisfactory accuracy in most cases and that the model-based estimates of SV are correlated with the reference bioimpedance-based SV estimates. However, the model seems to underestimate SV in both HD patients and healthy subjects. This may be at least partly an apparent result, given the possible inaccuracy of the reference bioimpedance measurements. If more accurate reference measurements confirm that the model does, indeed, underestimate SV, this could be due to: 1) limitations of our model, 2) too few fitted parameters of the model, or 3) a combination of the above factors. To fully and properly validate the model, a larger study should be conducted with a more accurate, gold-standard reference method for estimating SV, possibly with a larger number of model parameters to be fitted, selected after a more in-depth sensitivity and identifiability analysis.

Supporting information

S1 File. Supporting materials. The file presents simulated vs measured pressure waveforms in the radial artery.
(PDF)

S2 File. Supporting materials. The file presents the rationale behind the choice of model parameters to be fitted, a sensitivity analysis, as well as justification that the selected parameters uniquely determine the pulse wave.
(PDF)

S1 Fig. Exemplary outputs from the model at various locations of the arterial tree. The presented model outputs (i.e. blood pressure and flow rate waveforms) were obtained using the baseline values of all model parameters (see S1 supplementary materials), for a 175 cm man with a heart rate of 75 bpm.
(PNG)

S2 Fig. (a) Pearson correlation coefficients between the model-estimated (computed) SV and the SV measured using bioimpedance cardiography for HD patients (additionally divided into groups of measurements depending on the duration of the interdialytic break before the studied HD session and the moment of measurement during the HD session). (b) Scatter plots of model-estimated (computed) and bioimpedance-based SV values for HD patients corresponding to different moments of measurement. Correlations were computed after removing the outlier from the Before End group.
(PNG)

S3 Fig. Sankey diagram of the study dataset collected in HD patients. 136 cases were excluded from the analysis due to missing or clearly erroneous data or due to low quality of the recorded applanation tonometry or bioimpedance signals in accordance with the manufacturer's instructions (SphygmoCor "Operator index" < 80 or PhysioFlow "Signal Quality" < 90). The remaining cases were divided according to the length of the interdialytic break before

the studied HD session (a short, 2-day break vs a long, 3-day break) and according to the time of measurement during the HD session (before start, after start, before end and after end of the HD).
(PNG)

S4 Fig. Left-ventricular elastance function according to Eqs (7) and (8). E_{max}–maximal systolic elastance, E_{min}–minimal (diastolic) elastance, T–heart period, and t_m–time to the onset of constant (minimal) elastance.
(PNG)

S5 Fig. Exemplary pressure waveforms recorded in the radial artery by SphygmoCor along with their transformations into Fourier series with 6 harmonics. Results are presented for two healthy subjects and two HD patients and normalized against time, T–heart period.
(PNG)

Author Contributions

Conceptualization: Kamil Wołos, Jan Poleszczuk.

Data curation: Wojciech Dabrowski, Dorota Siwicka-Gieroba.

Formal analysis: Kamil Wołos.

Funding acquisition: Malgorzata Debowska, Wojciech Dabrowski, Dorota Siwicka-Gieroba, Jan Poleszczuk.

Investigation: Kamil Wołos.

Methodology: Kamil Wołos, Malgorzata Debowska, Wojciech Dabrowski, Jan Poleszczuk.

Project administration: Kamil Wołos, Jan Poleszczuk.

Resources: Dorota Siwicka-Gieroba, Jan Poleszczuk.

Software: Kamil Wołos.

Supervision: Leszek Pstras, Jan Poleszczuk.

Validation: Kamil Wołos, Leszek Pstras, Jan Poleszczuk.

Visualization: Kamil Wołos.

Writing – original draft: Kamil Wołos.

Writing – review & editing: Leszek Pstras, Malgorzata Debowska, Jan Poleszczuk.

References

1. Kalantar-Zadeh K, Jafar TH, Nitsch D, Neuen BL, Perkovic V. Chronic kidney disease. The Lancet [Internet]. 2021 Aug 28 [cited 2024 Jan 9]; 398(10302):786–802. Available from: http://www.thelancet.com/article/S0140673621005195/fulltext
2. Jankowski J, Floege J, Fliser D, Böhm M, Marx N. Cardiovascular Disease in Chronic Kidney Disease. Circulation [Internet]. 2021 Mar 16 [cited 2022 May 4]; 143:1157–72. Available from: https://www.ahajournals.org/doi/abs/10.1161/CIRCULATIONAHA.120.050686
3. Hill NR, Fatoba ST, Oke JL, Hirst JA, O'Callaghan CA, Lasserson DS, et al. Global Prevalence of Chronic Kidney Disease–A Systematic Review and Meta-Analysis. PLoS One [Internet]. 2016 Jul 1 [cited 2022 May 4]; 11(7):e0158765. Available from: https://journals.plos.org/plosone/article?id=10.1371/journal.pone.0158765 PMID: 27383068
4. Damman K, Voors AA, Navis G, Van Veldhuisen DJ, Hillege HL. The Cardiorenal Syndrome in Heart Failure. Prog Cardiovasc Dis. 2011 Sep 1; 54(2):144–53. https://doi.org/10.1016/j.pcad.2011.01.003 PMID: 21875513

5. Damman K, Voors AA, Navis G, Van Veldhuisen DJ, Hillege HL. The Cardiorenal Syndrome in Heart Failure. Prog Cardiovasc Dis. 2011 Sep 1; 54(2):144–53. https://doi.org/10.1016/j.pcad.2011.01.003 PMID: 21875513
6. Szlagor M, Dybiec J, Młynarska E, Rysz J, Franczyk B. Chronic Kidney Disease as a Comorbidity in Heart Failure. International Journal of Molecular Sciences 2023, Vol 24, Page 2988 [Internet]. 2023 Feb 3 [cited 2024 Jan 9];24(3):2988. Available from: https://www.mdpi.com/1422-0067/24/3/2988/htm https://doi.org/10.3390/ijms24032988 PMID: 36769308
7. Feng Y, Zou Y, Zheng Y, Levin NW, Wang L. The value of non-invasive measurement of cardiac output and total peripheral resistance to categorize significant changes of intradialytic blood pressure: A prospective study. BMC Nephrol [Internet]. 2018 Nov 6 [cited 2024 Feb 13]; 19(1):1–6. Available from: https://bmcnephrol.biomedcentral.com/articles/10.1186/s12882-018-1087-y
8. Bikia V, Papaioannou TG, Pagoulatou S, Rovas G, Oikonomou E, Siasos G, et al. Noninvasive estimation of aortic hemodynamics and cardiac contractility using machine learning. Sci Rep. 2020 Dec 1; 10 (1). https://doi.org/10.1038/s41598-020-72147-8 PMID: 32929108
9. Zhang X, Liu J, Cheng Z, Wu B, Xie J, Zhang L, et al. Personalized 0D-1D multiscale hemodynamic modeling and wave dynamics analysis of cerebral circulation for an elderly patient with dementia. Int J Numer Method Biomed Eng. 2021; https://doi.org/10.1002/cnm.3510 PMID: 34293250
10. Poleszczuk J, Debowska M, Dabrowski W, Wojcik-Zaluska A, Zaluska W, Waniewski J. Subject-specific pulse wave propagation modeling: Towards enhancement of cardiovascular assessment methods. PLoS One. 2018; 13(1):1–17. https://doi.org/10.1371/journal.pone.0190972 PMID: 29324835
11. Bikia V, Pagoulatou S, Trachet B, Soulis D, Protogerou AD, Papaioannou TG, et al. Noninvasive Cardiac Output and Central Systolic Pressure from Cuff-Pressure and Pulse Wave Velocity. IEEE J Biomed Health Inform. 2020; 24(7):1968–81. https://doi.org/10.1109/JBHI.2019.2956604 PMID: 31796418
12. Guala A, Camporeale C, Tosello F, Canuto C, Ridolfi L. Modelling and Subject-Specific Validation of the Heart-Arterial Tree System. Ann Biomed Eng. 2015; 43(1):222–37. https://doi.org/10.1007/s10439-014-1163-9 PMID: 25341958
13. Gray RA, Pathmanathan P. Patient-specific cardiovascular computational modeling: diversity of personalization and challenges. J Cardiovasc Transl Res. 2018 Apr 1; 11(2):80–8. https://doi.org/10.1007/s12265-018-9792-2 PMID: 29512059
14. Zhang X, Wu D, Miao F, Liu H, Li Y. Personalized Hemodynamic Modeling of the Human Cardiovascular System: A Reduced-Order Computing Model. IEEE Trans Biomed Eng. 2020; 67(10):2754–64. https://doi.org/10.1109/TBME.2020.2970244 PMID: 32142412
15. Stergiopulos N, Young DF, Rogge TR. Computer Simulation of Arterial Flow With Applications To Arterial and Aortic Stenoses. J Biomech. 1992; 25(12):1477–88. https://doi.org/10.1016/0021-9290(92)90060-e PMID: 1491023
16. Olufsen MS, Peskin CS, Kim WY, Pedersen EM, Nadim A, Larsen J. Numerical simulation and experimental validation of blood flow in arteries with structured-tree outflow conditions. Ann Biomed Eng. 2000; 28(11):1281–99. https://doi.org/10.1114/1.1326031 PMID: 11212947
17. Reymond P, Merenda F, Perren F, Rü D, Stergiopulos N. Validation of a one-dimensional model of the systemic arterial tree. Am J Physiol Heart Circ Physiol [Internet]. 2009; 297:208–22. Available from: http://www.ajpheart.orgH208 https://doi.org/10.1152/ajpheart.00037.2009 PMID: 19429832
18. Carson J, Warrander L, Johnstone E, van Loon R. Personalising cardiovascular network models in pregnancy: A two-tiered parameter estimation approach. Int J Numer Method Biomed Eng [Internet]. 2021 Nov 1 [cited 2024 Jan 18]; 37(11):e3267. Available from: https://onlinelibrary.wiley.com/doi/full/10.1002/cnm.3267 PMID: 31799783
19. Poleszczuk J, Debowska M, Dabrowski W, Wojcik-Zaluska A, Zaluska W, Waniewski J. Patient-specific pulse wave propagation model identifies cardiovascular risk characteristics in hemodialysis patients. PLoS Comput Biol. 2018; 14(9):1–15. https://doi.org/10.1371/journal.pcbi.1006417 PMID: 30216341
20. Giavarina D. Understanding Bland Altman analysis. Biochem Med (Zagreb) [Internet]. 2015 [cited 2023 Feb 8]; 25(2):141. Available from: /pmc/articles/PMC4470095/ https://doi.org/10.11613/BM.2015.015 PMID: 26110027
21. Germain MJ, Joubert J, O'Grady D, Nathanson BH, Chait Y, Levin NW. Comparison of stroke volume measurements during hemodialysis using bioimpedance cardiography and echocardiography. Hemodialysis International [Internet]. 2018 Apr 1 [cited 2024 Jan 9]; 22(2):201–8. Available from: https://onlinelibrary.wiley.com/doi/full/10.1111/hdi.12589 PMID: 28796425
22. Cybulski G, Strasz A, Niewiadomski W, Gąsiorowska A. Impedance cardiography: Recent advancements. NEW DRUGS AND TECHNOLOGIES IN CARDIOLOGY Cardiology Journal [Internet]. 2012 [cited 2024 Jan 9]; 19(5):550–6. Available from: www.cardiologyjournal.org https://doi.org/10.5603/cj.2012.0104 PMID: 23042327

23. Bogui P, Balayssac-Siransy E, Connes P, Tuo N, Ouattara S, Pichon A, et al. The PhysioFlow Thoracic Impedancemeter Is Not Valid for the Measurements of Cardiac Hemodynamic Parameters in Chronic Anemic Patients. PLoS One. 2013; 8(10). https://doi.org/10.1371/journal.pone.0079086 PMID: 24167637

24. Taylor K, Manlhiot C, McCrindle B, Grosse-Wortmann L, Holtby H. Poor accuracy of noninvasive cardiac output monitoring using bioimpedance cardiography [PhysioFlow®] compared to magnetic resonance imaging in pediatric patients. Anesth Analg [Internet]. 2012 Apr [cited 2024 Jan 9]; 114(4):771–5. Available from: https://journals.lww.com/anesthesia-analgesia/fulltext/2012/04000/poor_accuracy_of_noninvasive_cardiac_output.15.aspx

25. Vanholder R, Massy Z, Argiles A, Spasovski G, Verbeke F, Lameire N, et al. Chronic kidney disease as cause of cardiovascular morbidity and mortality. Nephrology Dialysis Transplantation [Internet]. 2005 Jun 1 [cited 2022 May 6]; 20(6):1048–56. Available from: https://academic.oup.com/ndt/article/20/6/1048/1818992 https://doi.org/10.1093/ndt/gfh813 PMID: 15814534

26. Himmelfarb J, Ikizler T Alp. Hemodialysis. n engl j med. 2010; 19(4):1833–78. https://doi.org/10.1056/NEJMra0902710 PMID: 21047227

27. Westerhof N, Stergiopulos N, Noble MIM, Westerhof BE. The Pressure-Volume Relation. Snapshots of Hemodynamics [Internet]. 2019 [cited 2024 Feb 13];101–13. Available from: https://link.springer.com/chapter/10.1007/978-3-319-91932-4_14

28. Claessens TE, Georgakopoulos D, Afanasyeva M, Vermeersch SJ, Millar HD, Stergiopulos N, et al. Nonlinear isochrones in murine left ventricular pressure-volume loops: How well does the time-varying elastance concept hold? Am J Physiol Heart Circ Physiol [Internet]. 2006 Apr [cited 2022 May 6]; 290(4):1474–83. Available from: https://journals.physiology.org/doi/full/10.1152/ajpheart.00663.2005 PMID: 16284239

29. Sagawa K. Cardiac contraction and the pressure-volume relationship. New York/Oxford: Oxford University Press; 1988.

30. SM-ICG Technology [Internet]. [cited 2024 Jan 10]. https://physioflow.com/sm_icg_technology.php

31. Charloux A, Lonsdorfer-Wolf E, Richard R, Lampert E, Oswald-Mammosser M, Mettauer B, et al. A new impedance cardiograph device for the non-invasive evaluation of cardiac output at rest and during exercise: comparison with the 'direct' Fick method. Eur J Appl Physiol [Internet]. 2000 [cited 2024 Jan 19]; 82(4):313–20. Available from: https://pubmed.ncbi.nlm.nih.gov/10958374/ https://doi.org/10.1007/s004210000226

32. Georgianos PI, Sarafidis PA, Sinha AD, Agarwal R. Adverse Effects of Conventional Thrice-Weekly Hemodialysis: Is It Time to Avoid 3-Day Interdialytic Intervals? Am J Nephrol [Internet]. 2015 Jul 1 [cited 2024 Jan 11]; 41(4–5):400–8. Available from: https://dx.doi.org/10.1159/000435842 PMID: 26139107

33. Van De Vosse FN, Stergiopulos N. Pulse Wave Propagation in the Arterial Tree. [Internet]. 2011 Jan 4 [cited 2022 May 4]; 43:467–99. Available from: https://www.annualreviews.org/doi/abs/10.1146/annurev-fluid-122109-160730

34. Westerhof N, Elzinga G, Sipkema P. An artificial arterial system for pumping hearts. [Internet]. 1971 [cited 2022 May 4]; 31(5):776–81. Available from: https://journals.physiology.org/doi/abs/10.1152/jappl.1971.31.5.776

35. Blanco PJ, Watanabe SM, Dari EA, Passos MARF, Feijóo RA. Blood flow distribution in an anatomically detailed arterial network model: criteria and algorithms. Biomech Model Mechanobiol [Internet]. 2014 Oct 7 [cited 2024 Feb 13]; 13(6):1303–30. Available from: https://link.springer.com/article/10.1007/s10237-014-0574-8 PMID: 24682727

36. Anemette Sofie Olufsen. Roskilde University. 1998 [cited 2022 May 4]. Modeling the arterial system with reference to an anesthesia simulator. Ph.D. Thesis. https://forskning.ruc.dk/en/publications/modeling-the-arterial-system-with-reference-to-an-anesthesia-simu

37. Zhang X, Noda S, Himeno R, Liu H. Gravitational effects on global hemodynamics in different postures: A closed-loop multiscale mathematical analysis. Acta Mechanica Sinica/Lixue Xuebao [Internet]. 2017 Jun 1 [cited 2024 Jan 11]; 33(3):595–618. Available from: https://link.springer.com/article/10.1007/s10409-016-0621-z

38. Anliker M, Rockwell RL, Ogden E. Nonlinear analysis of flow pulses and shock waves in arteries—Part I: Derivation and properties of mathematical model. Zeitschrift für angewandte Mathematik und Physik ZAMP [Internet]. 1971 Mar [cited 2024 Jan 17]; 22(2):217–46. Available from: https://link.springer.com/article/10.1007/BF01591407

39. Danielsen M, Ottesen JT. 6. A Cardiovascular Model. Mathematical Modeling and Computation [Internet]. 2004 Jan [cited 2022 May 4];137–55. Available from: https://epubs.siam.org/doi/abs/10.1137/1.9780898718287.ch6

40. Suga H, Sagawa K, Shoukas AA. Load independence of the instantaneous pressure-volume ratio of the canine left ventricle and effects of epinephrine and heart rate on the ratio. Circ Res [Internet]. 1973

[cited 2022 May 4]; 32(3):314–22. Available from: https://pubmed.ncbi.nlm.nih.gov/4691336/ https://doi.org/10.1161/01.res.32.3.314

41. Lax P, Wendroff B. Systems of conservation laws. Commun Pure Appl Math [Internet]. 1960 May 1 [cited 2024 Feb 15]; 13(2):217–37. Available from: https://onlinelibrary.wiley.com/doi/full/10.1002/cpa.3160130205

42. Kennedy J, Eberhart R. Particle swarm optimization. Proceedings of ICNN'95—International Conference on Neural Networks [Internet]. [cited 2022 May 5];4:1942–8. http://ieeexplore.ieee.org/document/488968/

43. Coleman TF, Li Y. An interior trust region approach for nonlinear minimization subject to bounds. SIAM Journal on Optimization. 1996; 6(2):418–45.

44. Coleman TF, Li Y. On the convergence of interior-reflective Newton methods for nonlinear minimization subject to bounds. Math Program. 1994 Oct; 67(1–3):189–224.

45. Wolos K, Debowska M, Dabrowski W, Siwicka-Gieroba D, Poleszczuk J. Pulse waveform and stroke volume/cardiac output measurements in healthy and hemodialysis patients. 2023 Jul 10 [cited 2023 Jul 10]; https://zenodo.org/record/8131393

Supplementary materials for the article

"Non-invasive assessment of stroke volume and cardiovascular parameters based on peripheral pressure waveform"

by

Kamil Wolos, Leszek Pstras, Malgorzata Debowska, Wojciech Dabrowski, Dorota Siwicka-Gieroba, Jan Poleszczuk

Choice of patient-specific parameters to be estimated and their identifiability

Compared to our previous work (1,2), in the present study we decided to limit the number of subject-specific parameters to be estimated to just four (described below), for two reasons. First, we wanted to ensure their identifiability, and second, we wanted to verify whether even such a low number of fitted parameters would allow for an assessment of patient-specific stroke volume and other parameters. One needs to remember, that the lower the number of estimated parameters, the faster the computations required to calibrate the model with data – an aspect important when thinking about future method implementation. The choice of parameters to be estimated was not a trivial matter. On the one hand, these parameters should enable a reasonably accurate fitting of the model to the recorded pressure waveforms in the radial artery. On the other hand, they should influence stroke volume (SV), the estimation of which was especially important in our study, given that this was the model output that was subject to validation. Therefore, we decided to estimate two parameters related to the time-varying left-ventricular elastance, E_{max}, and the time to the onset of constant elastance,t_m) and two parameters related to the peripheral arterial resistance and compliance, i.e. the scaling factors for the resistances and compliances of the terminal branches of the arterial tree (S_R and S_C).

The choice of the ventricular elastance-related parameters (E_{max} and t_m) was based on the observation that the left-ventricular elastance functions normalized by the time of the peak and its amplitude are similar in healthy and diseased hearts (3). The only differences between an intact and diseased heart should be in the peak value of the left-ventricular elastance (E_{max}) and the time of that peak (3). The latter is not used explicitly in our model, which is why we decided to estimate a slightly different time-related parameter used in our definition of the time-varying elastance function (see eq. (7) and

supplementary Figure S6 for more details), i.e. the time to the onset of constant (minimal) elastance, t_m, which we expect should be correlated with the time of the peak elastance. The remaining parameters of our elastance function, i.e. the parameter E_{min}, which describes the minimal left-ventricular diastolic elastance and parameters a and b, which are mainly responsible for the slope of $E_{lv}(t)$ have been assumed fixed, given the aforementioned regularity in the normalized shape of $E_{lv}(t)$.

The other two parameters chosen to be estimated are the scaling factors for the terminal resistances and compliances. The former is strictly related with the systemic resistance, which results mainly from the resistance of small arteries and arterioles (4) and has a crucial impact on arterial blood pressure and therefore on the heart function, given that the heart works against the pressure at the entry to the ascending aorta. The scaling factor for the peripheral (terminal) compliances, was chosen to be estimated given that it should affect the diastolic part of the peripheral pressure waveform and therefore should enable better overall fits to patient data.

In the future, the choice of the parameters for optimization should be addressed in a more systematic manner by analyzing various combinations of parameters used for model fitting and assessing their joint performance both in terms of fitting of the model to the recorded pressure waveforms in the radial artery as well as estimation of stroke volume using such a data-fitted model (while keeping the model identifiable). However, in order for such a systematic analysis to be robust, one should consider collecting more data, including additional measurement endpoints, preferably using gold-standard methods.

Parameter identifiability

To check if the set of the four chosen parameters can identify a pulse waveform in the radial artery, we performed an identifiability analysis based on the work of Brun et. al. (5). As the output from the model, we considered the Fourier expansion parameters of the computed pressure waveform, see equations (14) and (15) for more details.

We used the finite difference approximation to compute the local sensitivity matrix $V = \{v_{i,j}\}$ where each column v_j represents changes in model outputs caused by a small change in the value of parameter

$\theta_j \in \{E_{max},\ t_m,\ S_R,\ S_C\}$ with respect to its baseline level, θ_0, as presented in Supplementary Table 1. For each studied parameter, we increased its baseline value by 5%, leaving all other parameters unchanged (the elements of the vector v_j correspond to the elements of the vector c defined in equation (15), and j denotes the parameter being changed). Then, the scaled sensitivity matrix $S = \{s_{i,j}\}$ was computed as follows to obtain dimension-free sensitivity information:

$$s_{i,j} = \frac{v_{i,j}\Delta\theta_j}{MV_i}, \tag{17}$$

where, according to Brun et al. (5), $\Delta\theta_j$ should be an *a priori* measure of the reasonable range of θ_j, and the scale factor, MV_i, should have the same scale as the corresponding output $v_{i,j}$. Here we set $\Delta\theta_j = \theta_0$, (see Supplementary Table 1), assuming that for each parameter the expected range of its values is ±50%. For MV_i, we first calculated the Fourier expansion coefficients of all recorded pressure waveforms, as in equation (14), to obtain 13-element vectors as given by equation (15), and then we calculated the mean value (MV) of each element in those vectors and assigned it to the corresponding parameter MV_i.

SUPPLEMENTARY TABLE 1
PARAMETERS $\Delta\theta_j$ USED IN IDENTIFIABILITY ANALYSIS

Parameter	Unit	$\boldsymbol{\theta_0 = \Delta\theta_j}$
E_{max}	mmHg/ml	2.49[a]
t_m	s	0.41
S_R	-	1
S_C	-	1

[a] based on the work of Danielsen (6)

To assess the identifiability of a given set of parameters, we must consider the joint influence of these parameters on the model output. This can be done by checking the degree of near-linear dependence between the columns of the scaled sensitivity matrix. To that aim we calculated a collinearity index γ defined as in (5)

$$\gamma = \frac{1}{min_{||\beta||=1}||\tilde{S}\,\beta||} = \frac{1}{\sqrt{\lambda_k}}, \tag{18}$$

where $\tilde{S}$ is the normalized sensitivity matrix S, β is a 13-element vector, and λ_k is the smallest eigenvalue of $\tilde{S}^T\tilde{S}$. According to Brun et al., the parameters may be considered identifiable, if $\gamma < 20$. In our case, $\gamma = 2.1$. On this basis, we concluded that our model is identifiable and that the obtained solutions are unique.

78

79 **Sensitivity analysis**

80 We have also investigated changes in the simulated flow rate waveform in the ascending aorta and the
81 pulse waveform in the radial artery following changes in parameter values by $\pm 50\%$ for E_{max}, S_C and S_R,
82 and $\pm 10\%$ for t_m, similarly as done in (7). For t_m we studied smaller changes, because 50% of the
83 baseline value of t_m would fall below our accepted lower bound on this parameter which was set to
84 $0.45 \cdot T$, where T is the heartbeat period. The results of this sensitivity analysis are presented in Fig. S8.

85 The most prominent changes in the flow rate waveforms and pulse waveforms are visible for changes
86 in parameters E_{max} and S_R, particularly with regard to the vertical shifts of the pulse waveform, see
87 Fig. S6, b and c. Increasing E_{max} results in an increase of the aortic inflow, whereas the aortic inflow
88 decreases when S_R increases. Changes in E_{max} lead to changes in the maximal and total aortic inflow,
89 whereas changes in S_R affect mainly the timing of the blood flow from the heart. Slightly less visible is
90 the impact of t_m variations, which mainly influence the shape of the pulse waveform in the systolic
91 phase, especially with regard to the downslope of the pressure wave after reaching the peak systolic
92 pressure, see Fig. S6. The parameter S_C affects the diastolic part of the pulse waveform, although its
93 impact is relatively small, see Fig. S6d. It allows for somewhat better fitting of the recorded pulse
94 waveforms. However, it does not cause any noticeable changes in the flow rate in the ascending aorta.

95 The above analysis revealed, therefore, that each of the four chosen parameters influences the shape
96 of the pressure waveform in the radial artery and that all of them except Sc also affect stroke volume
97 (calculated from the flow rate waveform in the ascending aorta).

98

99 **Fixed parameters in the cardiovascular model**

100 Supplementary Table 2 presents the parameters that are fixed in the model. The values of these
101 parameters come mainly from the work of Olufsen (8) and Danielsen (6).

102

Supplementary Table 2
Fixed parameters of the model

Parameter	Unit	Value	Reference
E_{min}	$mmHg/ml$	0.049	(6)
a	-	0.9	(6)

b	-	0.25	(6)
k_1	$g/(s^2 \cdot cm)$	$2 \cdot 10^7$	(9)
k_2	cm^{-1}	-22.53	(9)
k_3	$g/(s^2 \cdot cm)$	$8.65 \cdot 10^5$	(9)
P_o	$mmHg$	97	(10)
R_{la}	$mmHg \cdot s/ml$	0.000089	(6)
L_{la}	$mmHg \cdot s^2/ml$	0.00005	(6)
p_{la}	$mmHg$	7.5	assumed
R_{lv}	$mmHg \cdot s/ml$	0.08	assumed
L_{lv}	$mmHg \cdot s^2/ml$	0.000416	(6)
$\overline{V_b}$	ml	2	(6)
V_o	ml	$15 \cdot S^3$	assumed

S is the ratio of the subject's height to the height of the reference man (175 cm)

REFERENCES

1. Poleszczuk J, Debowska M, Dabrowski W, Wojcik-Zaluska A, Zaluska W, Waniewski J. Subject-specific pulse wave propagation modeling: Towards enhancement of cardiovascular assessment methods. PLoS One. 2018;13(1):1–17.

2. Poleszczuk J, Debowska M, Dabrowski W, Wojcik-Zaluska A, Zaluska W, Waniewski J. Patient-specific pulse wave propagation model identifies cardiovascular risk characteristics in hemodialysis patients. PLoS Comput Biol. 2018;14(9):1–15.

3. Senzaki H, Chen CH, Kass DA. Single-Beat Estimation of End-Systolic Pressure-Volume Relation in Humans. Circulation [Internet]. 1996 Nov 15 [cited 2022 May 6];94(10):2497–506. Available from: https://www.ahajournals.org/doi/abs/10.1161/01.CIR.94.10.2497

4. Lax P, Wendroff B. Systems of conservation laws. Commun Pure Appl Math [Internet]. 1960 May 1 [cited 2024 Feb 15];13(2):217–37. Available from: https://onlinelibrary.wiley.com/doi/full/10.1002/cpa.3160130205

5. Brun R, Reichert P, Künsch HR. Practical identifiability analysis of large environmental simulation models. Water Resour Res [Internet]. 2001 Apr 1 [cited 2022 Oct 25];37(4):1015–30. Available from: https://onlinelibrary.wiley.com/doi/full/10.1029/2000WR900350

6. Danielsen M, Ottesen JT. 6. A Cardiovascular Model. Mathematical Modeling and Computation [Internet]. 2004 Jan [cited 2022 May 4];137–55. Available from: https://epubs.siam.org/doi/abs/10.1137/1.9780898718287.ch6

7. Zhang X, Liu J, Cheng Z, Wu B, Xie J, Zhang L, et al. Personalized 0D-1D multiscale hemodynamic modeling and wave dynamics analysis of cerebral circulation for an elderly patient with dementia. Int J Numer Method Biomed Eng. 2021;

8. Olufsen MS, Peskin CS, Kim WY, Pedersen EM, Nadim A, Larsen J. Numerical simulation and experimental validation of blood flow in arteries with structured-tree outflow conditions. Ann Biomed Eng. 2000;28(11):1281–99.

9. Anemette Sofie Olufsen. Roskilde University. 1998 [cited 2022 May 4]. Modeling the arterial system with reference to an anesthesia simulator. Ph.D. Thesis. Available from: https://forskning.ruc.dk/en/publications/modeling-the-arterial-system-with-reference-to-an-anesthesia-simu

10. Stergiopulos N, Young DF, Rogge TR. Computer Simulation of Arterial Flow With Applications To Arterial and Aortic Stenoses. J Biomech. 1992;25(12):1477–88.

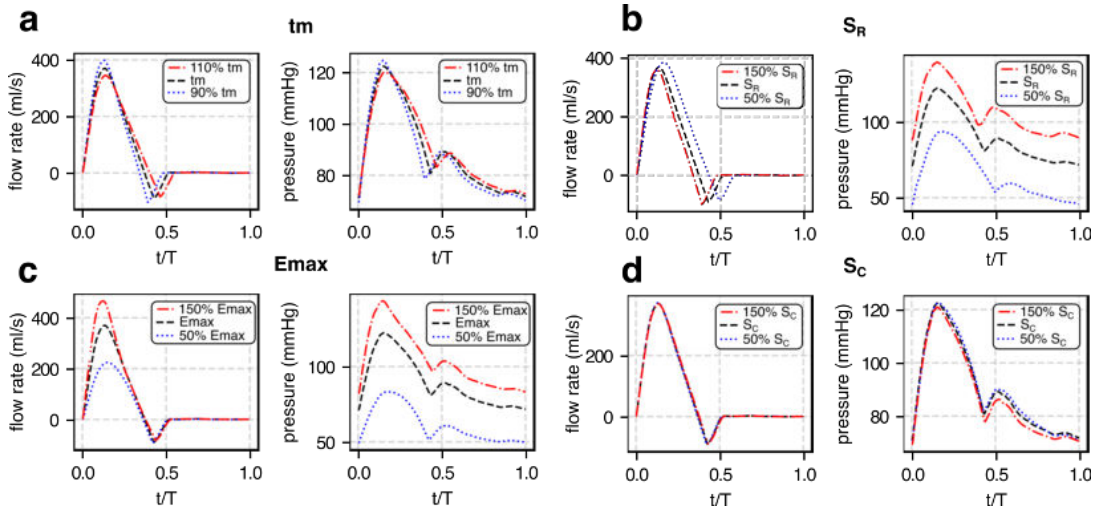

140

141 **S6 Fig. Sensitivity of the simulated flow rate waveform from the ascending aorta (left subpanels)**
142 **and pulse waveform in the radial artery (right subpanels) to relatively large changes in the**
143 **adjustable model parameters**. a) tm - time to the onset of constant elastance of the left ventricle; b) Sr
144 – scaling factor for the resistance of the terminal branches of the arterial tree; c) Emax - maximal
145 elastance of the left ventricle; d) Sc - scaling factor for the compliances of the terminal branches of the
146 arterial tree.

Supplementary material 2

Simulated vs measured pressure waveforms in the radial artery

Below we show the simulated vs measured (recorded) pressure waveforms in the radial artery (following fitting of the model to each measured waveform) for all cases analyzed in the present study, i.e. 144 measurements in 35 HD patients and 14 measurements in 14 healthy subjects (control group).

Legend

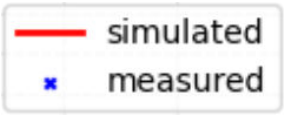

For the HD patients, the subpanels are titled using the following format:

[ID, interdialytic break, time of measurement, error]

where:
ID denotes patient ID

interdialytic break refers to the length of break since the last HD session:
SB – short interdialytic break (2 days)
LB – long interdialytic break (3 days)

time of measurement refers to the exact moment of measurement during the HD session:
BS – measurement taken 15 min before the start of HD session
AS – measurement taken 15 min after the start of HD session
BE – measurement taken 15 min before the end of HD session
AE – measurement taken 15 min after the end of HD session

error represents the fitting error, i.e. the mean absolute percentage error (MAPE) between the simulated and measured pressure waveforms (for all available data points)

Example:
The title "**9, SB, AS, err=2.2%**" describes the case of a patient with ID=9, with the pressure waveform measured during hemodialysis performed after a short interdialytic break and 15 min after the start of the hemodialysis session, where the MAPE between the simulated and measured pressure waveforms was 2.2%.

For the control group, the subpanels are titled using the analogous but shorter format:
[ID, error]


1, SB, BS, err=1.5%
1, SB, AS, err=1.6%
1, SB, BE, err=2.0%
1, SB, AE, err=4.6%
1, LB, AS, err=1.7%
1, LB, BE, err=1.6%
1, LB, AE, err=1.7%
2, LB, BS, err=7.8%
2, LB, AS, err=4.0%
2, LB, BE, err=6.1%
2, LB, AE, err=6.3%
3, SB, BS, err=7.2%
3, SB, AS, err=6.1%
3, SB, BE, err=1.7%
3, SB, AE, err=4.3%
3, LB, BS, err=8.0%
3, LB, AE, err=2.6%
4, SB, BS, err=8.1%
4, SB, AS, err=8.1%
4, SB, BE, err=3.8%
4, SB, AE, err=7.5%
4, LB, AS, err=10.5%
4, LB, AE, err=6.4%
5, SB, BS, err=2.4%
5, SB, BE, err=3.5%
5, LB, BS, err=4.1%
5, LB, BE, err=5.7%
6, SB, BS, err=5.8%
6, SB, AS, err=6.1%
6, SB, BE, err=6.3%
6, LB, AS, err=3.5%
7, SB, BS, err=5.7%
7, SB, AE, err=8.2%
7, LB, AS, err=1.6%
8, SB, BS, err=4.4%
8, SB, AS, err=2.7%
8, SB, BE, err=3.1%
8, SB, AE, err=2.9%
8, LB, BS, err=3.2%
8, LB, AS, err=2.6%
8, LB, BE, err=3.1%
8, LB, AE, err=2.7%
9, SB, BS, err=2.0%
9, SB, AS, err=2.2%
9, SB, BE, err=2.0%
9, SB, AE, err=1.8%
9, LB, BS, err=1.8%
9, LB, AS, err=2.2%
10, LB, BS, err=1.3%
10, LB, AS, err=2.4%
10, LB, AE, err=2.1%
11, SB, BS, err=3.4%
11, SB, AS, err=2.4%
11, LB, BS, err=3.3%
11, LB, AS, err=1.5%
12, SB, BS, err=4.8%
12, SB, AS, err=2.2%
12, SB, BE, err=3.5%
12, LB, AS, err=2.4%
12, LB, BE, err=5.6%
pressure (mmHg)
time (ms)

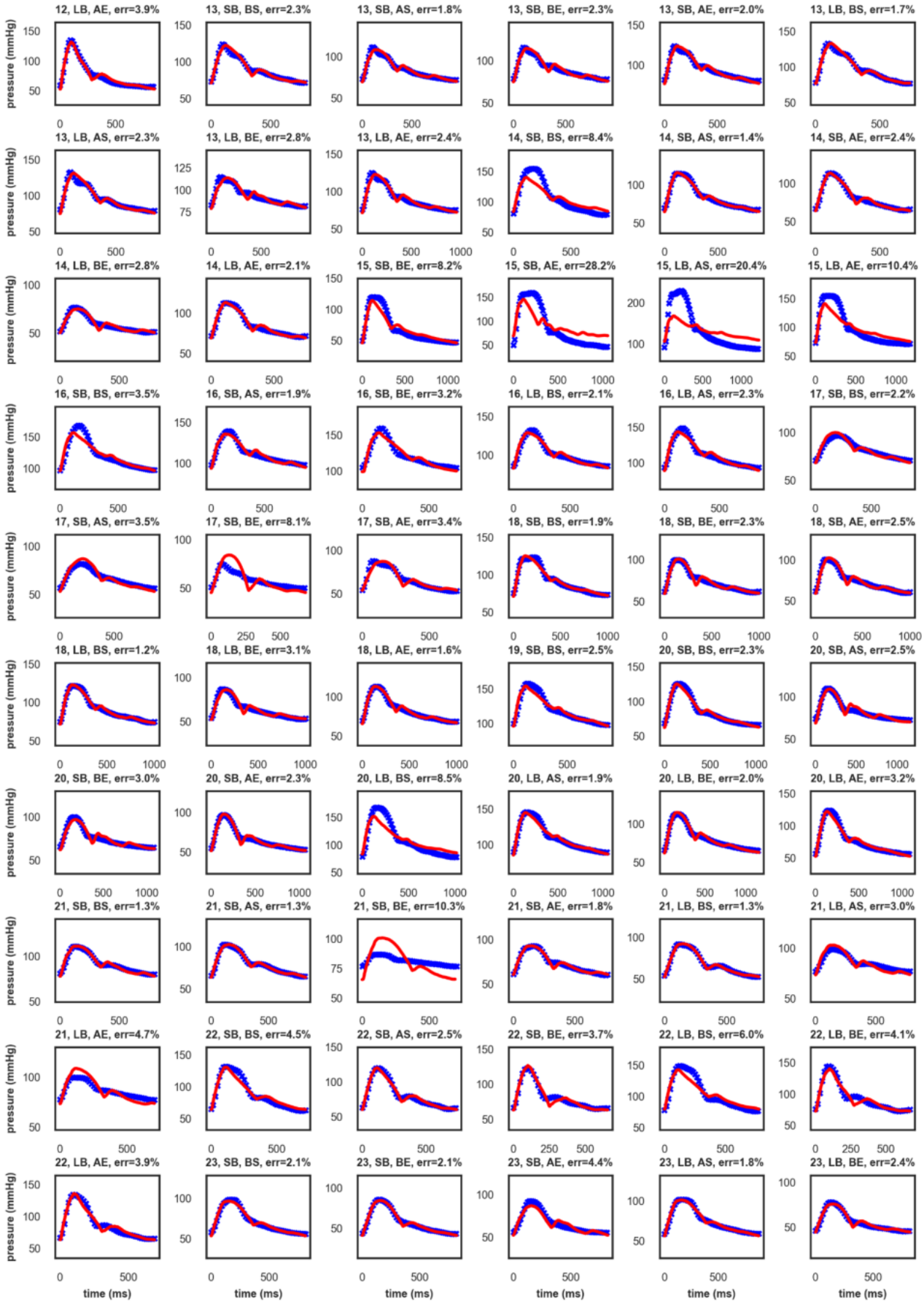
12, LB, AE, err=3.9%
13, SB, BS, err=2.3%
13, SB, AS, err=1.8%
13, SB, BE, err=2.3%
13, SB, AE, err=2.0%
13, LB, BS, err=1.7%
13, LB, AS, err=2.3%
13, LB, BE, err=2.8%
13, LB, AE, err=2.4%
14, SB, BS, err=8.4%
14, SB, AS, err=1.4%
14, SB, AE, err=2.4%
14, LB, BE, err=2.8%
14, LB, AE, err=2.1%
15, SB, BE, err=8.2%
15, SB, AE, err=28.2%
15, LB, AS, err=20.4%
15, LB, AE, err=10.4%
16, SB, BS, err=3.5%
16, SB, AS, err=1.9%
16, SB, BE, err=3.2%
16, LB, BS, err=2.1%
16, LB, AS, err=2.3%
17, SB, BS, err=2.2%
17, SB, AS, err=3.5%
17, SB, BE, err=8.1%
17, SB, AE, err=3.4%
18, SB, BS, err=1.9%
18, SB, BE, err=2.3%
18, SB, AE, err=2.5%
18, LB, BS, err=1.2%
18, LB, BE, err=3.1%
18, LB, AE, err=1.6%
19, SB, BS, err=2.5%
20, SB, BS, err=2.3%
20, SB, AS, err=2.5%
20, SB, BE, err=3.0%
20, SB, AE, err=2.3%
20, LB, BS, err=8.5%
20, LB, AS, err=1.9%
20, LB, BE, err=2.0%
20, LB, AE, err=3.2%
21, SB, BS, err=1.3%
21, SB, AS, err=1.3%
21, SB, BE, err=10.3%
21, SB, AE, err=1.8%
21, LB, BS, err=1.3%
21, LB, AS, err=3.0%
21, LB, AE, err=4.7%
22, SB, BS, err=4.5%
22, SB, AS, err=2.5%
22, SB, BE, err=3.7%
22, LB, BS, err=6.0%
22, LB, BE, err=4.1%
22, LB, AE, err=3.9%
23, SB, BS, err=2.1%
23, SB, BE, err=2.1%
23, SB, AE, err=4.4%
23, LB, AS, err=1.8%
23, LB, BE, err=2.4%
pressure (mmHg)
time (ms)

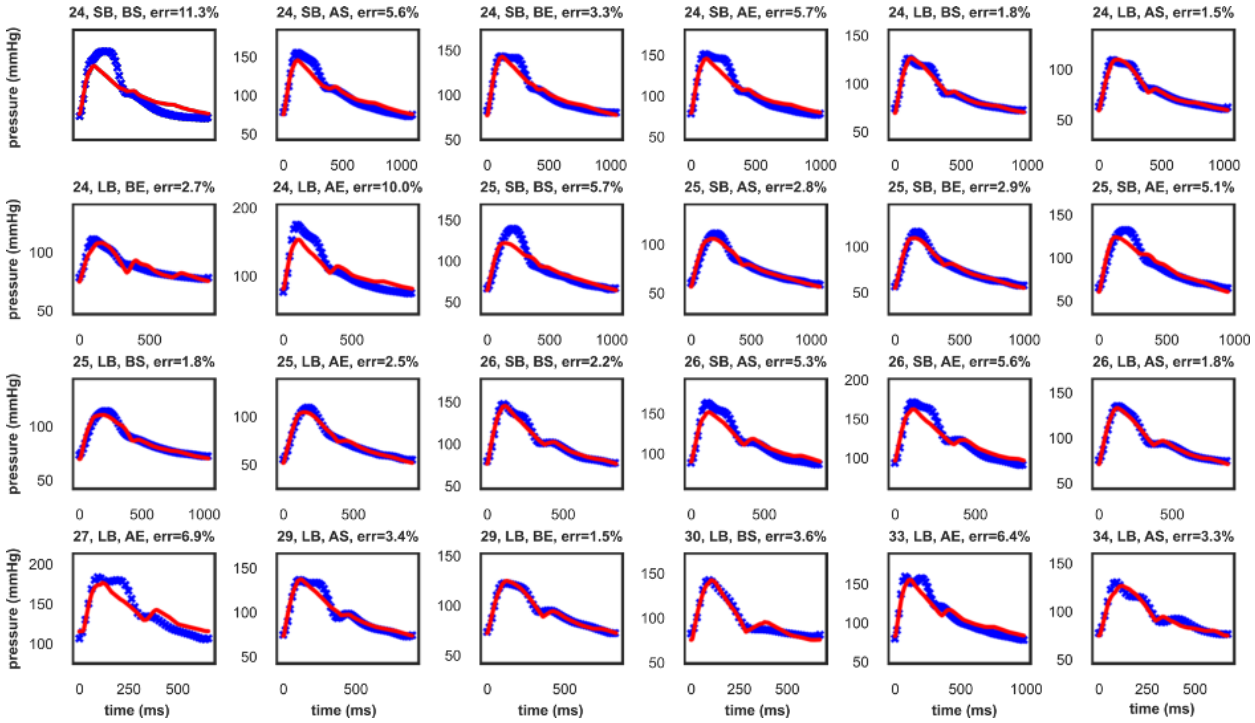

Control group:

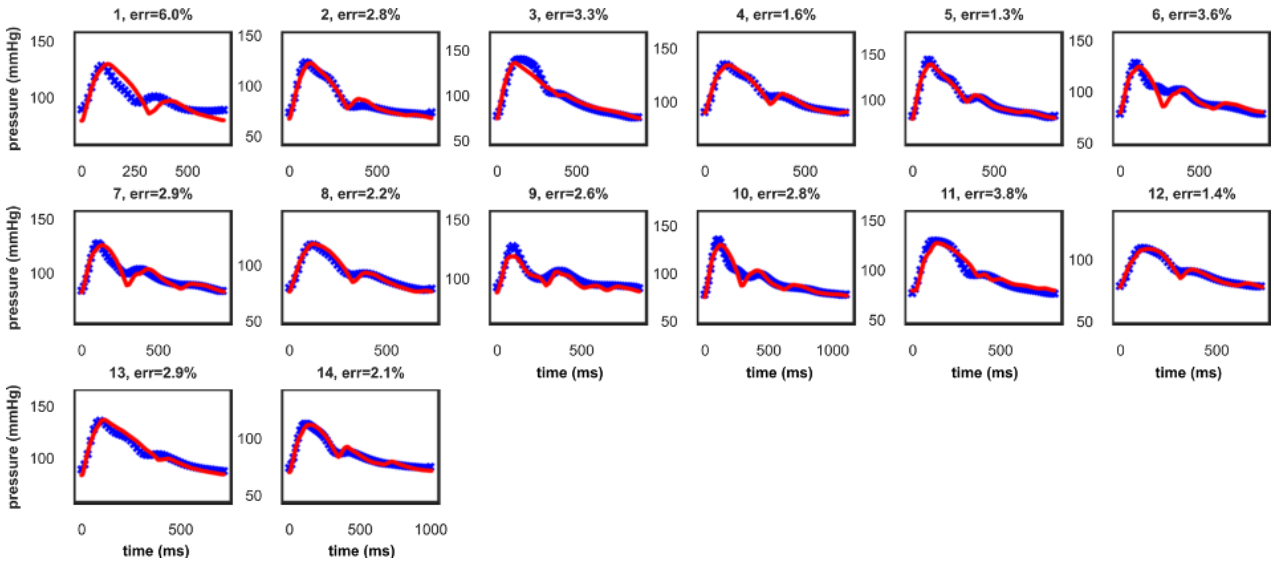

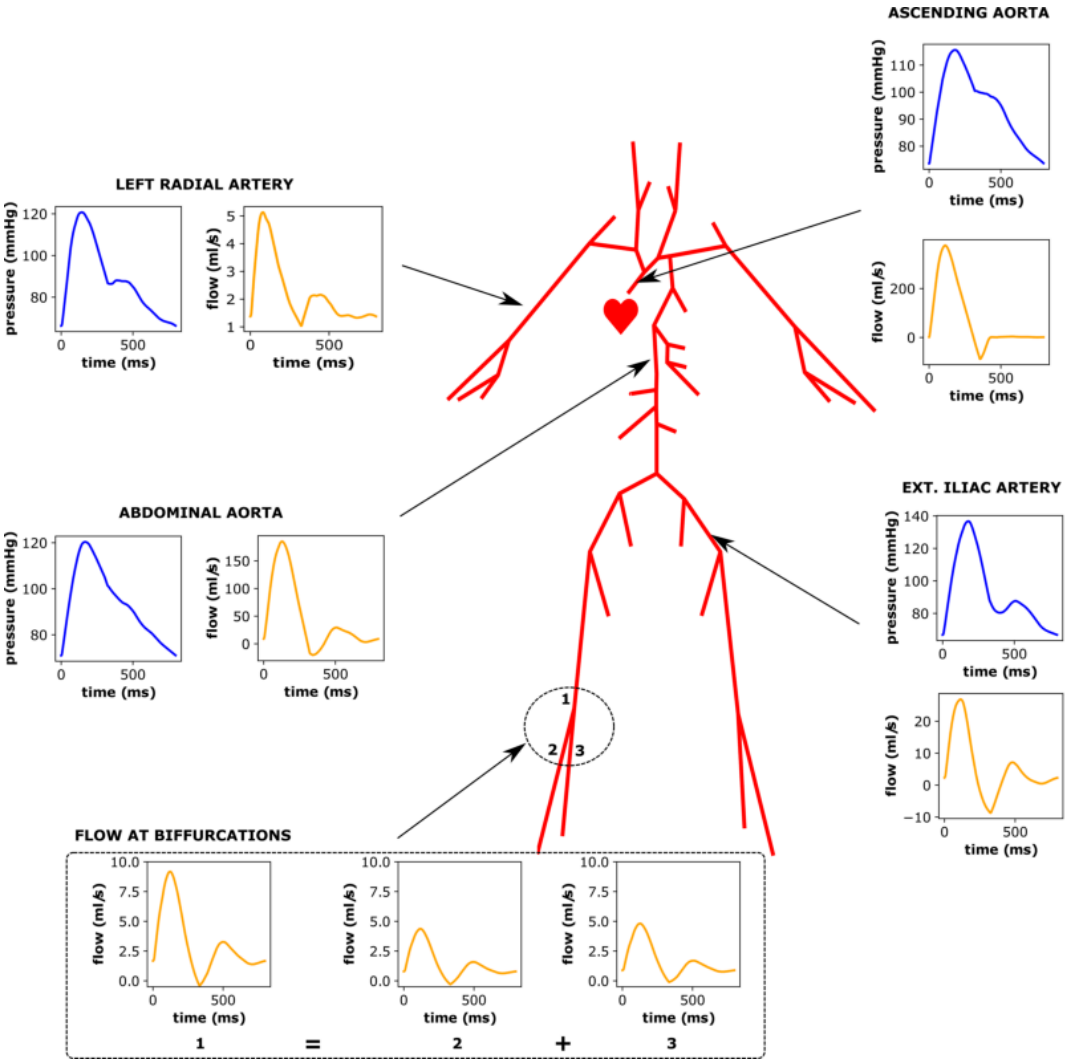

FIGURE S1: Exemplary outputs from the model at various locations of the arterial tree. The presented model outputs (i.e. blood pressure and flow rate waveforms) were obtained using the baseline values of all model parameters (see S1 supplementary materials), for a 175 cm man with a heart rate of 75 bpm.

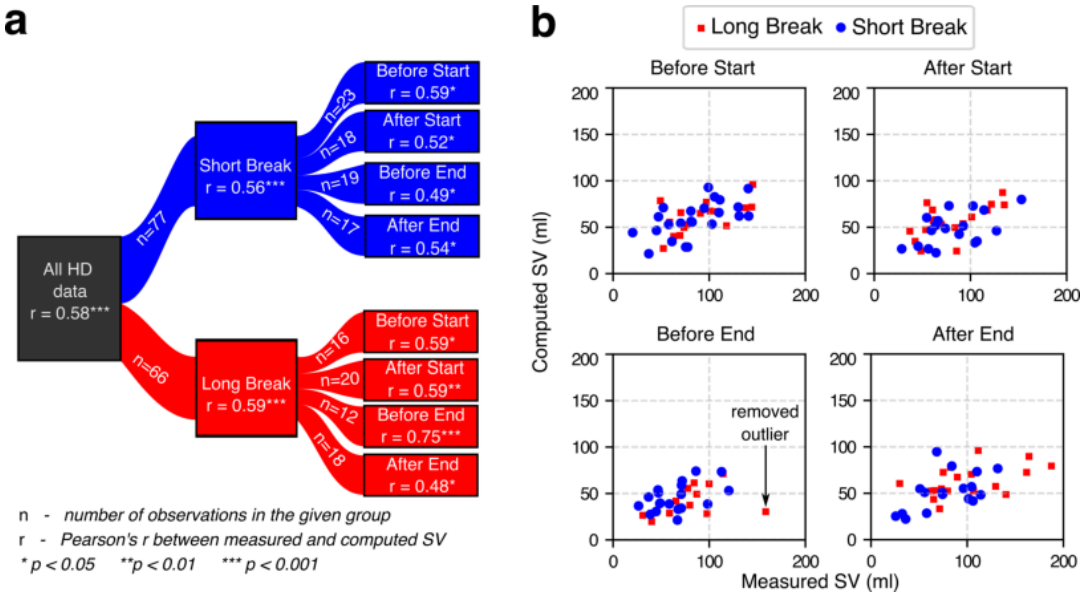

FIGURE S2: (a) Pearson correlation coefficients between the model-estimated (computed) SV and the SV measured using bioimpedance cardiography for HD patients (additionally divided into groups of measurements depending on the duration of the interdialytic break before the studied HD session and the moment of measurement during the HD session). (b) Scatter plots of model-estimated (computed) and bioimpedance-based SV values for HD patients corresponding to different moments of measurement. Correlations were computed after removing the outlier from the Before End group.

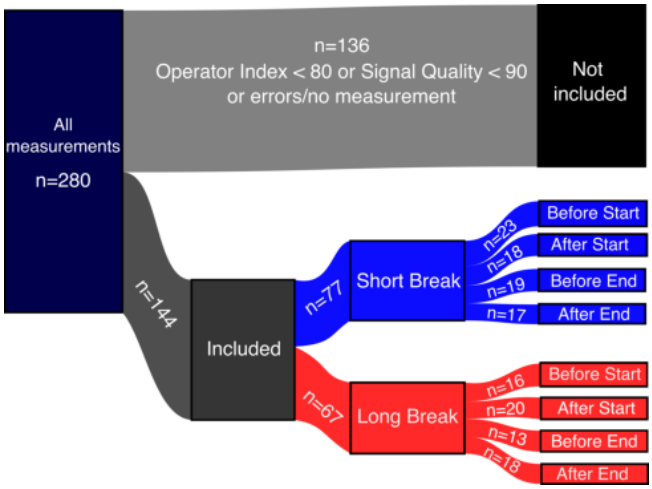

FIGURE S3: Sankey diagram of the study dataset collected in HD patients. 136 cases were excluded from the analysis due to missing or clearly erroneous data or due to low quality of the recorded applanation tonometry or bioimpedance signals in accordance with the manufacturer's instructions (SphygmoCor "Operator index" < 80 or PhysioFlow "Signal Quality" < 90). The remaining cases were divided according to the length of the interdialytic break before the studied HD session (a short, 2-day break vs a long, 3-day break) and according to the time of measurement during the HD session (before start, after start, before end and after end of the HD).

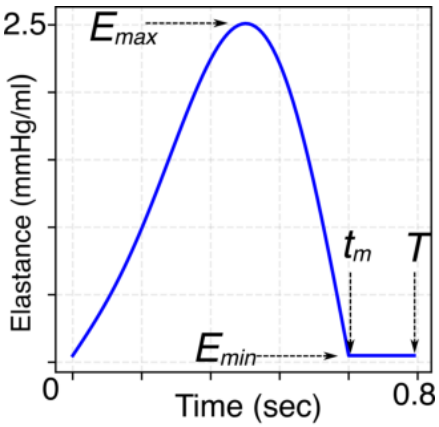

FIGURE S4: Left-ventricular elastance function according to Eqs (7) and (8). $E_{\max}$–maximal systolic elastance, $E_{\min}$–minimal (diastolic) elastance, T–heart period, and t_m–time to the onset of constant (minimal) elastance.

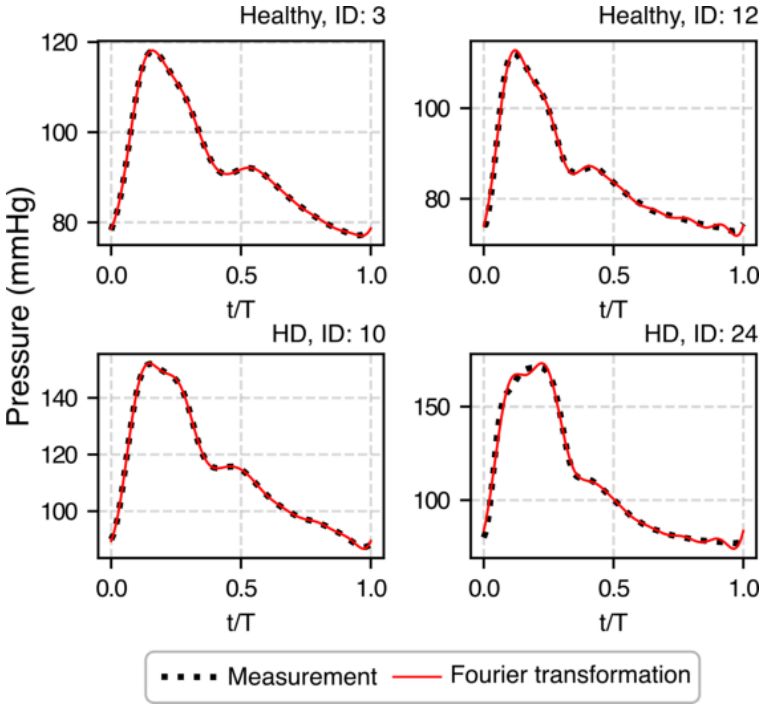

FIGURE S5: Exemplary pressure waveforms recorded in the radial artery by SphygmoCor along with their transformations into Fourier series with 6 harmonics. Results are presented for two healthy subjects and two HD patients and normalized against time, T–heart period.

Chapter 3

Publication [A2]: Personalized Pulse Wave Propagation Modeling to Improve Vasopressor Dosing Management in Patients with Severe Traumatic Brain Injury

3.1 Summary of the study

As discussed in Chapter 1, severe traumatic brain injury (sTBI) requires intensive medical care and long-term rehabilitation [16]. Arterial hypotension is a common and serious complication in sTBI patients, often necessitating the use of vasopressors to maintain adequate cerebral perfusion pressure and systemic hemodynamics [139]. However, determining the optimal vasopressor dosage is challenging due to the significant variability in cardiovascular responses to various drugs among patients. This variability can lead to under-treatment or over-treatment, both of which carry substantial risks.

Current clinical protocols for vasopressor administration are relatively general and often fail to account for individual patient differences. Dosing adjustments are typically made through trial and error or subjective clinical assessments, which may not fully capture the patient's cardiovascular status. Mathematical modeling offers a promising solution by enabling a more personalized and precise assessment of cardiovascular function.

In the second publication included in this dissertation, I investigated whether non-invasive arterial pulse wave recordings, analyzed through a physiology-based mathematical model of pulse wave propagation, could provide patient-specific cardiovascular information to improve vasopressor dosing strategies in an intensive care setting. To inform the model, I used non-invasive pulse wave measurements obtained with an oscillometric device (AngE, SOT Medical, Austria; see also Figure 1.4B), which simultaneously record pulse waveforms from both wrists and ankles. Thus, I formulated two hypotheses (H2 and H3, as outlined in Chapter 1.6):

(H2) *A pulse wave propagation model can approximate arterial pulse waveforms recorded simultaneously at multiple locations using the oscillometric technique.*

(H3) *Cardiovascular parameters estimated through personalization of a pulse wave propagation model may be used for prediction of vasopressor dosage adjustments in patients with severe traumatic brain injury.*

To address these hypotheses, I formulated four specific research questions:

(H2Q1) *Which parameters of a pulse wave propagation model should be adjusted to fit the model to four peripheral pulse waveforms (recorded on wrists and ankles)?*

(H2Q2) *Can a pulse wave propagation model approximate pulse waveforms recorded oscillometrically from four peripheral sites (wrists and ankles)?*

(H3Q1) *Do the values of cardiovascular parameters estimated from pulse wave propagation modeling allow for predictions of vasopressor dosing adjustments in patients with severe traumatic brain injury?*

(H3Q2) *Are the above-mentioned predictions better compared to predictions based on standard hemodynamic parameters and patient characteristics?*

In this study, I employed a 0-1D pulse wave propagation model coupled with a time-varying left ventricular elastance model, similar to the approach used in the previous publication discussed in Chapter 2. However, an important enhancement was the adoption of a more detailed arterial domain. The 55-element arterial tree described by Olufsen et al. [118, 106] was replaced with a 71-element domain based on the works of Alastruey et al. [140] and Stergiopulos et al. [105], providing a more accurate representation of the cerebral arterial system.

To inform the model, I used non-invasive arterial pulse (volumetric) wave recordings obtained simultaneously from wrists and ankles of 25 patients with sTBI treated with norepinephrine (five of whom also received dobutamine). These measurements were performed once daily for each patient using an oscillometric method. Unlike the typical approach of fitting the model to a single pulse waveform, this study utilized multiple waveforms to obtain a more comprehensive picture of the cardiovascular system.

The proposed mathematical model includes numerous parameters that describe the mechanical properties of the heart and arterial system and the dynamics of blood flow. To determine the most informative parameters for model fitting (H2Q1), I conducted a comprehensive Sobol sensitivity analysis [141, 142] and parameter identification analysis (following the procedure outlined by Olufsen et al. [143]). These analyses identified five key parameters (related to arterial stiffness, peripheral resistance, and cardiac function) as having the greatest influence on the pulse waveforms.

To personalize the model, I used the Levenberg-Marquardt optimization algorithm [144], which iteratively adjusted the selected model parameters to minimize the difference between the four measured and simulated waveforms. This fitting process was performed individually for each patient, resulting in a set of personalized cardiovascular parameters that reflected each patient's unique hemodynamic status during treatment (addressing H2Q1 and H2Q2).

The quality of the model fits to the recorded waveforms was satisfactory, with the mean coefficients of determination (R^2) of approximately 0.9 for all four measurement sites, indicating that the model could effectively capture the key features of the four recorded waveforms (addressing H2 and H2Q2). The resulting personalized parameters were then used to predict changes in norepinephrine dosing over the subsequent 24 hours (addressing H3). To this end, together with Urszula Białończyk, we developed two predictive models using machine learning techniques:

- Full model: a model that incorporated both the personalized model parameters and conventional clinical variables (such as patient demographics and standard hemodynamic measurements) – addressing H3Q1.
- Simple model: a model based solely on conventional clinical variables – addressing H3Q2.

The full predictive model incorporating the personalized cardiovascular parameters achieved higher accuracy, sensitivity, and precision compared with the simple model based solely on conventional measurements, suggesting that the pulse wave may contain additional "information" about the patient's cardiovascular status.

According to our findings, the proposed framework can predict the direction of norepinephrine dose changes within next 24h with balanced accuracy of 0.85 when trained and validated on the full dataset and 0.76 when using the leave-one-out cross-validation, despite the known variability in vasopressor responsiveness among sTBI patients. These results highlight the potential of combining non-invasive measurements with physiology-based modeling to support more individualized and responsive cardiovascular management in critically-ill patients. However, larger-scale validation is necessary before these approaches can be adopted clinically. According to my knowledge, this is the first study to demonstrate the feasibility of using personalized cardiovascular parameters from a pulse wave propagation model to predict vasopressor dosing adjustments in an intensive care setting.

The GitHub repository, which contains the implementation code of the mathematical model presented in this study and the anonymized data used for calibrating the model, can be found at: https://github.com/kwolos/STBI.

3.2 My contributions

I am the first author of this publication, responsible for the methodology and conceptualization, software implementation, validation, formal analysis, investigation, data curation, and drafting the first manuscript. I extended a previous mathematical model by incorporating a more detailed arterial network, implemented the optimization procedure for parameter estimation, and performed all simulations and analyses. I also conducted the sensitivity and parameter-identification analyses to select the most informative parameters to be used for fitting clinical data, prepared all figures and tables, and interpreted the results.

3.3 Author contributions

The conceptualization of the study was discussed collaboratively with my Advisors, Prof. Jan Poleszczuk, and Dr. Leszek Pstraś. Mgr Urszula Białończyk codeveloped predictive statistical models. Besides my Advisors, methodological discussions involved Prof. Małgorzata Debowska, Prof. Wojciech Dąbrowski, and Prof. Dorota Siwicka-Gieroba. Prof. Dąbrowski and Prof. Siwicka-Gieroba oversaw the collection of medical data used in the study. The manuscript underwent review and revisions by my Advisors and Prof. Debowska.

3.4 Publication

PLOS Computational Biology

RESEARCH ARTICLE

Personalized pulse wave propagation modeling to improve vasopressor dosing management in patients with severe traumatic brain injury

Kamil Wolos[1]*, Leszek Pstras[1], Urszula Bialonczyk[1], Malgorzata Debowska[1], Wojciech Dabrowski[2], Dorota Siwicka-Gieroba[2], Jan Poleszczuk[1]

1 Laboratory of Mathematical Modeling of Physiological Processes, Nalecz Institute of Biocybernetics and Biomedical Engineering, Polish Academy of Sciences, Warsaw, Poland, **2** Department of Anesthesiology and Intensive Therapy, Medical University of Lublin, Lublin, Poland

* kwolos@ibib.waw.pl

OPEN ACCESS

Citation: Wolos K, Pstras L, Bialonczyk U, Debowska M, Dabrowski W, Siwicka-Gieroba D, et al. (2025) Personalized pulse wave propagation modeling to improve vasopressor dosing management in patients with severe traumatic brain injury. PLoS Comput Biol 21(9): e1013501. https://doi.org/10.1371/journal.pcbi.1013501

Editor: Stacey D. Finley, University of Southern California, UNITED STATES OF AMERICA

Received: April 6, 2025

Accepted: September 8, 2025

Published: September 15, 2025

Data availability statement: The GitHub repository, which contains an implementation of the mathematical model presented in this study and the anonymized data, can be found at: https://github.com/kwolos/STBI.

Abstract

This study investigates whether examining the shape of arterial pulse waves and fitting to them a physiology-based mathematical model of pulse wave propagation can provide additional insights into the state of the cardiovascular system in patients with severe traumatic brain injury (sTBI), potentially enhancing vasopressor dosing strategies. We conducted a longitudinal study on 25 sTBI patients in an intensive care unit. Arterial pulse waves were recorded non-invasively from wrists and ankles using an oscillometric method and were used to inform a 0-1D model of the arterial blood flow dynamics. Model-estimated, patient-specific cardiovascular parameters were then used in a statistical model to predict changes in the administered dose of vasopressor (norepinephrine) in the next 24 hours. The model fits to the recorded pulse waves were satisfactory, with the coefficients of determination (R^2) of approximately 0.9 and the differences between the measured and model-estimated mean arterial pressure of 0.1 ± 1.0 mmHg (R^2=0.99). Except for a few patients, we found no clear association between the model-estimated parameters and norepinephrine dose at the time of pulse wave recording. Nevertheless, our predictive model achieved a balanced accuracy of 0.85 when trained and tested on the entire dataset and 0.76 when using the leave-one-out cross-validation, with 8 misclassifications among the total of 77 observations. Thus, despite the known inter-patient variability of hemodynamic response to vasopressors, the proposed method allowed predicting the direction of norepinephrine dose changes in the next 24 hours with satisfactory accuracy. Subject to further studies and extensive validation, our approach could inform a decision-support tool for optimizing vasopressor dosing on a per-patient basis.

PLOS Computational Biology

Funding: JP, MD, WD, DSG and KW were partly supported by the National Science Centre (Poland), grant No. 2018/31/D/ST7/03472. The funders had no role in study design, data collection and analysis, decision to publish, or preparation of the manuscript.

Competing interests: The authors have declared that no competing interests exist.

Authors summary

Hypotension is a dangerous complication in patients with severe traumatic brain injury (sTBI), making precise control of systemic blood pressure of utmost importance. To maintain blood pressure at prescribed levels, physicians often administer vasopressors (for example, norepinephrine). In current clinical practice, the vasopressor dose is frequently adjusted by trial and error, guided by continuous monitoring of the patient's hemodynamic state. This approach is time-consuming and likely sub-optimal, highlighting the need for more efficient methods to guide vasopressor therapy. In this study, we investigated whether non-invasive peripheral pulse wave recordings, combined with mathematical modeling of cardiovascular dynamics, could help predict changes in vasopressor dosing. Our results show that by incorporating personalized cardiovascular parameters into a statistical predictive model, it is possible to predict - with satisfactory accuracy - the direction of change (or lack thereof) in the administered norepinephrine dose within the next 24 hours. With further research and rigorous validation, this approach may support more effective vasopressor management using easily available, non-invasive clinical data.

Introduction

Severe traumatic brain injury (sTBI) can lead to permanent disability or death, and its treatment remains a challenge [1,2]. Among the many complications associated with sTBI, hemodynamic instability, particularly hypotension, is of utmost importance [3]. An abnormally low blood pressure poses a substantial risk to patients with sTBI, exacerbating cerebral ischemia and further compromising neurological function [4,5]. To avoid hypotension in sTBI patients, clinicians commonly use vasopressors, particularly norepinephrine (NE) [6] which, through various mechanisms, mainly peripheral vasoconstriction [7], leads to an increase in arterial blood pressure. Currently, adjusting vasopressor doses in critically ill patients is an iterative process based on observing mid- to long-term changes in vital physiological parameters such as mean arterial pressure (MAP) or systolic pressure (SP). According to the guidelines for sTBI patients, to decrease mortality and improve outcomes, MAP should be maintained above 80 mmHg [6], whereas SP should be maintained above 100 mmHg in patients aged 50–69 years, and above 110 mmHg in other patients [8]. However, such an iterative, often trial-and-error process might be far from optimal, carrying the risk of transient sub-optimal dose levels, which may lead to inadequate perfusion followed by hypoperfusion-related complications or to inadvertent overdosing, resulting in other adverse effects [9]. For instance, a study on 1093 ICU patients showed that their MAP was within the target range only in 43% of time (on average), while being below and above the target in 9% and 48% of time, respectively [10]. Therefore, there is a clear need to develop new tools that would help guide the process of vasopressor dosing in sTBI patients, to ensure the best possible treatment outcomes and minimize mortality.

Several approaches to the problem of guiding vasopressor dose adjustments in critically ill patients using mathematical modeling can be found in the literature. Bighamian et al. introduced a latency-dose-response cardiovascular model to predict MAP and other cardiovascular parameters in response to epinephrine dosing [11,12], employing phenomenological equations with parameters personalized for both normotensive and hypotensive patients, as well as piglets. Yapps et al. employed a logistic regression model to predict hypotension events using data on MAP and vasopressor dosing, either taken from a public database (MIMIC II) or collected in surgical ICU patients [13]. Tang et al. demonstrated a model for MAP prediction based on current MAP, heart period, NE infusion rate, and respiratory rate [14], which was later extended and validated using data from septic patients [15]. Recently, Kao et al. proposed a lumped-parameter cardiovascular model that incorporates baroreflex feedback and a dynamic dose-response model of vasopressors, validated using data from piglets receiving phenylephrine [16]. Also, machine-learning approaches have been explored to predict vasopressor requirements in critically ill patients [17–20]. However, none of the above studies addressed patients with sTBI.

Interestingly, Johnston et al., who investigated the pharmacodynamics and pharmacokinetics of dopamine and norepinephrine in a group of eight patients with moderate to severe head injury, found that the pharmacodynamics of NE seem to be unpredictable in these patients, showing no significant correlations between NE dose levels or plasma concentrations and MAP, cardiac index (CI), or systemic vascular resistance index (SVRI) [21]. While higher NE doses were generally associated with higher MAP and higher SVRI, they found no correlations between changes in plasma NE and changes in MAP, CI, or SVRI, which suggests inter-patient variability of hemodynamic response to NE. Therefore, it appears difficult to quantitatively predict the exact hemodynamic effects of increasing the dose of NE.

This apparent unpredictability of cardiovascular response to NE may stem from the fact that current methods primarily rely on analyzing only a few standard hemodynamic parameters, which may not be sufficient. The arterial pulse waveform can provide more detailed information on the status of the cardiovascular system, as it is the sum of the forward and reflected pulse waves, with reflections occurring wherever there is a change in blood flow, i.e., at vessel bifurcations or where the stiffness of the arteries changes [22]. Analysis of the pulse waveform can therefore provide additional information about the state of the arterial system [22]. For example, it can help assess arterial stiffness and evaluate the effects of vasoactive drugs [23,24]. Our goal was to determine whether information obtained from personalized pulse wave propagation modeling [25–29] could be useful in predicting the direction of change (or lack thereof) in the administered NE dose in sTBI patients.

Materials and methods

Ethics statement

The study was approved by the Bioethical Committee at the Medical University of Lublin, Poland (KE-0254/253/2020) and was performed in accordance with the Declaration of Helsinki and all applicable regulations. Written informed consent was obtained from each patient or their legal representative in case the patient was unconscious and/or under sedation at the time of enrolment in the study.

Study subjects

The study involved a cohort of 25 sTBI patients routinely treated at the intensive care unit; see Table 1 for group characteristics. Each patient was continuously monitored using a hemodynamic monitor, and based on its readings, especially MAP, and the patient's overall clinical condition, clinicians manually adjusted the vasopressor doses. All dose changes, along with the times of those changes, were documented. All patients received NE. Five patients received additionally dobutamine. Due to missing data on NE dosage, we had to exclude data from 3 patients. Data from further 2 patients were excluded due to poor quality of the recorded pulse waves. Thus, the final analysis is based on data from 20 patients.

Table 1. Characteristics of the studied patients and administered drugs.

	Unit	All patients (n = 25)	Analyzed patients (n = 20)
Male gender		18 (72%)	16 (80%)
Age	years	50.5 ± 19.5	50.7 ± 20.1
Body mass	kg	84.9 ± 16.6	85.7 ± 16.4
Height	cm	174.1 ± 9.5	175.0 ± 9.7
Norepinephrine		20 (80%)	16 (80%)
Norepinephrine + Dobutamine		5 (20%)	4 (20%)

Data are reported as frequencies (percentages) or means ± standard deviations.

https://doi.org/10.1371/journal.pcbi.1013501.t001

Pulse wave recordings

Arterial pulse waves were recorded once per day simultaneously on both wrists and ankles (four sites in total) using the AngE device (SOT Medical, Austria), which can perform simultaneous oscillometric recordings of pulse waves at multiple sites along with electrocardiogram (ECG); see Fig 1A for an overview of the measurement protocol. The device initially inflates the cuffs to 180 mmHg and records the pressure oscillations in all cuffs for 5 seconds. The pressure in all cuffs is then reduced by 10 mmHg and the 5-second recording is repeated. This process continues until the cuff pressure reaches 40 mmHg. Thus, the total duration of a single recording is about 2 minutes; see Fig 1B for exemplary pulse wave recording. The recorded oscillations represent changes in the cuff pressure caused by the pulsatile changes of arterial volume under the cuff (attenuated to some extent), and hence for cuff pressure close to the diastolic pressure the shape of the obtained wave may be treated as relatively closely resembling the shape of the arterial volume wave [30,31]. After the recording, for each cuff, the device selects the 5-second fragment of the wave with the highest amplitude, potentially recorded at different pressure levels in different cuffs (hence at different times). For our analysis, we took from all cuffs the pulse wave fragments corresponding to the same cuff pressure level (the closest to the average level selected by the device) to analyze the waves recorded simultaneously at all sites. For each recording site, we then averaged all beats from the selected fragment of the recorded wave to obtain a single arterial volume waveform. We did not observe any significant wave profile changes following the averaging procedure. Such average waveforms from all four recording sites were used in the model optimization step (see further sections).

Note that in order to obtain the waveform that would most closely reflect the shape of the true arterial volume waveform, one should perform the recording with the cuff pressure kept at a level slightly below the local diastolic pressure (DP), since cuff pressures above DP lead to temporary occlusion of the arteries and hence lead to some distortion of the recorded waves [30,31]. However, at low cuff pressures, the amplitude and the overall quality of the recorded wave are much lower, which in some cases makes it difficult to identify individual beats and ultimately makes the averaged shape of the waveform less reliable (especially in patients with low pressure amplitude). Therefore, in this study, we decided to use the waves with the highest amplitude (as mentioned earlier), which were recorded at cuff pressure close to MAP, thus somewhat higher than DP. In other words, we used waveforms whose shape may differ slightly from the shape of actual arterial volume waves, but this enabled us to efficiently identify individual beats and hence obtain the averaged waveforms that could be used in our framework. Moreover, even if there was no occlusion of the arteries below the cuff, the waveform observed at the cuff level could still be slightly different from the actual arterial volume waveform due to the fact that the tissues between the arteries and the cuff (including the artery wall itself) may transmit the volume changes to a different extent at different pressure levels (in all cases largely attenuated).

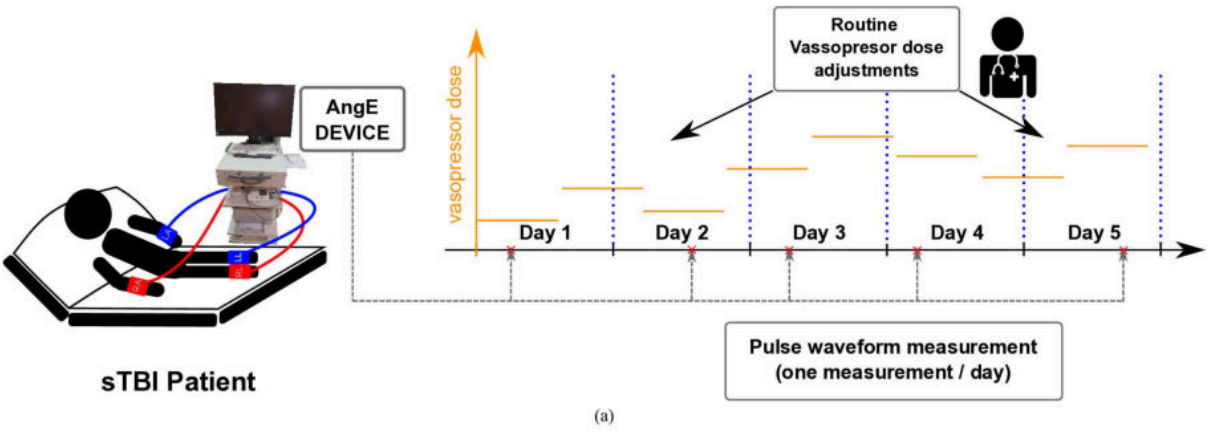

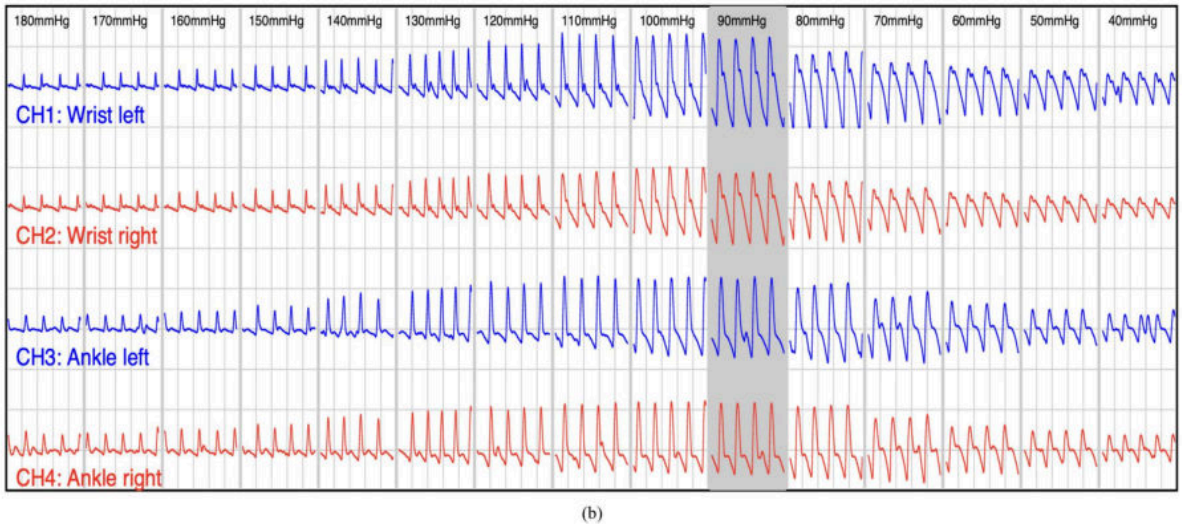

Fig 1. Study protocol and exemplary oscillometric waves recorded by the AngE device. (a) During the treatment (up to 5 days) one recording of pulse waves was taken each day (at various times of day) using the AngE device, while the vasopressor dose was routinely adjusted. (b) Exemplary pulse waves recorded by the AngE device.

https://doi.org/10.1371/journal.pcbi.1013501.g001

Note also that in this study, we fit the model-simulated volume waveforms from a specific artery under the cuff (e.g., the radial artery) to the cuff-recorded waveforms, which in fact, reflect blood volume changes not in one specific artery but in all arteries below the cuff (e.g., also in the ulnar artery). This is another simplification of our approach, in which we assumed that the shapes of the volume waveforms in the radial and ulnar arteries are relatively similar to each other, and hence we treated the waveform observed at the cuff level as corresponding to the volume waveform of the radial artery. Moreover, given the relatively low changes in the diameter of the radial artery along its length, we assume that the volume waveform of the fragment of the radial artery under the cuff is equivalent to volume waveforms in other parts of the radial artery, and hence, for simplicity, we analyze model-simulated volume waveform of the whole radial artery (similarly for the anterior tibial artery for the recordings at the ankle cuffs).

Other data obtained from the AngE device

In addition to recording the oscillometric waves, the AngE device also provides a number of cardiovascular parameters, some of which were used in our analysis. These include information on heart rate (HR) and blood pressure, i.e., systolic pressure (SP), diastolic pressure (DP), and mean arterial pressure (MAP), as well as parameters related to the recorded pulse waves, i.e., the duration of the rise in the pulse waveform from its foot to peak ('rise time'), and the ratio of the duration of the rise in the pulse waveform and the duration of its fall from peak to the foot of the next wave ('rise to fall'), calculated for the waveforms from each limb separately.

Pulse wave propagation model

We utilized a one-dimensional arterial network model composed of 71 main compliant arteries connected to zero-dimensional boundary conditions. For a detailed description of the model, please refer to our previous publications [32–34] and S1 File. The model simulates pulsatile blood flow and the corresponding blood pressure and volume waves in the whole modeled arterial tree, taking into account patient-specific characteristics, such as terminal vascular resistances, stiffness of arteries, and left-ventricular time-varying elastance function (LVTVE). We used the Levenberg-Marquardt optimization algorithm to minimize the objective (error) function by adjusting selected subject-specific model parameters. The objective function included the differences (errors) between simulated and recorded pulse waveforms (arterial volume waveforms) in four considered locations, the differences between recorded (on the cuff on the left wrist) and simulated (on the radial artery) SP and DP, and a penalty term to penalize abnormal (unphysiological) values of the simulated stroke volume (SV), according to the following equation:

$$\begin{aligned} \mathrm{err} = & \sum_{i\in(\mathrm{left/rightarm,left/rightleg})} \sum_{j=1}^{n} \left\| V_{\mathrm{norm,sim;i;j}} - V_{\mathrm{norm,meas;i;j}} \right\|^2 \\ & + \left\| DP_{\mathrm{sim}} - DP_{\mathrm{meas}} \right\|^2 /20 + \left\| SP_{\mathrm{sim}} - SP_{\mathrm{meas}} \right\|^2 /20 + \left(\frac{(SV_{\mathrm{sim}} - 70)}{40} \right)^6 \end{aligned} \tag{1}$$

where *norm*, *sim* and *meas* denote normalized, simulated and measured values, respectively, $\|\cdot\|$ is a l_2-norm, n=1000 is the number of analyzed time points in the normalized simulated and measured arterial volume waveforms (V); see S1 File and Fig 2 for details (including the explanation with regard to the weights of the individual terms in our objective function).

In order to select model parameters to be optimized during the above minimization procedure, we performed a sensitivity analysis combined with an identification analysis. To this end, we first performed the Sobol' sensitivity analysis [35,36] and calculated the first-order sensitivity indices (for each studied parameter, at multiple time points of the cardiac cycle), which quantify the direct contributions of individual parameters to the given model output variability (see Sensitivity analysis section in S1 File for details). Then we performed a parameter identification analysis using the procedure described by Olufsen et al. [37], which determines the possible pairwise correlations between the selected model parameters by calculating the relative local sensitivity matrix followed by the calculation of the inverse of the Hessian matrix (see Parameter identification section in S1 File for details). Following the above calculations, we selected five model parameters for which the analyzed outputs of the model (i.e. arterial volume waveforms at the considered locations as well as SP and DP) showed the greatest sensitivity and which were not highly correlated with each other. In particular, we selected the following model parameters: t_m (time to the onset of constant LVTVE), E_{max} (maximal value of the LVTVE function), S_R (scaling factor for the resistances of small arteries and arterioles), p_{la} (pressure in the left atrium), and k_3 (a parameter describing the stiffness of the large arteries). The values of all other parameters of the model were fixed at the levels taken from the literature as typical values for a 45-year-old man weighing 75 kg. Specifically, the values of parameters describing the stiffness of the arteries were based on a formula derived from the work of Olufsen et.al. [38], while the resistance and compliance parameters of small arteries and arterioles were taken from the work of Alastruey et al. [39]. In addition, some of the fixed parameter values were also scaled according to patient's height. More details on the selection of individual parameters and their exact values, along with references, can be found in S1 File.

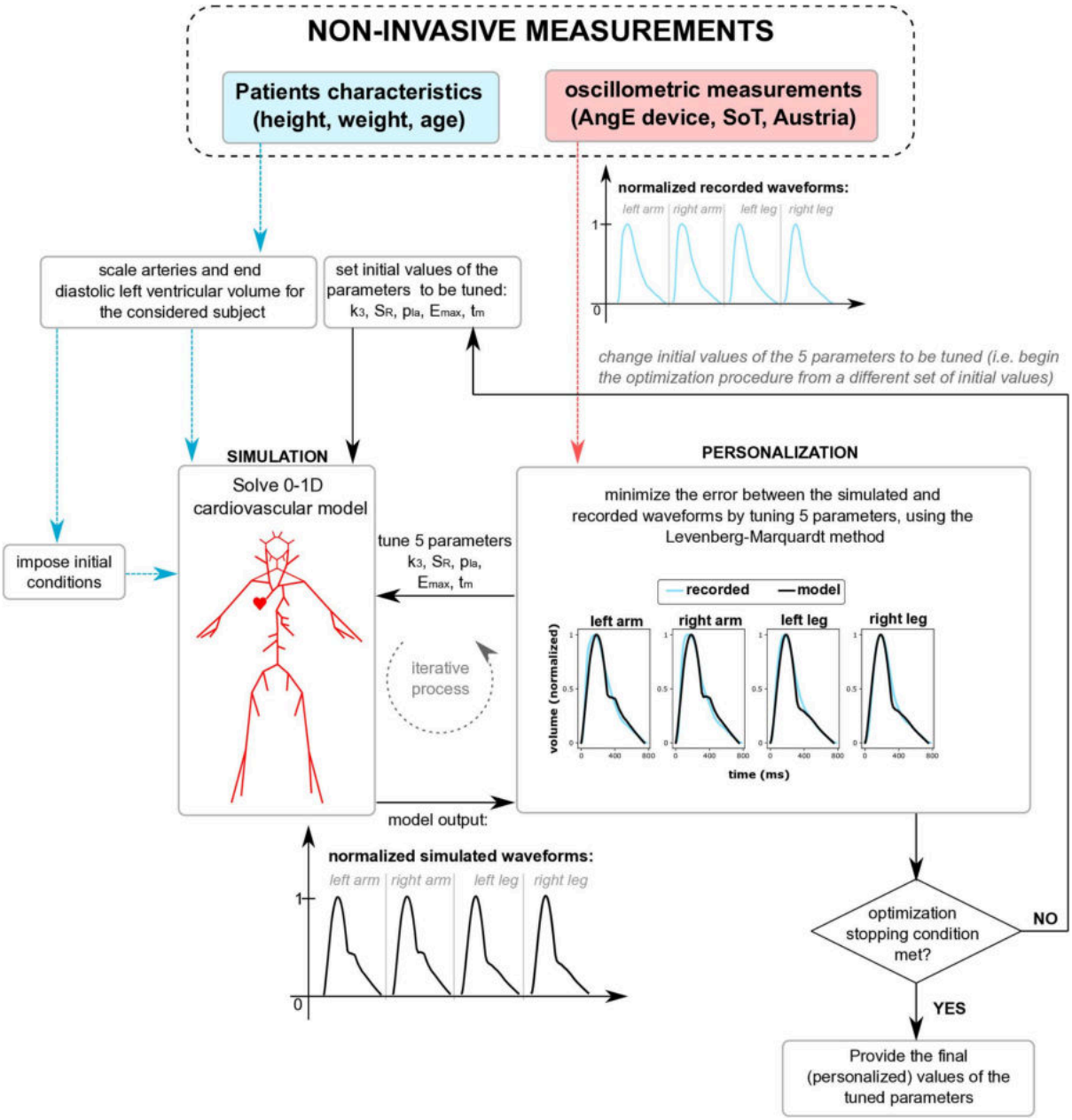

Fig 2. Overview of the personalization (i.e., patient-specific optimization) of the pulse wave propagation model. Fitting of the model-simulated arterial volume waveforms at four sites (wrists and ankles) to recorded waveforms by tuning selected model parameters.

https://doi.org/10.1371/journal.pcbi.1013501.g002

Predictive model

To investigate the clinical utility of the model-derived, patient-specific cardiovascular parameters, we incorporated them into a statistical model to predict whether the next NE dose adjustment within 24 hours will increase the dose or not. More precisely, for each case (i.e., each time of pulse wave recording), we assigned one of two labels as follows:

- 0 (negative class) - if within 24 hours from the given pulse wave measurement, there was no dose adjustment or the first adjustment lowered the NE dose,
- 1 (positive class) - if the first dose adjustment within 24 hours from the pulse wave measurement increased the NE dose.

We used a generalized mixed linear model with a binomial link function. This model can be viewed as a logistic regression classifier suitable for data where the assumption of observation independence is violated. A detailed description of the method can be found in [40] . We considered two versions of the predictive model – a full model and a simplified model. The features considered in our full model included five patient-specific cardiovascular parameters obtained from fitting the 0-1D model to recorded pulse waves and blood pressure data (t_m, E_{max}, p_{la}, k_3, and S_R), patient characteristics (age, height, and weight), standard cardiovascular parameters measured by the AngE device (HR, SP, DP, MAP), pulse wave-related parameters provided by the AngE device (rise time of the recorded waveform from all four cuffs, and 'rise to fall' ratio of the recorded waveform from all four cuffs), current NE dose, and pulse wave velocity (PWV) calculated using our pulse wave propagation model (between the beginning of the ascending aorta and the end of the femoral artery, using the foot-to-foot method). To assess the utility of the parameters related to pulse waveforms (both obtained from the AngE device and estimated from our model), we also analyzed a simplified model that excluded these parameters and was based solely on patient characteristics, HR and blood pressure data, and NE dose. All features were standardized to avoid numerical problems in the process of optimizing model parameters. For both full and simplified models, the feature selection for the final model was performed using the step-wise procedure based on the Akaike Information Criterion [41]. The model performance was validated using the leave-one-out cross-validation, a suitable approach for small datasets [42]. A probability threshold of 0.5 was used, meaning that patients with a predicted probability of having an increased vasopressor dose above 0.5 were classified as belonging to the positive class.

Results

Model fits to recorded pulse waveforms

The quality of the model fits to the recorded arterial volume waveforms was satisfactory, with the mean coefficients of determination (R^2) of 0.92, 0.91, 0.88, and 0.90 for the left arm, right arm, left leg, and right leg, respectively; Fig 3A shows the plots comparing all normalized model-estimated and recorded arterial volume waveforms. The model accurately estimated MAP with the mean difference between the model-derived and measured values of 0.1 ± 1.0 mmHg ($R^2 = 0.99$), with no dependence on the MAP level (Pearson's $r = 0.11$, p-value $= 0.35$), see Fig 3B. An exemplary model fit to the recorded waveform is presented in Fig 3C; see Figs A – D in S2 File for all model fits.

Correlations between vasopressor doses and estimated parameters

After fitting the model to the recorded waveforms and blood pressure data, we compared the estimated patient-specific cardiovascular parameters with the NE doses at the times of pulse wave recordings. We found no correlations between the model parameters and NE doses neither for the entire cohort, nor for individual patients. Only in a few patients (ID = 1, 2, 4) we observed some qualitative associations between the NE doses and parameters k_3 and S_R, see Fig 4. Similarly, we compared SP and DP (both estimated by the model and measured by AngE). In this case, we also did not observe any correlations, except for patient ID = 6, in whom SP and DP values also increased with increasing NE dose during treatment (see Figs A and B in S3 File).

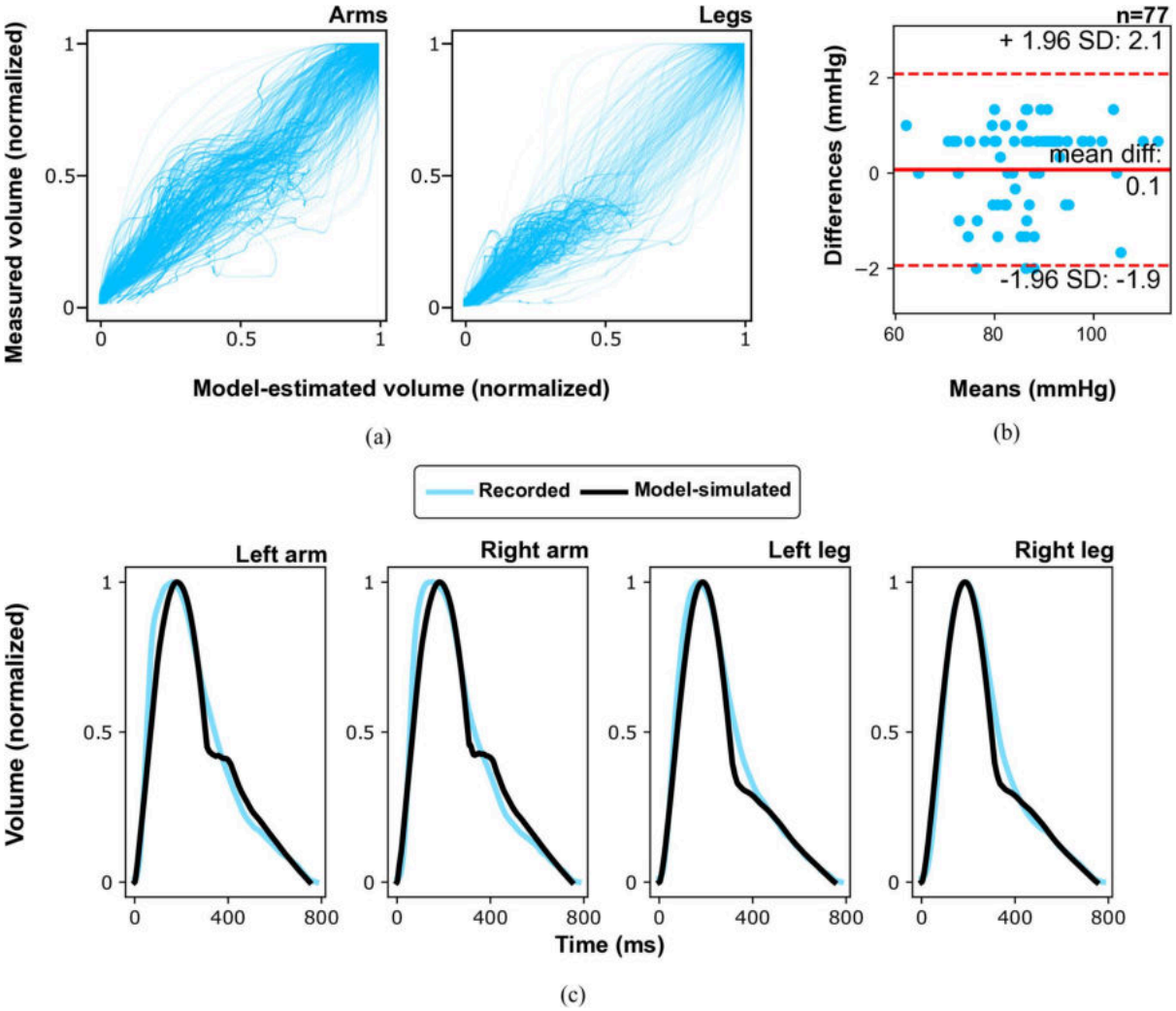

Fig 3. Quality of model fits to recorded data. (a) Comparison of the recorded arterial volume waveforms and corresponding in time model-simulated volume waveforms, with both the recorded and simulated waveforms normalized in amplitude (n = 77). The perfect match of the two waveforms corresponds to a diagonal line. (b) Bland-Altman plot comparing the measured and model-estimated mean arterial pressure for all analyzed cases (n = 77). (c) Typical model-simulated arterial volume waveforms (black lines) compared to the recorded (averaged) waveforms (light blue lines).

https://doi.org/10.1371/journal.pcbi.1013501.g003

Prediction of vasopressor dose change

The dataset used in our analysis consisted of 88 observations (i.e., separate pulse wave recordings) from a group of 20 patients, among which for 77 observations we were able to assign a label 0 or 1 (the remaining observations did not have sufficient follow-up time of 24 hours). During the step-wise feature selection for our predictive model (full model), 10 features were found to be associated with the target outcome; see Table 2. Notably, these features included two model-estimated cardiovascular parameters: p_{la}, and E_{max}, that is left-atrial pressure, and maximal value of the LVTVE function, respectively. When trained and tested on the entire dataset, the model achieved a balanced accuracy of 0.85 (accuracy

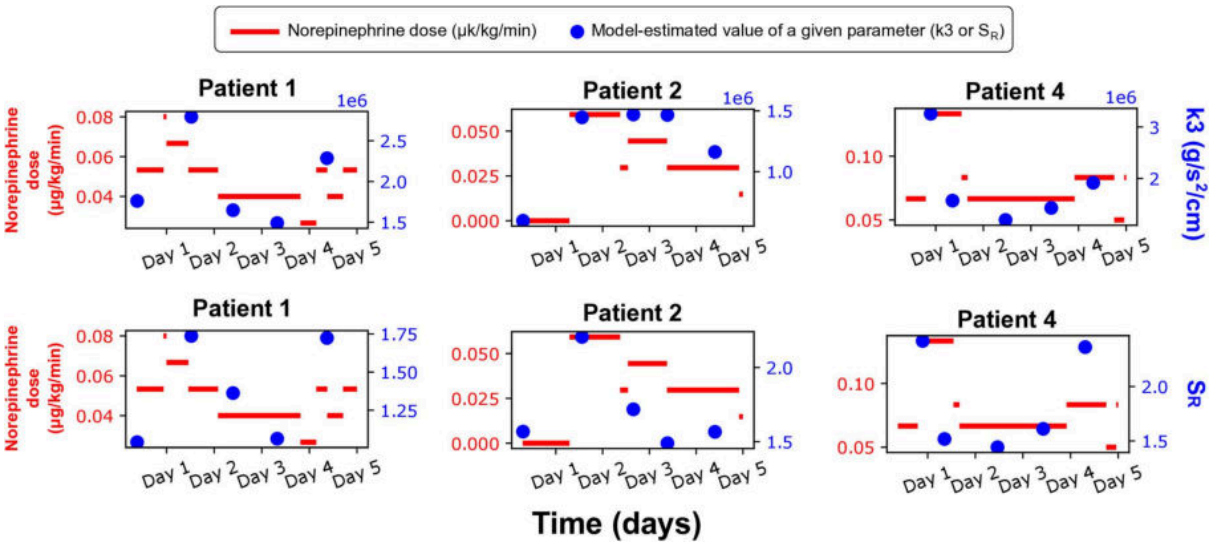

Fig 4. Norepinephrine dose vs patient-specific model-estimated parameters k_3 and S_R for three selected patients. Shown are values of the parameters (blue dots) and norepinephrine doses (red lines).

https://doi.org/10.1371/journal.pcbi.1013501.g004

0.90). When validated using the leave-one-out cross-validation (LOOCV), the model's balanced accuracy was 0.76 (accuracy 0.82). The confusion matrices for the full model trained and tested on the entire dataset or tested using LOOCV are presented in Table 3.

Table 2 also shows the features selected for the simplified model, which excluded pulse wave-related parameters (either derived from the AngE device or obtained from the pulse wave propagation model). This simplified model exhibits

Table 2. The coefficients of the full and simplified models predicting norepinephrine dose changes. The features included in the presented models were based on the step-wise feature selection procedure using the Akaike Information Criterion.

Feature	Full model		Simplified model		Description
	Coefficient	P-value	Coefficient	P-value	
Intercept	-1.82	<0.001	-2.48	0.05	
Norepinephrine dose	-1.80	<0.05	-2.77	<0.01	
HR	4.24	<0.05	0.06	<0.01	Heart rate
Height	1.21	<0.05	0.06	0.10	
Weight	-0.68	0.12	-0.05	0.07	
MAP	–	–	-0.11	<0.01	Mean arterial pressure
E_{max}	-1.48	0.09	–	–	Maximal value of the LVTVE function
p_{la}	-1.69	<0.05	–	–	Left-atrial pressure
Rise time (right wrist)	3.41	<0.01	–	–	Duration of the rise in the pulse waveform from the right arm (from foot to peak)
Rise to fall (right wrist)	-1.92	0.14	–	–	The ratio of the duration of the rise in the pulse waveform in the right arm (from foot to peak) and the duration of its fall (from peak to the foot of the next wave)
DP	-2.11	<0.01	–	–	Diastolic pressure measured with the left arm cuff
PWV	-1.24	<0.05	–	–	Pulse wave velocity calculated from the model

https://doi.org/10.1371/journal.pcbi.1013501.t002

Table 3. Confusion matrices for the predictions of the full model trained and tested on the entire dataset or validated using the leave-one-out cross validation (LOOCV).

	Entire dataset		LOOCV	
	Predicted Negative	Predicted Positive	Predicted Negative	Predicted Positive
Actual Negative	53	2	49	6
Actual Positive	6	16	8	14

https://doi.org/10.1371/journal.pcbi.1013501.t003

lower balanced accuracy compared to the full model, both when trained and tested on the entire dataset (0.75) and when validated using LOOCV (0.67). A detailed comparison of the performance metrics of the two models is provided in Table 4.

In S4 File, we illustrated the predictions of the NE dose adjustments corresponding to all pulse wave recordings in all analyzed patients (the results from the full model trained and tested on the entire dataset). In some cases, despite the incorrect prediction, the model correctly anticipated the overall trend in dose adjustments (see patients with ID 7 and 18). Interestingly, in the case of the patient with ID = 18, the prediction in Day 1 was a false negative (see Fig A in S4 File) with a very low probability value (0.02). This prediction was false because at the next dose adjustment the NE dose was increased; however, this dose increase was only transient, and soon the dose was decreased to much lower levels.

For some observations from the last day, we did not have information about the potential changes in NE dose in the following 24 hours. These cases were excluded from our main analysis, but we proceeded with predictions for these cases anyway, even if their accuracy could not be assessed. In each of these cases, the model predicted that the dose would remain constant or be decreased within the next 24 hours, which seems to be expected, as one would expect the patient's condition to improve after 4–5 days of treatment.

Discussion

In our study on patients with severe traumatic brain injury, we explored the potential of using information extracted from arterial pulse waveforms (either directly or through pulse wave propagation modeling) to predict changes in NE dose administration that will likely be needed within the next 24 hours. We showed that knowledge of selected patient-specific cardiovascular parameters derived from the pulse waveforms, which are not measured during standard treatment procedures, appears to be useful for predicting changes in the administered NE dose in these patients possibly providing some insights into the mid- to long-term effects of the current NE dose considering the current state of patient's cardiovascular system, thus providing the basis for a tool that could be potentially used to guide vasopressor dosing, in particular with regard to adjusting the doses sooner.

Table 4. Metrics of performance of the full predictive model trained and tested on the entire dataset (see the confusion matrix in Table 3), along with the comparison with the simplified model (also trained and tested on the entire dataset).

	Full model	Simplified model	Advantage of the full model (%)
Accuracy	0.90	0.83	7.8
Sensitivity/True Positive Rate/Recall	0.73	0.55	33.3
Specificity/True Negative Rate	0.96	0.95	1.9
Balanced Accuracy	0.85	0.75	13.4
False Positive Rate	0.04	0.05	-33.3
Precision	0.89	0.80	11.1
F1-score	0.80	0.65	23.3

https://doi.org/10.1371/journal.pcbi.1013501.t004

Key results

The proposed statistical model predicting NE dose adjustments (full model) is based on 10 features, including three features derived from the 0-1D cardiovascular model (E_{max}, p_{la}, and PWV) and two features computed directly from the recorded pulse waveform ('rise time' and 'rise to fall' ratio in the right arm). Integrating the parameters available from the AngE measurements with parameters obtained from the cardiovascular model optimization enhances the performance of our predictive model. Specifically, the model that included pulse-wave-derived features (full model), exhibited a 33.3% higher sensitivity (i.e., the rate of correct predictions of NE dose increases) and 13.4% higher balanced accuracy compared to the model without those features (simplified model) when trained and tested on the entire dataset; see Table 4 for more details. The markedly higher sensitivity while maintaining similar specificity is essential from our perspective, as accurately predicting that the vasopressor dose is likely to be increased within the next 24 hours seems to be particularly important when focused on preventing episodes of hypotension in sTBI patients.

All analyzed patients were treated with NE; four patients were also given dobutamine. The effects of NE include, among others, vasoconstriction, which leads to increased arterial stiffness [43]. In line with this, the proposed predictive model accounts for the model-estimated PWV, a standard marker of arterial stiffness [44]. NE also improves end-systolic elastance [45] and increases the heart rate [46] and systemic diastolic blood pressure [47], all of which are features of our full model (end-systolic elastance is described by E_{max}). According to our predictive model, higher values of p_{la} and PWV are associated with a decreased likelihood of requiring an increased NE dose within the next 24 h. This is not unexpected, given that these parameters are related to blood pressure. The fact that they were selected as predictors for our predictive model suggests that they may carry information on the current state of the cardiovascular system that may not be captured by standard cardiovascular parameters. Interestingly, our full predictive model does not include MAP as a predictor, although it is the main parameter used by clinicians to determine vasopressor dosage. However, MAP can be estimated from systolic blood pressure (SP) and diastolic pressure (DP) using a linear relationship, such as MAP = 2/3DP + 1/3SP [48], which may explain the absence of MAP and presence of DP in our full model. Indeed, during our various tests, when we removed SP and DP from the set of potential predictors, MAP emerged as an important predictor.

Secondary findings

We also compared the patient-specific cardiovascular parameters estimated during model optimization (i.e., k_3, S_R, t_m, E_{max} and p_{la}) with the NE doses. In general, we did not find any relationship between NE doses and the estimated parameter values. As shown in previous studies [21,49] the pharmacodynamics of NE appear unpredictable and may be due to patient variability. Such variability may explain the observed lack of relationship between the values of the estimated parameters and the administered NE doses in our cohort. However, in three patients (ID = 1, 2, 4) we observed relatively similar patterns between NE doses and the values of two estimated parameters: k_3 and S_R. We believe that this was not coincidental and may be due to the fact that NE is responsible, among others, for the increase in peripheral resistance (S_R is the scaling factor for the resistances of small arteries and arterioles) and arterial stiffness (k_3 describes the stiffness of large arteries). The fact that such relationships were not observed in other patients may be due to the effects of other vasoactive substances, e.g., endogenous catecholamines, which can disrupt the relationship between NE dose and the discussed parameters [50], or due to impact of other drugs not considered in our study, or due to neural mechanisms controlling vascular tone (also not considered in our study).

Other studies

The problem of optimizing the dosing of vasopressors in critically ill patients has been the subject of multiple studies. For predicting a patient's condition or the required vasopressor dose, researchers mainly use standard hemodynamic parameters that are routinely measured during standard treatment procedures and validate their methods using data from ICU

patients [17–20]. In the case of mathematical models of the hemodynamic response to vasopressors, the models are mainly validated using data from either healthy individuals [11,12], septic patients [14,15], or animals [16]. To our knowledge, however, no such predictive or modelling studies have focused on sTBI patients, and hence our study seems to be the first to use personalized cardiovascular parameters estimated from a pulse wave propagation model (based on non-invasive oscillometric measurements of arterial pulse waveforms) to be fully conducted on data from a cohort of sTBI patients treated with NE.

Recently, a novel approach to vasopressor dosing has been proposed by Rinehart et. al. who developed a closed-loop controller for automatized vasopressor administration (targeting MAP) in perioperative or intensive care settings [51,52].This controller has been subsequently tested by Joostens et. al. in a randomized controlled study on titrating NE in 18 sTBI patients [53], showing that in patients in whom NE was titrated in an automatically controlled manner, MAP remained within the target range 96% of time on average (over the four-hour study period), as compared to only 43% of time in the group with standard, manual NE titration. The approach by Rinehart and Joostens, i.e., automatized NE titration, is entirely different to that considered in our study, and while it offers a great perspective for a fully automatized process of vasopressor dosing (not only in sTBI patients but in other critically ill patients or in patients undergoing surgeries), it requires special or modified equipment for drug titration. On the other hand, our approach could potentially lead to improved vasopressor dosing strategies within standard care using the existing equipment. Moreover, it is possible that integrating pulse wave features in a controller targeting MAP could potentially lead to even better performance of such a controller.

Limitations

Our study has certain limitations. First, our findings are based on relatively limited data from a small cohort of patients, with only one pulse wave recording per day at various, arbitrary times, unrelated to vasopressor dose adjustments (although despite this, our full model was able to predict with relatively high balanced accuracy (0.85) whether the NE dose would be increased within the next 24 hours). Second, the data to which the model is fitted is subject to error measurement and natural variability (especially blood pressure), and therefore it may not necessarily reflect accurately the current (average) state of the cardiovascular system. Moreover, although the model parameters that were fixed rather than adjusted appear to have little effect on the arterial volume waveforms and blood pressure, possible changes in many of these parameters could collectively have a non-negligible effect on the behavior of the modeled system and thus on the values of the estimated (adjusted) parameters, which in turn could affect the predictions in our statistical model. Furthermore, by adjusting the value of parameter S_R, we assume that the resistance of all small arteries and arterioles (the terminal 0D elements in our model) changes to the same extent (in percentage terms, from their baseline values), which is a simplification, given that vessels in different tissues and organs may respond differently to vasoactive substances (not only in terms of the magnitude of the change in their tone but even in terms of the direction of this change) and may be also subject to varying degrees of vascular autoregulation (e.g., in cerebral vessels, although in patients with sTBI cerebrovascular autoregulation is frequently impaired [54]). Also, for simplicity, in all our simulations we assumed intact cerebral vasculature, thus ignoring the fact that patients with sTBI will likely experience alterations in cerebrovascular function, which could affect the total cerebral resistance and compliance and thus could influence central and peripheral hemodynamics, potentially affecting the results of our study. Finally, the presented approach is based on recording pulse waveforms at multiple locations (to account for the possible differences in peripheral pulse waveforms between different limbs, we chose to fit our cardiovascular model to pulse waveforms from four sites, recorded oscillometrically). We want to highlight, however, that the proposed methodology could be potentially used with pulse waveform recorded only at a single site, thus not necessarily requiring recordings on four limbs. Moreover, one could use arterial volume waveforms recorded using other methods, or use arterial pressure waveforms (e.g., recorded using applanation tonometry).

Conclusions and future work

This study provides a preliminary demonstration of the potential of pulse wave propagation modeling for sTBI patient management. Using the data collected in sTBI patients, we developed a statistical model to predict vasopressor dose increases within 24 hours with relatively high balanced accuracy (0.85). Including in this predictive model the patient-specific parameters related to arterial stiffness and heart function, estimated from the pulse wave propagation model, turned out to provide a higher model sensitivity compared to the model without pulse wave-related features. The proposed framework could be potentially used to adjust vasopressor doses not only based on the current condition of the patient (as is currently done) but also (to some extent) taking into account predictions of vasopressor dose adjustments that are likely to be needed in the future. However, it is not obvious yet how exactly the vasopressor doses could be adjusted taking into account the predictions of the proposed model and whether this would lead to improved patient outcomes. Moreover, here we proposed a model for predicting whether the vasopressor dose will be increased by clinicians within 24 hours from the given time (the time of recording the pulse wave and blood pressure), which can be treated only as indirect information of the likely future state of the patient. Ideally, a similar framework should be developed with a model predicting directly the future state of the patient (e.g., MAP). Future studies should investigate these aspects using more comprehensive models (with various cardiovascular regulatory mechanisms) and more data, including more frequent pulse wave recordings, continuous vital parameter monitoring, and data on endogenous catecholamines.

Supporting information

S1 File. Detailed description of the mathematical model and sensitivity analysis.
(PDF)

S2 File. Fits of the model-simulated arterial volume waveforms to the recorded waveforms.
(PDF)

S3 File. Visualization of changes of systolic and diastolic pressure during the treatment.
(PDF)

S4 File. Visualization of the vasopressor doses and their adjustments during the observation period, along with the predictions of the statistical model (full model) with regard to the changes in vasopressor dose within the next 24 hours from the time of pulse wave recording.
(PDF)

Author contributions

Conceptualization: Kamil Wołos, Jan Poleszczuk.

Data curation: Wojciech Dabrowski, Dorota Siwicka-Gieroba.

Formal analysis: Kamil Wołos.

Funding acquisition: Malgorzata Debowska, Wojciech Dabrowski, Dorota Siwicka-Gieroba, Jan Poleszczuk.

Investigation: Kamil Wołos.

Methodology: Kamil Wołos, Leszek Pstras, Urszula Bialonczyk, Malgorzata Debowska, Wojciech Dabrowski, Dorota Siwicka-Gieroba, Jan Poleszczuk.

Project administration: Kamil Wołos, Jan Poleszczuk.

Software: Kamil Wołos.

Supervision: Leszek Pstras, Malgorzata Debowska, Jan Poleszczuk.

Validation: Kamil Wołos, Leszek Pstras, Urszula Bialonczyk, Jan Poleszczuk.

Visualization: Kamil Wołos.

Writing – original draft: Kamil Wołos.

Writing – review & editing: Leszek Pstras, Urszula Bialonczyk, Jan Poleszczuk.

References

1. Yan A, Torpey A, Morrisroe E, Andraous W, Costa A, Bergese S. Clinical Management in Traumatic Brain Injury. Biomedicines. 2024;12(4):781. https://doi.org/10.3390/biomedicines12040781 PMID: 38672137
2. Rakhit S, Nordness MF, Lombardo SR, Cook M, Smith L, Patel MB. Management and Challenges of Severe Traumatic Brain Injury. Semin Respir Crit Care Med. 2021;42(1):127–44. https://doi.org/10.1055/s-0040-1716493 PMID: 32916746
3. Robbins B, Almassalkhi L, Baum R, Blackburn M, Davis J, Edwards L. Pharmacotherapy adjuncts for traumatic brain injury: A narrative review of evidence and considerations in the emergency department. Am J Emerg Med. 2025;89:78–84.
4. Sookplung P, Siriussawakul A, Malakouti A, Sharma D, Wang J, Souter MJ, et al. Vasopressor use and effect on blood pressure after severe adult traumatic brain injury. Neurocrit Care. 2011;15(1):46–54. https://doi.org/10.1007/s12028-010-9448-9 PMID: 20878264
5. Toro C, Ohnuma T, Komisarow J, Vavilala MS, Laskowitz DT, James ML. Early vasopressor utilization strategies and outcomes in critically ill patients with severe traumatic brain injury. Anesth Analg. 2022;135(6):1245.
6. Rossaint R, Afshari A, Bouillon B, Cerny V, Cimpoesu D, Curry N, et al. The European guideline on management of major bleeding and coagulopathy following trauma: sixth edition. Crit Care. 2023;27(1):80.
7. Stampfl M, DeBlieux P. A clinical review of vasopressors in emergency medicine. J Emerg Med. 2024;67(1):e31-41.
8. Carney N, Totten AM, O'Reilly C, Ullman JS, Hawryluk GWJ, Bell MJ, et al. Guidelines for the Management of Severe Traumatic Brain Injury, Fourth Edition. Neurosurgery. 2017;80(1):6–15. https://doi.org/10.1227/NEU.0000000000001432 PMID: 27654000
9. Russell JA, Gordon AC, Williams MD, Boyd JH, Walley KR, Kissoon N. Vasopressor Therapy in the Intensive Care Unit. Semin Respir Crit Care Med. 2021;42(1):59–77. https://doi.org/10.1055/s-0040-1710320 PMID: 32820475
10. Rinehart J, Ma M, Calderon MD, Bardaji A, Hafiane R, Van der Linden P, et al. Blood pressure variability in surgical and intensive care patients: Is there a potential for closed-loop vasopressor administration?. Anaesth Crit Care Pain Med. 2019;38(1):69–71. https://doi.org/10.1016/j.accpm.2018.11.009 PMID: 30513357
11. Bighamian R, Reisner AT, Jin-Oh Hahn. An analytic tool for prediction of hemodynamic responses to vasopressors. IEEE Trans Biomed Eng. 2014;61(1):109–18. https://doi.org/10.1109/TBME.2013.2277867 PMID: 23955691
12. Bighamian R, Soleymani S, Reisner AT, Seri I, Hahn J-O. Prediction of Hemodynamic Response to Epinephrine via Model-Based System Identification. IEEE J Biomed Health Inform. 2016;20(1):416–23. https://doi.org/10.1109/JBHI.2014.2371533 PMID: 25420273
13. Yapps B, Shin S, Bighamian R, Thorsen J, Arsenault C, Quraishi SA, et al. Hypotension in ICU Patients Receiving Vasopressor Therapy. Sci Rep. 2017;7(1):8551. https://doi.org/10.1038/s41598-017-08137-0 PMID: 28819101
14. Tang Y, Brown S, Sorensen J, Harley JB. Reduced Rank Least Squares for Real-Time Short Term Estimation of Mean Arterial Blood Pressure in Septic Patients Receiving Norepinephrine. IEEE J Transl Eng Health Med. 2019;7:4100209. https://doi.org/10.1109/JTEHM.2019.2919020 PMID: 31475080
15. Tang Y, Brown SM, Sorensen J, Harley JB. Physiology-Informed Real-Time Mean Arterial Blood Pressure Learning and Prediction for Septic Patients Receiving Norepinephrine. IEEE Trans Biomed Eng. 2021;68(1):181–91. https://doi.org/10.1109/TBME.2020.2997929 PMID: 32746013
16. Kao YM, Sampson CM, Shah SA, Salsbury JR, Tivay A, Bighamian R. A Mathematical Model for Simulation of Vasoplegic Shock and Vasopressor Therapy. IEEE Transactions on Biomedical Engineering. 2023;70(5):1565–74.
17. Holder AL, Shashikumar SP, Wardi G, Buchman TG, Nemati S. A Locally Optimized Data-Driven Tool to Predict Sepsis-Associated Vasopressor Use in the ICU. Crit Care Med. 2021;49(12):e1196–205. https://doi.org/10.1097/CCM.0000000000005175 PMID: 34259450
18. Kwak GH, Ling L, Hui P. Predicting the Need For Vasopressors in the Intensive Care Unit Using an Attention Based Deep Learning Model. Shock. 2021;56(1):73–9. https://doi.org/10.1097/SHK.0000000000001692 PMID: 33177372
19. Choi Y, Kim KH, Kim Y, Choi DH, Joo YH, Choi SW, et al. Prediction of vasopressor needs in hypotensive emergency department patients using serial arterial blood pressure data with deep learning. Hong Kong J Emerg Med. 2024;31(5):233–41.
20. Prasad V, Reisner AT, Lynch JC, Filbin MR, Heldt T. Modeling of Usual Care: Vasopressor Initiation for Sepsis With Hypotension. Front Med (Lausanne). 2022;9:715856. https://doi.org/10.3389/fmed.2022.715856 PMID: 35360743
21. Johnston AJ, Steiner LA, O'Connell M, Chatfield DA, Gupta AK, Menon DK. Pharmacokinetics and pharmacodynamics of dopamine and norepinephrine in critically ill head-injured patients. Intensive Care Med. 2004;30(1):45–50. https://doi.org/10.1007/s00134-003-2032-4 PMID: 14586494
22. Westerhof N, Stergiopulos N, Noble MIM, Westerhof BE. Wave Travel and Reflection. Snapshots of Hemodynamics. Springer International Publishing. 2018. 75–88. https://doi.org/10.1007/978-3-319-91932-4_12

23. O'Rourke M, Adji A. Contour of pressure and flow waves in arteries. McDonald's blood flow in arteries. 7th ed. CRC Press. 2022.
24. Reavette RM, Ramakrishnan A, Rowland EM, Tang MX, Mayet J, Weinberg PD. Detecting heart failure from B-mode ultrasound characterization of arterial pulse waves. Am J Physiol-Heart Circ Physiol. 2024;327(1):H80-8.
25. Bikia V, Rovas G, Stergiopulos N. Cardiac output estimated from an uncalibrated radial blood pressure waveform: validation in an in-silico-generated population. Front Bioeng Biotechnol. 2023.
26. Bikia V, Papaioannou TG, Pagoulatou S, Rovas G, Oikonomou E, Siasos G, et al. Noninvasive estimation of aortic hemodynamics and cardiac contractility using machine learning. Sci Rep. 2020;10(1):15015. https://doi.org/10.1038/s41598-020-72147-8 PMID: 32929108
27. Bikia V, Pagoulatou S, Trachet B, Soulis D, Protogerou AD, Papaioannou TG, et al. Noninvasive Cardiac Output and Central Systolic Pressure From Cuff-Pressure and Pulse Wave Velocity. IEEE J Biomed Health Inform. 2020;24(7):1968–81. https://doi.org/10.1109/JBHI.2019.2956604 PMID: 31796418
28. Zhang X, Wu D, Miao F, Liu H, Li Y. Personalized Hemodynamic Modeling of the Human Cardiovascular System: A Reduced-Order Computing Model. IEEE Trans Biomed Eng. 2020;67(10):2754–64. https://doi.org/10.1109/TBME.2020.2970244 PMID: 32142412
29. Zhang X, Liu J, Cheng Z, Wu B, Xie J, Zhang L, et al. Personalized 0D-1D multiscale hemodynamic modeling and wave dynamics analysis of cerebral circulation for an elderly patient with dementia. Int J Numer Methods Biomed Eng. 2021.
30. Stork M, Jilek J, Stork M, Jilek J. Cuff pressure pulse waveforms: their current and prospective applications in biomedical instrumentation. Biomedical engineering, trends in electronics, communications and software. IntechOpen. 2011.
31. Jilek J, Stork M. The contours of arterial pulsations in the blood pressure cuff are hemodynamic waveforms rather than oscillations. In: Proceedings of the 2nd international conference on Circuits, systems, control, signals, Stevens Point, Wisconsin, USA, 2011. 140–3.
32. Poleszczuk J, Debowska M, Dabrowski W, Wojcik-Zaluska A, Zaluska W, Waniewski J. Patient-specific pulse wave propagation model identifies cardiovascular risk characteristics in hemodialysis patients. PLoS Comput Biol. 2018;14(9):e1006417. https://doi.org/10.1371/journal.pcbi.1006417 PMID: 30216341
33. Poleszczuk J, Debowska M, Dabrowski W, Wojcik-Zaluska A, Zaluska W, Waniewski J. Subject-specific pulse wave propagation modeling: Towards enhancement of cardiovascular assessment methods. PLoS One. 2018;13(1):e0190972. https://doi.org/10.1371/journal.pone.0190972 PMID: 29324835
34. Wołos K, Pstras L, Debowska M, Dabrowski W, Siwicka-Gieroba D, Poleszczuk J. Non-invasive assessment of stroke volume and cardiovascular parameters based on peripheral pressure waveform. PLoS Comput Biol. 2024;20(4):e1012013. https://doi.org/10.1371/journal.pcbi.1012013 PMID: 38635856
35. Sobol' IM. Global sensitivity indices for nonlinear mathematical models and their Monte Carlo estimates. Math Comput Simul. 2001;55(1):271–80.
36. Saltelli A, Annoni P, Azzini I, Campolongo F, Ratto M, Tarantola S. Variance based sensitivity analysis of model output. Design and estimator for the total sensitivity index. Comput Phys Commun. 2010;181(2):259–70.
37. Olufsen MS, Ottesen JT. A practical approach to parameter estimation applied to model predicting heart rate regulation. J Math Biol. 2013;67(1):39–68.
38. Olufsen MS, Peskin CS, Kim WY, Pedersen EM, Nadim A, Larsen J. Numerical simulation and experimental validation of blood flow in arteries with structured-tree outflow conditions. Ann Biomed Eng. 2000;28(11):1281–99. https://doi.org/10.1114/1.1326031 PMID: 11212947
39. Alastruey J, Khir AW, Matthys KS, Segers P, Sherwin SJ, Verdonck PR. Pulse wave propagation in a model human arterial network: assessment of 1-D visco-elastic simulations against in vitro measurements. J Biomech. 2011;44(12):2250–8.
40. Gałecki A, Burzykowski T. Linear Mixed-Effects Models Using R. Springer New York. 2013. https://doi.org/10.1007/978-1-4614-3900-4
41. Akaike H. A new look at the statistical model identification. IEEE Trans Autom Control. 1974;19(6):716–23.
42. James G, Witten D, Hastie T, Tibshirani R. An Introduction to Statistical Learning. Springer US. 2021. https://doi.org/10.1007/978-1-0716-1418-1
43. Vallée F, Passouant O, Le Gall A, Joachim J, Mateo J, Mebazaa A, et al. Norepinephrine reduces arterial compliance less than phenylephrine when treating general anesthesia-induced arterial hypotension. Acta Anaesthesiol Scand. 2017;61(6):590–600. https://doi.org/10.1111/aas.12905 PMID: 28543052
44. Pilz N, Heinz V, Ax T, Fesseler L, Patzak A, Bothe TL. Pulse Wave Velocity: Methodology, Clinical Applications, and Interplay with Heart Rate Variability. Rev Cardiovasc Med. 2024;25(7):266. https://doi.org/10.31083/j.rcm2507266 PMID: 39139426
45. Zhou X, Pan J, Wang Y, Wang H, Xu Z, Zhuo W. Left ventricular-arterial coupling as a predictor of stroke volume response to norepinephrine in septic shock - a prospective cohort study. BMC Anesthesiol. 2021;21(1):56. https://doi.org/10.1186/s12871-021-01276-y PMID: 33596822
46. Tank AW, Lee Wong D. Peripheral and central effects of circulating catecholamines. Compr Physiol. 2015;5(1):1–15. https://doi.org/10.1002/cphy.c140007 PMID: 25589262
47. Procaccini DE, Sawyer JE, Watt KM. 19 - Pharmacology of Cardiovascular Drugs. In: Ungerleider RM, Meliones JN, Nelson McMillan K, Cooper DS, Jacobs JP. Critical Heart Disease in Infants and Children. Third ed. Philadelphia: Elsevier. 2019. 192-212.e6.
48. DeMers D, Wachs D. Physiology, Mean Arterial Pressure. StatPearls. Treasure Island (FL): StatPearls Publishing. 2024.
49. Beloeil H, Mazoit JX, Benhamou D, Duranteau J. Norepinephrine kinetics and dynamics in septic shock and trauma patients. Br J Anaesth. 2005;95(6):782–8.

50. Kinoshita K. Traumatic brain injury: pathophysiology for neurocritical care. J Intensive Care. 2016;4:29. https://doi.org/10.1186/s40560-016-0138-3 PMID: 27123305

51. Rinehart J, Ma M, Calderon MD, Cannesson M. Feasibility of automated titration of vasopressor infusions using a novel closed-loop controller. J Clin Monit Comput. 2018;32(1):5–11.

52. Rinehart J, Joosten A, Ma M, Calderon MD, Cannesson M. Closed-loop vasopressor control: in-silico study of robustness against pharmacodynamic variability. J Clin Monit Comput. 2019;33(5):795–802.

53. Joosten A, Rinehart J, Cannesson M, Coeckelenbergh S, Pochard J, Vicaut E. Control of mean arterial pressure using a closed-loop system for norepinephrine infusion in severe brain injury patients: the COMAT randomized controlled trial. J Clin Monit Comput. 2024;38(1):25–30.

54. Sviri GE, Aaslid R, Douville CM, Moore A, Newell DW. Time course for autoregulation recovery following severe traumatic brain injury. J Neurosurg. 2009;111(4):695–700. https://doi.org/10.3171/2008.10.17686 PMID: 19392589

S1 FILE: SUPPLEMENTARY MATERIAL
FOR THE ARTICLE
PERSONALIZED PULSE WAVE PROPAGATION MODELING TO IMPROVE VASOPRESSOR DOSING MANAGEMENT IN PATIENTS WITH SEVERE TRAUMATIC BRAIN INJURY

Kamil Wolos[1], Leszek Pstras[1], Urszula Bialonczyk[1], Malgorzata Debowska[1], Wojciech Dabrowski[2], Dorota Siwicka-Gieroba[2], Jan Poleszczuk[1]

[1]Laboratory of Mathematical Modeling of Physiological Processes
Nalecz Institute of Biocybernetics and Biomedical Engineering
Polish Academy of Sciences, Warsaw, Poland

[2]Department of Anesthesiology and Intensive Therapy,
Medical University of Lublin, Lublin, Poland

In this supplement, we present in more detail the methods used in our study. First, we present a detailed description of the 0-1D cardiovascular model. Next, we describe how we selected patient-specific parameters to be used in the model optimization procedure. Finally, we describe the optimization procedure.

1 The Cardiovascular Model

The mathematical foundations of the model that we present in this section come from the work of Sterigiopulos et. al [1], Olufsen et. al. [2], and Ottesen et. al, [3], [4].

1.1 Geometry of the arterial tree

The one-dimensional arterial bifurcation tree represents 71 major human arteries, including cerebral circulation; see Fig A for more details. Each segment (artery) is modeled as a compliant axi-symmetric, tapering cylinder with impermeable walls. The geometric parameters of each segment (length L, inlet internal radius r_{in}, and outlet internal radius r_{out}) are adapted from the work of Stergiopulos and Alastruey, [1], [5], see Table A for more details. Tapering of a given vessel is described by the following equation:

$$r_0(x) = r_{\text{in}} \left(\frac{r_{\text{out}}}{r_{\text{in}}} \right)^{x/L}, \tag{1}$$

where $r_0(x)$ denotes the internal radius of a given artery at point x at the nominal pressure P_0, [2].

1.2 Blood flow through the artery

The presented mathematical model is based on the Navier-Stokes equations and describes the changes in flow $Q(t, x)$, internal cross-sectional area $A(t, x)$, and pressure $P(t, x)$ along the vessel. We assume that blood is an incompressible fluid with constant density ρ and viscosity μ, and that the flow in the artery has a Poiseuille (parabolic) velocity profile. The continuity and momentum equations, derived using standard methods (detailed in [2], [3]), are given by,

$$\frac{\partial Q(t,x)}{\partial x} + \frac{\partial A(t,x)}{\partial t} = 0, \tag{2}$$

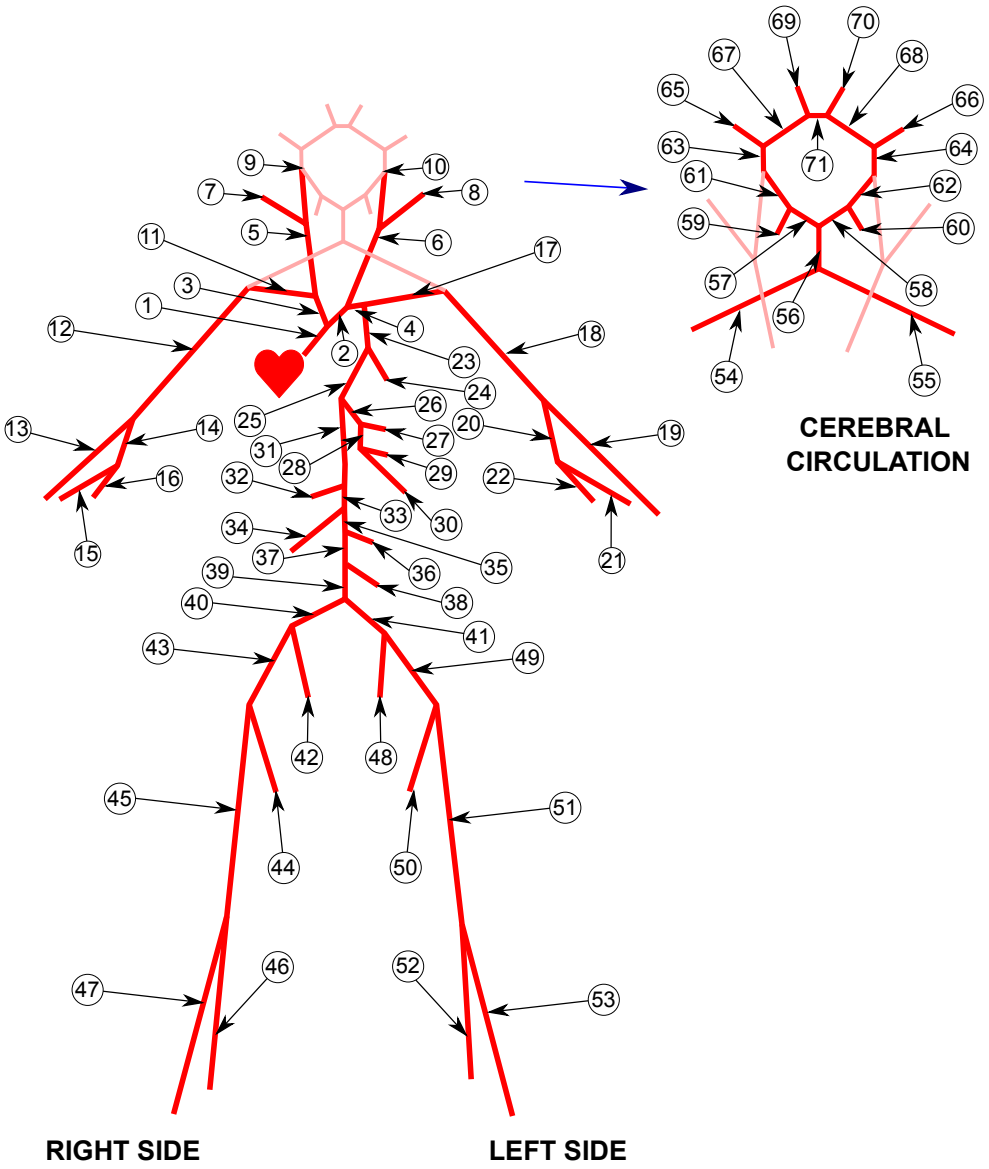

Fig A. **Overview of the modelled arterial tree.** For more information on individual arteries, see Table A.

$$\frac{\partial Q(t,x)}{\partial t} + \frac{\partial}{\partial x}\left(\frac{Q(t,x)^2}{A(t,x)}\right) + \frac{A(t,x)}{\rho}\frac{\partial P(t,x)}{\partial x} = \frac{-8\pi\mu}{\rho}\frac{Q(t,x)}{A(t,x)}. \tag{3}$$

Since in equation (3) the pressure appears only in the gradient, we need to add one more equation using P to ensure that the solution is unique. Assuming that the arterial walls are purely elastic, we can introduce the following equation, relating pressure to the internal cross-section of the artery [2]:

$$P(t,x) - P_0 = f(x)\left(1 - \sqrt{\frac{A_0(x)}{A(t,x)}}\right), \tag{4}$$

Table A: **Geometry of the modelled arterial tree and the corresponding peripheral resistances and compliances.** Length, r_{in} and r_{out} are provided in centimeters. Total peripheral resistance, $\left(R_T,\ 10^4\,\text{g/cm}^4/\text{s}\right)$ and compliance $\left(C_T,\ 10^6\,\text{cm}^4\text{s}^2/\text{g}\right)$ are provided only for terminal arteries. L and R stands for left and right, respectively. Data adapted from [1], [5].

ID	**Artery name**	**Length**	$\mathbf{r_{in}}$	$\mathbf{r_{out}}$	$\mathbf{R_T}$	$\mathbf{C_T}$
1	Ascending aorta	4	1.2	1.18	-	-
2	Aortic arch (I)	2	1.12	1.11	-	-
3	Brachiocephalic	3.4	0.62	0.61	-	-
4	Aortic arch (II)	3.9	1.07	1.06	-	-
5/6	Common Carotid R/L	17.7/20.8	0.25	0.25	-	-
7/8	External Carotid R/L	17.7	0.15	0.14	5.43	12.70
9/10	Internal Carotid (I) R/L	17.7	0.2	0.2	-	-
11/17	Subclavian (I) R/L	3.4	0.42	0.42	-	-
12/18	Subclavian (II) R/L	42.2	0.4	0.24	-	-
13/19	Radial R/L	23.5	0.17	0.14	5.28	3.52
14/20	Ulnar (I) R/L	6.7	0.22	0.22	-	-
15/21	Interosseous R/L	7.9	0.1	0.1	8.40	0.22
16/22	Ulnar (II) R/L	17.1	0.2	0.18	5.28	3.52
23	Thoracic aorta (I)	5.2	1	1	-	-
24	Intercostals	8	0.2	0.15	1.39	13.38
25	Thoarcic aorta (II)	10.4	0.68	0.65	-	-
26	Celiac (I)	1	0.39	0.39	-	-
27	Hepatic	6.6	0.22	0.22	3.64	5.13
28	Celiac (II)	1.0	0.2	0.2	-	-
29	Gastric	7.1	0.18	0.17	5.43	3.44
30	Splenic	6.3	0.18	0.17	2.32	8.01
31	Abdominal aorta (I)	5.3	0.61	0.6	-	-
32	Superior mesenteric	5.9	0.44	0.42	0.93	20.0
33	Abdominal aorta (II)	1	0.6	0.59	-	-
34/36	Renal R/L	3	0.26	0.25	1.13	16.46
35	Abdominal aorta (III)	3	0.59	0.58	-	-
37	Abdominal aorta (IV)	10.6	0.58	0.55	-	-
38	Inferior mesenteric	5.0	0.17	0.16	6.89	2.70
39	Abdominal aorta (V)	1.0	0.54	0.52	-	-
40/41	Common iliac R/L	5.8	0.37	0.35	-	-
42/48	Internal iliac R/L	5	0.2	0.19	7.96	2.34
43/49	External iliac R/L	14.5	0.32	0.27	-	-
44/50	Deep femoral R/L	12.6	0.26	0.19	4.79	3.90
45/51	Femoral R/L	44.5	0.26	0.19	-	-
46/52	Posterior tibial R/L	32.1	0.16	0.14	4.79	3.90
47/53	Anterior tibial R/L	34.3	0.13	0.12	5.60	3.33
47/53	Anterior tibial R/L	34.3	0.13	0.12	5.60	3.33
54/55	Vertebral R/L	14.8	0.14	0.14	-	-
56	Basilar artery	3	0.16	0.11	-	-
57/58	Posterior cerebral (I) R/L	0.5	0.11	0.11	-	-
59/60	Posterior cerebral (II) R/L	8.5	0.11	0.11	11.08	6.20
61/62	Posterior communicating R/L	1.5	0.07	0.07	-	-
63/64	Internal carotid (II) R/L	0.5	0.2	0.19	-	-
65/66	Middle cerebral R/L	12	0.14	0.12	5.97	11.60
67/68	Anterior cerebral (I) R/L	1.2	0.12	0.12	-	-
69/70	Anterior cerebral (II) R/L	10	0.12	0.12	8.48	8.20
71	Anterior communicating	0.3	0.07	0.07	-	-

where $A_0(x)$ is the artery's internal cross-sectional area at nominal pressure, i.e., $A_0(x) = \pi r_0^2(x)$, and the function $f(x)$ describes the elasticity of the artery wall as follows:

$$f(x) = \frac{4}{3}\left(k_1 \exp\left(k_2 r_0(x)\right) + k_3\right), \tag{5}$$

where parameters k_1, k_2 and k_3 are global subject-specific constants. Parameter k_3 describes the stiffness of large arteries, parameter k_1 describes the increasing stiffness of smaller arteries, and k_2 reflects the transition between the large, elastic arteries and smaller, less-elastic arteries [6].

1.3 Bifurcations

We assume pressure continuity and mass conservation (i.e. no blood leakage) at the vessel nodes. For a discussion on the validity of these assumptions, see [3]. If by p we denote the parent vessel, and d_1, d_2 are the daughter vessels, then the above conditions may be expressed as follows:

$$P_{\text{out},p} = P_{\text{in},d_1} = P_{\text{in},d_2}, \quad \text{and} \quad Q_{\text{out},p} = Q_{\text{in},d_1} + Q_{\text{in},d_2}. \tag{6}$$

1.4 Inflow Boundary Condition

The inflow boundary condition describes the blood ejection from the left heart ventricle and is based on the work of Suga et al. [7], [8], and Danielsen and Ottensen [4]. Changes of the pressure in the left ventricle, P_{lv}, can be described using a time-varying left-ventricle elastance function $E_{lv}(t)$:

$$P_{lv} = E_{lv}(t)\left(V_{lv}(t) - V_0\right), \tag{7}$$

where V_{lv} is the ventricular volume and V_0 is the volume of the left ventricle at zero transmural pressure. According to [4], the function $E_{lv}(t)$ may be expressed as follows:

$$E_{lv}(t) = E_{\text{min}}\left(1 - \phi(t)\right) + E_{\text{max}}\phi(t), \tag{8}$$

where the parameters E_{min} and E_{max} are minimal and maximal values of the elastance function $E_{lv}(t)$. Function ϕ is defined by the following equation:

$$\phi(t) = \begin{cases} a\sin\left(\frac{\pi t}{t_m}\right) + b\sin\left(\frac{2\pi t}{t_m}\right) & \text{for} \quad 0 \le t < t_m \\ 0 & \text{for} \quad t_m \le t < T \end{cases}, \tag{9}$$

where T is the heart period, t_m denotes the onset of constant (minimal) elastance, and parameters a and b are responsible for the shape of the $\phi(t)$. Additionally, a and b must be chosen so that $\max_{t\in[0,T]}\phi(t) = 1$. The example of the simulated left ventricle elastance is shown in Fig B.

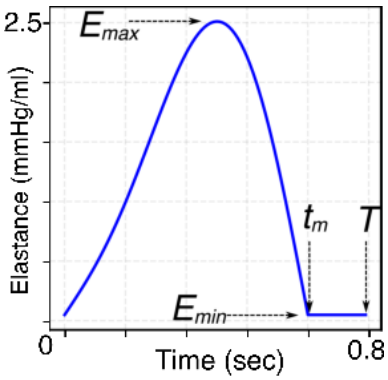

Fig B. **Left-ventricle time-varying elastance function.** $E_{\text{min}}, E_{\text{max}}$ - minimal and maximal value of the elastance function, t_m - onset of the constant (minimal) elastance, T - heart period.

The work of the left ventricle can be divided into four stages. We will begin with isovolumic relaxation. During this phase, the pressure in the left ventricle decreases. When P_{lv} is smaller than the pressure in the left atrium, P_{la}, then the mitral valve opens.

In the next phase (ventricular filling) blood flows from the left atrium to the left ventricle. This flow, Q_{la}, is described by the following equation:

$$\frac{dQ_{la}}{dt} = \frac{1}{L_{la}}\left(P_{la} - P_{lv}\right) - \frac{R_{la}}{L_{la}}Q_{la}. \tag{10}$$

Parameter L_{la} is an inertia term, and R_{la} describes the resistance against the flow from the atrium to the ventricle, caused mainly by the viscous properties of the blood. Simultaneously, due to the inflow of blood into the left ventricle, V_{lv} increases, given by the following equation:

$$\frac{dV_{lv}}{dt} = Q_{la}. \tag{11}$$

When V_{lv} is greater than end-diastolic volume V_{ed}, the mitral valve closes, and isovolumic contraction begins.

During this phase, there is no flow between the left atrium and ventricle ($Q_{la} = 0$), and P_{lv} increases. When P_{lv} is greater than the pressure in the ascending aorta, P_a, the aortic valve opens, and the last phase of the cycle (ventricular ejection) begins.

The flow between the ventricle and aorta is expressed by an equation similar to equation (10), namely:

$$\frac{dQ_{lv}}{dt} = \frac{1}{L_{lv}}\left(P_{la} - P_a\right) - \frac{R_{lv}}{L_{lv}}Q_{lv}. \tag{12}$$

The pressure P_a is taken directly from the 1-D model of the arterial tree. The volume V_{lv} decreases according to the following equation:

$$\frac{dV_{lv}}{dt} = -Q_{lv}. \tag{13}$$

At the end of this phase, some amount of blood, V_b, returns from the ascending aorta to the left ventricle, which is associated with the negative value of Q_{lv} (backflow). V_b is given by the following equation:

$$V_b = \int_{t^*}^{t} \left|Q_{lv}\right|, \quad \text{for} \quad t > t^*, \tag{14}$$

where t^* denotes the moment, when Q_{lv} becomes negative. At the time t, when $V_b > \overline{V_b}$ we end the last phase by setting $Q_{lv} = 0$, and then the cycle repeats.

1.5 Outflow boundary conditions

The outflow boundary conditions are modeled using a three-element Windkessel model [9], [10], which describes compliance and resistance effects of the vessels beyond the modeled terminal arteries:

$$R_1 R_2 C_T \frac{dQ_{\text{end}}(t)}{dt} = R_2 C_T \frac{dP_{\text{end}}(t)}{dt} + \left(P_{\text{end}}(t) - P_T\right) - (R_1 + R_2)Q_{\text{end}}(t). \tag{15}$$

In the above equation, R_1 and R_2 are proximal and distal resistances, respectively, C_T is the total compliance of the terminal vascular branch, and P_T is the reference terminal pressure. Moreover, we assume that $R_1/R_T = 0.2$, where R_T is the total terminal resistance, and $R_T = R_1 + R_2$ as in [1], [10]. Table A lists all values of C_T and R_T, adapted from [1] and [5].

1.6 Solving the model equations

The procedure of solving the model equationsis similar to the one presented in our previous work [11]. The governing equations for blood flow in the 1D domain were solved using the Lax-Wendroff scheme [12]. The inflow and outflow boundary conditions were integrated into the 1D model using the "ghost point" method [13], [14]. The inflow boundary condition was solved with the Runge-Kutta scheme, and the 3-element Windkessel models were solved using the explicit Euler method. The time step was set to $\Delta t = 2 \cdot 10^{-4}$ s, and spacial discretization was set to $\Delta x = 0.5$ cm (Courant number in radial artery for a default parameters is $C = 0.016$).

2 Model parameters

2.1 Arterial tree geometry

The procedure of personalizing the arterial tree geometry was similar to that employed in our previous publications [11], [15], [16]. The default arterial tree (Table A) represents the typical arterial geometry for a 175 cm tall man. To personalize the arterial tree for a given patient, we multiplied all nominal artery lengths as well as internal proximal and distal artery radii by a scaling factor S=H/175, where H is patient's height in cm.

2.2 Blood flow and vascular parameters

We set blood density as $\mu = 1.04\frac{\text{g}}{\text{cm}^3}$ and kinematic viscosity as $\rho = 0.04\frac{\text{cm}^2}{\text{s}}$ [10]. The nominal mean arterial pressure, P_0, was set to 97 mmHg [1]. With regard to parameters describing the stiffness of the arteries (equation (5)), as in [6], we set parameter k_2 to $-13.5\frac{1}{\text{cm}}$. The other two parameters (k_1 and k_3) were considered in the sensitivity analysis discussed later (see Table B for their assumed baseline values).

2.3 Inflow boundary condition

The blood pressure in the left ventricle, P_{lv}, is computed using a time-varying elastance function $E_{lv}(t)$, see eq. (7). Since the shape of the left-ventricular elastance function (normalized for amplitude and time to peak) remains relatively constant, even in various cardiovascular diseases [17], we decided to fix the parameters describing the shape of the elastance function, $a = 0.9$ and $b = 0.25$, as in [4]. We assumed that the volume of blood backflow to the left ventricle at the end of each cycle ($\overline{V_b}$), equals 2 ml [4]. Based on the work of Parikh et. al. [18], we determined the relation between the left end-diastolic volume index (LEDVi) and the age, corrected for the body surface area (BSA), calculated using the Du Bois formula, as follows [19]:

$$BSA = 0.007184 \cdot \text{Weight}^{0.425} \cdot \text{Height}^{0.725}. \tag{16}$$

After performing linear fitting to data from [18], we obtained the following relation:

$$V_{ed} = (-0.29 \cdot \text{Age} + 81) \cdot BSA. \tag{17}$$

The parameters that describe the flow from the left atrium to the left ventricle (L_{la}, R_{la}) and from the left ventricle to the ascending aorta ($L_{lv}, R_{lv}, E_{\text{min}}, E_{\text{max}}$ and P_{la}) were considered in the sensitivity analysis described later (see Table B for their assumed baseline values).

2.4 Outflow boundary condition

Each terminal artery was connected to a three-element Windkessel model, describing the behavior of small arteries, arterioles, and capillaries downstream of the given terminal artery, characterized by the total resistance, R_T and compliance, C_T. The nominal values of these parameters for each terminal artery are presented in Table A, based on data from the literature [1], [5]. Similarly to other studies [11], [14], [20] these parameters are scaled globally, using separate scaling factors for resistances and compliances (S_R and S_C, respectively). The reference terminal pressure, P_T, was set at 15 mmHg as in our previous study [16].

3 Sensitivity analysis

The sensitivity analysis was performed to identify model parameters with the greatest impact on the shape of the pulse waveform. The following parameters were analyzed: k_1, k_3 – parameters describing the stiffness of the artery wall in the state equation, $E_{\text{min}}, E_{\text{max}}, t_m$ – parameters describing the shape of the left ventricular elastance function, R_{lv}, L_{lv} – parameters describing blood flow from the left ventricle to the ascending aorta, L_{la}, R_{la} – parameters describing the blood flow from the left atrium to the left ventricle, V_0 – volume of the left ventricle at zero transmural pressure, $\overline{V_b}$ – the amount of backflow to the left ventricle, S_R, S_C – scaling factors for teminal resistances and compliances, P_{la} – the pressure in the left atrium, and V_{ed} – left ventricular end-diastolic volume.

The analysis was performed for a 45-year old 175 cm tall man with a heart rate (HR) of 75 bpm. We performed the Sobol sensitivity analysis, as described in [21], [22]. All computations were done using the Python library SaLiB v. 1.4.8, [23], [24].

For all analyzed parameters, the initial (nominal) values were taken from the literature and the lower/upper bounds were set at $\pm 50\%$ of the nominal value, except for parameter V_{ed}, for which individual physiological limits were defined (see Table B).

To generate input data, we used a Saltelli sampler [26], which generates $N \cdot (D + 1)$ sets of parameter values, where D is the number of parameters (in our case, $D = 15$), and N is an arbitrary number, preferably a power of 2. The more sets of parameters are generated, the more reliable, although time-consuming, the sensitivity analysis. As a compromise, we took $N = 1024$, which gave us 16384 samples. For each set of parameter values, we simulated the volumetric pulse waves (described in more detail in the next section) in the two arms (radial artery) and the left leg (anterior tibial artery). We decided to use only one leg in the analysis given that the modelled arteries in the two legs are symmetrical. In addition, for each simulation, we also computed stroke volume (SV). To obtain a stable output of the model, we performed 8 seconds of simulation. We present an exemplary output in Fig C.

Table B: **Parameters studied in the sensitivity analysis with adopted limits ($\pm 50\%$ of the nominal values).**

Parameter	Unit	Boundaries	Nominal value	Source of the nominal value
k_1	$\frac{\text{g}}{\text{s}^2\cdot\text{cm}}$	$[1.5 \cdot 10^6, 4.5 \cdot 10^6]$	$3 \cdot 10^6$	[25]
k_3	$\frac{\text{g}}{\text{s}^2\cdot\text{cm}}$	$[4.2 \cdot 10^5, 12.6 \cdot 10^5]$	$8.4 \cdot 10^5$	computed from [6], for age = 45
E_{max}	$\frac{\text{mmHg}}{\text{ml}}$	$[1.3, 3.8]$	2.5	[4]
E_{min}	$\frac{\text{mmHg}}{\text{ml}}$	$[0.025, 0.074]$	0.049	[4]
t_m	s	$[0.23, 0.68]$	0.45	computed from [4], for HR$=75$
V_{ed}	ml	$[90, 150]^*$	127	[4]
V_b	ml	$[1, 3]$	2	[4]
V_0	ml	$[5, 15]$	10	[4]
R_{lv}	$\frac{\text{mmHg}\cdot\text{s}}{ml}$	$[0.0167, 0.0501]$	0.0334	[4]
L_{lv}	$\frac{\text{mmHg}\cdot\text{s}^2}{\text{ml}}$	$[2.08 \cdot 10^{-4}, 6.24 \cdot 10^{-4}]$	0.000416	[4]
R_{la}	$\frac{\text{mmHg}\cdot\text{s}}{\text{ml}}$	$[4.45 \cdot 10^{-5}, 1.34 \cdot 10^{-4}]$	0.000089	[4]
L_{la}	$\frac{\text{mmHg}\cdot\text{s}^2}{\text{ml}}$	$[2.5 \cdot 10^{-5}, 7.5 \cdot 10^{-5}]$	0.00005	[4]
P_{la}	mmHg	$[2.5, 7.5]$	5	[4]
S_R	-	$[0.5, 1.5]$	1	assumed
S_C	-	$[0.5, 1.5]$	1	assumed

* individual limits were adopted to obtain physiological values

From the 8 seconds of simulated arterial volume waves, we took the data from the last 1 second sampled at 100Hz, excluding simulations with corrupted results. Then, we conducted the Sobol sensitivity analysis for each considered time point, i.e., $t_1, t_2, \ldots, t_{100}$ separately for waveforms from each limb. The results of this analysis were the first-order sensitivity indices S1 (computed for each studied parameter), which quantify the direct contribution of the given parameter to the model output variability at the given time point of the cardiac cycle. We present the results of this analysis in Fig. D A, C, E. In Fig. D B, D, F, we present the ranked (from smallest to largest) maximal values of S1 for a given limb. A simillar sensitivity analysis was also performed for SP and DP (separately for each limb) and SV. The S1 coefficients for SP, DP, and SV are presented in Fig E. As a cutoff point, we took the value of S1 = 0.05, i.e., we considered the parameters with a maximum S1 coefficient below 0.05 as having little influence on the model output. According to the performed sensitivity analysis, the parameters $E_{\text{min}}, P_{la}, S_R, t_m, E_{\text{max}}$, and k_3 have the highest impact on the studied model outputs (i.e. the arterial volume waveform, SP, DP, and SV) and hence these parameters were included in the identifiability analysis.

4 Parameter identification

To determine possible pairwise correlations between the selected model parameters to limit the number of parameters involved in the patient-specific model optimization, we used the method described by Olufsen et. al., [27]. Let $V_{\text{right arm}}$, $V_{\text{left arm}}$, V_{leg} be arterial volume waveforms in the considered peripheral locations simulated as described in the previous section. To check the local sensitivity of the output $y \in (V_{\text{right arm}}, V_{\text{left arm}}, V_{\text{leg}})$ to the model parameters $\theta = (\theta_1, \ldots, \theta_6) = (E_{\text{min}}, P_{la}, S_R, t_m, E_{\text{max}}, k_3)$, we first determined the relative sensitivity matrix, as follows:

$$\tilde{S} = \frac{\partial y}{\partial \theta}\frac{\theta}{y}, \quad y \neq 0, \tag{18}$$

where

$$\frac{\partial y}{\partial \theta} = \begin{bmatrix} \frac{\partial y}{\partial \theta_1(t_1)} & \cdots & \frac{\partial y}{\partial \theta_6(t_1)} \\ \frac{\partial y}{\partial \theta_1(t_2)} & \cdots & \frac{\partial y}{\partial \theta_6(t_2)} \\ \vdots & \vdots & \vdots \\ \frac{\partial y}{\partial \theta_1(t_{100})} & \cdots & \frac{\partial y}{\partial \theta_6(t_{100})} \end{bmatrix}. \tag{19}$$

To compute the sensitivity matrix we used the central difference approximation, with the steps equal to 0.1% of the nominal value of the given parameter. Then we approximated the model Hessian:

$$H = \tilde{S}^T \tilde{S}. \tag{20}$$

Finally, we calculated the correlation matrix c, where

$$c_{ij} = \frac{C_{i,j}}{\sqrt{C_{ii}C_{jj}}}, \tag{21}$$

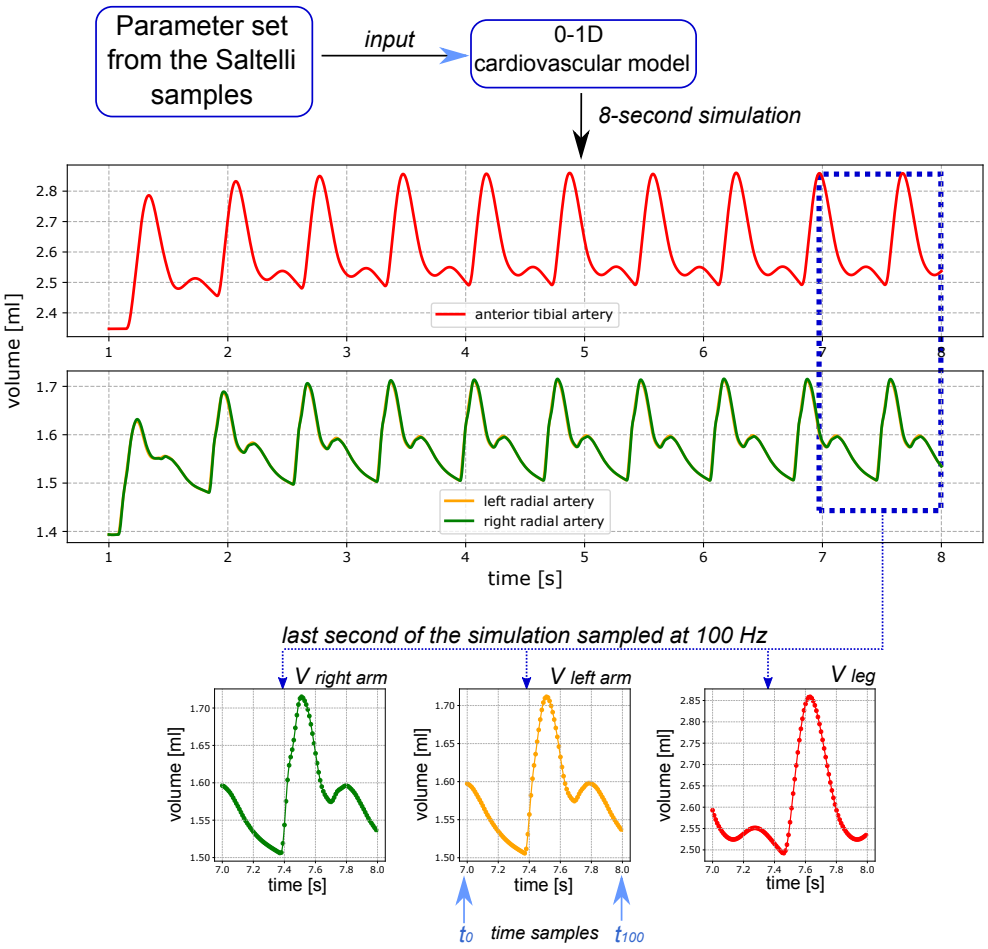

Fig C. **Data processing scheme for the Sobol global sensitivity analysis**. First, we generated 16384 sets of values of 15 parameters (the ranges of parameter values are shown in Table B). Then, for each set of parameter values, using the 0-1D cardiovascular model, we performed 8 seconds simulations of the arterial volume in three analyzed arteries. We used the last second for analysis, sampling the arterial volume waves from the left and right radial artery and anterior tibial artery at 100Hz. We labeled the successive time stamps as $t_0, t_1, \ldots, t_{100}$.

and $C = H^{-1}$ (but only if $\det(H) \neq 0$). A pair of parameters (i, j) is correlated if $|c_{i,j}| > \gamma$ for $\gamma \to 1$. Here, we assumed that two parameters are correlated if $|c_{ij}| > 0.9$. The correlations between parameters can be significantly affected by the values of parameters, for which we compute the corresponding derivatives in the matrix $\tilde{S}$. To understand these correlations better, we computed the coefficients c_{ij} for 150 randomly selected points from the parameter space defined in Table B (assuming uniform distribution of each parameter). Then, for all pairs of parameters, we plotted the coefficients c_{ij} on histograms; see Fig. F. For the vast majority of the generated cases, there was a significant correlation (> 0.9) between the parameters P_{la} and E_{min}. It is noteworthy that in 39% of cases, the correlation was observed only between these two parameters (i.e. $|c_{ij}| > 0.9$ only for the pair E_{min} and P_{la}).

We repeated this procedure in a similar manner for SP, DP (from two arms and one leg) and SV, obtaining a similar relationship between E_{min} and P_{la}. Based on that, we concluded that there is a relationship between E_{min} and P_{la}, and hence we decided to set E_{min} to a fixed value of $0.049 \frac{\text{mmHg}}{\text{ml}}$ [4], and use only P_{la} in the optimization process. Hence, we decided that the patient-specific optimization of the model will be performed using the following five parameters: $P_{la}, S_R, t_m, E_{\text{max}}, k_3$. The values of all other parameters studied in the sensitivity analysis were set at their nominal values as shown in Table B.

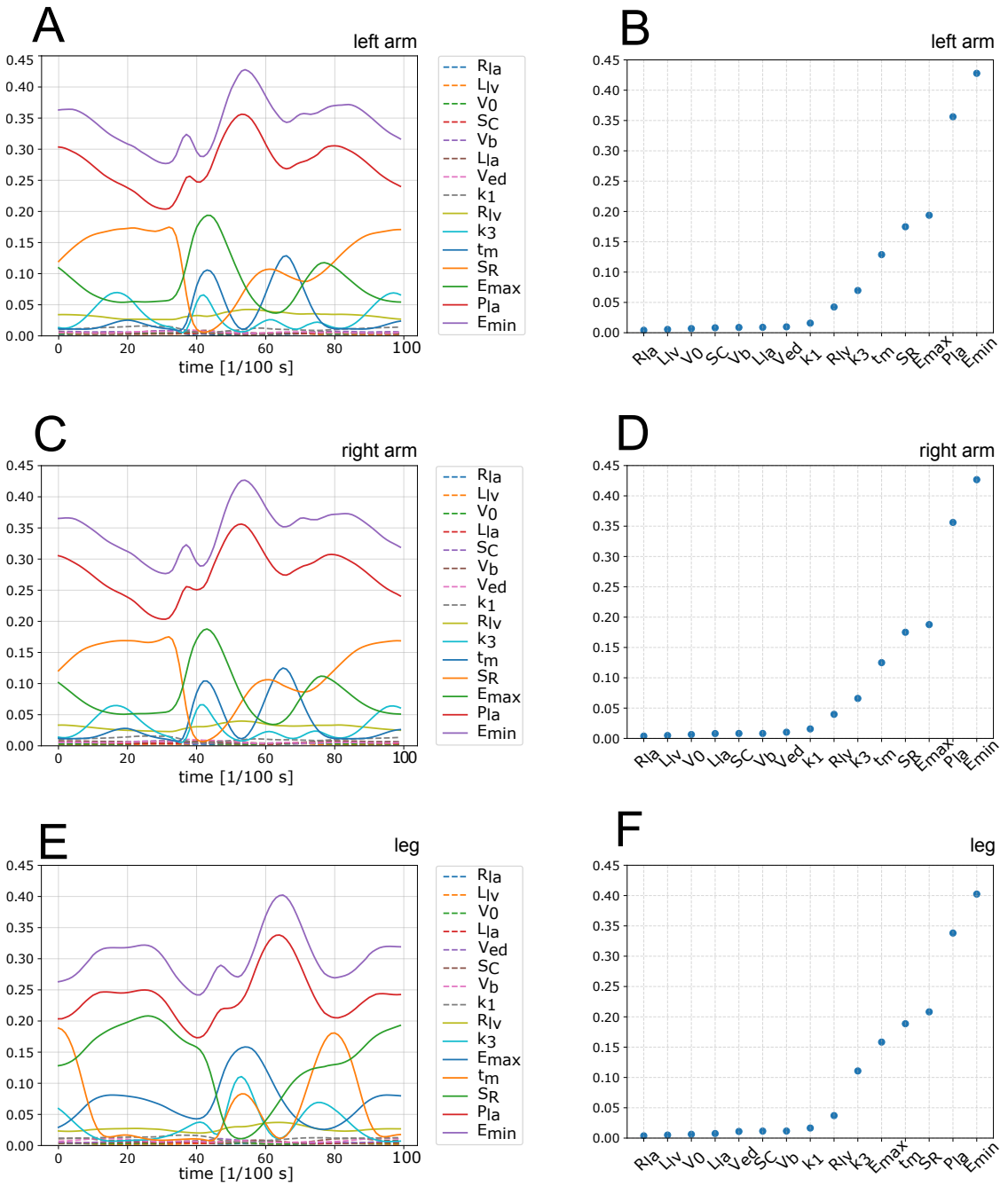

Fig D. **Results of the sensitivity analysis for arterial volume waveforms**. **A, C, E** - time varying values of the S1 index for the last second of the simulation for the left arm, right arm, and leg respectively. **B, D, F** - maximal values of the S1 index computed for the left arm, right arm and leg respectively; since the values of S1 may come from different timestamps, their sum may exceed 1.

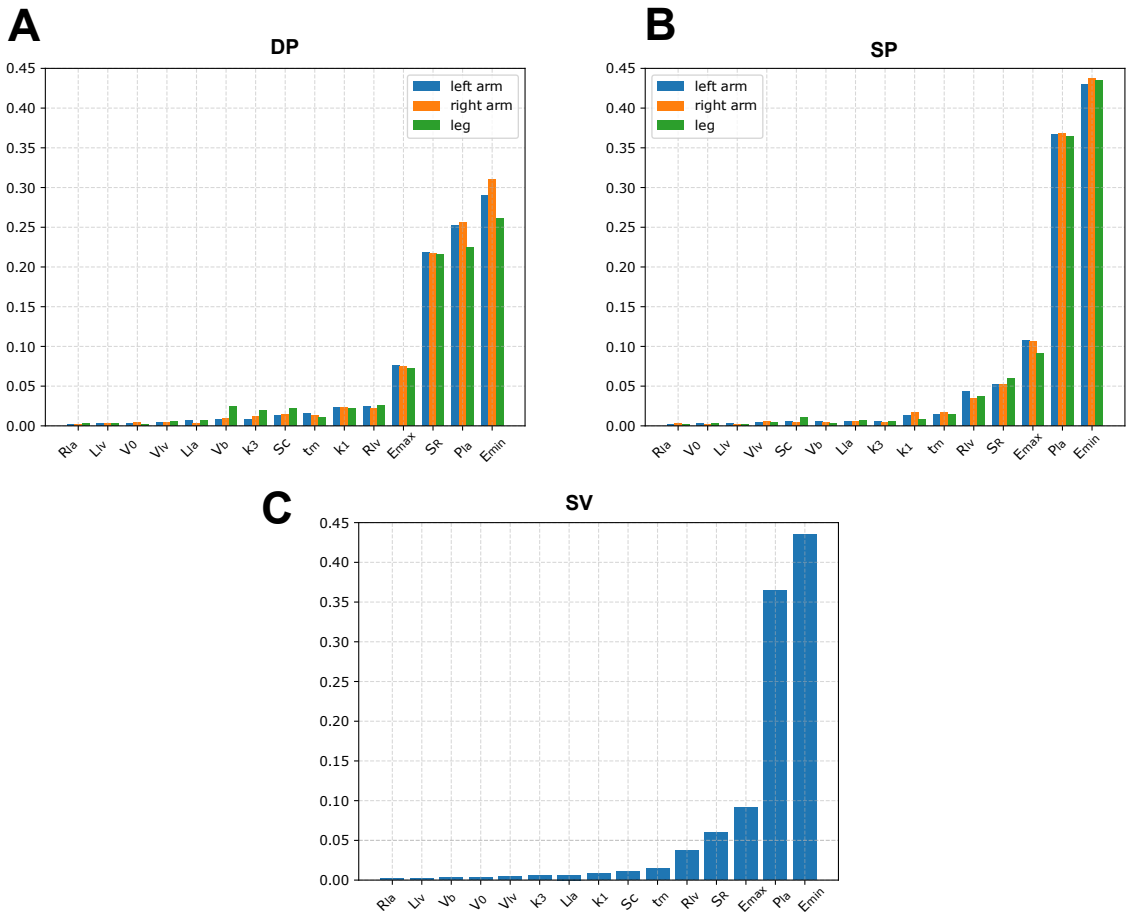

Fig E. **Results of the sensitivity analysis (S1 index) for systolic pressure (A), diastolic pressure (B), and stroke volume (C).**

5 Model optimization

As a result of solving the system of equations described in Section 1, we obtain changes in pressure P, arterial internal cross-sectional area A, and blood flow Q for each point of the 1D arterial domain over time. The model was fitted to pulse waveform data obtained from oscillometric measurements using cuffs on wrists and ankles inflated to a certain level of pressure (see the main text for more details). Since the pulse waves obtained by this method describe changes in blood volume under the cuff, the recorded pulse waveform was fitted by model-simulated changes in the volume of the large artery under the given cuff (e.g. radial artery) V, i.e. the wave computed by integrating the changes in the internal cross-sectional area A over the artery length.

To define the error function to be minimized during the model optimization, first, we normalized in amplitude the recorded and computed pulse waveforms. Then, we approximated the computed waveforms at time points corresponding to the time points of the the recorded waveforms (obtained at 1000 Hz) and compared their differences. Our primary goal was to match the waveform shapes, but to ensure physiological accuracy, we also incorporated into the error function deviations between the diastolic and systolic pressure measured by the AngE device on the left arm (DP_{meas} and SP_{meas}, respectively) and that computed by the model in the left radial artery ($DP_{\text{sim}}, SP_{\text{sim}}$). Additionally, we included a penalty for excessively low (< 40 ml) or high (> 110 ml) stroke volumes, SV_{sim}. Hence, the objective

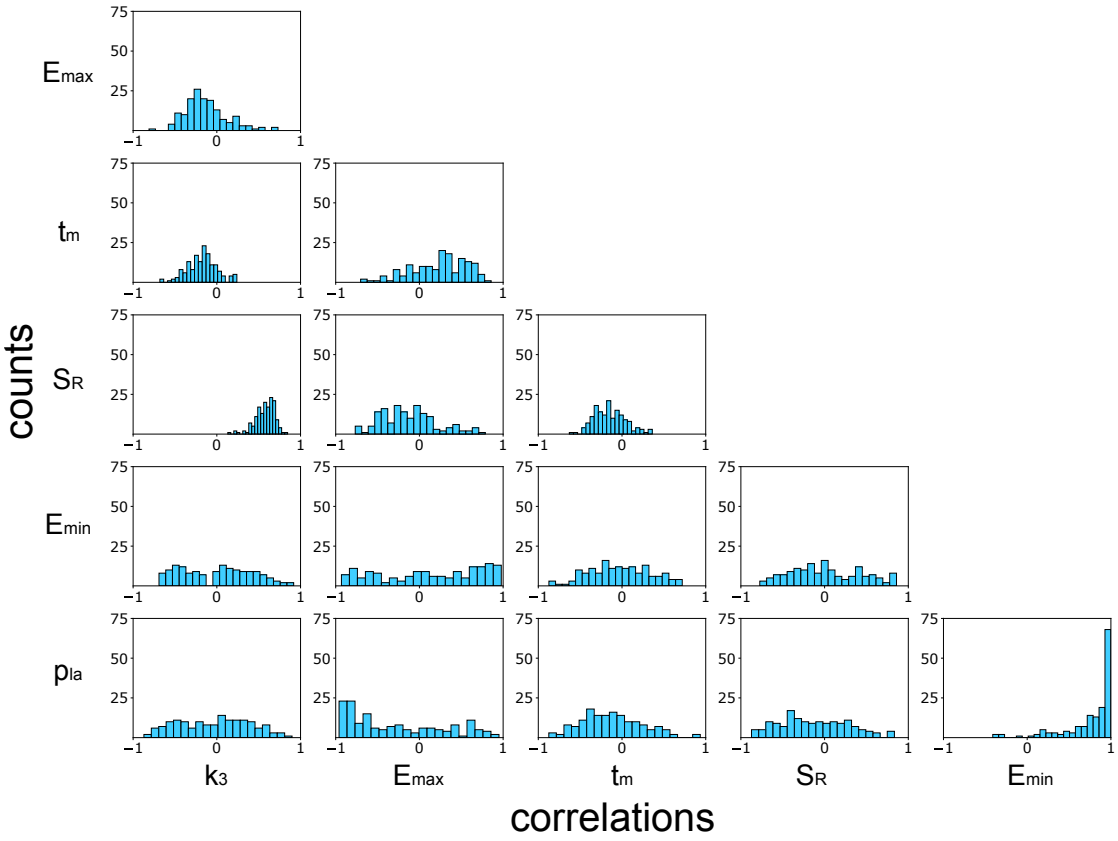

Fig F. **Histograms of correlation coefficients (c_{ij}) for each pair of the studied parameters, generated for 150 randomly selected points from the parameter space**. We set the number of bins in the histograms to 20.

function was as follows

$$\begin{aligned} \text{err} = & \sum_{i \in (\text{left/right arm, left/right leg})} \sum_{j=1}^{n} \left\| V_{\text{norm, sim; i; j}} - V_{\text{norm, meas; i; j}} \right\|^2 \\ & + \|DP_{\text{sim}} - DP_{\text{meas}}\|^2/20 + \|SP_{\text{sim}} - SP_{\text{meas}}\|^2/20 + \left((SV_{\text{sim}} - 70)/40\right)^6, \end{aligned} \tag{22}$$

where *norm*, *sim* and *meas* denotes normalized, simulated and measured values respectively, $\|\cdot\|$ is a ℓ_2-norm, and $n = 1000$ is the number of time points from simulated and measured arterial volume waveforms V. The penalty terms are scaled by fixed values (20 or 40; for all performed fittings) in order to obtain comparable orders of magnitude for first sum and the other terms. The last term is defined in such a way that for SV values between 40 ml and 110 ml it is close to 0, whereas for values smaller or larger the penalty increases exponentially. Indeed, the values of the individual terms may depend on how well the first term is fitted (i.e., the poorer the fit of the normalized waveforms, the more significant the first term). Nevertheless, our priority was to first capture the shape of the volume waves, and only then the pressure values.

To minimize the objective function (22), we used the Levenberg-Marquardt algorithm, [28]. The initial point (i.e. the initial values of the five model parameters being optimized) was set as a combination of parameter values corresponding to the minimal value of the error function amongst the randomly chosen 50 combinations from the parameter space defined in Table B. We present the simplified scheme of the optimization procedure in Fig. 2 in the main text.

References

[1] N. Stergiopulos, D. F. Young, and T. R. Rogge, "Computer simulation of arterial flow with applications to arterial and aortic stenoses," *Journal of Biomechanics*, vol. 25, no. 12, pp. 1477–1488, 1992, ISSN: 0021-9290. DOI: 10.1016/0021-9290(92)90060-E.

[2] M. S. Olufsen, C. S. Peskin, W. Y. Kim, E. M. Pedersen, A. Nadim, and J. Larsen, "Numerical simulation and experimental validation of blood flow in arteries with structured-tree outflow conditions," *Annals of Biomedical Engineering*, vol. 28, no. 11, pp. 1281–1299, 2000, ISSN: 1573-9686. DOI: 10.1114/1.1326031.

[3] J. T. Ottesen, M. S. Olufsen, J. K. Larsen, and M. S. Olufsen, "5. modeling flow and pressure in the systemic arteries," in *Applied Mathematical Models in Human Physiology*, ser. Mathematical Modeling and Computation, Society for Industrial and Applied Mathematics, 2004, pp. 91–136, ISBN: 978-0-89871-539-2. DOI: 10.1137/1.9780898718287.ch5.

[4] J. T. Ottesen, M. S. Olufsen, J. K. Larsen, M. Danielsen, and J. T. Ottesen, "6. a cardiovascular model," in *Applied Mathematical Models in Human Physiology*, ser. Mathematical Modeling and Computation, Society for Industrial and Applied Mathematics, 2004, pp. 137–155, ISBN: 978-0-89871-539-2. DOI: 10.1137/1.9780898718287.ch6.

[5] J. Alastruey, K. H. Parker, J. Peiró, S. M. Byrd, and S. J. Sherwin, "Modelling the circle of Willis to assess the effects of anatomical variations and occlusions on cerebral flows," *Journal of Biomechanics*, vol. 40, no. 8, pp. 1794–1805, 2007, ISSN: 0021-9290. DOI: 10.1016/j.jbiomech.2006.07.008.

[6] P. H. Charlton, J. Mariscal Harana, S. Vennin, Y. Li, P. Chowienczyk, and J. Alastruey, "Modeling arterial pulse waves in healthy aging: A database for in silico evaluation of hemodynamics and pulse wave indexes," *American Journal of Physiology-Heart and Circulatory Physiology*, vol. 317, no. 5, H1062–H1085, 2019. DOI: 10.1152/ajpheart.00218.2019.

[7] H. Suga, K. Sagawa, and D. P. Kostiuk, "Controls of ventricular contractility assessed by pressure-volume ratio, Emax1," *Cardiovascular Research*, vol. 10, no. 5, pp. 582–592, 1976, ISSN: 0008-6363. DOI: 10.1093/cvr/10.5.582.

[8] H. Suga, K. Sagawa, and A. A. Shoukas, "Load independence of the instantaneous pressure-volume ratio of the canine left ventricle and effects of epinephrine and heart rate on the ratio," *Circulation Research*, vol. 32, no. 3, pp. 314–322, 1973, ISSN: 0009-7330. DOI: 10.1161/01.res.32.3.314.

[9] N. Westerhof, G. Elzinga, and P. Sipkema, "An artificial arterial system for pumping hearts," *Journal of Applied Physiology*, vol. 31, no. 5, pp. 776–781, 1971, ISSN: 0021-8987. DOI: 10.1152/jappl.1971.31.5.776.

[10] P. J. Blanco, S. M. Watanabe, E. A. Dari, M. A. R. F. Passos, and R. A. Feijóo, "Blood flow distribution in an anatomically detailed arterial network model: Criteria and algorithms," *Biomechanics and Modeling in Mechanobiology*, vol. 13, no. 6, pp. 1303–1330, 2014, ISSN: 1617-7940. DOI: 10.1007/s10237-014-0574-8.

[11] K. Wołos, L. Pstras, M. Debowska, W. Dabrowski, D. Siwicka-Gieroba, and J. Poleszczuk, "Non-invasive assessment of stroke volume and cardiovascular parameters based on peripheral pressure waveform," *PLOS Computational Biology*, vol. 20, no. 4, e1012013, 2024, ISSN: 1553-7358. DOI: 10.1371/journal.pcbi.1012013.

[12] P. Lax and B. Wendroff, "Systems of conservation laws," *Communications on Pure and Applied Mathematics*, vol. 13, no. 2, pp. 217–237, 1960, ISSN: 1097-0312. DOI: 10.1002/cpa.3160130205.

[13] X. Zhang, S. Noda, R. Himeno, and H. Liu, "Gravitational effects on global hemodynamics in different postures: A closed-loop multiscale mathematical analysis," *Acta Mechanica Sinica*, vol. 33, no. 3, pp. 595–618, 2017, ISSN: 1614-3116. DOI: 10.1007/s10409-016-0621-z.

[14] X. Zhang, D. Wu, F. Miao, H. Liu, and Y. Li, "Personalized hemodynamic modeling of the human cardiovascular system: A reduced-order computing model," *IEEE Transactions on Biomedical Engineering*, vol. 67, no. 10, pp. 2754–2764, 2020, ISSN: 1558-2531. DOI: 10.1109/TBME.2020.2970244.

[15] J. Poleszczuk, M. Debowska, W. Dabrowski, A. Wojcik-Zaluska, W. Zaluska, and J. Waniewski, "Patient-specific pulse wave propagation model identifies cardiovascular risk characteristics in hemodialysis patients," *PLOS Computational Biology*, vol. 14, no. 9, e1006417, 2018, ISSN: 1553-7358. DOI: 10.1371/journal.pcbi.1006417.

[16] J. Poleszczuk, M. Debowska, W. Dabrowski, A. Wojcik-Zaluska, W. Zaluska, and J. Waniewski, "Subject-specific pulse wave propagation modeling: Towards enhancement of cardiovascular assessment methods," *PLOS ONE*, vol. 13, no. 1, e0190972, 2018, ISSN: 1932-6203. DOI: 10.1371/journal.pone.0190972.

[17] H. Senzaki, C.-H. Chen, and D. A. Kass, "Single-beat estimation of end-systolic pressure-volume relation in humans," *Circulation*, vol. 94, no. 10, pp. 2497–2506, 1996. DOI: 10.1161/01.CIR.94.10.2497.

[18] J. D. Parikh, K. G. Hollingsworth, D. Wallace, A. M. Blamire, and G. A. MacGowan, "Normal age-related changes in left ventricular function: Role of afterload and subendocardial dysfunction," *International Journal of Cardiology*, vol. 223, pp. 306–312, 2016, ISSN: 0167-5273. DOI: 10.1016/j.ijcard.2016.07.252.

[19] D. Du Bois and E. F. Du Bois, "A formula to estimate the approximate surface area if height and weight be known," *Archives of Internal Medicine*, vol. XVII, no. 6, pp. 863–871, 1916, ISSN: 0730-188X. DOI: 10.1001/archinte.1916.00080130010002.

[20] V. Bikia et al., "Noninvasive estimation of aortic hemodynamics and cardiac contractility using machine learning," *Scientific Reports*, vol. 10, no. 1, p. 15 015, 2020, ISSN: 2045-2322. DOI: 10.1038/s41598-020-72147-8.

[21] I. M. Sobol', "Global sensitivity indices for nonlinear mathematical models and their Monte Carlo estimates," *Mathematics and Computers in Simulation*, The Second IMACS Seminar on Monte Carlo Methods, vol. 55, no. 1, pp. 271–280, 2001, ISSN: 0378-4754. DOI: 10.1016/S0378-4754(00)00270-6.

[22] A. Saltelli, P. Annoni, I. Azzini, F. Campolongo, M. Ratto, and S. Tarantola, "Variance based sensitivity analysis of model output. Design and estimator for the total sensitivity index," *Computer Physics Communications*, vol. 181, no. 2, pp. 259–270, 2010, ISSN: 0010-4655. DOI: 10.1016/j.cpc.2009.09.018.

[23] T. Iwanaga, W. Usher, and J. Herman, "Toward SALib 2.0: Advancing the accessibility and interpretability of global sensitivity analyses," *Socio-Environmental Systems Modelling*, vol. 4, p. 18 155, 2022. DOI: 10.18174/sesmo.18155.

[24] J. Herman and W. Usher, "SALib: An open-source python library for sensitivity analysis," *The Journal of Open Source Software*, vol. 2, no. 9, 2017. DOI: 10.21105/joss.00097.

[25] J. P. Mynard and J. J. Smolich, "One-dimensional haemodynamic modeling and wave dynamics in the entire adult circulation," *Annals of Biomedical Engineering*, vol. 43, no. 6, pp. 1443–1460, 2015, ISSN: 1573-9686. DOI: 10.1007/s10439-015-1313-8.

[26] A. Saltelli, "Making best use of model evaluations to compute sensitivity indices," *Computer Physics Communications*, vol. 145, no. 2, pp. 280–297, 2002, ISSN: 0010-4655. DOI: 10.1016/S0010-4655(02)00280-1.

[27] M. S. Olufsen and J. T. Ottesen, "A practical approach to parameter estimation applied to model predicting heart rate regulation," *Journal of Mathematical Biology*, vol. 67, no. 1, pp. 39–68, 2013, ISSN: 1432-1416. DOI: 10.1007/s00285-012-0535-8.

[28] J. J. Moré, "The Levenberg-Marquardt algorithm: Implementation and theory," in *Numerical Analysis*, G. A. Watson, Ed., Berlin, Heidelberg: Springer, 1978, pp. 105–116, ISBN: 978-3-540-35972-2. DOI: 10.1007/BFb0067700.

S2 FILE: SUPPLEMENTARY MATERIAL
FOR THE ARTICLE
PERSONALIZED PULSE WAVE PROPAGATION MODELING TO IMPROVE VASOPRESSOR DOSING MANAGEMENT IN PATIENTS WITH SEVERE TRAUMATIC BRAIN INJURY

Kamil Wolos[1], **Leszek Pstras**[1], **Urszula Bialonczyk**[1], **Malgorzata Debowska**[1], **Wojciech Dabrowski**[2], **Dorota Siwicka-Gieroba**[2], **Jan Poleszczuk**[1]

[1]Laboratory of Mathematical Modeling of Physiological Processes
Nalecz Institute of Biocybernetics and Biomedical Engineering
Polish Academy of Sciences, Warsaw, Poland

[2]Department of Anesthesiology and Intensive Therapy,
Medical University of Lublin, Lublin, Poland

In this Supplementary Figures, we show the fits of the model-simulated arterial volume waveforms (shown in black) to the recorded (averaged) waveforms (shown in light blue). All waveforms were normalized in amplitude. For each patient a few cases are shown corresponding to pulse wave recordings performed on different days. For each case, four fits are shown corresponding to four measurement sites: left arm (LA), right arm (RA), left leg (LL), and right leg (RL).

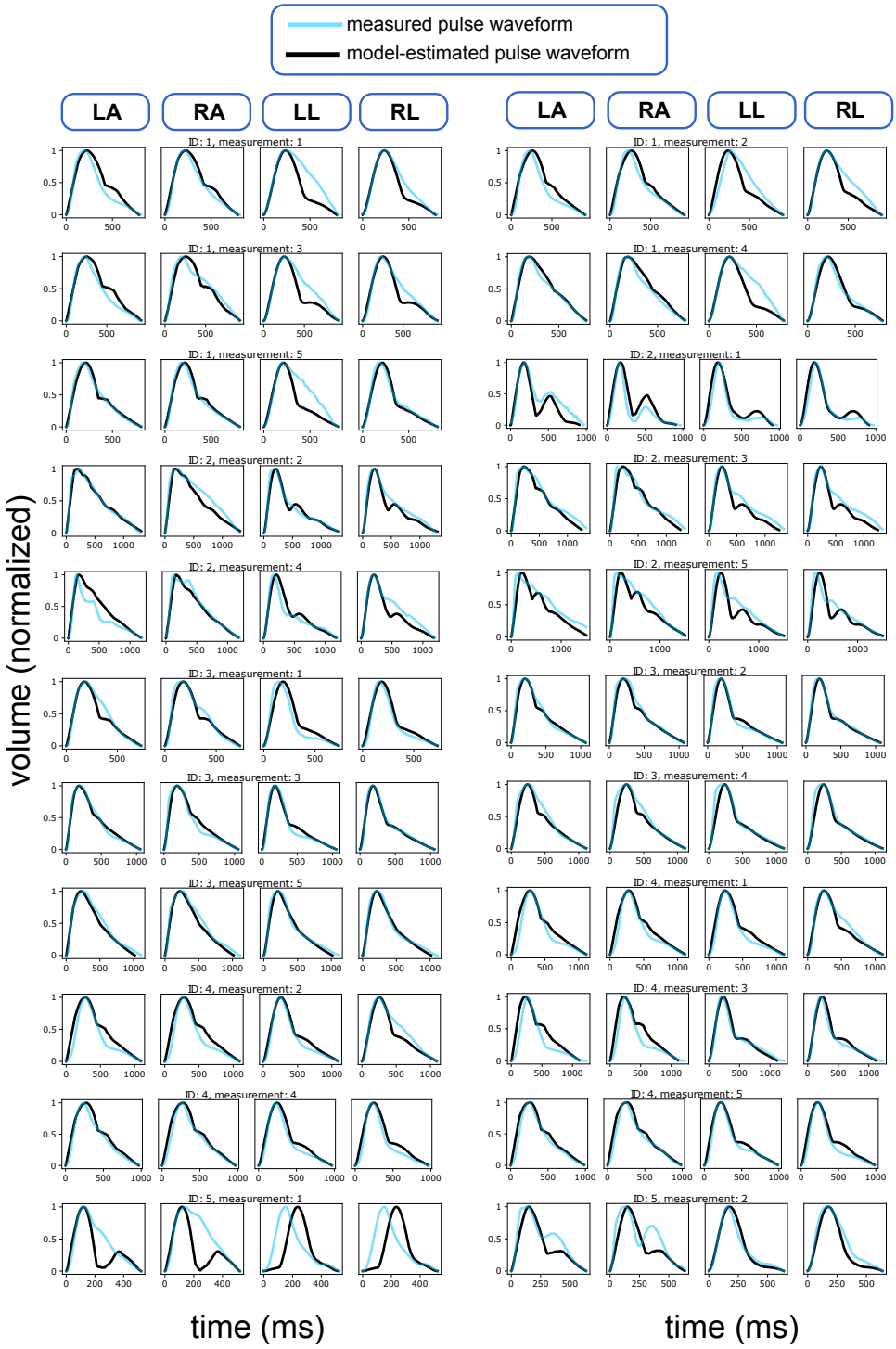

Fig A. Model-simulated vs. recorded arterial volume waveforms

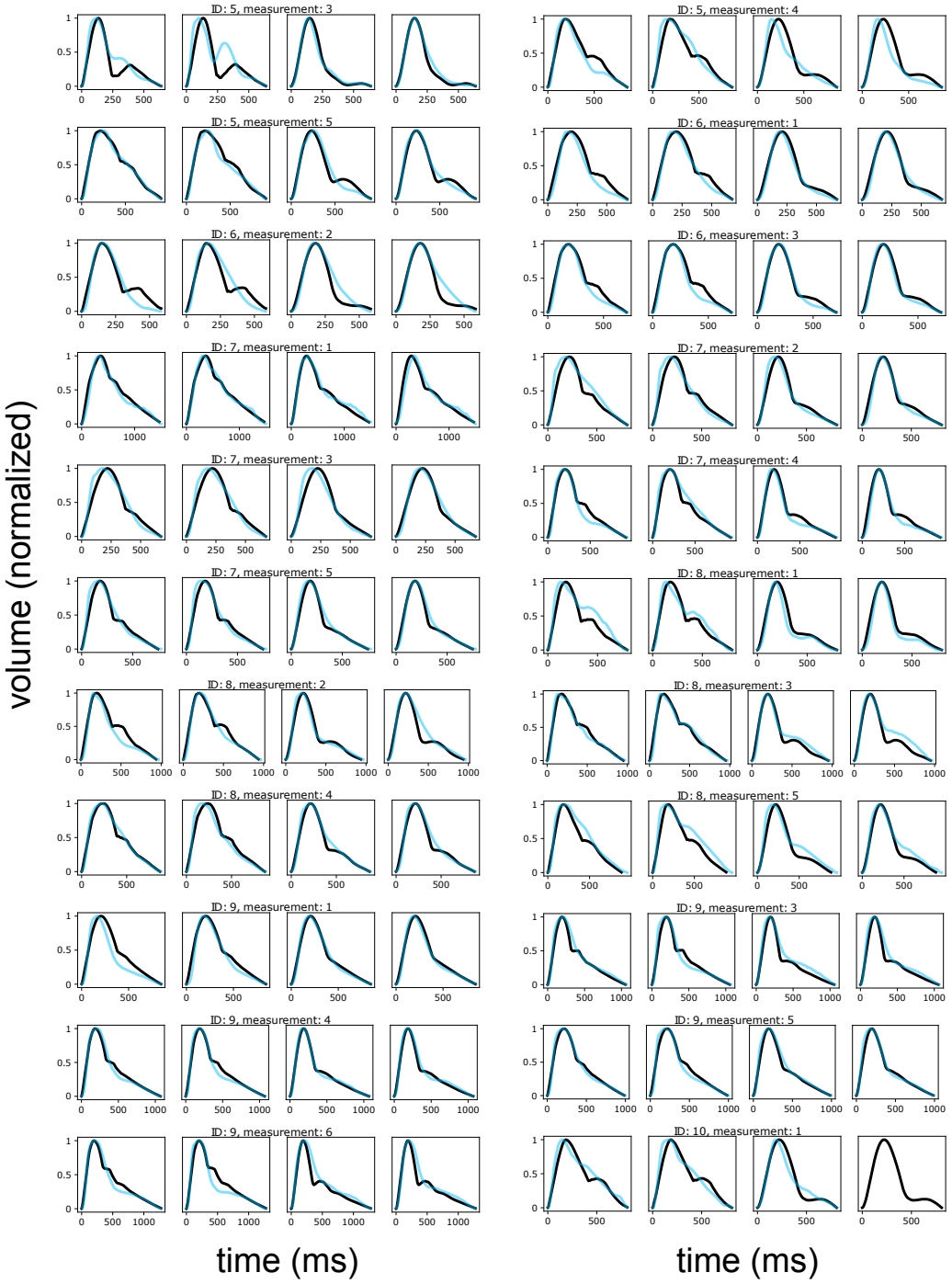

Fig B. Model-simulated vs. recorded arterial volume waveforms

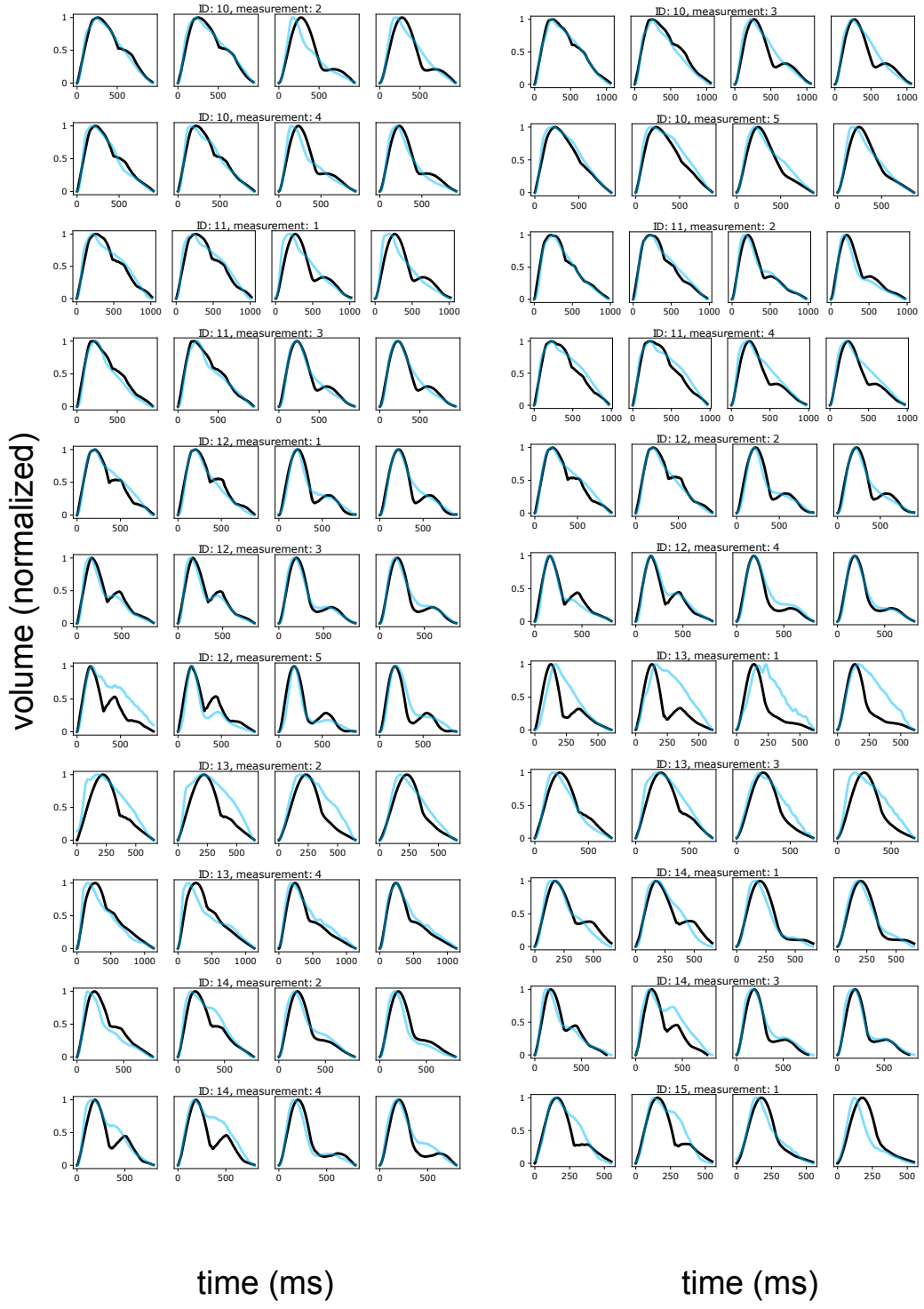

Fig C. Model-simulated vs. recorded arterial volume waveforms

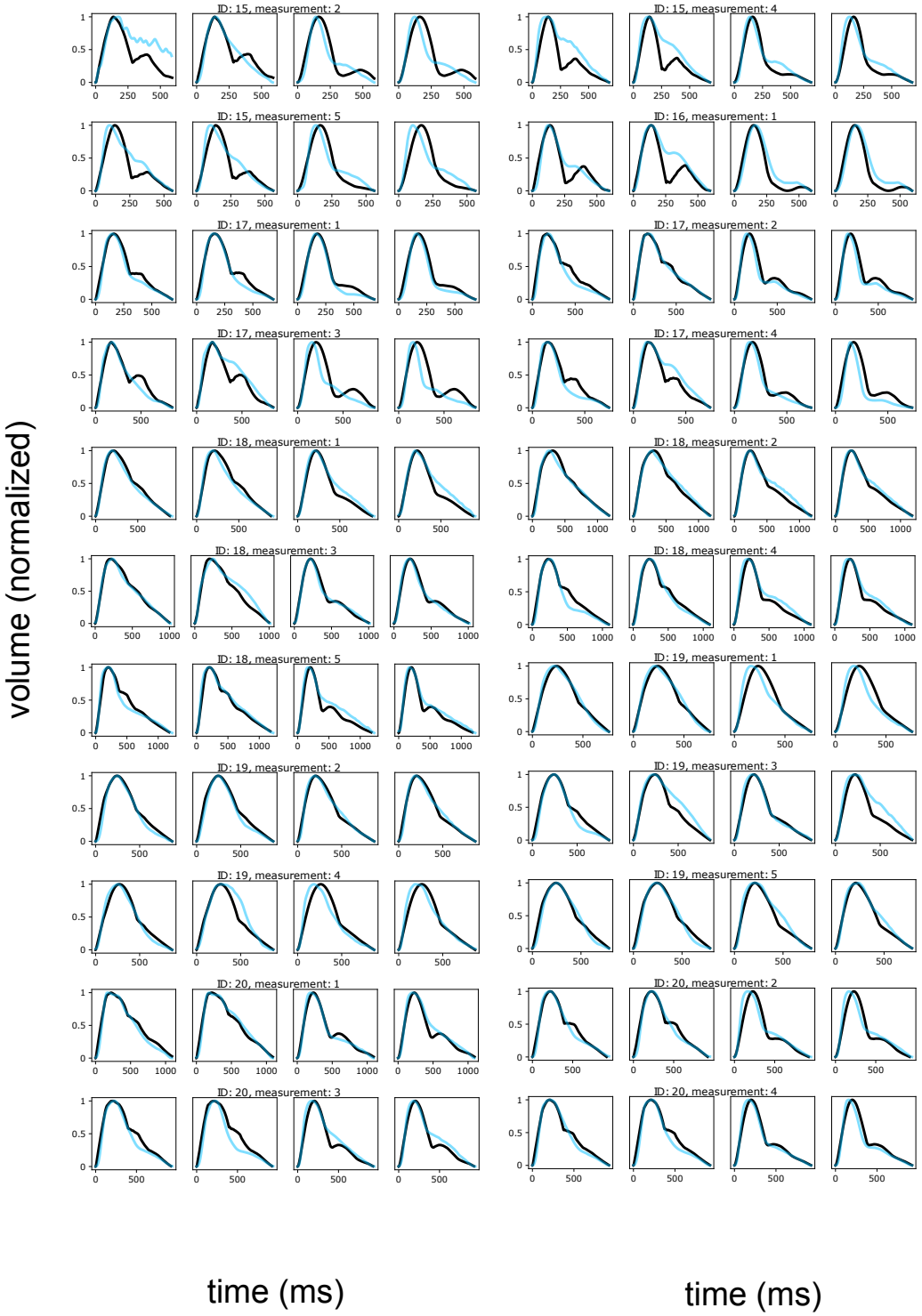

Fig D. Model-simulated vs. recorded arterial volume waveforms

S3 FILE: SUPPLEMENTARY MATERIAL
FOR THE ARTICLE
PERSONALIZED PULSE WAVE PROPAGATION MODELING TO IMPROVE VASOPRESSOR DOSING MANAGEMENT IN PATIENTS WITH SEVERE TRAUMATIC BRAIN INJURY

Kamil Wolos[1], **Leszek Pstras**[1], **Urszula Bialonczyk**[1], **Malgorzata Debowska**[1], **Wojciech Dabrowski**[2], **Dorota Siwicka-Gieroba**[2], **Jan Poleszczuk**[1]

[1]Laboratory of Mathematical Modeling of Physiological Processes
Naleczow Institute of Biocybernetics and Biomedical Engineering
Polish Academy of Sciences, Warsaw, Poland

[2]Department of Anesthesiology and Intensive Therapy
Medical University of Lublin, Lublin, Poland

This supplement presents changes of measured (on the left wrist cuff; shown in blue) and model estimated (on the radial artery; shown in orange) values of systolic pressure (SP; left column) and diastolic pressure (DP; right column) during the treatment. Additionally, for comparison, the dosage of vasopressors is shown (in light red).

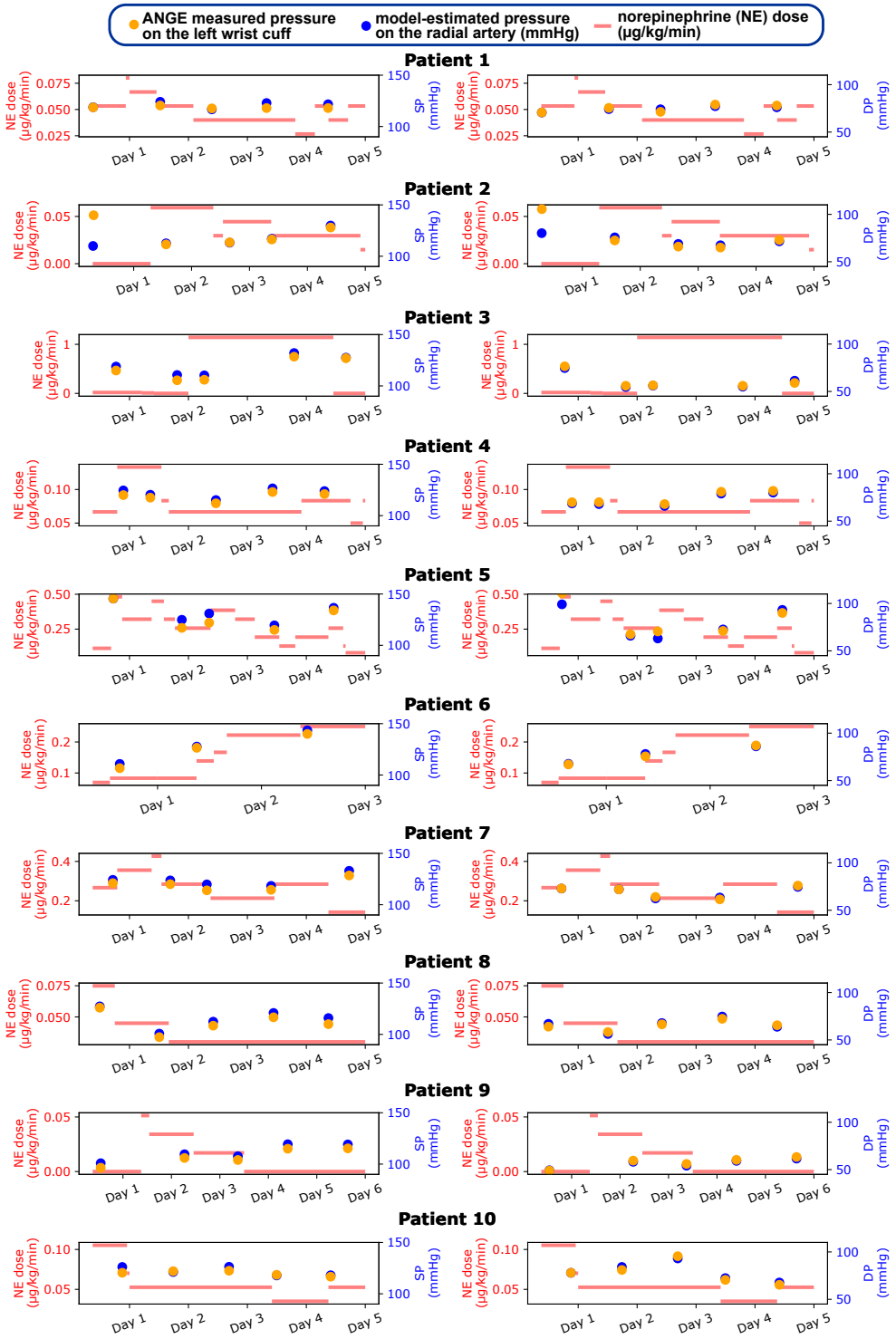

Fig A. Comparison of measured SP and DP (left wrist cuff, blue) and model-estimated values (radial artery, orange) over time during treatment. Vasopressor dosage is indicated in light red for reference (patients 1 – 10).

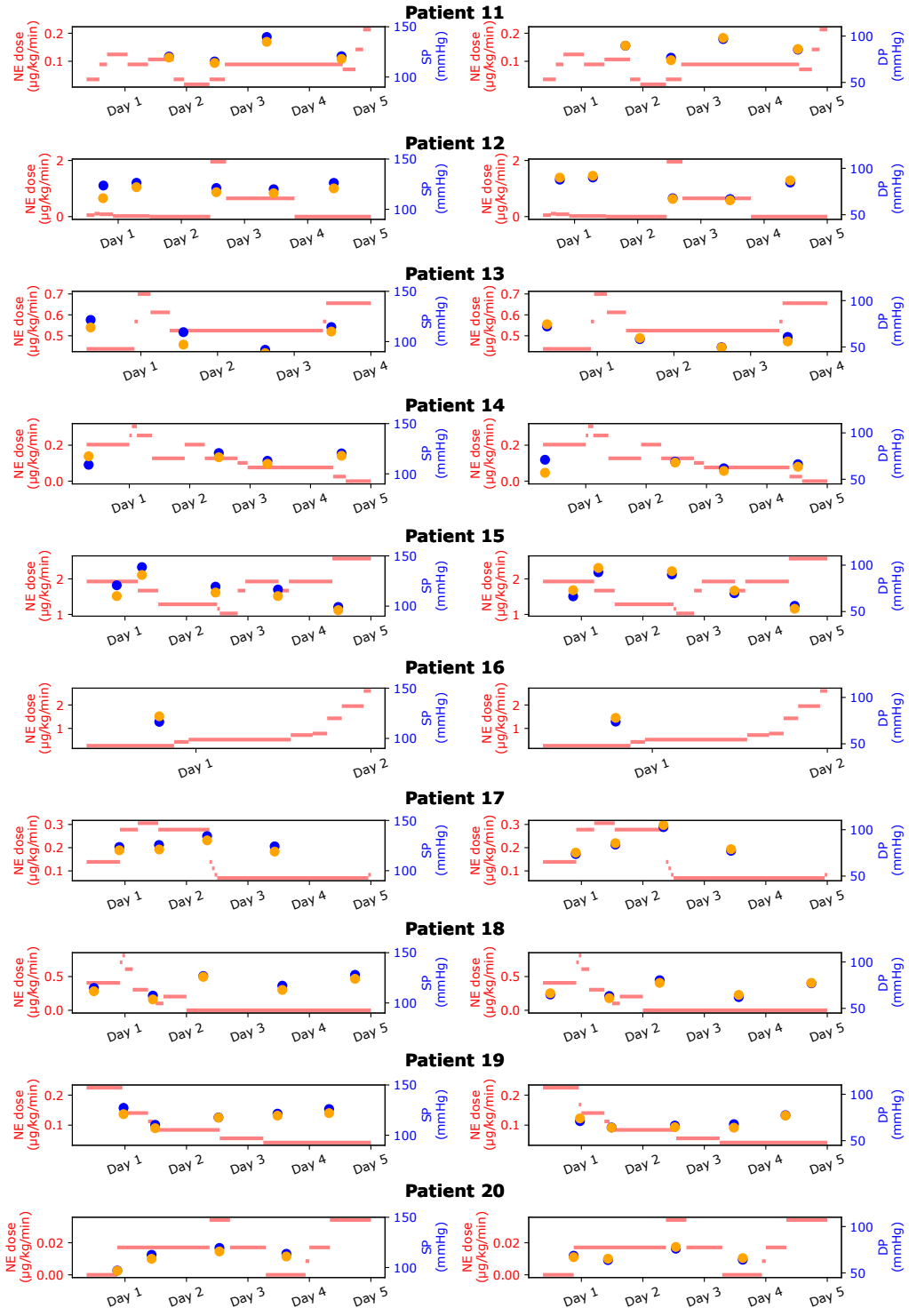

Fig B. Comparison of measured SP and DP (left wrist cuff, blue) and model-estimated values (radial artery, orange) over time during treatment. Vasopressor dosage is indicated in light red for reference (patients 11 – 20).

S4 File: Supplementary Material
for the article
Personalized Pulse Wave Propagation Modeling to Improve Vasopressor Dosing Management in Patients with Severe Traumatic Brain Injury

Kamil Wolos[1], Leszek Pstras[1], Urszula Bialonczyk[1], Malgorzata Debowska[1], Wojciech Dabrowski[2], Dorota Siwicka-Gieroba[2], Jan Poleszczuk[1]

[1]Laboratory of Mathematical Modeling of Physiological Processes
Naleczi Institute of Biocybernetics and Biomedical Engineering
Polish Academy of Sciences, Warsaw, Poland

[2]Department of Anesthesiology and Intensive Therapy,
Medical University of Lublin, Lublin, Poland

Here, we present a visualization of the vasopressor doses and their adjustments during the observation period, along with the predictions of our statistical model (full model) with regard to the changes in vasopressor dose within the next 24 hours from the time of pulse wave recording. The numbers next to the symbols of predictions indicate the probability assigned to the given prediction.

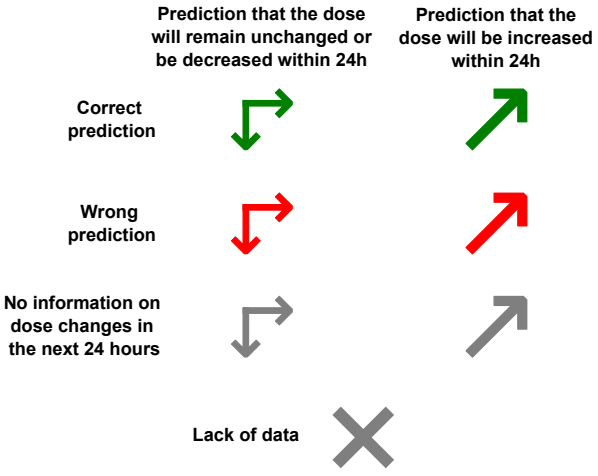

LEGEND

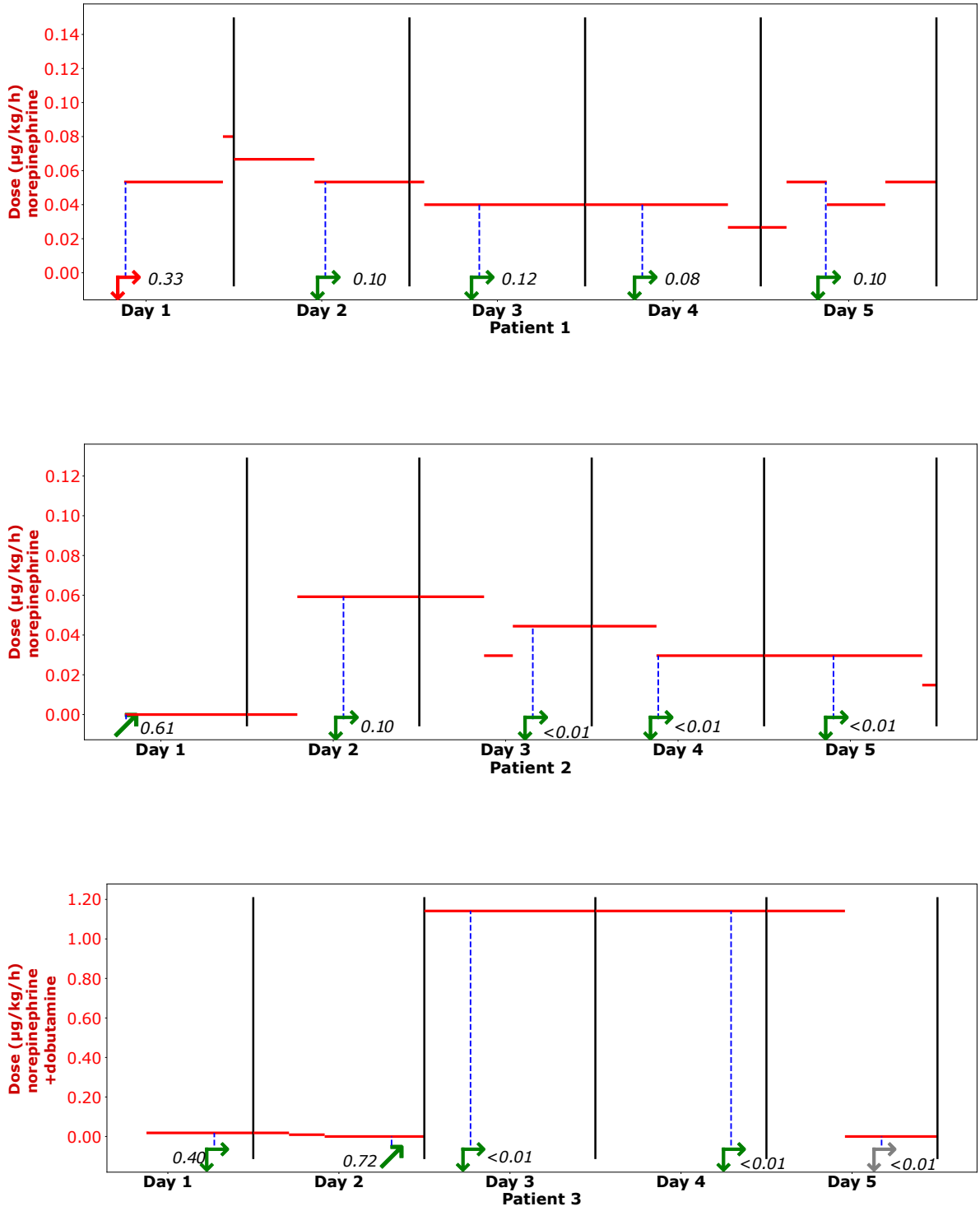

Fig A. Visualization of vasopressor dosage (shown in red) and model predictions for patients 1–3. The full model's predictions for changes in vasopressor dose within the next 24 hours are indicated, with probabilities displayed next to each prediction symbol. Refer to the Legend for further details.

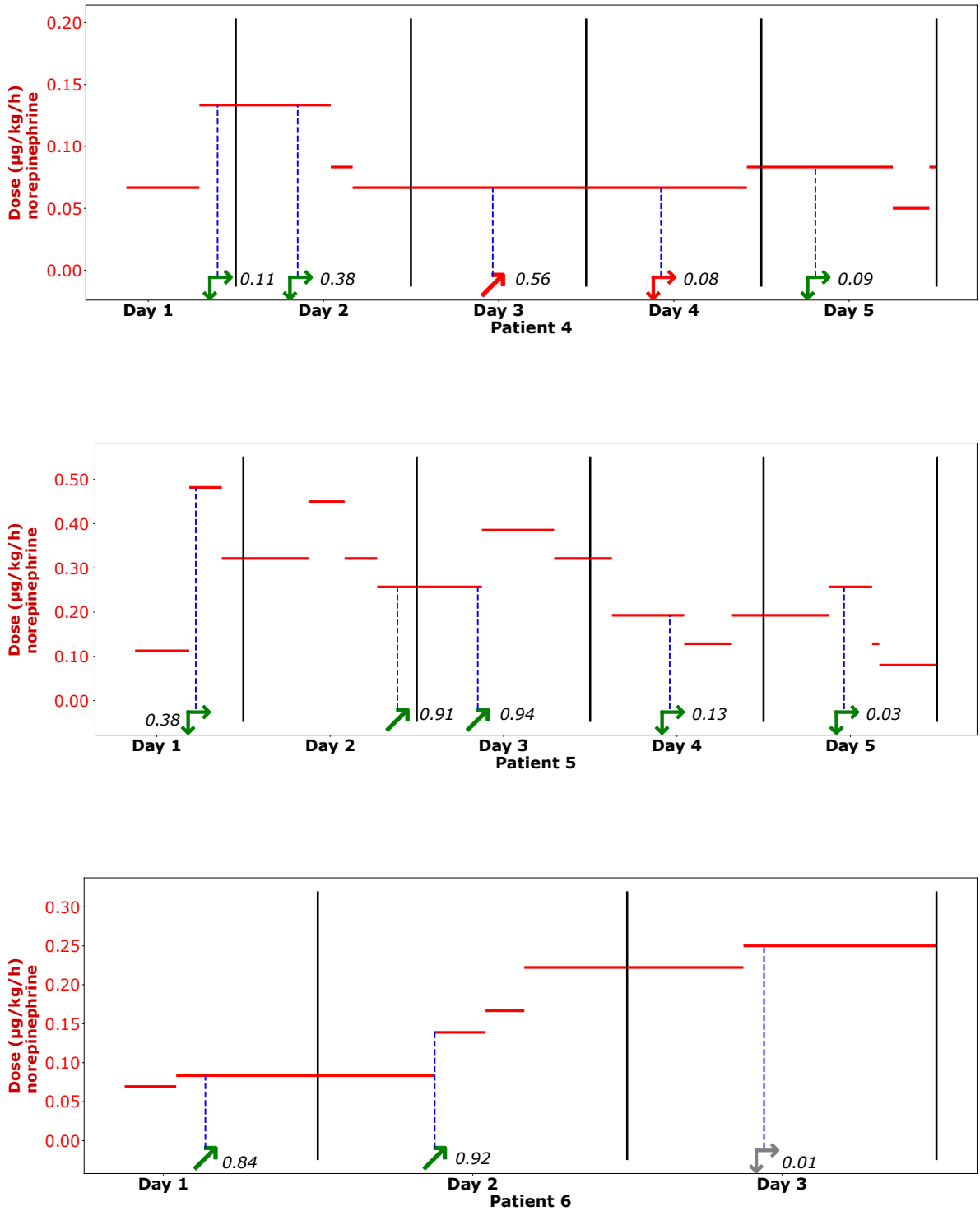

Fig B. Visualization of vasopressor dosage (shown in red) and model predictions for patients 4–6. The full model's predictions for changes in vasopressor dose within the next 24 hours are indicated, with probabilities displayed next to each prediction symbol. Refer to the Legend for further details.

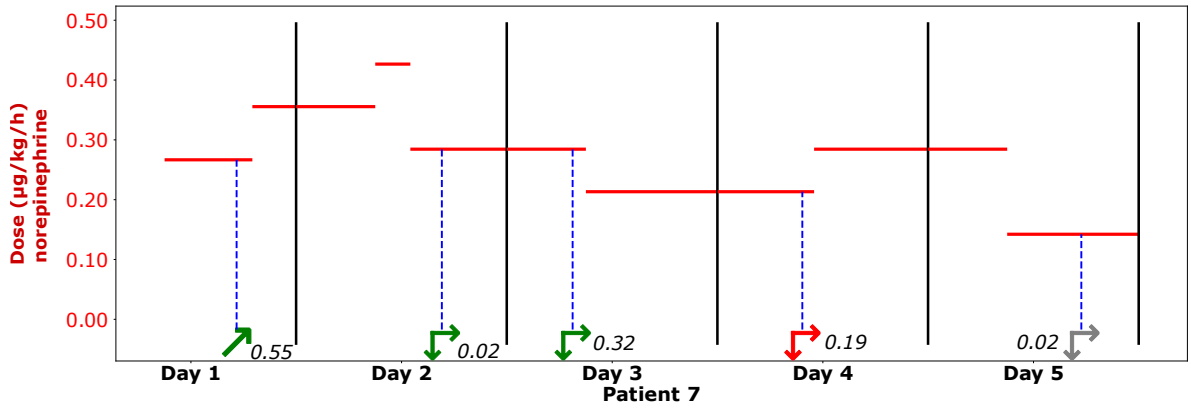

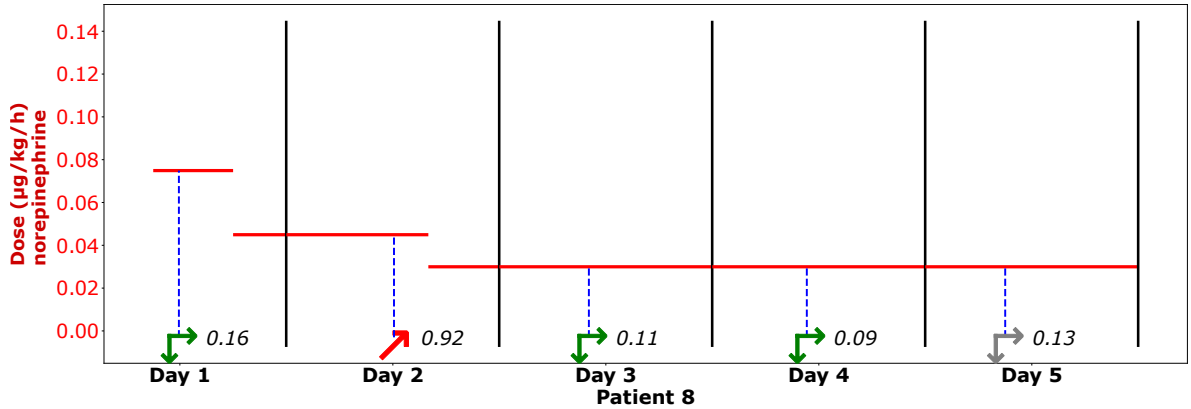

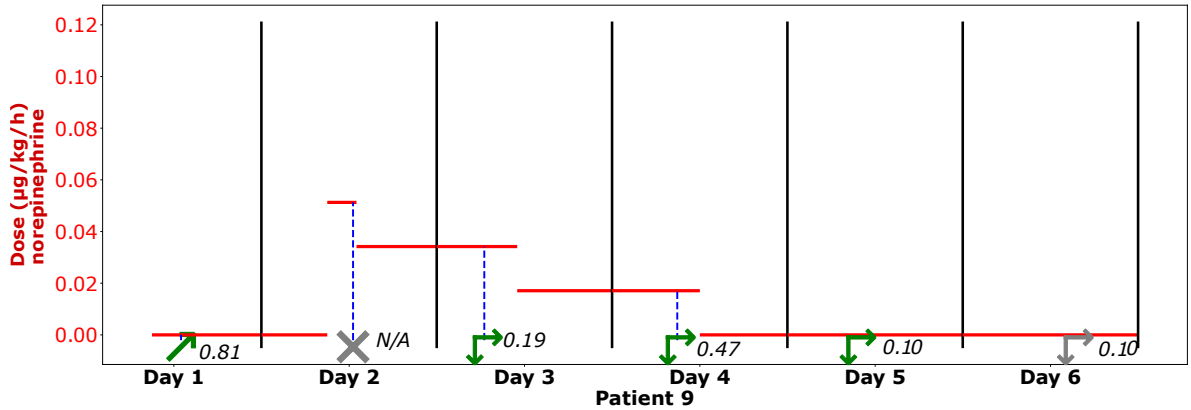

Fig C. Visualization of vasopressor dosage (shown in red) and model predictions for patients 7–9. The full model's predictions for changes in vasopressor dose within the next 24 hours are indicated, with probabilities displayed next to each prediction symbol. Refer to the Legend for further details.

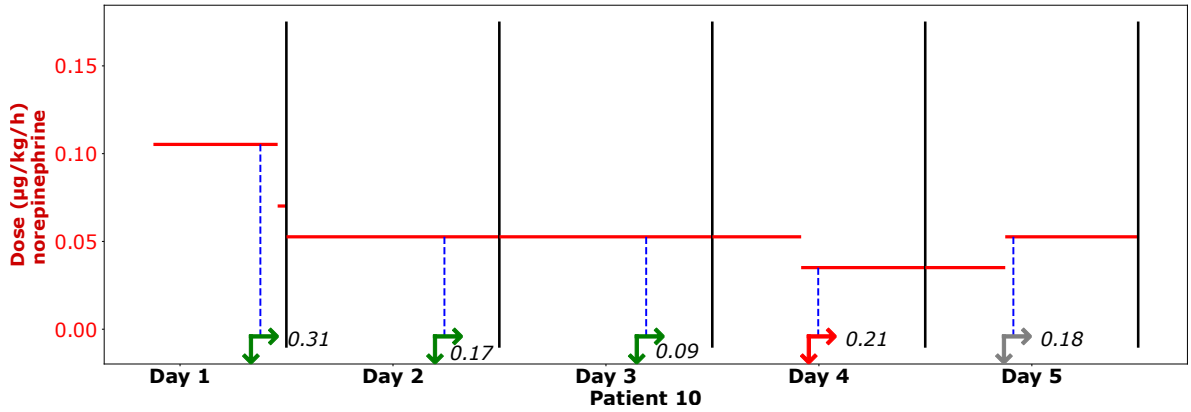

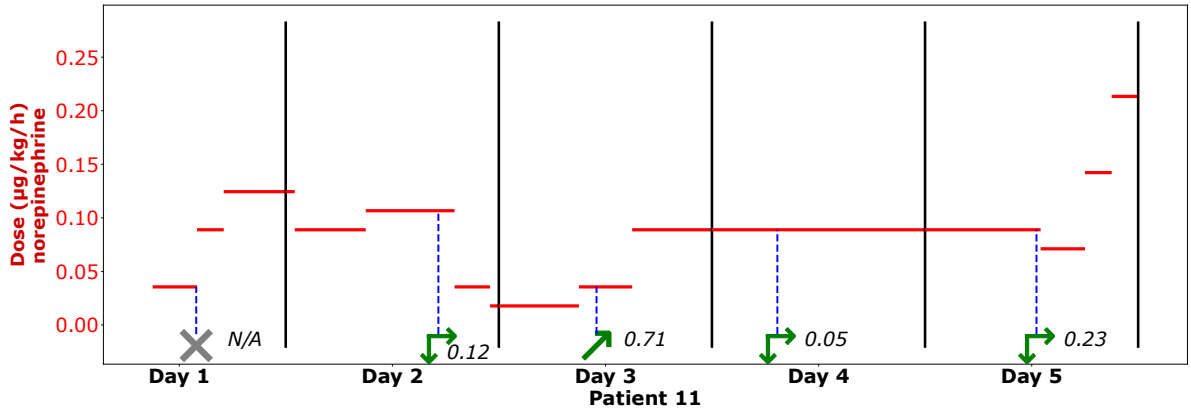

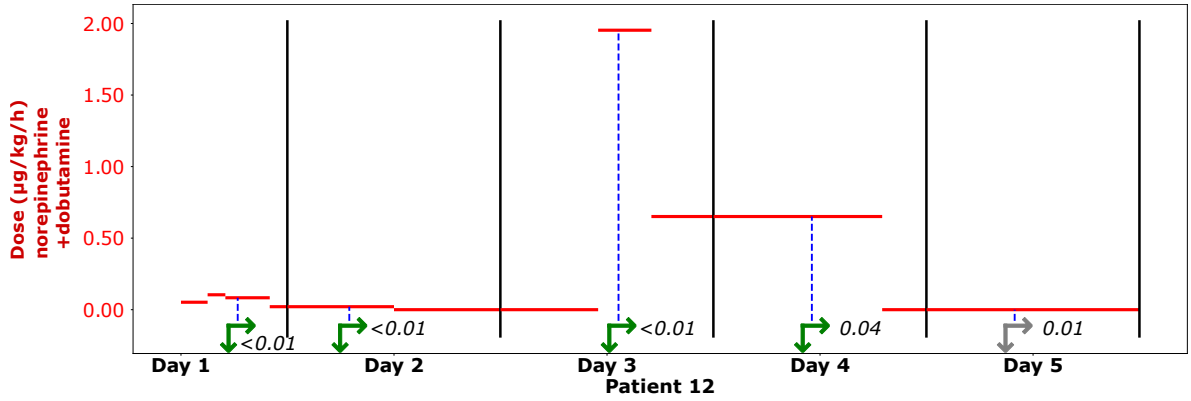

Fig D. Visualization of vasopressor dosage (shown in red) and model predictions for patients 10–12. The full model's predictions for changes in vasopressor dose within the next 24 hours are indicated, with probabilities displayed next to each prediction symbol. Refer to the Legend for further details.

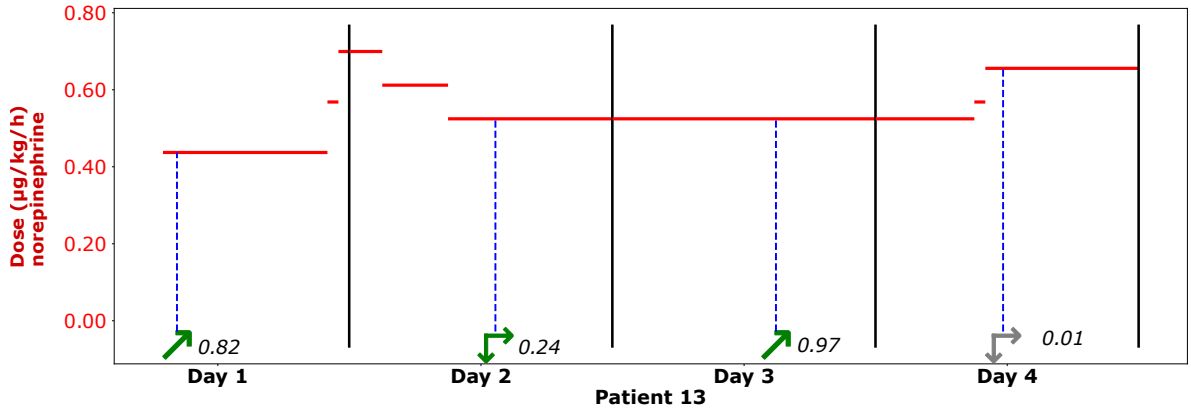

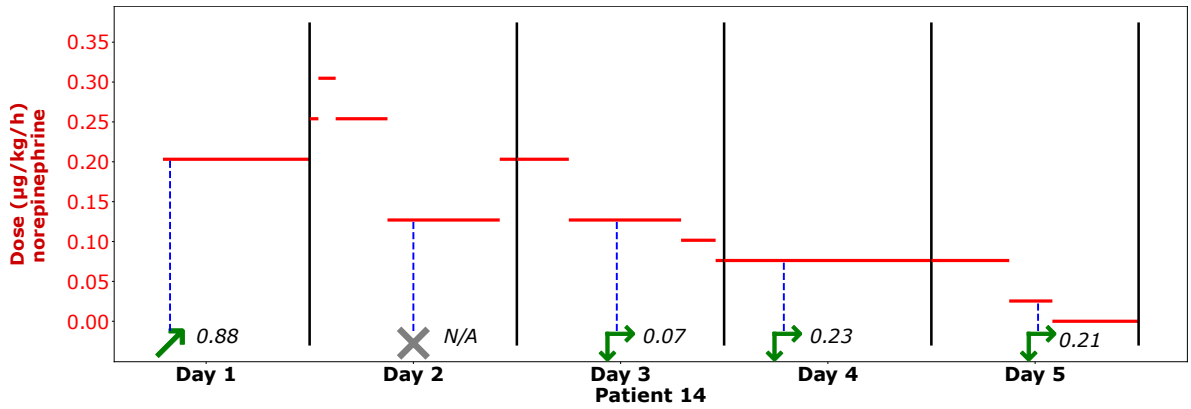

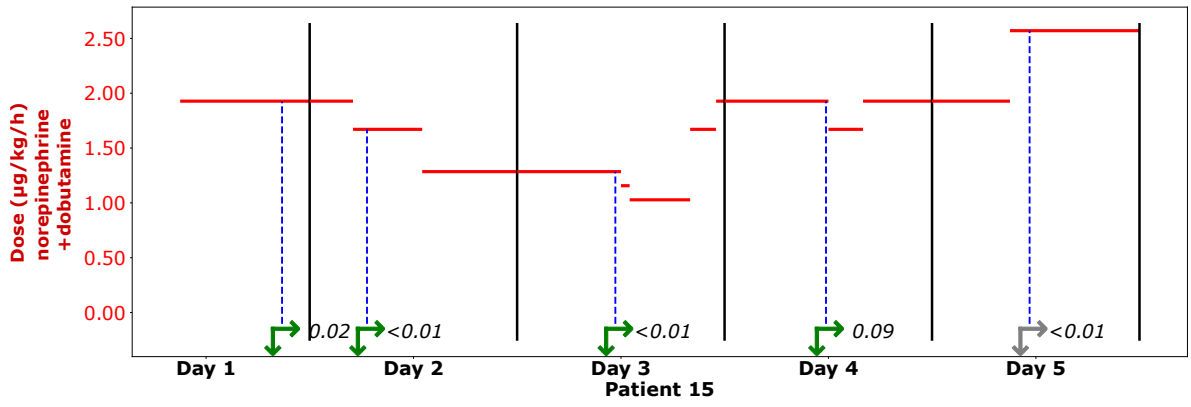

Fig E. Visualization of vasopressor dosage (shown in red) and model predictions for patients 13–15. The full model's predictions for changes in vasopressor dose within the next 24 hours are indicated, with probabilities displayed next to each prediction symbol. Refer to the Legend for further details.

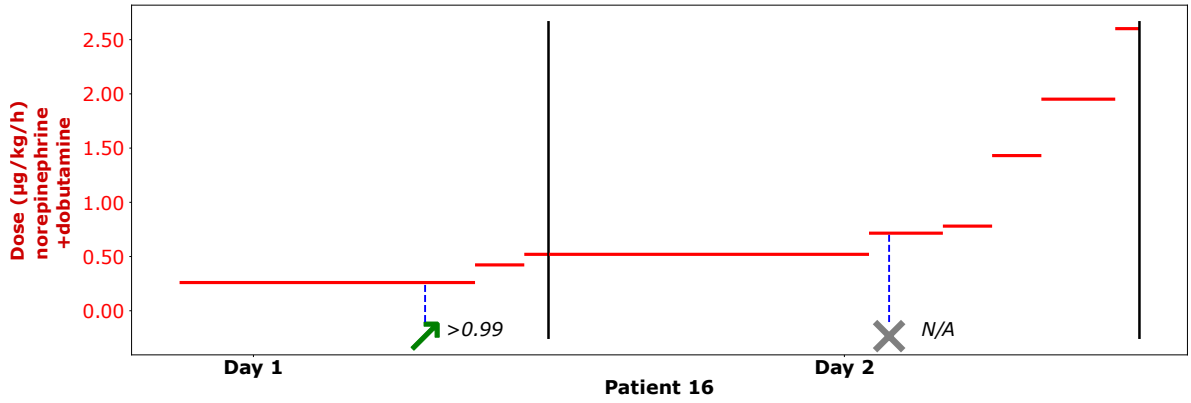

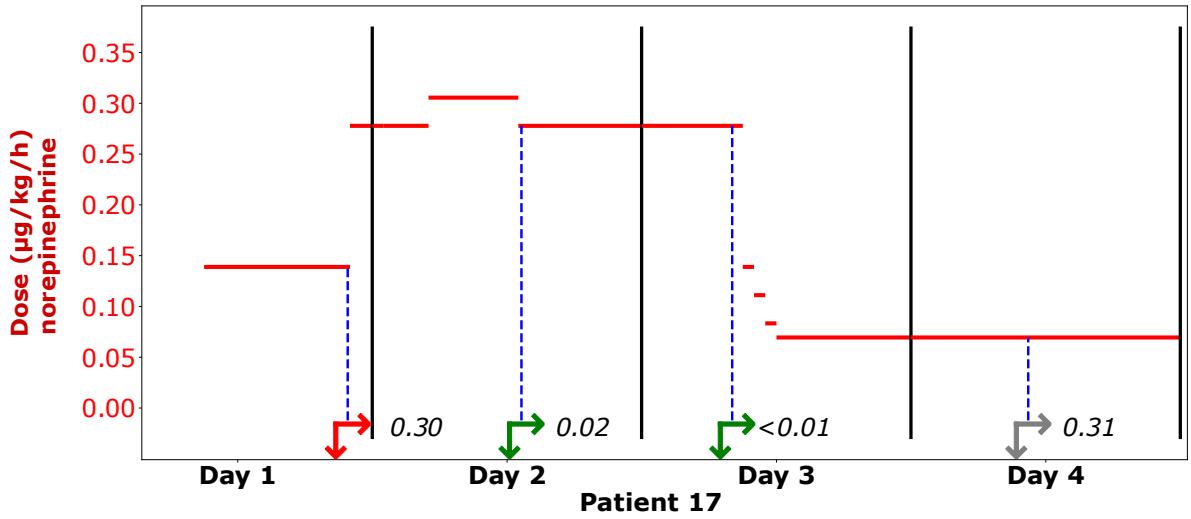

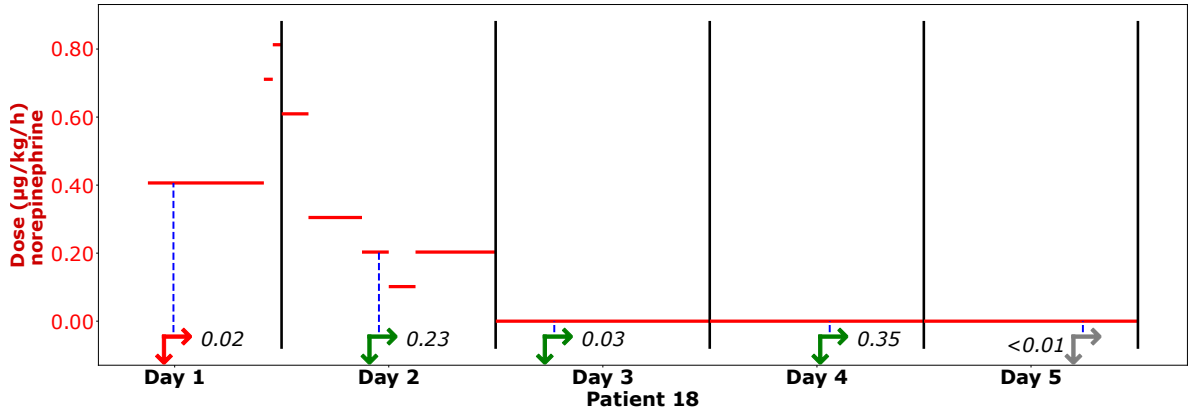

Fig F. Visualization of vasopressor dosage (shown in red) and model predictions for patients 16–18. The full model's predictions for changes in vasopressor dose within the next 24 hours are indicated, with probabilities displayed next to each prediction symbol. Refer to the Legend for further details.

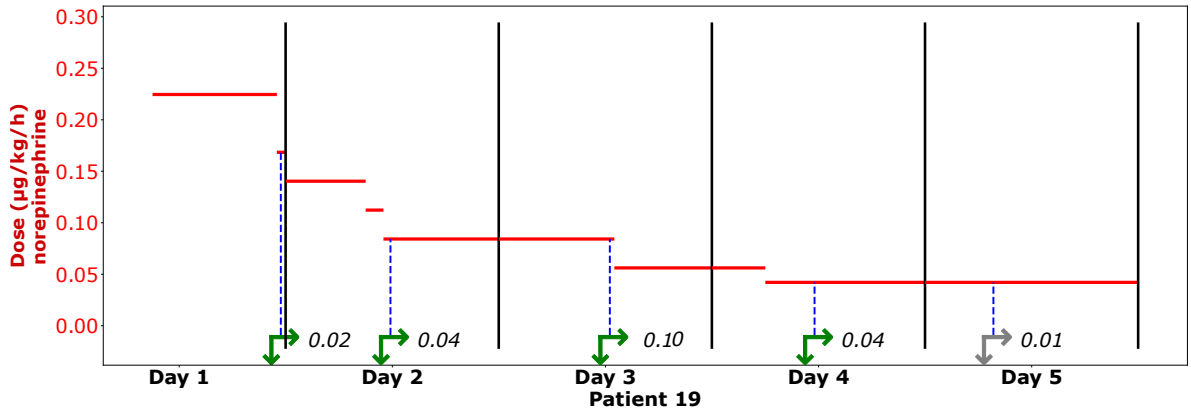

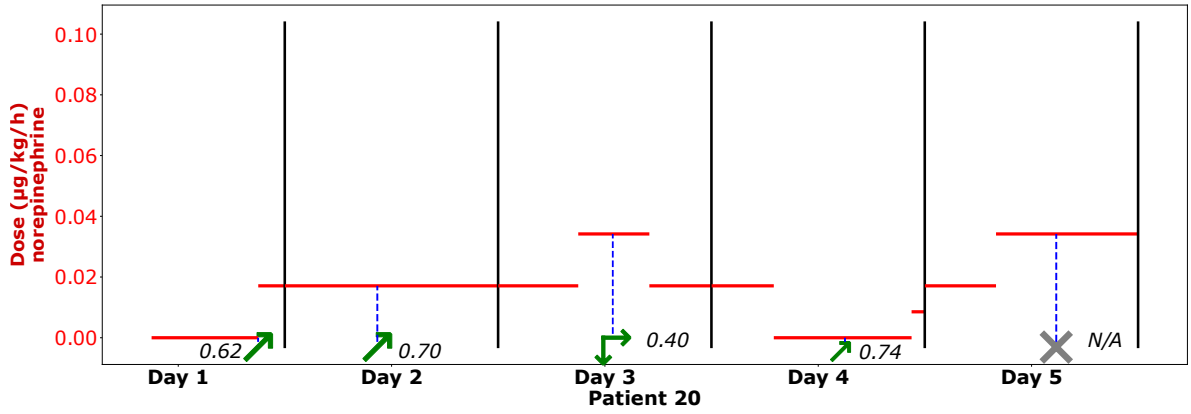

Fig G. Visualization of vasopressor dosage (shown in red) and model predictions for patients 19 and 20. The full model's predictions for changes in vasopressor dose within the next 24 hours are indicated, with probabilities displayed next to each prediction symbol. Refer to the Legend for further details.

Chapter 4

Publication [A3]: Impact of Multi-Limb Oscillometric Cuff Measurements on Hemodynamics: Insights from Pulse Wave Propagation Modeling

4.1 Summary of the study

In this study, I addressed an important and underexplored aspect of non-invasive cuff-based assessment of cardiovascular system, i.e., the hemodynamic consequences of simultaneous multi-limb arterial occlusion due to oscillometric cuff inflation. Although oscillometric cuffs applied to multiple limbs are increasingly used for cardiovascular diagnostics to estimate various vascular parameters and detect their potential differences between body sides, their effects on central and peripheral hemodynamics remain insufficiently understood. This topic is especially important given our previous study, in which we used such an oscillometric device (AngE, SOT Medical, Austria) to measure pulse waves and hemodynamic parameters in patients with severe traumatic brain injury (sTBI). My goal was to determine how inflating oscillometric cuffs on the wrists and/or ankles affects mean arterial pressure (MAP) and blood flow in key arterial locations, especially in conditions where cardiovascular regulatory mechanisms may be impaired or absent. With this aim, I formulated the following research hypothesis:

(H4) *A pulse wave propagation model can be used to assess the hemodynamic effects of peripheral arterial occlusions due to oscillometric cuff measurements.*

To address this hypothesis, I formulated the following research question:

(H4Q1) *How can a pulse wave propagation model be adapted to simulate peripheral arterial occlusion due to oscillometric cuff measurements?*

(H4Q2) *What are the local and central hemodynamic consequences of a single-limb oscillometric cuff measurement?*

(H4Q3) *What are the local and central hemodynamic consequences of multi-limb oscillometric cuff measurements?*

(H4Q4) *Are the central hemodynamic consequences of multi-limb oscillometric cuff measurements similar in different subjects?*

To address H4Q1, my first step was to extend the existing 0-1D pulse wave propagation model to account for the effects of cuff inflation on selected arterial segments. In our 0-1D arterial tree model, vessel wall mechanics are represented by a standard elastic model relating cross-sectional area to transmural pressure [118, 106]. However, during cuff inflation above arterial pressure, transmural pressure becomes negative and leads to vessel collapse, which the elastic model cannot capture. To address this, I incorporated the framework of Drzewiecki et al. [145], which combines arterial elastic distension with the vessel collapse at negative pressures. For computational simplicity, the relation from Drzewiecki's study was applied only to arterial segments under the cuff and approximated locally by scaling the standard elastic model around the expected mean transmural pressure (for full details, see the publication). This allowed me to preserve the structure of the original model while accounting for the vessel collapse effects. Since this study was focused on steady-state conditions after cuff inflation, viscoelastic effects and dynamic inflation/deflation processes were not modeled. Instead, each simulation was run until a steady state was achieved for a given cuff pressure, representing the worst-case hemodynamic scenario, assuming no cardiovascular regulation. The absence of modeling of pressure regulatory mechanisms (e.g., baroreflex) was justified by the fact that impairment of these functions is common in patients with sTBI [146, 147]. In such sensitive populations, a transient increase in cerebral blood pressure may increase intracranial pressure (especially with the common impairment of cerebral autoregulation in such patients [148]) and therefore increase the risk of secondary injury.

The proposed model extension allowed me to model a complete arterial occlusion caused by suprasystolic cuff pressure (i.e., exceeding systolic arterial pressure). By simulating different cuff pressures, I obtained detailed insights into the local and systemic hemodynamic perturbations induced by single- or multi-limb cuff inflation (H4Q2 and H4Q3).

The model reliably captures the local hemodynamic changes induced by cuff inflation: the volumetric waveforms remain almost unaffected when cuff pressure is below systolic levels, while the cross-sectional areas of arteries beneath the cuff decrease progressively as cuff pressure increases (H4Q2, H4Q3). Simulation results showed that a single-limb (left wrist) occlusion had minimal impact on central hemodynamics, with changes in MAP and aortic blood flow remaining below 3%. In contrast, a four-limb occlusion increased central MAP by approximately 10% and carotid artery blood flow by about 11%, while modestly reducing the aortic flow (H4Q2, H4Q3).

Using a local sensitivity analysis, I identified the key cardiovascular parameters influencing the hemodynamic response to multi-limb arterial occlusion. For the four-cuff occlusion scenario, this analysis indicated that blood pressure and mean flow in the left common carotid artery were most sensitive to variations in the heart period, left ventricular elastance, end-diastolic volume, left atrial pressure, and terminal arterial resistance scaling factor. The global sensitivity analysis confirmed these results, identifying the same parameters as the primary contributors to the variability in the studied model outputs (i.e., MAP and mean flow in the left common carotid artery). Additional simulations accounting for inter-patient variability (performed on a large set of virtual patients with randomly adjusted values of cardiovascular parameters) confirmed that the four-limb peripheral arterial occlusion can increase MAP by $\sim$10% and mean carotid blood flow by $\sim$12% on average; however, the magnitude of these changes may depend on baseline cardiovascular properties (H4Q4).

In summary, this *in-silico* study contributes to a better understanding of the systemic and central hemodynamic effects that may be induced by simultaneous cuff-based measurements on multiple limbs in patients with impaired blood pressure regulation. To my knowledge, this is the first study to use a pulse wave propagation model to investigate the hemodynamic consequences of multi-limb oscillometric cuff inflation. The findings highlight the importance of considering these effects in clinical practice, especially in vulnerable populations, and provide a foundation for future experimental validation.

4.2 My contributions

I am the first author of this publication, responsible for the conceptualization, methodology, software implementation, validation, formal analysis, data curation, investigation, and original draft writing. I extended the mathematical model by integrating the effects of arterial occlusion due to cuff inflation. I implemented the simulation framework to analyze local and systemic hemodynamic changes induced by single- and multi-limb cuff inflation. Furthermore, I also conducted the sensitivity analyses to identify key cardiovascular parameters influencing the hemodynamic response to multi-limb arterial occlusion. Additionally, I prepared all figures and tables presented in the article and supplementary materials.

4.3 Author contributions

The conceptualization and methodology of the study were developed in collaboration with my Advisors, Prof. Jan Poleszczuk and Dr. Leszek Pstraś, and with Prof. Małgorzata Dębowska. Prof. Poleszczuk and Dr. Pstraś also provided supervision, project administration, and guidance throughout the research. All authors contributed to the validation and critical review of the study. The manuscript was revised and edited with the support of my Advisors and Prof. Dębowska.

4.4 Publication

frontiers | Frontiers in Physiology

TYPE Original Research
PUBLISHED 15 August 2025
DOI 10.3389/fphys.2025.1642645

OPEN ACCESS

EDITED BY
Lisheng Xu,
Northeastern University, China

REVIEWED BY
Hao-Nan Wang,
Sichuan University, China
Yujia Zhong,
Northeastern University Archives,
Northeastern University, China

*CORRESPONDENCE
Kamil Wolos,
kwolos@ibib.waw.pl

RECEIVED 06 June 2025
ACCEPTED 28 July 2025
PUBLISHED 15 August 2025

CITATION
Wolos K, Pstras L, Debowska M and Poleszczuk J (2025) Impact of multi-limb oscillometric cuff measurements on hemodynamics: insights from pulse wave propagation modeling.
Front. Physiol. 16:1642645.
doi: 10.3389/fphys.2025.1642645

Impact of multi-limb oscillometric cuff measurements on hemodynamics: insights from pulse wave propagation modeling

Kamil Wolos*, Leszek Pstras, Malgorzata Debowska and Jan Poleszczuk

Laboratory of Mathematical Modeling of Physiological Processes, Nalecz Institute of Biocybernetics and Biomedical Engineering, Polish Academy of Sciences, Warsaw, Poland

Objective: Multi-limb oscillometric cuff measurements can be used for estimating various vascular parameters and evaluating side differences in arterial pulse waveforms. In this study, we conduct an *in silico* investigation to evaluate the potential impact of such measurements on hemodynamics.

Methods: We employed a 0–1D model of pulse wave propagation to examine the relationship between different levels of oscillometric cuff pressure applied simultaneously at multiple sites (right above the wrists and/or ankles) and the resulting changes in blood pressure and flow at selected sites in the vascular system, assuming the absence of cardiovascular regulatory mechanisms. The simulations included various combinations of cuff placements, including four cuffs applied simultaneously on all limbs. In addition, we conducted both global and local sensitivity analysis to evaluate the impact of selected cardiovascular parameters on the simulation results.

Results: In the case of cuffs placed on all four limbs and inflated to suprasystolic pressure - effectively occluding the vessels beneath the cuffs - our simulations indicated an increase in mean arterial pressure (MAP) of approximately 10% in the ascending aorta, left common carotid artery, and abdominal aorta. Additionally, the mean carotid artery blood flow increased by approximately 11% compared to baseline value. In contrast, for the case with a cuff placed only on one wrist, we observed a significantly smaller MAP increase of only 2.5%, with a 3% rise in mean carotid artery flow. Our sensitivity analysis revealed that these changes can be mitigated by relatively small adjustments in specific cardiovascular parameters, suggesting that properly functioning physiological regulatory mechanisms should easily compensate for the cuff induced hemodynamic alterations. Furthermore, global sensitivity analysis demonstrated that relatively similar increases in MAP and mean carotid blood flow are expected for different combinations of cardiovascular parameters values, indicating the robustness of our findings.

Significance: This *in silico* study suggests that multi-limb cuff-based measurements may induce measurable central hemodynamic alterations if

not counteracted by cardiovascular regulatory mechanisms. This suggests that such measurements may not be innocuous to individuals with some deficiencies in cardiovascular regulation. Further investigation is warranted to verify this *in vivo* and, if necessary, establish appropriate safety protocols.

KEYWORDS

cardiovascular modeling, oscillometric measurement, hemodynamics, blood pressure, pulse wave propagation

1 Introduction

Oscillometric blood pressure (BP) measurement is a widely used non-invasive technique, leveraging cuff-induced arterial occlusion and cuff pressure oscillations to estimate systolic and diastolic arterial blood pressure (Muntner et al., 2019). The most common version of this method involves relatively rapid inflation of a cuff wrapped around a limb (usually around the upper arm) to suprasystolic pressure, temporarily occluding blood flow in the underlying blood vessels. During subsequent cuff deflation, the gradual arterial reopening generates oscillations in the cuff pressure that correlate with pulsatile arterial blood volume changes (Alpert et al., 2014) and form the basis for blood pressure estimation. While the traditional oscillometric method uses a single-cuff measurement with relatively continuous inflation and deflation of the cuff, devices such as AngE (SoT Medical, Austria) utilize simultaneous multi-limb cuff measurements with a more stepped deflation process and longer periods of maintaining the cuff inflated for advanced cardiovascular diagnostics, especially for estimating various vascular parameters and evaluating side differences in arterial pulse waveforms. However, concurrent occlusion of peripheral arteries in multiple limbs for longer periods of time raises questions about hemodynamic interference, particularly in populations with deficiencies in cardiovascular regulation.

Previous studies suggested that arterial occlusion using a cuff on one or two upper limbs can transiently affect central hemodynamics. Liang et al., in an *in silico* study (Liang et al., 2013), demonstrated that the pulse waveform proximal to a single cuff placed around the brachial artery can vary significantly with cuff pressure. Trachet et al. also demonstrated *in silico* local changes in the brachial artery pulse waveform associated with single cuff-induced occlusion (Trachet et al., 2010). However, none of the aforementioned *in silico* studies looked directly at central blood flow and pressure changes following peripheral cuff-induced occlusions. On the other hand, Kashyap et al. found *in vivo* that bilateral brachial artery occlusion, achieved by inflating cuffs on both arms, can lead to changes in carotid and vertebral artery blood flow in asymptomatic patients with a complete circle of Willis (Kashyap et al., 2005). This underscores the potential impact of peripheral vascular flow alterations on cerebral hemodynamics, which is particularly relevant in clinical contexts where maintaining stable cerebral perfusion is crucial. For example, cerebral blood flow alterations are critically important in patients with severe traumatic brain injury (sTBI), as they can cause secondary brain damage and negatively influence long-term outcomes (Graves et al., 2015). A key concern in sTBI is the frequent impairment of cerebrovascular autoregulation, which has been reported in over 70% of patients (Sviri et al., 2009), which renders cerebral blood flow pressure passive and heightens vulnerability to systemic blood pressure fluctuations (Toth et al., 2016; Rangel-Castilla et al., 2008). Moreover, evidence suggests that, in addition to changes in baroreflex sensitivity (BRS) occurring directly after brain trauma (Uryga et al., 2023), both mild and severe TBI can lead to persistent autonomic dysfunction, manifesting as altered heart rate variability, reduced BRS, and impaired cardiovascular responses to physiological stressors such as posture changes or Valsalva maneuver (Hilz et al., 2011; Hilz et al., 2017; Hilz et al., 2016). These impairments have been linked to increased morbidity and mortality in acute brain injury patients (Hilz et al., 2015; Papaioannou et al., 2008; Sykora et al., 2016). Additionally, studies have shown that heart rate responses to both lowering and elevating blood pressure are depressed by propofol anesthesia (Sato et al., 2005), which is frequently administered in intensive care units during the days following severe brain injury to help manage intracranial pressure.

The purpose of our study was to analyze the potential hemodynamic consequences of multi-limb oscillometric measurements using a physiology-based modeling approach. Primarily, we sought to estimate the effect of multi-site cuff inflation on hemodynamic parameters such as mean arterial pressure (MAP) and blood flow at various locations in the arterial tree (with a particular focus on the central arteries), assuming the absence of cardiovascular regulatory mechanisms. For this purpose, we applied a previously developed cardiovascular model of pulse wave propagation (Poleszczuk et al., 2018a; Poleszczuk et al., 2018b; Wołos et al., 2024), which we here adapted to simulate the effects of oscillometric cuffs placed right above the wrists and/or ankles.

To our knowledge, no previous *in silico* study has examined the effects of multiple cuff-induced occlusions on central hemodynamics. We hypothesized that occlusion of arteries at wrists and ankles, in the absence of regulatory mechanisms, may significantly influence blood flow and blood pressure at other sites.

2 Materials and methods

2.1 Cardiovascular model

In this study, we utilized a previously developed and validated 0-1D cardiovascular model; for more details, see (Poleszczuk et al., 2018a; Poleszczuk et al., 2018b; Wołos et al., 2024) and Supplementary Material S1. The modeled arterial network consists of 71 axisymmetric elastic vessel segments with tapered walls. Blood was modeled as an incompressible Newtonian fluid with a constant

density and viscosity. At arterial bifurcations, pressure continuity and flow conservation were imposed. Blood flow was governed by equations derived from the Navier-Stokes equations, describing changes in blood flow, arterial cross-sectional area, and transmural pressure over time. For the inflow boundary condition, we used a time-varying elastance model of the left heart ventricle, whereas the outflow from the terminal arteries of our arterial tree was modeled using 3-element Windkessel models. In Supplementary Material S1, we present the values of all model parameters used in our baseline simulations.

2.2 Cuff modeling

In our 1-D model of the arterial tree, we use an elastic model of the arterial wall to describe the relationship between arterial cross-sectional area and transmural pressure (see Supplementary Material S1). However, when a cuff is inflated to a pressure above the arterial blood pressure, the transmural pressure in the arteries under the cuff becomes negative, leading to the so-called vessel collapse (cross-sectional area approaching zero), which cannot be described by the elastic model. To address this, we used indirectly the model proposed by Drzewiecki et al. (1994), which combines the model of elastic distention of arterial wall with the model of its collapse at negative transmural pressures, thus describing the (static) arterial cross-sectional area (A) for a wide range of transmural pressures (P_T) as follows:

$$A = d\frac{\ln(aP_T + b)}{1 + \exp(-cP_T)} \tag{1}$$

where a, b, c, and d are empirical constants.

For simplicity, we used the above relationship only for the arterial segments under the considered cuffs. Moreover, to maintain the computational tractability of our 1-D model of the arterial network, we did not use the above (somewhat complex) relationship explicitly in those arterial segments, but we kept there our standard elastic model, which for each simulation (for a given cuff pressure) was scaled so that it would approximate locally the above relationship around the new expected mean arterial transmural pressure (assuming that the transmural pressure is reduced by an amount equal to the cuff pressure) - see Supplementary Material S1 for further details. This approach allowed us to keep the original structure of our model, while effectively describing the arteries under the cuffs using the appropriate (approximated) parts of the relationship proposed by Drzewiecki et al.

Note that the Equation 1 describes steady-state conditions of an artery, thus disregarding its viscoelasticity. However, in our study we did not attempt to model in detail the process of cuff inflation/deflation (for which viscoelasticity would be particularly important). Instead, we were interested only in steady-state conditions following inflation of cuff(s) to a given pressure and maintaining this pressure for some time (as, for example, in the aforementioned AngE device). For each considered cuff pressure (treated as a parameter in our model), we ran the simulation until a steady state was reached and we reported the results for that steady state to provide an estimate of what could happen in terms of hemodynamics in the worst-case scenario (with no cardiovascular regulation).

In our simulations, oscillometric cuffs were modeled at four locations: the wrists and ankles. At the wrist, we considered a cuff placed above the distal parts of the radial, interosseous, and ulnar arteries. At the ankles, the cuff pressure was applied to the distal parts of the anterior and posterior tibial arteries. We assumed that all cuffs were 15 cm wide (the size of the medium cuffs of the AngE device). Given the unequal lengths of terminal arteries in the considered cuff locations (e.g., the anterior and posterior tibial arteries), we assumed that each cuff was located so that it ended at the distal end of the longest artery. For example, with a 15 cm wide cuff and a 2.5 cm difference in length between the anterior and posterior tibial arteries, the posterior tibial artery (shorter) was covered at its distal end by 12.5 cm of cuff. To ensure that cuff pressure was exerted only on the arterial segments directly under the cuff (i.e., not along the entire length of the underlying arteries), each artery under the considered cuff locations was divided into two segments: one located under the cuff and the other before the cuff. In the arterial segments under the cuffs, the arterial blood pressure was the sum of transmural pressure and the cuff pressure (we assumed that the cuff pressure is transmitted entirely to the underlying arterial segments), whereas in the preceding arterial segments and in all other arteries in our model, the arterial blood pressure was equal to the transmural pressure (for simplicity, we assumed the same zero external pressure for all arteries). All simulations assumed a uniform pressure distribution across the entire cuff width, with the same cuff pressure applied simultaneously to all arterial segments covered by the cuff(s).

2.3 Workflow

For baseline simulations, we assumed parameter values representing a 25-year-old healthy male with a height of 175 cm (see Supplementary Material S1). First, we simulated a single cuff scenario (with the cuff above the left wrist) and analyzed the local hemodynamic effects of cuff inflation by assessing the waveforms representing pressure and cross-sectional area in three locations in the radial artery beneath or before the cuff (for different cuff pressure levels). Then, we simulated various multi-cuff scenarios (again, for different cuff pressure levels) and obtained model-predicted waveforms of blood pressure and flow at three central locations within the arterial tree (in the ascending aorta, left common carotid artery, and abdominal artery; see Figure 1). We then compared the simulation results obtained for different cuff pressure levels to assess the impact of varying arterial occlusion levels for different cuff configurations. In all simulations, the same cuff pressure (P_{cuff}) was applied simultaneously to all cuffs considered in the given scenario. We considered cuff pressures from 0 mmHg to 150 mmHg (in 10 mmHg steps). We did not analyze cases with cuff pressures above 150 mmHg, given that the results of our simulations reached a plateau for a cuff pressure of 140 mmHg, and higher cuff pressures caused numerical instability of the calculations due to the cross-sectional area of compressed arteries approaching zero. The cuff pressure of 150 mmHg was 25 mmHg higher than the systolic pressure of our baseline virtual patient, thus leading to near complete occlusion of the arteries.

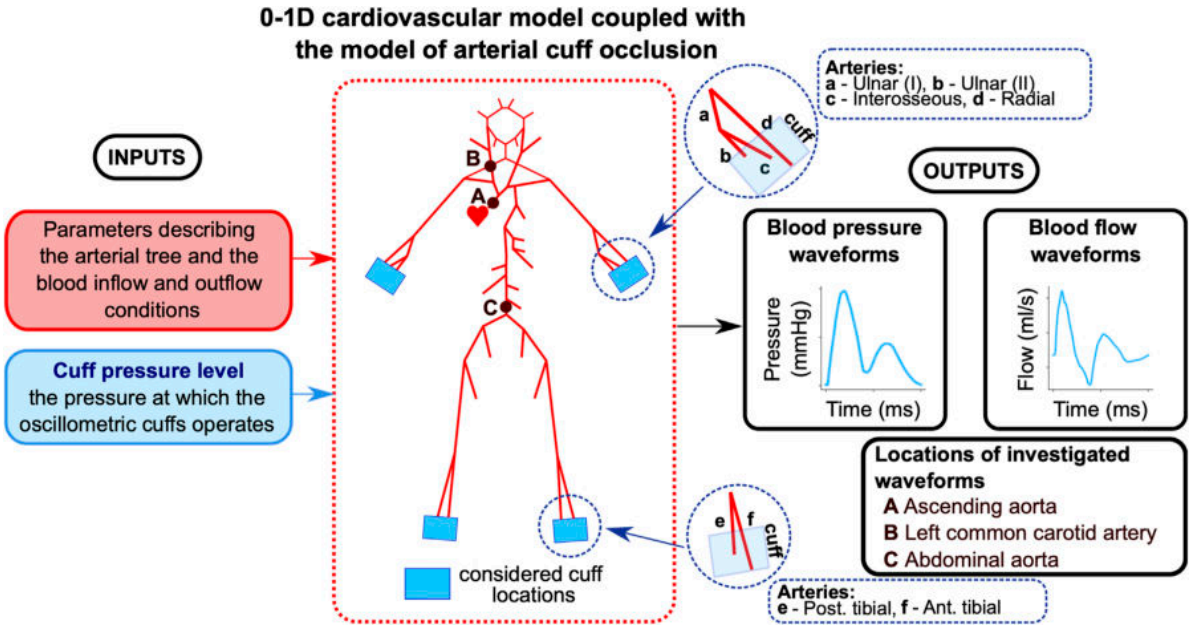

FIGURE 1
Workflow of the study. The model describes pulse wave propagation in the arterial tree with cuff-induced peripheral arterial occlusion (above wrists and/or ankles), assuming no cardiovascular regulatory mechanisms. The baseline model uses parameter values describing the cardiovascular tree of a 25-year-old healthy man. Arterial pressure and blood flow waveforms are analyzed at the indicated locations.

3 Results

3.1 Local effects of cuff occlusion

Figure 2 illustrates how inflation of the cuff placed above the wrist affects pressure and cross-sectional area waveforms at three locations in the radial artery relative to the cuff: 1) proximal (2 cm before the cuff), 2) in the middle of the cuff, and 3) distal (at the end of the cuff). Similar waveform alterations were observed for other arteries beneath the cuff (i.e., the interosseous and ulnar arteries).

When P_{cuff} remained below diastolic pressure (DP; around 80 mmHg), the pressure waveforms exhibited relatively small changes. Significant pulse pressure waveform alterations began to appear around P_{cuff} = 90 mmHg, particularly for the distal segment of the radial artery. The arterial cross-sectional area under the cuff decreased with rising cuff pressure, while the amplitude of its pulsations peaked for cuff pressure near MAP level (95 mmHg), which is an expected effect that is used in the classic oscillometric BP measurement (Drzewiecki et al., 1994). Noticeable changes in the arterial cross-sectional area proximal to the cuff began to appear once P_{cuff} exceeded the MAP level, mirroring pressure waveform alterations. Virtually complete vessel occlusion (>99% reduction in mean blood flow) occurred for P_{cuff} of 130 mmHg, i.e., when P_{cuff} exceeded the systolic pressure (SP; 125 mmHg), as evidenced by the virtually zeroed cross-sectional area waveforms beneath the cuff.

3.2 Central effects of multi-limb cuff occlusion

For simultaneous four-limb total arterial occlusion (P_{cuff} = 150 mmHg), our simulations demonstrated a 9.9% increase in MAP in the ascending aorta, left common carotid artery (CCA), and abdominal aorta relative to baseline values (P_{cuff} = 0 mmHg); see Figure 3. At the same time, mean carotid artery blood flow increased by 11.2% compared to baseline, while the mean blood flow in the abdominal aorta and ascending aorta decreased by 3.5% and 11.6%, respectively, relative to baseline. Similar changes were observed for all cuff pressure levels above the baseline systolic pressure (i.e., above 125 mmHg).

We also performed additional simulations to assess the impact of total arterial occlusion with other cuff placement configurations. In Figure 3 we show the results for unilateral (left) wrist occlusion, bilateral wrist occlusion, and hemilateral occlusion (left wrist and left ankle). Due to the relatively symmetrical structure of our arterial model (complete symmetry in the case of the arteries in the legs and close to symmetry in the case of the arms), right-sided occlusions yielded analogous results. Across all analyzed cuff configurations, a consistent trend was observed: when cuff pressure remained below the baseline MAP, central hemodynamic changes were negligible. Significant changes in blood pressure and mean blood flow in the analyzed central arteries began to appear when cuff pressure approached and exceeded the baseline MAP (95 mmHg).

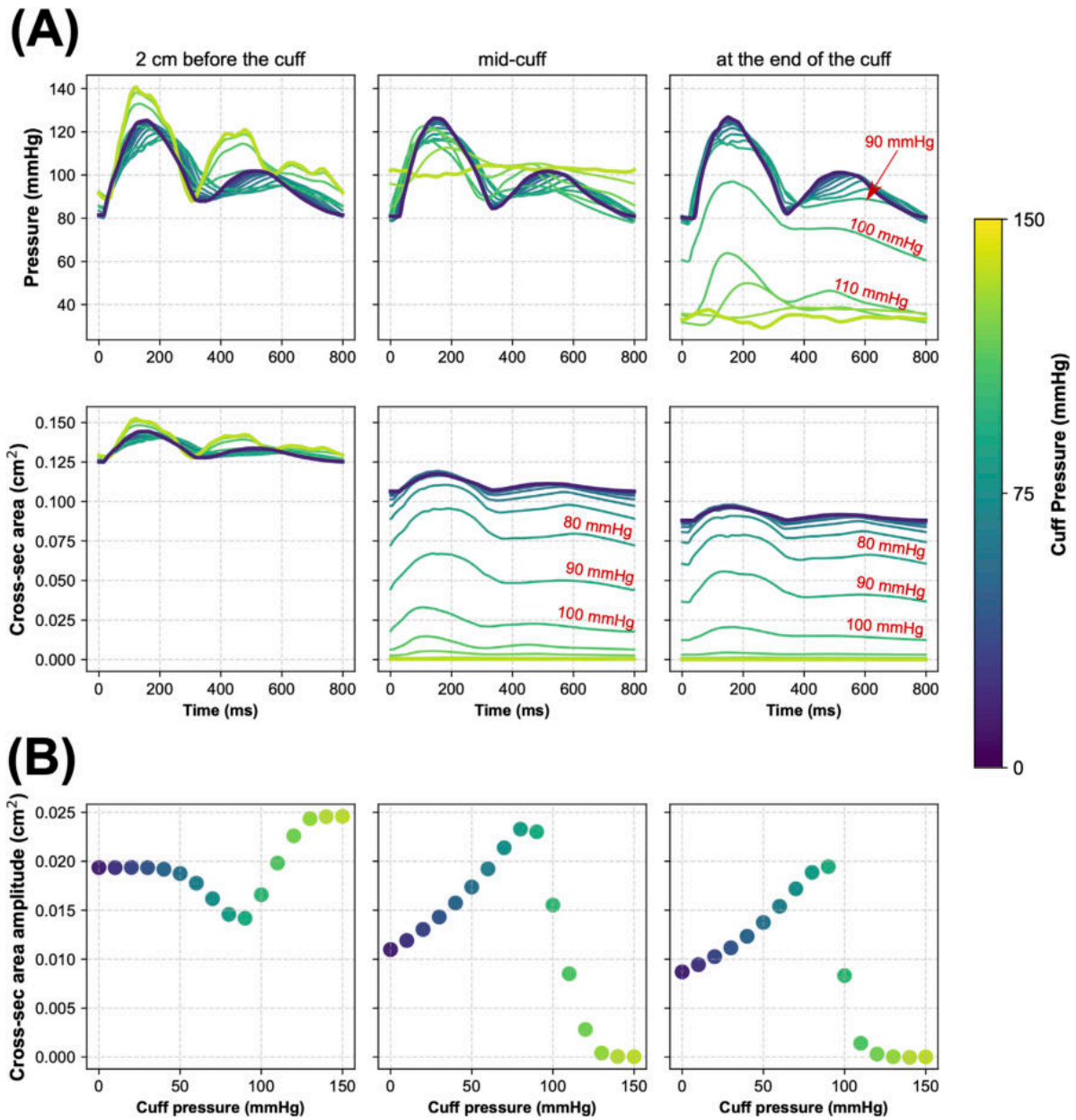

FIGURE 2
Simulated local hemodynamic effects of cuff-induced arterial occlusion above the left wrist (in the radial artery). **(A)** Blood pressure and cross-sectional area of the radial artery during one cardiac cycle simulated for different levels of cuff pressure in three locations of the radial artery before and under the cuff, i.e., 2 cm before the cuff (left panels), in the middle of the cuff (middle panels), and at the end of the cuff (right panels). **(B)** The amplitude of cross-sectional area pulsations of the radial artery simulated for different cuff pressure levels in the same three locations of the radial artery.

Upper-limb total occlusion (bilateral wrist cuffs) induced a 6.4% increase in the abdominal aorta blood flow toward the lower limbs relative to the baseline value. Conversely, left-sided hemilateral total peripheral occlusion reduced abdominal aorta flow by 1.8% compared to baseline. The mean blood flow in the left CCA increased by 6.2% and 5.2% for the total occlusion by upper-limb cuffs and left-limb cuffs, respectively. These changes were less pronounced than those observed during four-limb total occlusion. Accordingly smaller changes were observed for unilateral (left) wrist total occlusion, which resulted in approximately fourfold smaller changes than during the four-limb total occlusion. Specifically, in the case of single wrist occlusion, MAP in the ascending aorta, abdominal aorta, and left CCA increased by only 2.5% relative to baseline, while the mean blood flow in the left CCA rose by only 3%.

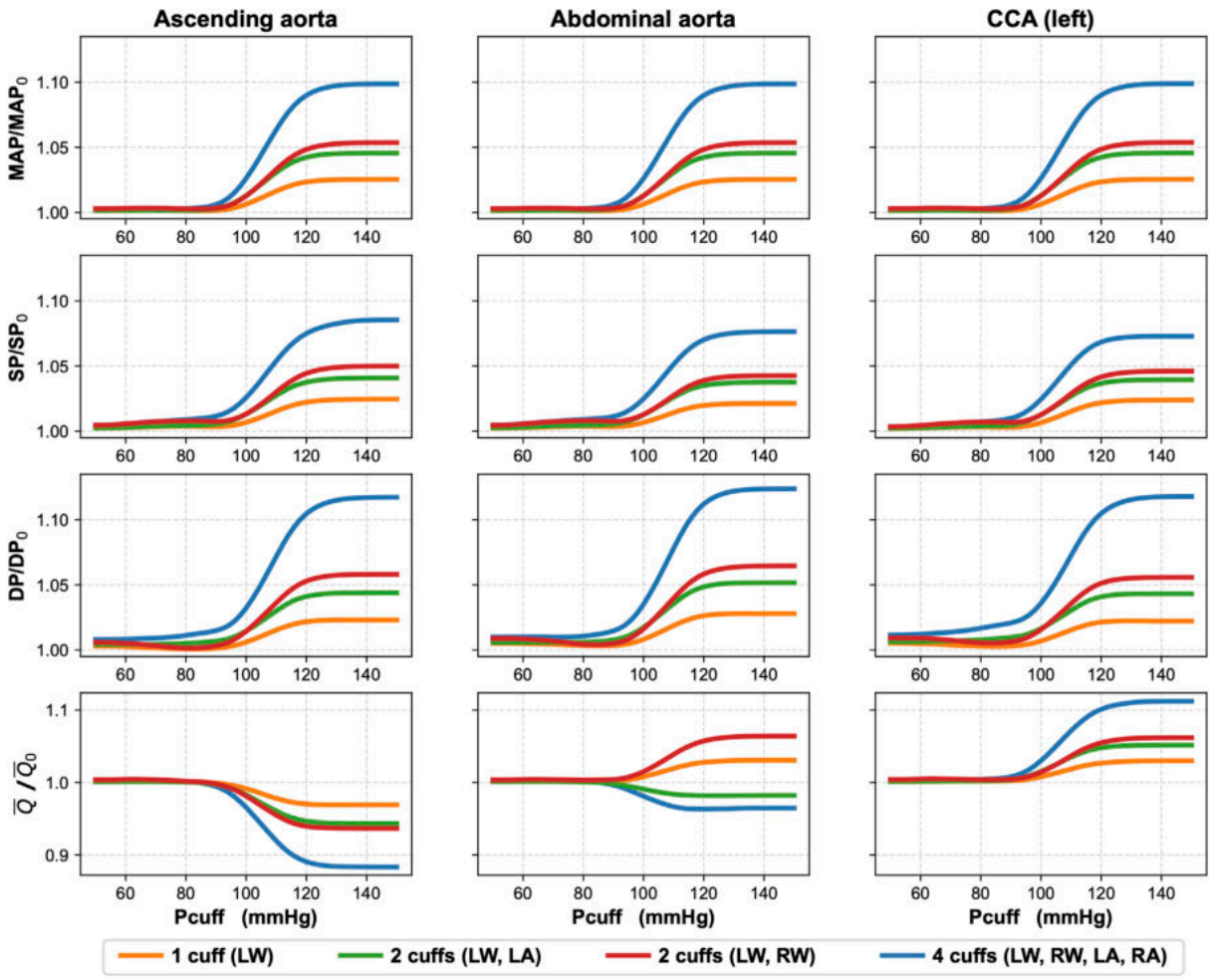

FIGURE 3
Effects of single and multi-limb cuff occlusions on blood pressure and blood flow in three arteries: ascending aorta, abdominal aorta, and left common carotid artery (CCA). The simulations present relative changes in mean arterial pressure (MAP), systolic pressure (SP), diastolic pressure (DP), and mean blood flow ($\overline{Q}$) in the three considered arteries for different cuff pressure levels (P_{cuff}), compared to baseline values (i.e., for $P_{cuff} = 0$). Various combinations of cuff occlusions were considered. LW and RW denote the left and right wrist, respectively, and LA, RA denote the left and right ankle, respectively. Subscripts 0 indicate baseline values.

3.3 Sensitivity analysis

To assess how changes in the values of selected cardiovascular parameters could counteract the central hemodynamic changes caused by the cuff-induced arterial occlusions, we conducted a local sensitivity analysis. Namely, we studied the sensitivity of selected model outputs to the combined effect of inflating the cuffs to 150 mmHg and changing locally the values of selected (single) model parameters. The analyzed model outputs included blood pressure (SP, DP, and MAP) and mean blood flow ($\overline{Q}$) in the left CCA. We have focused on the artery supplying blood to the brain, as blood pressure and blood flow in this artery may be crucial in patients with impaired cerebral autoregulation. Each of the studied parameters (see Supplementary Material S1 for a list of the parameters considered in the sensitivity analysis) was varied within ±10% of its default value (with other parameters unchanged), and the corresponding changes in the analyzed model outputs were expressed in relation to their baseline values. Our analysis revealed that the two considered model outputs are most sensitive to variations in the following cardiovascular parameters: heart period (T), minimal and maximal left ventricular elastance ($E_{\min}$ and $E_{\max}$), end-diastolic left ventricular volume (V_{lv}), left atrial pressure (p_{la}), and the scaling factor for terminal arterial resistances (S_R); see Figure 4.

To investigate the impact of simultaneous variations in all analyzed cardiovascular parameters on mean blood flow and MAP in the left CCA following the four-limb cuff occlusion, we also performed a global sensitivity analysis for all considered parameters. To this end, we computed first-order Sobol' indices (Sobol′, 2001; Saltelli et al., 2010) based on 8,000 simulations of the four-limb cuff occlusion (again with $P_{\text{cuff}} = 150$ mmHg) with different sets of cardiovascular parameter values sampled randomly from a uniform

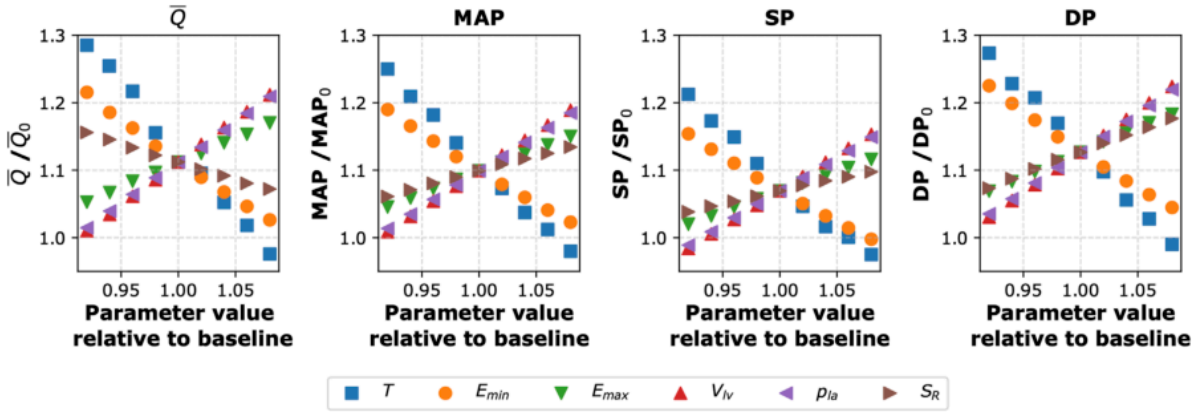

FIGURE 4
Sensitivity of selected model outputs to the combined effect of inflating the cuffs to 150 mmHg (on all four limbs) and changing the values of selected (single) model parameters. The y-axis shows the percentage of the given model output relative to baseline value (without the cuffs and with the baseline parameter values). The considered model outputs (for the left common carotid artery): $\overline{Q}$ – mean blood flow, MAP–mean arterial pressure, SP–systolic pressure, DP–diastolic pressure; The tested model parameters: T–heart period, E_{min},E_{max} – minimal and maximal left ventricular elastance, V_{lv} – left ventricular end-diastolic volume, p_{la} – left atrial pressure, S_R – scaling factor for resistances of small arteries and arterioles (terminal segments of the arterial tree). Subscript 0 indicates baseline values (i.e., simulations for P_{cuff} = 0 and baseline parameter values).

distribution within ±10% of their default values. This approach allowed us to quantify the contribution of each parameter to the total variance in the analyzed model outputs (i.e., either MAP or mean blood flow in the left CCA following the four-limb total cuff occlusion). This analysis showed that the parameters with the most significant impact on the studied model outputs are almost identical to those identified in the local sensitivity analysis, see Figure 5.

It is also worth noting that the magnitude of potential changes in MAP and mean carotid blood flow induced by peripheral arterial occlusion by cuffs (assuming the absence of cardiovascular regulation) can depend on the baseline values of cardiovascular parameters, which are naturally subject to inter-patient variability. For instance, older individuals typically exhibit increased arterial stiffness (Vatner et al., 2021), compared to younger individuals. To explore this inter-patient variability, we performed another global sensitivity analysis with 8,000 pairs of simulations (i.e., a baseline simulation without cuffs and a simulation with cuffs on all four limbs inflated to 150 mmHg) using different combinations of cardiovascular parameter values randomly sampled from a ±10% range around their default values. The histograms illustrating the distributions of relative changes in MAP and mean blood flow in the left CCA across these 8,000 simulations are presented in Figure 6. On average, these simulations demonstrated an approximate 10% increase in MAP and a 12% increase in mean blood flow in the left CCA relative to baseline values.

4 Discussion

In this study, we employed a pulse wave propagation model to investigate the hemodynamic effects of cuff-induced peripheral arterial occlusion at single or multiple limbs, assuming the absence of cardiovascular regulatory mechanisms and considering steady-state conditions after inflating the cuff(s) to a given pressure. While previous mathematical modeling studies have investigated single cuff mechanics (Liang et al., 2013; Trachet et al., 2010; Liang et al., 2012), to our knowledge, this is the first study to analyze the cumulative impact of simultaneous multi-limb cuff occlusion, as used for advanced cardiovascular diagnostics. Our *in silico* study demonstrates that multi-limb cuff-based measurements, if not counteracted by the properly functioning cardiovascular regulatory mechanisms, can alter MAP and the central blood flow distribution. As expected, the most pronounced changes were observed when cuffs were placed on all four limbs and inflated to suprasystolic pressure. Specifically, we observed an increase in MAP of approximately 10% in our baseline virtual patient and up to approximately 14% in the analyzed cohort of virtual patients (see Figure 6). It should be emphasized that this represents a theoretical "worst-case" scenario, as our model intentionally did not account for cardiovascular regulation. It is to be expected that properly functioning regulatory mechanisms should compensate the effects of cuff occlusion, as has been shown in an *in-vivo* study in healthy subjects (Kashyap et al., 2005).

The proposed model seems to reliably reflect the local physiological responses to cuff inflation. As illustrated in Figure 2, the higher the cuff pressure, the higher the reduction in the cross-sectional area of the arteries under the cuff (represented by the radial artery for the wrist cuff scenario). Concurrently, the maximal amplitude of the pulsations of the arterial cross-sectional area was observed for $P_{cuff} \approx$ MAP. This aligns with the known relationship between arterial compliance and transmural pressure, with the maximal compliance occurring at transmural pressure close to zero (i.e., when $P_{cuff} \approx$ MAP), which corresponds to the point of mechanical buckling of the arterial wall, where buckling is defined as the transition of the vessel shape form circular to non-circular (Drzewiecki et al., 1994), although in our model we always assume a circular cross-section of the vessels.

Regardless of cuff configuration, for P_{cuff} values below MAP, relative changes in blood pressure in the central arteries (compared to baseline) were generally negligible, as shown in Figure 3. Bilateral

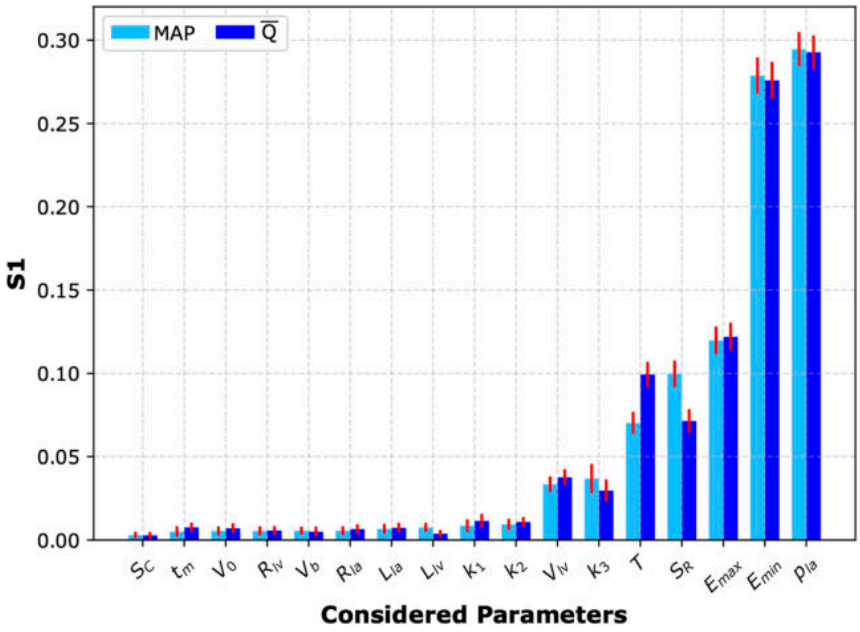

FIGURE 5
Sobol' sensitivity analysis. First-order Sobol' indices (S1) with 95% confidence intervals (red bars) representing sensitivity of the two analyzed model outputs (mean arterial pressure, MAP, and mean blood flow in the left common carotid artery, $\overline{Q}$) to changes in the values of selected cardiovascular parameters (during four-limb cuff occlusion). The considered parameters included: S_C– scaling factor for compliances of small arteries and arterioles, t_m – time to the onset of the constant left ventricular elastance, V_0 – volume of the left ventricle at zero transmural pressure, R_{lv} – resistance against blood flow from the left ventricle to the ascending aorta, V_b – volume of the backflow from the ascending aorta to the left ventricle, R_{la},L_{la} – resistance and inertia terms for the blood flow from the left atrium to the left ventricle, respectively, L_{lv}– inertia term for the blood flow between the left ventricle and ascending aorta, k_1,k_2,k_3- parameters describing stiffness of the small, medium and large arteries, respectively, V_{lv} – left ventricular end-diastolic volume, T – heart period, S_R – scaling factor for resistances of small arteries and arterioles (terminal segments of the arterial tree), E_{max},E_{min} – maximal and minimal left ventricular elastance, p_{la} – left atrial pressure.

wrist occlusion produced a slightly distinct pattern for different cuff inflation levels, compared to other cuff configurations: first, a minor increase in blood pressure, followed by a slight decrease before the main rise for higher cuff pressures. This could be related to wave reflection and superposition effects, which are modulated by varying degrees of cuff inflation, although, also in this case, the changes in central blood pressure were rather negligible. For cuff pressures above MAP, we observed that the higher the cuff pressure, the lower the mean blood flow in the ascending aorta (up to a plateau for P_{cuff} = 140 mmHg). This was an entirely expected effect as peripheral arterial occlusions increase systemic vascular resistance, requiring the heart to work against a higher afterload (the phenomenon accounted for in our model), leading to a reduced left ventricular stroke volume and hence reduced cardiac output (assuming the absence of cardiac regulation). The increase in central MAP is caused mainly by the increase in the total systemic vascular resistance but partly also by additional reflection of pressure waves from the cuff occlusion sites (see Figure 2 for these additional reflections visible in arterial pressure waveforms before the cuff when the cuff is inflated to high pressures). In the case with cuff(s) on one or both ankles, the mean blood flow in the abdominal aorta is reduced, despite the increase in central MAP, which can be explained by the increased peripheral resistance in one or both legs, respectively. In contrast, in the case with cuff(s) on one or both wrists, the mean blood flow in the abdominal aorta is increased, because in this case the increase in central MAP is combined with no change in peripheral resistance of the lower body. This increase in the mean blood flow in the abdominal aorta may seem paradoxical, given the reduced cardiac output. This can be explained by redistribution of central blood flow–a higher arterial resistance in the upper limbs translates to relatively higher proportion of cardiac output being directed towards the lower body. For a similar reason, the mean blood flow in the common carotid artery increases in all considered cuff configurations.

As already mentioned, our simulations did not account for cardiovascular regulatory mechanisms (e.g., baroreflex mechanisms or cerebral autoregulation). However, this approach may be physiologically relevant for populations with impaired regulatory mechanisms, such as patients with severe traumatic brain injury (Toth et al., 2016). In such patients (assuming a significant regulatory impairment), the potential increase in cerebral blood flow induced by four-limb cuff inflation to suprasystolic pressure could elevate intracranial pressure, potentially leading to secondary brain injury.

An example of a device utilizing multi-limb oscillometric measurements is AngE (SoT Medical, Austria), which typically employs the following measurement protocol: initial inflation of the cuffs to suprasystolic pressure (180 mmHg by default), followed by cuff pressure reductions by 10 mmHg every 5 s, until 40 mmHg is reached. This means that the cuffs may remain inflated to

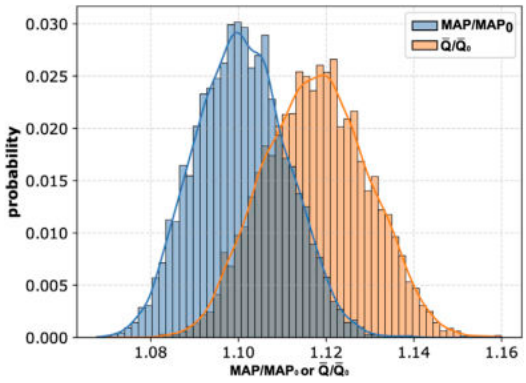

FIGURE 6
Histograms of relative changes in mean arterial pressure (MAP) and mean blood flow in the left common carotid artery ($\overline{Q}$) following peripheral arterial occlusion simulated for 8,000 combinations of cardiovascular parameter values. Parameter values were sampled within ±10% of their default values. Simulations were performed for the case with four cuffs placed above the wrists and ankles and inflated to 150 mmHg. Subscript 0 indicates baseline values (i.e., simulations without cuff occlusions).

a suprasystolic pressure for a much longer time compared to the standard blood pressure measurement. Moreover, in clinical practice, such a measurement protocol may be repeated for data averaging, which could therefore lead to repeated increases in blood pressure in patients with impaired cardiovascular regulation, with a possible accumulation of their potentially negative effects. On the other hand, assuming fully functional regulatory mechanisms, changes in the cardiovascular system initiated by the autonomic nervous system (ANS) and the humoral system to counteract the effects of peripheral arterial occlusion induced by cuff inflation may potentially lead to some distortion of the measurement results, i.e., the measured or estimated parameters may not necessarily correspond to resting conditions but may partly reflect the changes that occurred in the cardiovascular system in response to cuff inflation. For instance, devices such as the AngE, provide an average waveform of the recorded cuff pressure fluctuations (reflecting fluctuations in blood volume under the cuff). However, the morphology of these waveforms could be affected by the activation of the ANS following cuff inflation. ANS controls the heart rate, heart contractility, peripheral arterial resistance, and venous compliance, all of which may affect the observed waveform morphology. Similarly, measurements of pulse wave velocity using the time shift between waveforms recorded in wrist and ankle cuffs may be somewhat distorted by changes in heart rate possibly induced by cuff inflation, although there are conflicting results regarding whether the effect of heart rate on arterial stiffness is a pressure-independent phenomenon (Tan et al., 2018).

Our sensitivity analyses revealed that the cardiac function parameters have the largest impact on the central hemodynamic response to cuff inflation. Specifically, the local sensitivity analysis identified heart period (T), maximal and minimal left ventricular elastance ($E_{\min}$, $E_{\max}$), and left atrial pressure (p_{la}) as the key factors influencing central blood pressure and blood flow following the four-limb cuff occlusion (as assessed in the left CCA). The global sensitivity analysis confirmed these findings, highlighting p_{la} and $E_{\min}$ as the primary determinants of MAP and mean blood flow in the left CCA. This is because p_{la} and E_{min} directly determine cardiac output by governing the left ventricular preload and compliance, respectively. Since MAP is fundamentally driven by cardiac output, these cardiac-related parameters have a dominant influence on central hemodynamics. While arterial stiffness parameters (such as k_3) also affect central blood pressure, their impact on the MAP is secondary. This suggests that during oscillometric cuff measurements blood pressure may be most effectively controlled by regulating the cardiac function.

5 Limitations and directions for future research

This *in silico* study has several limitations. First, we assumed the absence of any cardiovascular regulatory mechanisms (e.g., baroreflex). On the one hand, this allowed us to investigate the potential hemodynamic effects of simultaneous multi-limb arterial cuff occlusion in hypothetical patients with complete cardiovascular regulatory dysfunction. On the other hand, however, we could not investigate the effects of partial impairment (either underactivity or overactivity) of all or selected regulatory mechanisms. Moreover, we used a pulse wave propagation model that involves only the pulsatile outflow of blood from the left heart ventricle and its subsequent flow through the arterial tree, without taking into account microcirculation, venous return, and cardiopulmonary circulation, thus neglecting the closed-loop nature of the cardiovascular system (in our model, the left atrial pressure is assumed constant). This means that the results of our simulations (in particular, the observed increase in central blood pressure and carotid blood flow following peripheral arterial occlusion) should be treated only as potential short-term effects since even in the assumed absence of cardiovascular regulatory mechanisms, an increase in arterial blood volume (associated with an increase in arterial blood pressure), combined with a decrease in cardiac output (manifested by decreased blood flow in the ascending aorta), should lead to a decrease in venous blood volume and therefore a decrease in central venous pressure, ultimately leading to a further decrease in cardiac output, which would counteract the increase in arterial blood pressure (in addition to the decrease in cardiac output due to the increased afterload, which we accounted for). On the other hand, the decrease in the left ventricular stroke volume caused by increased afterload should lead to a transient increase in the left atrial pressure (kept constant in our model), thus limiting to some extent a further decrease in cardiac output, at least transiently. Therefore, even considering the scenario without cardiovascular regulatory mechanisms, the prediction of the central hemodynamic effects of peripheral arterial occlusion is not straightforward without using a full closed-loop model of the cardiovascular system. Furthermore, we only analyzed steady-state conditions following cuff inflation to different cuff pressure levels, thus ignoring arterial viscoelasticity and hence disregarding the time it takes for the arteries under the cuffs to collapse under high (suprasystolic) cuff pressures. We did not model the dynamic cuff inflation/deflation processes or the impact of the duration of maintaining the cuffs inflated to a high pressure. Similarly, we did not analyze the potential cumulative

effects of repeated cuff-based measurements as is often the case in clinical protocols. Finally, another limitation of our study is the lack of validation of our cuff occlusion model. Therefore, *in vivo* validation would be, essential to confirm the clinical relevance of our findings. In case these model-based observations are confirmed, future studies should establish appropriate safety protocols for multi-limb cuff-based measurements in vulnerable populations (e.g., in severe traumatic brain injury patients), especially with regard to maximal time of maintaining suprasystolic cuff pressure. However, designing such a validation protocol requires careful ethical consideration. One approach could involve performing the multi-limb cuff measurements in sTBI patients with continuous monitoring of central hemodynamic parameters and intracranial pressure (ICP), but instead of a rapid inflation of the cuffs to a pressure substantially above the systolic pressure, it would be recommended to first inflate the cuffs to a lower pressure (e.g., to a pressure equal to MAP) and then gradually increase the cuff pressure while closely monitoring ICP, so that the test could be quickly aborted in the event of a dangerous rise in ICP. An alternative protocol could involve assessing changes in central hemodynamic parameters following multi-limb cuff inflation in healthy volunteers under pharmacological autonomic blockade to temporarily and reversibly impair cardiovascular regulation.

6 Conclusion

We used a pulse wave propagation model to assess the short-term influence of multi-limb cuff occlusion on central hemodynamics in the case of inactive cardiovascular regulatory mechanisms. In such a scenario, according to our simulations, four-limb arterial occlusion can potentially increase MAP by about 10% in the ascending aorta, left common carotid artery, and abdominal aorta, with concurrent central blood flow redistribution (an 11.2% increase in the mean carotid blood flow despite an 11.6% decrease in the ascending aorta blood flow). Our results suggest that simultaneous multi-limb arterial occlusion can lead to noticeable changes in central hemodynamics if not counteracted by properly functioning cardiovascular regulatory mechanisms. This suggests that caution should be exercised when performing this type of measurement in patients with significant impairments in regulatory mechanisms, although further research is required to confirm the clinical relevance of our findings.

Data availability statement

The raw data supporting the conclusions of this article will be made available by the authors, without undue reservation.

Author contributions

KW: Investigation, Software, Conceptualization, Writing – review and editing, Formal Analysis, Writing – original draft, Data curation, Visualization, Methodology, Validation. LP: Conceptualization, Supervision, Investigation, Writing – review and editing, Validation, Methodology. MD: Conceptualization, Funding acquisition, Validation, Methodology, Supervision, Investigation, Writing – review and editing. JP: Validation, Project administration, Methodology, Investigation, Conceptualization, Writing – review and editing, Supervision, Funding acquisition.

Funding

The author(s) declare that financial support was received for the research and/or publication of this article. KW, MD, and JP were partly supported by the National Science Centre (Poland), grant No. 2018/31/D/ST7/03472. The funder had no role in the study design, analysis, or interpretation; in the writing of the manuscript; or in the decision to submit the article for publication.

Conflict of interest

The authors declare that the research was conducted in the absence of any commercial or financial relationships that could be construed as a potential conflict of interest.

Generative AI statement

The author(s) declare that no Generative AI was used in the creation of this manuscript.

Publisher's note

Supplementary material

The Supplementary Material for this article can be found online at: https://www.frontiersin.org/articles/10.3389/fphys.2025.1642645/full#supplementary-material

References

Alpert, B. S., Quinn, D., and Gallick, D. (2014). Oscillometric blood pressure: a review for clinicians. *J. Am. Soc. Hypertens.* 8 (12), 930–938. doi:10.1016/j.jash.2014.08.014

Drzewiecki, G., Hood, R., and Apple, H. (1994). Theory of the oscillometric maximum and the systolic and diastolic detection ratios. *Ann. Biomed. Eng.* 22 (1), 88–96. doi:10.1007/BF02368225

Graves, J. C., and Kreipke, C. W. (2015). "Endothelin, cerebral blood flow, and traumatic brain injury: implications for a future therapeutic target," in *Brain neurotrauma: molecular, neuropsychological, and rehabilitation aspects*. Editor F. H. Kobeissy (Boca Raton (FL): CRC Press/Taylor and Francis).

Hilz, M. J., DeFina, P. A., Anders, S., Koehn, J., Lang, C. J., Pauli, E., et al. (2011). Frequency analysis unveils cardiac autonomic dysfunction after mild traumatic brain injury. *J. Neurotrauma* 28 (9), 1727–1738. doi:10.1089/neu.2010.1497

Hilz, M. J., Aurnhammer, F., Flanagan, S. R., Intravooth, T., Wang, R., Hösl, K. M., et al. (2015). Eyeball pressure stimulation unveils subtle autonomic cardiovascular dysfunction in persons with a history of mild traumatic brain injury. *J. Neurotrauma* 32 (22), 1796–1804. doi:10.1089/neu.2014.3842

Hilz, M. J., Liu, M., Koehn, J., Wang, R., Ammon, F., Flanagan, S. R., et al. (2016). Valsalva maneuver unveils central baroreflex dysfunction with altered blood pressure control in persons with a history of mild traumatic brain injury. *BMC Neurol.* 16 (61), 61. doi:10.1186/s12883-016-0584-5

Hilz, M. J., Wang, R., Markus, J., Ammon, F., Hösl, K. M., Flanagan, S. R., et al. (2017). Severity of traumatic brain injury correlates with long-term cardiovascular autonomic dysfunction. *J. Neurol.* 264, 1956–1967. doi:10.1007/s00415-017-8581-1

Kashyap, V. S., Franklin, K. S., and Fitzpatrick, C. M. (2005). Bilateral brachial artery occlusion decreases internal carotid artery volume flow: a simple adjunct for cerebral protection? *J. Endovasc. Ther.* 12 (4), 454–460. doi:10.1583/05-1518MR.1

Liang, F., Takagi, S., and Liu, H. (2012). The influences of cardiovascular properties on suprasystolic brachial cuff wave studied by a simple arterial-tree model. *J. Mech. Med. Biol.* 12, 1250040. doi:10.1142/s0219519411004605

Liang, F., Takagi, S., Himeno, R., and Liu, H. (2013). A computational model of the cardiovascular system coupled with an upper-arm oscillometric cuff and its application to studying the suprasystolic cuff oscillation wave, concerning its value in assessing arterial stiffness. *Comput. Methods Biomech. Biomed. Engin* 16 (2), 141–157. doi:10.1080/10255842.2011.610305

Muntner, P., Shimbo, D., Carey, R. M., Charleston, J. B., Gaillard, T., Misra, S., et al. (2019). Measurement of blood pressure in humans: a scientific statement from the American heart association. *Hypertension* 73 (5), e35–e66. doi:10.1161/HYP.0000000000000087

Papaioannou, V., Giannakou, M., Maglaveras, N., Sofianos, E., and Giala, M. (2008). Investigation of heart rate and blood pressure variability, baroreflex sensitivity, and approximate entropy in acute brain injury patients. *J. Crit. Care* 23 (3), 380–386. doi:10.1016/j.jcrc.2007.04.006

Poleszczuk, J., Debowska, M., Dabrowski, W., Wojcik-Zaluska, A., Zaluska, W., and Waniewski, J. (2018a). Patient-specific pulse wave propagation model identifies cardiovascular risk characteristics in hemodialysis patients. *PLoS Comput. Biol.* 14 (9), e1006417–15. doi:10.1371/journal.pcbi.1006417

Poleszczuk, J., Debowska, M., Dabrowski, W., Wojcik-Zaluska, A., Zaluska, W., and Waniewski, J. (2018b). Subject-specific pulse wave propagation modeling: towards enhancement of cardiovascular assessment methods. *PLoS ONE* 13 (1), e0190972–17. doi:10.1371/journal.pone.0190972

Rangel-Castilla, L., Gasco, J., Nauta, H. J. W., Okonkwo, D. O., and Robertson, C. S. (2008). Cerebral pressure autoregulation in traumatic brain injury. *Neurosurg. Focus* 25 (4), E7. doi:10.3171/FOC.2008.25.10.E7

Saltelli, A., Annoni, P., Azzini, I., Campolongo, F., Ratto, M., and Tarantola, S. (2010). Variance based sensitivity analysis of model output. Design and estimator for the total sensitivity index. *Comput. Phys. Commun.* 181 (2), 259–270. doi:10.1016/j.cpc.2009.09.018

Sato, M., Tanaka, M., Umehara, S., and Nishikawa, T. (2005). Baroreflex control of heart rate during and after propofol infusion in humans. *Br. J. Anaesth.* 94 (5), 577–581. doi:10.1093/bja/aei092

Sobol′, I. M. (2001). Global sensitivity indices for nonlinear mathematical models and their Monte Carlo estimates. *Math. Comput. Simul.* 55 (1), 271–280. doi:10.1016/s0378-4754(00)00270-6

Sviri, G. E., Aaslid, R., Douville, C. M., Moore, A., and Newell, D. W. (2009). Time course for autoregulation recovery following severe traumatic brain injury: clinical article. *J. Neurosurg.* 111 (4), 695–700. doi:10.3171/2008.10.17686

Sykora, M., Czosnyka, M., Liu, X., Donnelly, J., Nasr, N., Diedler, J., et al. (2016). Autonomic impairment in severe traumatic brain injury: a multimodal neuromonitoring study. *Crit. Care Med.* 44 (6), 1173–1181. doi:10.1097/CCM.0000000000001624

Tan, I., Butlin, M., Spronck, B., Xiao, H., and Avolio, A. (2018). Effect of heart rate on arterial stiffness as assessed by pulse wave velocity. *Curr. Hypertens. Rev.* 14 (2), 107–122. doi:10.2174/1573402113666170724100418

Toth, P., Szarka, N., Farkas, E., Ezer, E., Czeiter, E., Amrein, K., et al. (2016). Traumatic brain injury-induced autoregulatory dysfunction and spreading depression-related neurovascular uncoupling: pathomechanisms, perspectives, and therapeutic implications. *Am. J. Physiol. - Heart Circ. Physiol.* 311 (5), H1118–H1131. doi:10.1152/ajpheart.00267.2016

Trachet, B., Reymond, P., Kips, J., Swillens, A., De Buyzere, M., Suys, B., et al. (2010). Numerical validation of a new method to assess aortic pulse wave velocity from a single recording of a brachial artery waveform with an occluding cuff. *Ann. Biomed. Eng.* 38 (3), 876–888. doi:10.1007/s10439-010-9945-1

Uryga, A., Kasprowicz, M., Burzyńska, M., Kazimierska, A., Czosnyka, M., and Nasr, N. (2023). Association between temporal patterns of baroreflex sensitivity after traumatic brain injury and prognosis: a preliminary study. *Neurol. Sci.* 44, 1653–1663. doi:10.1007/s10072-022-06579-7

Vatner, S. F., Zhang, J., Vyzas, C., Mishra, K., Graham, R. M., and Vatner, D. E. (2021). Vascular stiffness in aging and disease. *Front. Physiol.* 12, 762437. doi:10.3389/fphys.2021.762437

Wołos, K., Pstras, L., Debowska, M., Dabrowski, W., Siwicka-Gieroba, D., and Poleszczuk, J. (2024). Non-invasive assessment of stroke volume and cardiovascular parameters based on peripheral pressure waveform. *PLOS Comput. Biol.* 20 (4), e1012013. doi:10.1371/journal.pcbi.1012013

Supplementary Material 1

1 Cardiovascular model

Here, we provide a brief description of the mathematical model of the cardiovascular system used in our study. A more detailed explanation is available in our previous publications (1,2).

1.1 Arterial tree

The vascular tree considered in this study consists of 71 major human arteries (see Supp. Figure 1). The geometric properties of the considered arteries are listed in Table 1. Each arterial segment is defined by its length L, inlet internal radius r_{in}, and outlet internal radius r_{out}. Arterial segments are modeled as compliant, axisymmetric, tapering cylinders with impermeable walls. The vessel tapering is described by the following equation:

$$r_0(x) = r_{\text{in}} \left(\frac{r_{\text{out}}}{r_{\text{in}}} \right)^{x/L}, \quad \textbf{(1)}$$

where $r_0(x)$ denotes the internal radius of a given artery at point x at the nominal pressure P_0 (3).

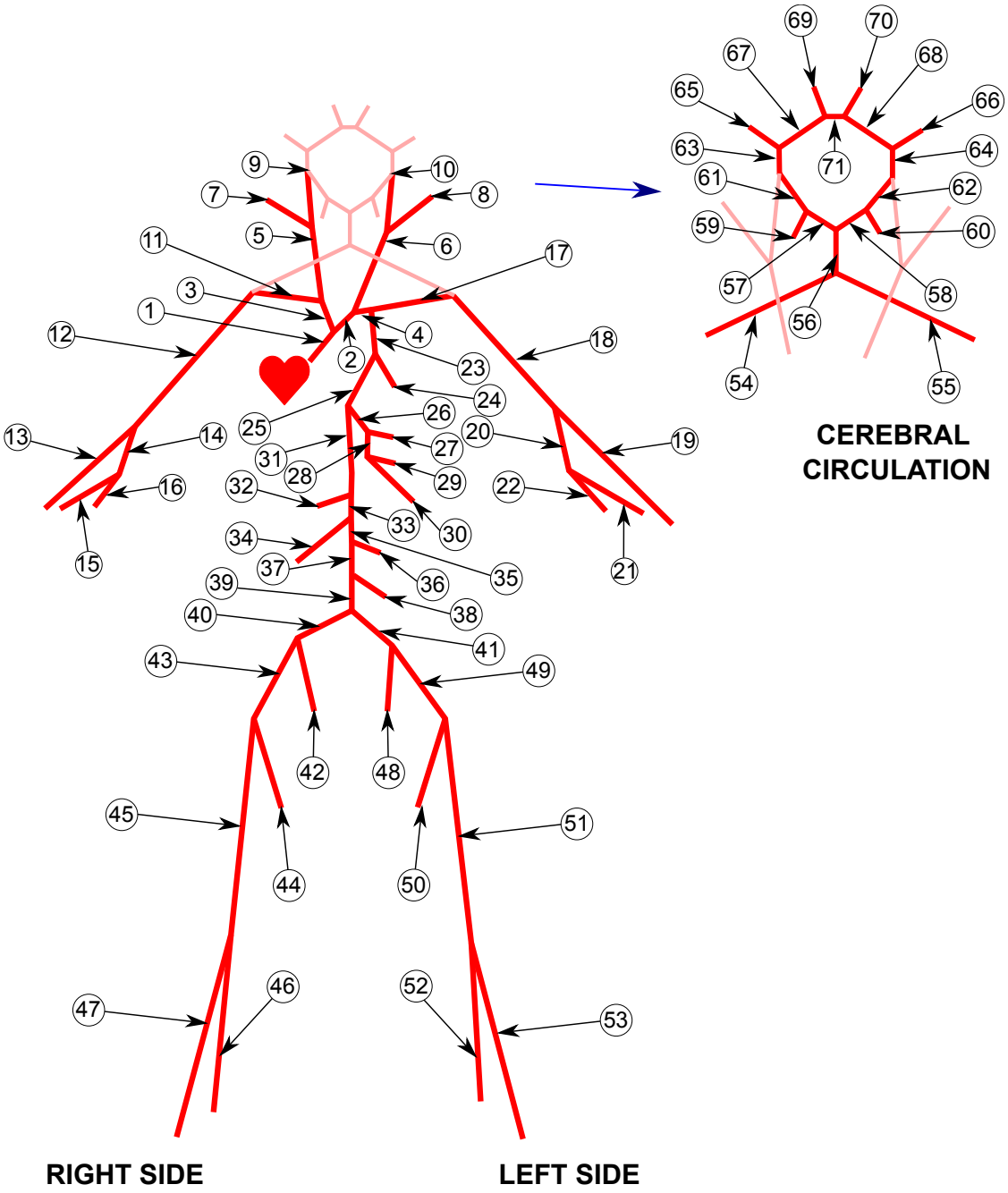

Supp. Figure 1 Overview of the modelled arterial tree. For more information on individual arteries, see **Table 1**.

Table 1 Geometry of the modelled arteries and the corresponding peripheral resistances and compliances. Arterial length (as well as inlet and outlet internal radii (r_{in} and r_{out}) are provided in centimeters. Peripheral resistance (R_T, 10^4 g/cm^4/s) and compliance (C_T, 10^6 cm^{4}s^2/g) are provided only for terminal arteries. L and R stand for left and right, respectively. Data adapted from (4,5).

ID	Artery name	Length	r_{in}	r_{out}	R_T	C_T
1	Ascending aorta	4	1.2	1.18	-	-
2	Aortic arch (I)	2	1.12	1.11	-	-
3	Brachiocephalic	3.4	0.62	0.61	-	-
4	Aortic arch (II)	3.9	1.07	1.06	-	-
5/6	Common carotid R/L	17.7/20.8	0.25	0.25	-	-
7/8	External carotid R/L	17.7	0.15	0.14	5.43	12.7
9/10	Internal carotid (I) R/L	17.7	0.2	0.2	-	-
11/17	Subclavian (I) R/L	3.4	0.42	0.42	-	-
12/18	Subclavian (II) R/L	42.2	0.4	0.24	-	-
13/19	Radial R/L	23.5	0.17	0.14	5.28	3.52
14/20	Ulnar (I) R/L	6.7	0.22	0.22	-	-
15/21	Interosseous R/L	7.9	0.1	0.1	8.40	0.22
16/22	Ulnar (II) R/L	17.1	0.2	0.18	5.28	3.52
23	Thoracic aorta (I)	5.2	1	1	-	-
24	Intercostals	8	0.2	0.15	1.39	13.38
25	Thoracic aorta (II)	10.4	0.68	0.65	-	-
26	Celiac (I)	1	0.39	0.39	-	-
27	Hepatic	6.6	0.22	0.22	3.64	5.13
28	Celiac (II)	1	0.2	0.2	-	-
29	Gastric	7.1	0.18	0.17	5.43	3.44
30	Splenic	6.3	0.18	0.17	2.32	8.01
31	Abdominal aorta (I)	5.3	0.61	0.6	-	-
32	Superior mesenteric	5.9	0.44	0.42	0.93	20.0
33	Abdominal aorta (II)	1	0.6	0.59	-	-
34/36	Renal R/L	3	0.26	0.25	1.13	16.46
35	Abdominal aorta (III)	1	0.59	0.58	-	-
37	Abdominal aorta (IV)	10.6	0.58	0.55	-	-
38	Inferior mesenteric	5	0.17	0.16	6.89	2.7
39	Abdominal aorta (V)	1	0.54	0.52	-	-
40/41	Common iliac R/L	5.8	0.37	0.35	-	-
42/48	Internal iliac R/L	5	0.2	0.19	7.96	2.34
43/49	External Iliac R/L	14.5	0.32	0.27	-	-
44/50	Deep femoral R/L	12.6	0.26	0.19	4.79	3.90
45/51	Femoral R/L	44.5	0.26	0.19	-	-
46/52	Posterior tibial R/L	32.1	0.16	0.14	4.79	3.90
47/53	Anterior tibial R/L	34.3	0.13	0.12	5.60	3.33
54/55	Vertebral R/L	14.8	0.14	0.14	-	-
56	Basilar	3	0.16	0.11	-	-
57/58	Posterior cerebral (I) R/L	0.5	0.11	0.11	-	-

59/60	Posterior cerebral (II) R/L	8.5	0.11	0.11	11.08	6.20
61/62	Posterior communicating R/L	1.5	0.07	0.07	-	-
63/64	Internal carotid (II) R/L	0.5	0.2	0.19	-	-
65/66	Middle cerebral R/L	12	0.14	0.12	5.97	11.60
67/68	Anterior cerebral (I) R/L	1.2	0.12	0.12	-	-
69/70	Anterior cerebral (II) R/L	10	0.12	0.10	8.48	8.20
71	Anterior communicating	0.3	0.07	0.07	-	-

1.2 Blood flow

The equations governing blood flow in the arteries are derived from the incompressible Navier-Stokes equations, assuming constant blood density ρ and viscosity μ, and a Poiseuille velocity profile. These equations describe the flow rate $Q(x,t)$, internal cross-sectional area $A(x,t)$, and transmural pressure $P(x,t)$. A system of equations is formed with the following three equations. The continuity and momentum equations are derived using standard methods (3,6):

$$\frac{\partial Q(t,x)}{\partial x} + \frac{\partial A(t,x)}{\partial t} = 0 \quad \textbf{(2)}$$

$$\frac{Q(t,x)}{\partial t} + \frac{\partial}{\partial x}\left(\frac{Q(t,x)}{A(t,x)}\right) + \frac{A(t,x)}{\rho}\frac{\partial P(t,x)}{\partial x} = -\frac{8\pi\mu}{\rho}\frac{Q(t,x)}{A(t,x)} \quad \textbf{(3)}$$

The third equation describes the relationship between arterial cross-sectional area and transmural pressure P_T, assuming the arterial walls are purely elastic (3):

$$P_T(t,x) - P_0 = f(x)\left(1 - \sqrt{\frac{A_0(x)}{A(t,x)}}\right), \quad \textbf{(4)}$$

where $A_0(x)$ is the arterial internal cross-sectional area at point x at nominal pressure P_0, i.e., $A_0(x) = \pi r_0^2(x)$, and the function $f(x)$ describes the elasticity of the artery wall as follows:

$$f(x) = \frac{4}{3}\left(k_1\, exp\left(k_2 r_0(x)\right) + k_3\right), \quad \textbf{(5)}$$

where parameter k_1 describes the stiffness of smaller arteries, k_2 reflects the transition between the large, elastic arteries and smaller, less-elastic arteries, and k_3 may be interpreted as the stiffness of large arteries (the vast majority of arteries in our model) (7).

1.3 Model of the cuff inflation

To model the impact of cuff inflation on arteries beneath the cuff, we used a nonlinear relationship between arterial internal cross-section (A_d) and transmural pressure (P_T) proposed by Drzewiecki et al. (8) (following its calibration, as described below):

$$A_d = d\frac{\ln(aP_T + b)}{1 + \exp(-cP_T)}, \quad \textbf{(6)}$$

where a, b, c, and d are empirical constants. This relationship combines the model of elastic distention of arterial wall with the model of its collapse at negative transmural pressures (cross-sectional area approaching zero), thus describing the (static) arterial cross-sectional area for a wide range of transmural pressures.

For simplicity, we used the above relationship only for the arterial segments under the considered cuffs. Moreover, to maintain the computational tractability of our 1-D model of the arterial network, we did not use the above relationship explicitly in those arterial segments, but we kept there our standard elastic model (equation (4)), which for each simulation (for a given cuff pressure) was scaled so that it would approximate locally the above relationship around the new expected mean arterial transmural pressure (assuming that the transmural pressure is reduced by an amount equal to the cuff pressure).

Our methodology involved the following calibration process (see. Supp. Figure 2). First, we calibrated the parameters a, b, c, and d of the Drzewiecki model to closely match our standard elastance model of the arterial wall (as given by Olufsen (3)) within the physiological pressure range, i.e. the range 80-120 mmHg. This ensured alignment with our baseline model under normal conditions. Next, to simulate cuff inflation, we used the Drzewiecki model to predict the reduced arterial cross-sectional area at external pressure corresponding to cuff pressure. Then, for each considered cuff pressure level, we scaled the Olufsen-based elastance model, i.e., we found the values of parameters P_{new} and g modifying equation (4), as follows:

$$P_T(t,x) = P_0 + P_{new} + g \cdot f(x)\left(1 - \sqrt{\frac{A_0(x)}{A(t,x)}}\right), \quad \textbf{(7)}$$

to approximate locally the Drzewiecki model within $\pm$ 20 mmHg around the estimated mean transmural pressure (for the given cuff pressure level). This scaling method allowed us to capture the nonlinear behavior of selected arterial segments during cuff occlusion while preserving the computational efficiency and structure of our existing 0-1D model.

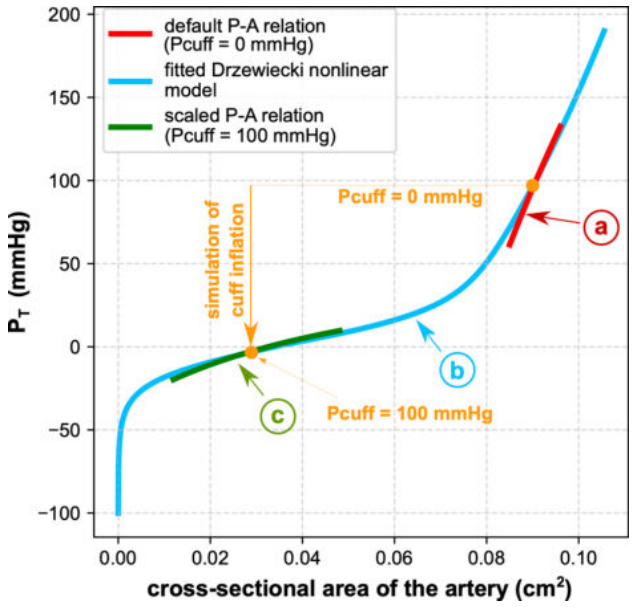

Supp. Figure 2 Calibration of the arterial pressure-area (P-A) relationship to simulate cuff inflation (example provided for the cuff pressure $\boldsymbol{P_{cuff}}$ = 100 mmHg). The calibration process for a given artery consists of three steps: (a) calibrating the parameters of the Drzewiecki model (equation 6) to fit as closely as possible the default P-A relationship (equation 4, red line) in the physiological pressure range (i.e. the range 80-120 mmHg); (b) using the fitted Drzewiecki model (blue line) to predict the arterial cross-sectional area at the given cuff pressure (assuming that the transmural pressure is reduced by an amount corresponding to the cuff pressure), and (c) scaling the default P-A relationship (equation 4) to approximate locally the Drzewiecki model (green line). By $\boldsymbol{P_T}$ we denoted transmural pressure.

1.4 Arterial bifurcations

At all modeled arterial bifurcations, we assume pressure continuity and mass conservation (i.e., no blood leakage). Let p represent the parent vessel and d_1, d_2 the daughter vessels. The assumed conditions can be expressed as follows:

$$P_{\text{out},p} = P_{\text{in},d_1} = P_{\text{in},d_2} \quad \text{and} \quad Q_{\text{out},p} = Q_{\text{in},d_1} + Q_{\text{in},d_2}, \tag{8}$$

where in and out denote inlet and outlet of a given artery, respectively.

1.5 Inflow boundary condition

Since venous return to the heart is not modeled, the inflow boundary conditions represent the outflow from the left heart ventricle. This is modeled based on the works of Suga et al. (9,10), and Danielsen and Ottesen (11). The pressure in the left ventricle, P_{lv}, is described using a time-varying elastance function $E_{lv}(t)$:

$$P_{lv} = E_{lv}(t)(V_{lv}(t) - V_0), \tag{9}$$

where $V_{lv}(t)$ is the ventricular volume at time t and V_0 is the volume of the left ventricle at zero transmural pressure. According to (11), the function $E_{lv}(t)$ may be expressed as follows:

$$E_{lv}(t) = E_{\min}\big(1 - \phi(t)\big) + E_{\max}\phi(t), \tag{10}$$

where the parameters $E_{\min}$ and $E_{\max}$ are minimal and maximal values of the elastance function $E_{lv}(t)$. Function ϕ is defined by the following equation:

$$\phi(t) = \begin{cases} \alpha \sin\left(\frac{\pi t}{t_m}\right) + \beta \sin\left(\frac{2\pi t}{t_m}\right) \text{ for } 0 \le t < t_m \\ 0 \text{ for } t_m \le t < T \end{cases} \tag{11}$$

where T is the heart period, t_m denotes the time to the onset of constant (minimal) elastance, and parameters α and β are responsible for the shape of the $\phi(t)$. Additionally, α and β must be chosen so that $\max_{t\in[0,T]} \phi\,(t) = 1$.

The work of the left ventricle can be divided into four stages. We will begin with isovolumic relaxation. During this phase, the pressure in the left ventricle decreases. When P_{lv} is smaller than the pressure in the left atrium, P_{la}, then the mitral valve opens.

In the next phase (ventricular filling) blood flows from the left atrium to the left ventricle. This flow, Q_{la}, is described by the following equation:

$$\frac{dQ_{la}}{dt} = \frac{1}{L_{la}}(P_{la} - P_{lv}) - \frac{R_{la}}{L_{la}}Q_{la}. \tag{12}$$

Parameter L_{la} is an inertia term, and R_{la} describes the resistance against the flow from the left atrium to the left ventricle, caused mainly by the viscous properties of the blood. Simultaneously, due to the inflow of blood into the left ventricle, V_{lv} increases, as given by the following equation:

$$\frac{dV_{lv}}{dt} = Q_{la}. \tag{13}$$

When V_{lv} is greater than the end-diastolic volume V_{ed}, the mitral valve closes, and isovolumic contraction begins.

During this phase, there is no flow between the left atrium and ventricle ($Q_{la} = 0$), and P_{lv} increases. When P_{lv} is greater than the pressure in the ascending aorta, P_a, the aortic valve opens, and the last phase of the cycle (ventricular ejection) begins.

The flow between the left ventricle and aorta is expressed by an equation similar to equation (11), namely:

$$\frac{dQ_{lv}}{dt} = \frac{1}{L_{lv}}(P_{la} - P_a) - \frac{R_{lv}}{L_{lv}}Q_{lv}. \quad \textbf{(14)}$$

The pressure P_a is taken directly from the 1D model of the arterial tree. The volume V_{lv} decreases according to the following equation:

$$\frac{dV_{lv}}{dt} = -Q_{lv}. \quad \textbf{(15)}$$

At the end of this phase, some amount of blood, V_b, returns from the ascending aorta to the left ventricle, which is associated with the negative value of Q_{lv} (backflow). V_b is given by the following equation:

$$V_b = \int_{t^*}^{t} |Q_{lv}|, \quad \text{for} \quad t > t^*, \quad \textbf{(16)}$$

where t^* denotes the moment, when Q_{lv} becomes negative. At the time t, when $V_b > \overline{V_b}$ we end the last phase by setting $Q_{lv} = 0$, and then the cycle repeats.

1.6 Outflow boundary conditions

To model blood flow in the small arteries and arterioles downstream from the terminal arteries in our vascular model, we use the three-element Windkessel model (12,13):

$$R_1 R_2 C_T \frac{dQ_{\text{end}}(t)}{dt} = R_2 C_T \frac{dP_{\text{end}}(t)}{dt} + (P_{\text{end}}(t) - P_{\text{term}}) - (R_1 + R_2)Q_{\text{end}}(t) \quad \textbf{(17)}$$

where R_1, R_2 are proximal and distal resistances, respectively, C_T is the compliance of the given terminal vascular branch, and P_{term} is the reference terminal pressure. We assume that $R_1/R_T = 0.2$, where $R_T = R_1 + R_2$ is the total terminal resistance (5,14). The assumed values of R_T and C_T are shown in Table 1. We personalize the model by applying the scaling factors: S_C for compliances and S_R for resistances, see (15) for more details.

2 Default Parameter Values

For our baseline model, we employed parameter values representative of a 25-year-old male with a height of 175 cm. The values of these parameters are provided in Table 2.

Table 2 Default parameter values considered in the cardiovascular model.

Parameter	Unit	Nominal value	Reference	Studied in the sensitivity analysis	Sampling range for sensitivity analyses ($\pm$ 10%)
μ	$\frac{\text{g}}{\text{cm}^3}$	1.04	(13)	No	-

ρ	$\frac{\mathrm{cm}^2}{\mathrm{s}}$	0.04	(13)	No	-
P_0	mmHg	97	(14)	No	-
k_1	$\frac{\mathrm{g}}{\mathrm{s}^2 \cdot \mathrm{cm}}$	$3 \cdot 10^6$	(16)	Yes	$[2.7 \cdot 10^6, 3.3 \cdot 10^6]$
k_2	$\frac{1}{\mathrm{cm}}$	-13.5	(7)	Yes	[-12.15, -14.85]
k_3	$\frac{\mathrm{g}}{\mathrm{s}^2 \cdot \mathrm{cm}}$	$5.36 \cdot 10^5$	Computed for age=25 from (7)	Yes	$[4.82, 5.90] \cdot 10^5$
a	$-$	0.9	(11)	No	-
b	$-$	0.25	(11)	No	-
$E_{\max}$	$\frac{\mathrm{mmHg}}{\mathrm{ml}}$	2.5	(11)	Yes	[2.25, 2.75]
$E_{\min}$	$\frac{\mathrm{mmHg}}{\mathrm{ml}}$	0.049	(11)	Yes	[0.0441, 0.0539]
t_m	s	0.45	(11)	Yes	[0.405, 0.495]
T	$\frac{1}{s}$	0.8	assumed	Yes	[0.72, 0.88]
V_{ed}	ml	127	(11)	Yes	[114, 140]
V_b	ml	2	(11)	Yes	[1.8, 2.2]
V_0	ml	10	(11)	Yes	[9, 11]
$\overline{V_b}$	ml	2	(11)	No	-
R_{lv}	$\frac{\mathrm{mmHg} \cdot \mathrm{s}}{\mathrm{ml}}$	0.0334	(11)	Yes	[0.03, 0.037]
L_{lv}	$\frac{\mathrm{mmHg} \cdot \mathrm{s}^2}{\mathrm{ml}}$	0.000416	(11)	Yes	[0.0003744, 0.0004576]
R_{la}	$\frac{\mathrm{mmHg} \cdot \mathrm{s}}{\mathrm{ml}}$	0.000089	(11)	Yes	$[8.0 \cdot 10^{-5}, 9.8 \cdot 10^{-5}]$
L_{la}	$\frac{\mathrm{mmHg} \cdot \mathrm{s}^2}{\mathrm{ml}}$	0.00005	(11)	Yes	$[4.5 \cdot 10^{-5}, 5.5 \cdot 10^{-5}]$
P_{la}	mmHg	5	(11)	Yes	[4.5, 5.5]

S_R	$-$	1	assumed	Yes	[0.9, 1.1]
S_C	$-$	1	assumed	Yes	[0.9, 1.1]
P_{term}	mmHg	15	(2)	No	-

References

1. Poleszczuk J, Debowska M, Dabrowski W, Wojcik-Zaluska A, Zaluska W, Waniewski J. Patient-specific pulse wave propagation model identifies cardiovascular risk characteristics in hemodialysis patients. PLoS Comput Biol. 2018;14(9):1–15.

2. Poleszczuk J, Debowska M, Dabrowski W, Wojcik-Zaluska A, Zaluska W, Waniewski J. Subject-specific pulse wave propagation modeling: Towards enhancement of cardiovascular assessment methods. PLoS ONE. 2018;13(1):1–17.

3. Olufsen MS, Peskin CS, Kim WY, Pedersen EM, Nadim A, Larsen J. Numerical simulation and experimental validation of blood flow in arteries with structured-tree outflow conditions. Ann Biomed Eng. 2000;28(11):1281–99.

4. Stergiopulos N, Young DF, Rogge TR. Computer simulation of arterial flow with applications to arterial and aortic stenoses. J Biomech. 1992 Dec 1;25(12):1477–88.

5. Alastruey J, Parker KH, Peiró J, Byrd SM, Sherwin SJ. Modelling the circle of Willis to assess the effects of anatomical variations and occlusions on cerebral flows. J Biomech. 2007 Jan 1;40(8):1794–805.

6. Ottesen JT, Olufsen MS, Larsen JK, Olufsen MS. 5. Modeling Flow and Pressure in the Systemic Arteries. In: Applied Mathematical Models in Human Physiology. Society for Industrial and Applied Mathematics; 2004. p. 91–136. (Mathematical Modeling and Computation).

7. Charlton PH, Mariscal Harana J, Vennin S, Li Y, Chowienczyk P, Alastruey J. Modeling arterial pulse waves in healthy aging: a database for in silico evaluation of hemodynamics and pulse wave indexes. Am J Physiol Heart Circ Physiol. 2019 Nov 1;317(5):H1062–85.

8. Drzewiecki G, Hood R, Apple H. Theory of the oscillometric maximum and the systolic and diastolic detection ratios. Ann Biomed Eng. 1994;22(1):88–96.

9. Suga H, Sagawa K, Kostiuk DP. Controls of ventricular contractility assessed by pressure-volume ratio, Emax1. Cardiovasc Res. 1976 Sep 1;10(5):582–92.

10. Suga H, Sagawa K, Shoukas AA. Load independence of the instantaneous pressure-volume ratio of the canine left ventricle and effects of epinephrine and heart rate on the ratio. Circ Res. 1973 Mar;32(3):314–22.

11. Ottesen JT, Olufsen MS, Larsen JK, Danielsen M, Ottesen JT. 6. A Cardiovascular Model. In: Applied Mathematical Models in Human Physiology. Society for Industrial and Applied Mathematics; 2004. p. 137–55. (Mathematical Modeling and Computation).

12. Westerhof N, Elzinga G, Sipkema P. An artificial arterial system for pumping hearts. J Appl Physiol. 1971 Nov;31(5):776–81.

13. Blanco PJ, Watanabe SM, Dari EA, Passos MARF, Feijóo RA. Blood flow distribution in an anatomically detailed arterial network model: criteria and algorithms. Biomech Model Mechanobiol. 2014 Nov 1;13(6):1303–30.

14. Stergiopulos N, Young DF, Rogge TR. Computer simulation of arterial flow with applications to arterial and aortic stenoses. J Biomech. 1992 Dec 1;25(12):1477–88.

15. Wołos K, Pstras L, Debowska M, Dabrowski W, Siwicka-Gieroba D, Poleszczuk J. Non-invasive assessment of stroke volume and cardiovascular parameters based on peripheral pressure waveform. PLOS Comput Biol. 2024 Apr 18;20(4):e1012013.

16. Mynard JP, Smolich JJ. One-Dimensional Haemodynamic Modeling and Wave Dynamics in the Entire Adult Circulation. Ann Biomed Eng. 2015 Jun 11;43(6):1443–60.

Chapter 5

General Discussion and Conclusions

5.1 Summary of Key Findings

This dissertation focuses on developing personalized pulse wave propagation models, utilizing non-invasive measurements of arterial pulse waveforms to estimate cardiovascular parameters that may help elucidate the cardiovascular state of patients. To achieve this, I introduced four research hypotheses (H1-H4) and corresponding research questions (H1Q1, H1Q2, H2Q1, H2Q2, H3Q1, H3Q2, H4Q1, H4Q2, H4Q3, H4Q4), as outlined in Chapter 1.6. All these hypotheses and research questions were addressed in the publications included in this dissertation.

To investigate my first research hypothesis (H1), I conducted a study to assess the feasibility of estimating stroke volume (SV) and selected cardiovascular parameters using a mathematical model of pulse wave propagation [A1]. The study included both healthy controls and patients with chronic kidney disease (CKD), with SV measured via bioimpedance cardiography (PhysioFlow, Manatec Biomedical, France). To describe the left ventricular function, the previously developed model was extended by incorporating a time-varying elastance model of the left ventricle. Personalization of the model was achieved using radial artery pulse waveforms acquired by applanation tonometry (SphygmoCor, AtCor Medical, Australia), enabling the estimation of clinically important but difficult-to-measure cardiovascular parameters, such as end-systolic elastance of the left ventricle. The model was able to reproduce the recorded peripheral pressure waveforms with high accuracy and the results demonstrated a moderate correlation between model-derived and bioimpedance-based SV in both study groups. Furthermore, the model-estimated end-systolic elastance showed a strong correlation with peripheral systolic pressure. These findings suggest that peripheral pulse wave recordings may provide clinically relevant information about SV and ventricular function, thereby supporting my first research hypothesis (H1). This study represents a novel application of pulse wave propagation modeling, utilizing peripheral pulse waveforms to estimate SV and ventricular function in both CKD patients and healthy individuals.

In the second publication [A2], I applied the extended pulse wave propagation model (featuring a more detailed arterial tree, including cerebral arteries) to estimate selected cardiovascular parameters in patients with severe traumatic brain injury (sTBI). This patient group presents particular challenges for both, researchers and clinicians due to frequent impairments in cerebral blood flow and the use of vasoactive drugs, which directly affect cardiovascular and thus model parameters. Clinical data were collected from 25 patients, including the history of vasopressor dosage and the peripheral pulse waveforms recorded using a four-limb oscillometric device (AngE, SoT Medical, Austria) on wrists and ankles. Prior to personalization of the model,

a comprehensive sensitivity and identifiability analysis was conducted to identify the parameters most relevant for data fitting. Based on these findings, a model optimization procedure was developed and applied to personalize the model for individual patient's multi-limb waveform recordings. The quality of the fits was satisfactory, which supported my second research hypothesis (H2). To test my third research hypothesis (H3), a statistical model was constructed using both the estimated cardiovascular parameters and routinely available clinical parameters to predict whether the next vasopressor dose would be increased, remain unchanged, or decreased. For comparison, a simplified predictive model was developed that relied solely on the current vasopressor dose and routinely available clinical parameters (e.g., body weight, height, and systolic/diastolic pressure). Incorporating model-estimated cardiovascular parameters improved the predictive accuracy compared to the simplified approach.

Simultaneous multi-limb oscillometric cuff inflation raises concerns about its potential impact on central hemodynamics, especially in patients with impaired cardiovascular regulation, which is a common complication in sTBI. To address this, I formulated the fourth hypothesis (H4) and developed a model to investigate the effects of simultaneous multi-limb arterial occlusion due to inflation of the cuffs [A3]. Specifically, I investigated how different combinations of cuff occlusions influence central hemodynamics. The model reliably reproduced local physiological responses to cuff inflation. Notably, during total arterial occlusion on all four limbs (in the absence of cardiovascular regulatory mechanisms), significant increases in mean arterial pressure and blood flow in the left common carotid artery were observed. These findings indicate that caution is warranted when performing such measurements in patients with compromised regulatory functions. However, further research is required to confirm these results and their clinical relevance.

5.2 Limitations and Future Perspectives

Mathematical modeling of the cardiovascular system is inherently complex. The models developed and presented in this dissertation sought to balance physiological fidelity with computational efficiency, enabling relatively accurate reproduction of recorded pulse waveforms while necessarily omitting certain physiological details. As a result, all presented studies are subject to both model-related and data-related limitations that should be considered when interpreting the results.

A general limitation arises from the simplified structure of the proposed model of the cardiovascular system. For instance, the model assumes a constant left atrial pressure, which overlooks the pulmonary circulation and interactions between the heart and the venous system. This simplification limits the ability to reflect cardiac regulatory mechanisms, such as the Frank-Starling mechanism, which is crucial for regulating stroke volume in response to changes in venous return [61]. Additionally, the presented studies did not incorporate autoregulatory mechanisms (such as cerebral autoregulation), which are essential for maintaining cerebral perfusion in patients with sTBI [148]. Although there are models in the literature that account for these phenomena, the parameters describing them are often difficult to estimate from non-invasive measurements. Future research should consider integrating a more detailed representation of the heart and accounting for the closed-loop nature of the cardiovascular system to better capture these interactions and enhance the model's predictive capabilities of cardiovascular or hemodynamic parameters, while maintaining computational efficiency and ensuring parameter identifiability from available data.

Another limitation concerns the availability and quality of input data. In the first study ([A1] presented in the Chapter 2), pulse waveforms were recorded using applanation tonometry, while stroke volume was estimated via bioimpedance cardiography. Due to poor quality of the recorded pulse waves or poor signal quality estimated by the device during stroke volume measurement procedure, nearly half of the data from CKD patients had to be excluded from analysis. Furthermore, the bioimpedance method itself has certain limitations compared to gold-standard techniques such as thermodilution or cardiac magnetic resonance imaging, which were not feasible in this patient group (during HD). In the second study ([A2], Chapter 3), pulse waveforms were obtained using a four-limb oscillometric device. However, as investigated in the third study ([A3], Chapter 4), inflation of multiple cuffs can potentially affect both central and local hemodynamics (and therefore the peripheral waveforms), particularly in patients with impaired cardiovascular regulation. Additionally, the recordings were performed only once per day at arbitrary time points. Future protocols should consider more frequent measurements to better capture the dynamic nature of cardiovascular responses to vasopressor administration in sTBI patients. In studies [A1] and [A2], presented in Chapter 2 and Chapter 3, the number of patients and pulse wave recordings was limited, so the presented findings should be regarded as preliminary and require validation in larger cohorts. Finally, the third study ([A3], Chapter 4) was purely theoretical, and the model predictions regarding the hemodynamic effects of multi-limb cuff inflation require *in vivo* validation. Future research should aim to confirm these findings in clinical settings, particularly in vulnerable to cardiovascular disease populations.

Despite these limitations, the studies presented in this thesis highlight promising directions for future research. Incorporating additional physiological details (such as the venous system, pulmonary circulation, and regulatory mechanisms) should enhance the model's ability to capture complex cardiovascular dynamics. This may enable the investigation of parameters like intracranial pressure or cerebral perfusion pressure, which are particularly relevant in patients with sTBI. Methodologically, integrating advanced machine learning techniques with traditional modeling approaches could improve parameter estimation and predictive accuracy of cardiovascular parameters. Such approaches are beginning to be explored in cardiovascular modeling and hold promise for further enhancing model performance [149, 150, 151]. Clinically, validating pulse wave propagation models in larger, more diverse patient cohorts using gold-standard measurements is essential to establish their utility in routine practice. This would help confirm my preliminary findings and verify whether the models presented in this dissertation could effectively support clinical decision-making across various patient populations.

5.3 Concluding Remarks

In summary, this dissertation presents three studies that collectively provide encouraging evidence that personalized pulse wave propagation modeling, informed by data from non-invasive measurements, can offer a novel method for SV and other cardiac parameter estimation in CKD patients, support vasopressor dosing decisions in sTBI patients, and elucidate the hemodynamic effects of multi-limb oscillometric cuff inflation. While each of the presented studies has its limitations, together they highlight the potential of mathematical models and may pave the way for future research to refine and validate these models for broader clinical application. Importantly, the presented work fits within the field of biomedical engineering, as it combines

mathematical modeling, computational simulation, and physiological measurements to develop tools that may enhance diagnosis, monitoring, and therapy optimization. Addressing the identified limitations and exploring the suggested future directions will be crucial for advancing the field and realizing the full potential of personalized cardiovascular modeling in clinical practice.

KAMIL WOŁOS

@ kwolos@ibib.waw.pl linkedin.com/in/kamilwolos github.com/kwolos 0000-0003-4655-1732

EDUCATION

PhD Studies, Biomedical Engineering

Nalecz Institute of Biocybernetics and Biomedical Engineering, Polish Academy of Sciences

2020–2025 Warsaw

- PhD thesis: *Optimization of Vasopressor Dose in Severe Traumatic Brain Injuries Using Pulse-Wave Propagation Modeling*.

Master's degree in Mathematics in Technical Science

Faculty of Mathematics and Information Science, Warsaw University of Technology

2016–2019 Warsaw

- Diploma thesis: *Theoretical and numerical analysis of selected boundary conditions for fluid mechanics equations.*

Bachelors's degree in Mathematics

Faculty of Mathematics and Information Science, Warsaw University of Technology

2013–2016 Warsaw

- Diploma thesis: *Special, global solutions to magnetohydrodynamic equations.*

PUBLICATIONS

1. Kosewski, Przemysław, and **Kamil Wołos**. "Existence and regularity result for Stokes system with special inlet/outlet condition." Mathematical Methods in the Applied Sciences 44.17 (2021): 12797-12809.
2. **Wołos, Kamil**, et al. "Non-invasive assessment of stroke volume and cardiovascular parameters based on peripheral pressure waveform." PLOS Computational Biology 20.4 (2024): e1012013.
3. **Wołos, Kamil**, et al. "Impact of multi-limb oscillometric cuff measurements on hemodynamics: insights from pulse wave propagation modeling." Frontiers in Physiology 16 (2025): 1642645.
4. **Wołos, Kamil**, et al. "Personalized pulse wave propagation modeling to improve vasopressor dosing management in patients with severe traumatic brain injury." PLOS Computational Biology 21.9 (2025): e1013501.

CONFERENCES

1. International Congress on Industrial and Applied Mathematics (ICIAM 2019), 15-19 July 2019, Valencia, Spain, *Mathematical analysis and numerical methods for internal incompressible flows with inertial-dissipative inflow/outflow conditions* – **poster**.
2. 22nd Polish Conference on Biocybernetics and Biomedical Engineering, 19-21 May 2021, Warsaw, Poland (online), *Pulse wave propagation modeling for non-invasive assessment of heart function* – **poster**.
3. Computing in Cardiology Conference, 04-07 September 2022, Tampere, Finland, *Cardiac function assessment using personalized reduced-order pulse wave modelling* – **poster**.
4. The 12th European Conference on Mathematical and Theoretical Biology, 19-23 September 2022, Heidelberg, Germany, *Cardiac function assessment in patients with chronic kidney disease using subject-specific cardiovascular modelling* – **presentation**.

5. 23rd Polish Conference on Biocybernetics and Biomedical Engineering, 27-29 September 2023, Łódź, Poland, *A Model of Cerebral Hemodynamics Incorporating Interstitial Fluid Flow in Cerebral Edema* – **presentation**.
6. Joint 20th Nordic-Baltic Conference on Biomedical Engineering and the 24th Polish Conference on Biocybernetics and Biomedical Engineering, 16-18 June 2025, Warsaw, poster 1: *Patient-specific Pulse Wave Propagation Modeling for Improving Vasopressor Therapy in Severe Traumatic Brain Injury Patients (presentation)*, poster 2: *Model-Based Investigation of the Effect of Multi-Site Arterial Occlusion by Cuffs on the Distribution of Blood Flow in the Arterial Tree*, (presenting Author: Jan Poleszczuk) – **poster**.

PARTICIPATION IN RESEARCH PROJECTS

- **Rector's Grant for Scientific Clubs** for the project *Theoretical and Numerical Analysis of a Boundary Value Problem Simulating Airflow in the Lungs*, Warsaw University of Technology, 2019.
- **SONATA 14, grant No. 2018/31/D/ST7/03472**, "Optimization of vasopressor dose in severe traumatic brain injuries using pulse-wave propagation modeling", funded by the National Science Centre (Poland), 2019-2025 (Principal investigator: Jan Poleszczuk).
- **Internal grant FBW/2.5/22**, „System do symulacji hydrodynamicznych układu krążenia", Nalecz Institute of Biocybernetics and Biomedical Sciences, 2022, (Principal investigator: Krzysztof Zieliński).

RECEIVED SCHOLARSHIPS AND AWARDS

- Rector's Scholarship of Warsaw University of Technology for top students (academic year 2016/17).
- Rector's Scholarship of Warsaw University of Technology for scientific achievements (academic year 2016/17).
- John Paul II Scholarship of the City of Warsaw (academic year 2016/2017).
- Scholarship under the grant SONATA 14, grant No. 2018/31/D/ST7/03472, "Optimization of vasopressor dose in severe traumatic brain injuries using pulse-wave propagation modeling", funded by the National Science Centre (Poland).
- Scholarship under the program "POWER OCH!DOK", supported by ESF, POWR.03.02.00-00-I028/17-00.

PARTICIPATION IN TRAININGS, WORKSHOPS, SUMMER SCHOOLS

- ENTHRAL Summer School on vascular bioengineering, 28.06-1.07.2021, online, Gliwice, Poland.
- International Summer School on Modeling Nature, BIOMAT 2022, 06.06-10.06.2022, Granada, Spain.
- Apache Spark z wykorzystaniem języka Python, 15.02-16.02.2024, online, Sages Company, Poland.
- Python Średnio-Zaawansowany, 18.03-22.03.2024, online, Sages Company, Poland.
- Python Zaawansowany, 15.04-19.04.2024, online, Sages Company, Poland.

PRIZES, DISTINCTIONS

- Second place in the best poster competition in the Joint 20th Nordic-Baltic Conference on Biomedical Engineering and the 24th Polish Conference on Biocybernetics and Biomedical Engineering.

GENERAL SKILLS

Python | MATLAB | C/C++ | LaTeX | Git | Linux | Data Analysis | Mathematical Modeling | Numerical Methods | TensorFlow | Keras | Scikit-learn | Pandas | NumPy | SciPy

OTHER ACTIVITIES

Member of the Faculty Student Council (Wydziałowa Rada Samorządowa)

Faculty of Mathematics and Information Science, Warsaw University of Technology

2014–2018 Warsaw, Poland

- Member of the Faculty Council (Rada Wydziału), Faculty of Mathematics and Information Science, Warsaw University of Technology.
- Member of the Faculty Curriculum Committee (Komisja Programowa) for the Mathematics program.
- Member of the Faculty Scholarship and Social Affairs Committee (Komisja Socjalna i Stypendialna).

Student Research Group in Mathematical Modelling (Koło Naukowe Modelowania Matematycznego)

Faculty of Mathematics and Information Science, Warsaw University of Technology

2017–2018 Warsaw, Poland

- Co-founder and first Chair.
- Co-organizer and Head of the Organizing Committee of the first edition of the conference *Applications of Mathematics* ("DwuMIan").

Volunteering

Akademia Przyszłości

2017–2018 Warsaw, Poland

- Supported a child in overcoming educational barriers and fostering equal opportunities for those from disadvantaged backgrounds.

WORK EXPERIENCE

Engineer in the R&D department

Euros Energy

2018–2020 Koprki

Development of mathematical models and control optimization for cold storage and freezer systems. Numerical simulation of a single vertical borehole heat exchanger with underground heat storage.

Specialist

Centrum e-zdrowia (e-Health Centre)

2023–2024 Warsaw

Support for data processing, integration, and analysis, enabling the construction of models based on machine learning and artificial intelligence methods.

Specialist (research-technical position)

Nalecz Institute of Biocybernetics and Biomedical Engineering, Polish Academy of Sciences

2024–2025 Warsaw

Development of a zero-dimensional mathematical model describing intracerebral hemodynamics, integrated with a 1D pulse wave propagation model and investigating the effect of oscillometric pressure measurement on hemodynamics utilizing the pulse wave propagation model.

Authorship declaration for the article: *„Non-invasive assessment of stroke volume and cardiovascular parameters based on peripheral pressure waveform"*, published in PLOS Computational Biology, 20(4):e1012013.

The Authors declare that they have made the following contributions to the article:

Kamil Wołos (first author, corresponding author):
Conceptualization, Formal analysis, Investigation, Methodology, Project administration, Software, Validation, Visualization, Writing – original draft.

Leszek Pstraś:
Supervision, Validation, Writing – review and editing.

Małgorzata Dębowska:
Funding acquisition, Methodology, Writing – review and editing.

Wojciech Dąbrowski:
Data curation, Funding acquisition, Methodology.

Dorota Siwicka-Gieroba:
Data curation, Funding acquisition, Resources.

Jan Poleszczuk: Conceptualization, Funding acquisition, Methodology, Project administration, Resources, Supervision, Validation, Writing – review and editing.

Kamil Wołos
Signature: 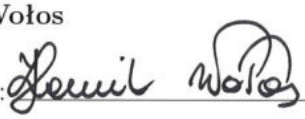

Leszek Pstraś
Signature: *Signature provided on another page*

Małgorzata Dębowska
Signature: 

Wojciech Dąbrowski
Signature: *Signature provided on another page*

Dorota Siwicka-Gieroba
Signature: *Signature provided on another page*

Jan Poleszczuk
Signature: 

Authorship declaration for the article: *„Non-invasive assessment of stroke volume and cardiovascular parameters based on peripheral pressure waveform"*, published in PLOS Computational Biology, 20(4):e1012013.

The Authors declare that they have made the following contributions to the article:

Kamil Wołos (first author, corresponding author):
Conceptualization, Formal analysis, Investigation, Methodology, Project administration, Software, Validation, Visualization, Writing – original draft.

Leszek Pstraś:
Supervision, Validation, Writing – review and editing.

Małgorzata Dębowska:
Funding acquisition, Methodology, Writing – review and editing.

Wojciech Dąbrowski:
Data curation, Funding acquisition, Methodology.

Dorota Siwicka-Gieroba:
Data curation, Funding acquisition, Resources.

Jan Poleszczuk: Conceptualization, Funding acquisition, Methodology, Project administration, Resources, Supervision, Validation, Writing – review and editing.

Kamil Wołos

Signature: *Signature provided on another page*

Leszek Pstraś

Signature:

Małgorzata Dębowska

Signature: *Signature provided on another page*

Wojciech Dąbrowski

Signature: *Signature provided on another page*

Dorota Siwicka-Gieroba

Signature: *Signature provided on another page*

Jan Poleszczuk

Signature: *Signature provided on another page*

Authorship declaration for the article: *„Non-invasive assessment of stroke volume and cardiovascular parameters based on peripheral pressure waveform"*, published in PLOS Computational Biology, 20(4):e1012013.

The Authors declare that they have made the following contributions to the article:

Kamil Wołos (first author, corresponding author):
Conceptualization, Formal analysis, Investigation, Methodology, Project administration, Software, Validation, Visualization, Writing – original draft.

Leszek Pstraś:
Supervision, Validation, Writing – review and editing.

Małgorzata Dębowska:
Funding acquisition, Methodology, Writing – review and editing.

Wojciech Dąbrowski:
Data curation, Funding acquisition, Methodology.

Dorota Siwicka-Gieroba:
Data curation, Funding acquisition, Resources.

Jan Poleszczuk: Conceptualization, Funding acquisition, Methodology, Project administration, Resources, Supervision, Validation, Writing – review and editing.

Kamil Wołos
Signature: *Signature provided on another page*

Leszek Pstraś
Signature: *Signature provided on another page*

Małgorzata Dębowska
Signature: *Signature provided on another page*

Wojciech Dąbrowski
Signature: *Signature provided on another page*

Dorota Siwicka-Gieroba
Signature: Siwicka

Jan Poleszczuk
Signature: *Signature provided on another page*

Authorship declaration for the article: *„Non-invasive assessment of stroke volume and cardiovascular parameters based on peripheral pressure waveform"*, published in PLOS Computational Biology, 20(4):e1012013.

The Authors declare that they have made the following contributions to the article:

Kamil Wołos (first author, corresponding author):
Conceptualization, Formal analysis, Investigation, Methodology, Project administration, Software, Validation, Visualization, Writing – original draft.

Leszek Pstraś:
Supervision, Validation, Writing – review and editing.

Małgorzata Dębowska:
Funding acquisition, Methodology, Writing – review and editing.

Wojciech Dąbrowski:
Data curation, Funding acquisition, Methodology.

Dorota Siwicka-Gieroba:
Data curation, Funding acquisition, Resources.

Jan Poleszczuk: Conceptualization, Funding acquisition, Methodology, Project administration, Resources, Supervision, Validation, Writing – review and editing.

Kamil Wołos

Signature: *Signature provided on another page*

Leszek Pstraś

Signature: *Signature provided on another page*

Małgorzata Dębowska

Signature: *Signature provided on another page*

Wojciech Dąbrowski

Signature:

Dorota Siwicka-Gieroba

Signature: *Signature provided on another page*

Jan Poleszczuk

Signature: *Signature provided on another page*

Authorship declaration for the article: *„Personalized pulse wave propagation modeling to improve vasopressor dosing management in patients with severe traumatic brain injury"*, published in PLOS Computational Biology, 21(9):e1013501.

The Authors declare that they have made the following contributions to the article:

Kamil Wołos (first author, corresponding author):
Conceptualization, Data curation, Formal analysis, Investigation, Methodology, Project Administration, Software, Validation, Visualization, Writing - original draft.

Leszek Pstraś:
Methodology, Supervision, Validation, Writing - review and editing

Urszula Białończyk:
Methodology, Validation, Writing – review and editing.

Małgorzata Dębowska:
Funding acquisition, Methodology, Supervision.

Wojciech Dąbrowski:
Data curation, Funding acquisition, Methodology.

Dorota Siwicka-Gieroba:
Data curation, Funding acquisition, Methodology.

Jan Poleszczuk: Conceptualization, Funding acquisition, Methodology, Project administration, Supervision, Validation, Writing – review and editing.

Kamil Wołos
Signature: 

Leszek Pstraś
Signature: *Signature provided on another page*

Urszula Białończyk
Signature: 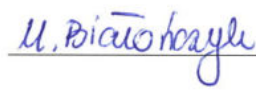

Małgorzata Dębowska
Signature: 

Wojciech Dąbrowski
Signature: *Signature provided on another page*

Dorota Siwicka-Gieroba
Signature: *Signature provided on another page*

Jan Poleszczuk
Signature: 

Authorship declaration for the article: *„Personalized pulse wave propagation modeling to improve vasopressor dosing management in patients with severe traumatic brain injury"*, published in PLOS Computational Biology, 21(9):e1013501.

The Authors declare that they have made the following contributions to the article:

Kamil Wołos (first author, corresponding author):
Conceptualization, Data curation, Formal analysis, Investigation, Methodology, Project Administration, Software, Validation, Visualization, Writing - original draft.

Leszek Pstraś:
Methodology, Supervision, Validation, Writing - review and editing

Urszula Białończyk:
Methodology, Validation, Writing – review and editing.

Małgorzata Dębowska:
Funding acquisition, Methodology, Supervision.

Wojciech Dąbrowski:
Data curation, Funding acquisition, Methodology.

Dorota Siwicka-Gieroba:
Data curation, Funding acquisition, Methodology.

Jan Poleszczuk: Conceptualization, Funding acquisition, Methodology, Project administration, Supervision, Validation, Writing – review and editing.

Kamil Wołos
Signature: *Signature provided on another page*

Leszek Pstraś
Signature: 

Urszula Białończyk
Signature: *Signature provided on another page*

Małgorzata Dębowska
Signature: *Signature provided on another page*

Wojciech Dąbrowski
Signature: *Signature provided on another page*

Dorota Siwicka-Gieroba
Signature: *Signature provided on another page*

Jan Poleszczuk
Signature: *Signature provided on another page*

Authorship declaration for the article: *„Personalized pulse wave propagation modeling to improve vasopressor dosing management in patients with severe traumatic brain injury"*, published in PLOS Computational Biology, 21(9):e1013501.

The Authors declare that they have made the following contributions to the article:

Kamil Wołos (first author, corresponding author):
Conceptualization, Data curation, Formal analysis, Investigation, Methodology, Project Administration, Software, Validation, Visualization, Writing - original draft.

Leszek Pstraś:
Methodology, Supervision, Validation, Writing - review and editing

Urszula Białończyk:
Methodology, Validation, Writing – review and editing.

Małgorzata Dębowska:
Funding acquisition, Methodology, Supervision.

Wojciech Dąbrowski:
Data curation, Funding acquisition, Methodology.

Dorota Siwicka-Gieroba:
Data curation, Funding acquisition, Methodology.

Jan Poleszczuk: Conceptualization, Funding acquisition, Methodology, Project administration, Supervision, Validation, Writing – review and editing.

Kamil Wołos
Signature: *Signature provided on another page*

Leszek Pstraś
Signature: *Signature provided on another page*

Urszula Białończyk
Signature: *Signature provided on another page*

Małgorzata Dębowska
Signature: *Signature provided on another page*

Wojciech Dąbrowski
Signature: *Signature provided on another page*

Dorota Siwicka-Gieroba
Signature: Siwicka

Jan Poleszczuk
Signature: *Signature provided on another page*

Authorship declaration for the article: *„Personalized pulse wave propagation modeling to improve vasopressor dosing management in patients with severe traumatic brain injury”*, published in PLOS Computational Biology, 21(9):e1013501.

The Authors declare that they have made the following contributions to the article:

Kamil Wołos (first author, corresponding author):
Conceptualization, Data curation, Formal analysis, Investigation, Methodology, Project Administration, Software, Validation, Visualization, Writing - original draft.

Leszek Pstraś:
Methodology, Supervision, Validation, Writing - review and editing

Urszula Białończyk:
Methodology, Validation, Writing – review and editing.

Małgorzata Dębowska:
Funding acquisition, Methodology, Supervision.

Wojciech Dąbrowski:
Data curation, Funding acquisition, Methodology.

Dorota Siwicka-Gieroba:
Data curation, Funding acquisition, Methodology.

Jan Poleszczuk: Conceptualization, Funding acquisition, Methodology, Project administration, Supervision, Validation, Writing – review and editing.

Kamil Wołos

Signature: *Signature provided on another page*

Leszek Pstraś

Signature: *Signature provided on another page*

Urszula Białończyk

Signature: *Signature provided on another page*

Małgorzata Dębowska

Signature: *Signature provided on another page*

Wojciech Dąbrowski

Signature: Podpisuję z Cencert

Podpisany elektronicznie przez WOJCIECH ROBERT DĄBROWSKI 16.09.2025 20:41:01 +02'00'

Dorota Siwicka-Gieroba

Signature: *Signature provided on another page*

Jan Poleszczuk

Signature: *Signature provided on another page*

Authorship declaration for the article: *„Impact of multi-limb oscillometric cuff measurements on hemodynamics: insights from pulse wave propagation modeling"*, published in Frontiers in Physiology, 16:1642645.

The Authors declare that they have made the following contributions to the article:

Kamil Wołos (first author, corresponding author):
Investigation, Software, Conceptualization, Writing - review and editing, Formal Analysis, Writing - original draft, Data curation, Visualization, Methodology, Validation.

Leszek Pstraś:
Conceptualization, Supervision, Investigation, Writing – review and editing, Validation, Methodology.

Małgorzata Dębowska:
Conceptualization, Funding acquisition, Validation, Methodology, Supervision, Investigation, Writing – review and editing.

Jan Poleszczuk:
Validation, Project administration, Methodology, Investigation, Conceptualization, Writing – review and editing, Supervision, Funding acquisition.

Kamil Wołos

Signature: 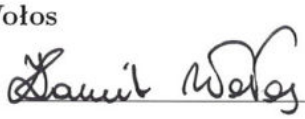

Leszek Pstraś

Signature: *Signature provided on another page*

Małgorzata Dębowska

Signature: 

Jan Poleszczuk

Signature: 

Authorship declaration for the article: *„Impact of multi-limb oscillometric cuff measurements on hemodynamics: insights from pulse wave propagation modeling"*, published in Frontiers in Physiology, 16:1642645.

The Authors declare that they have made the following contributions to the article:

Kamil Wołos (first author, corresponding author):
Investigation, Software, Conceptualization, Writing - review and editing, Formal Analysis, Writing - original draft, Data curation, Visualization, Methodology, Validation.

Leszek Pstraś:
Conceptualization, Supervision, Investigation, Writing – review and editing, Validation, Methodology.

Małgorzata Dębowska:
Conceptualization, Funding acquisition, Validation, Methodology, Supervision, Investigation, Writing – review and editing.

Jan Poleszczuk:
Validation, Project administration, Methodology, Investigation, Conceptualization, Writing – review and editing, Supervision, Funding acquisition.

Kamil Wołos

Signature: *Signature provided on another page*

Leszek Pstraś

Signature: 

Małgorzata Dębowska

Signature: *Signature provided on another page*

Jan Poleszczuk

Signature: *Signature provided on another page*

Bibliography

[A1] Kamil Wołos et al. “Non-Invasive Assessment of Stroke Volume and Cardiovascular Parameters Based on Peripheral Pressure Waveform”. In: *PLOS Computational Biology* 20.4 (2024), e1012013. ISSN: 1553-7358.

[A2] Kamil Wolos et al. “Personalized Pulse Wave Propagation Modeling to Improve Vasopressor Dosing Management in Patients with Severe Traumatic Brain Injury”. In: *PLOS Computational Biology* 21.9 (2025), e1013501. ISSN: 1553-7358.

[A3] Kamil Wolos et al. “Impact of Multi-Limb Oscillometric Cuff Measurements on Hemodynamics: Insights from Pulse Wave Propagation Modeling”. In: *Frontiers in Physiology* 16 (2025). ISSN: 1664-042X.

[1] World Health Organization. *Cardiovascular Diseases (CVDs)*. https://www.who.int/news-room/fact-sheets/detail/cardiovascular-diseases-(cvds). Accessed: 2025-08-30.

[2] Gregory A. Roth et al. “Global Burden of Cardiovascular Diseases and Risk Factors, 1990–2019”. In: *JACC* 76.25 (2020), pp. 2982–3021.

[3] Bryan Chong et al. “Global Burden of Cardiovascular Diseases: Projections from 2025 to 2050”. In: *European Journal of Preventive Cardiology* 32.11 (2025), pp. 1001–1015. ISSN: 2047-4881.

[4] Sarah J. Pickersgill et al. “Modeling Global 80-80-80 Blood Pressure Targets and Cardiovascular Outcomes”. In: *Nature Medicine* 28.8 (2022), pp. 1693–1699. ISSN: 1078-8956.

[5] Joachim Jankowski et al. “Cardiovascular Disease in Chronic Kidney Disease”. In: *Circulation* 143.11 (2021), pp. 1157–1172.

[6] Kunihiro Matsushita et al. “Epidemiology and Risk of Cardiovascular Disease in Populations with Chronic Kidney Disease”. In: *Nature Reviews Nephrology* 18.11 (2022), pp. 696–707. ISSN: 1759-507X.

[7] Kamyar Kalantar-Zadeh et al. “Chronic Kidney Disease”. In: *The Lancet* 398.10302 (2021), pp. 786–802. ISSN: 0140-6736, 1474-547X.

[8] Boris Bikbov et al. “Global, Regional, and National Burden of Chronic Kidney Disease, 1990–2017: A Systematic Analysis for the Global Burden of Disease Study 2017”. In: *The Lancet* 395.10225 (2020), pp. 709–733. ISSN: 0140-6736, 1474-547X.

[9] Luca Di Lullo et al. “Chronic Kidney Disease and Cardiovascular Complications”. In: *Heart Failure Reviews* 20.3 (2015), pp. 259–272. ISSN: 1573-7322.

[10] Stephanie Thompson et al. “Cause of Death in Patients with Reduced Kidney Function”. In: *Journal of the American Society of Nephrology* 26.10 (2015), p. 2504. ISSN: 1046-6673.

[11] Zhen Zhang and Yaqiong Wang. “Management of Cardiovascular Diseases in Chronic Hemodialysis Patients”. In: *Reviews in Cardiovascular Medicine* 24.7 (2023), p. 185. ISSN: 1530-6550.

[12] David K. Menon et al. “Position Statement: Definition of Traumatic Brain Injury”. In: *Archives of Physical Medicine and Rehabilitation* 91.11 (2010), pp. 1637–1640. ISSN: 0003-9993.

[13] Juliet Haarbauer-Krupa et al. “Epidemiology of Chronic Effects of Traumatic Brain Injury”. In: *Journal of Neurotrauma* 38.23 (2021), pp. 3235–3247. ISSN: 0897-7151.

[14] Andrew I. R. Maas et al. “Traumatic Brain Injury: Progress and Challenges in Prevention, Clinical Care, and Research”. In: *The Lancet Neurology* 21.11 (2022), pp. 1004–1060. ISSN: 1474-4422, 1474-4465.

[15] Bob Roozenbeek, Andrew I. R. Maas, and David K. Menon. “Changing Patterns in the Epidemiology of Traumatic Brain Injury”. In: *Nature Reviews Neurology* 9.4 (2013), pp. 231–236. ISSN: 1759-4766.

[16] Simon R. Finfer and Jeremy Cohen. “Severe Traumatic Brain Injury”. In: *Resuscitation* 48.1 (2001), pp. 77–90. ISSN: 0300-9572.

[17] Jeffrey V. Rosenfeld et al. “Early Management of Severe Traumatic Brain Injury”. In: *The Lancet* 380.9847 (2012), pp. 1088–1098. ISSN: 0140-6736, 1474-547X.

[18] Nancy Carney et al. “Guidelines for the Management of Severe Traumatic Brain Injury, Fourth Edition”. In: *Neurosurgery* 80.1 (2017), p. 6. ISSN: 0148-396X.

[19] Camilo Toro et al. “Early Vasopressor Utilization Strategies and Outcomes in Critically Ill Patients with Severe Traumatic Brain Injury”. In: *Anesthesia and analgesia* 135.6 (2022), p. 1245.

[20] John A. Kellum and Michael R. Pinsky. “Use of Vasopressor Agents in Critically Ill Patients”. In: *Current Opinion in Critical Care* 8.3 (2002), pp. 236–241. ISSN: 1070-5295.

[21] Helene Beloeil et al. “Norepinephrine Kinetics and Dynamics in Septic Shock and Trauma Patients”. In: *British Journal of Anaesthesia* 95.6 (2005), pp. 782–788. ISSN: 00070912.

[22] Matthieu Legrand and Alexander Zarbock. “Ten Tips to Optimize Vasopressors Use in the Critically Ill Patient with Hypotension”. In: *Intensive Care Medicine* 48.6 (2022), pp. 736–739. ISSN: 1432-1238.

[23] Michael Böhm et al. “Heart Rate as a Risk Factor in Chronic Heart Failure (SHIFT): The Association between Heart Rate and Outcomes in a Randomised Placebo-Controlled Trial”. In: *The Lancet* 376.9744 (2010), pp. 886–894. ISSN: 0140-6736, 1474-547X.

[24] William B. Kannel et al. “Heart Rate and Cardiovascular Mortality: The Framingham Study”. In: *American Heart Journal* 113.6 (1987), pp. 1489–1494. ISSN: 0002-8703.

[25] Paolo Palatini and Stevo Julius. “Relevance of Heart Rate as a Risk Factor in Hypertension”. In: *Current Hypertension Reports* 1.3 (1999), pp. 219–224. ISSN: 1534-3111.

[26] Leonard S. Dreifus et al. “Heart Rate Variability for Risk Stratification of Life-Threatening Arrhythmias”. In: *Journal of the American College of Cardiology* 22.3 (1993), pp. 948–950. ISSN: 0735-1097.

[27] Becky Schroeder et al. “Cardiovascular Monitoring”. In: *Miller’s Anesthesia, 2-Volume Set*. 2024. ISBN: 978-0-323-93592-0.

[28] S. Magder. "The Meaning of Blood Pressure". In: *Critical Care* 22.1 (2018), p. 257. ISSN: 1364-8535.

[29] Katherine T. Mills et al. "Global Disparities of Hypertension Prevalence and Control". In: *Circulation* 134.6 (2016), pp. 441–450.

[30] Bin Zhou et al. "Worldwide Trends in Hypertension Prevalence and Progress in Treatment and Control from 1990 to 2019: A Pooled Analysis of 1201 Population-Representative Studies with 104 Million Participants". In: *The Lancet* 398.10304 (2021), pp. 957–980. ISSN: 0140-6736, 1474-547X.

[31] Johanna Kuipers et al. "The Prevalence of Intradialytic Hypotension in Patients on Conventional Hemodialysis: A Systematic Review with Meta-Analysis". In: *American Journal of Nephrology* 49.6 (2019), pp. 497–506. ISSN: 0250-8095.

[32] Geoffrey Manley et al. "Hypotension, Hypoxia, and Head Injury: Frequency, Duration, and Consequences". In: *Archives of Surgery* 136.10 (2001), pp. 1118–1123. ISSN: 0004-0010.

[33] Keita Shibahashi et al. "Defining Hypotension in Patients with Severe Traumatic Brain Injury". In: *World Neurosurgery* 120 (2018), e667–e674. ISSN: 1878-8750.

[34] Andrew Rhodes et al. "Surviving Sepsis Campaign: International Guidelines for Management of Sepsis and Septic Shock: 2016". In: *Critical Care Medicine* 45.3 (2017), p. 486. ISSN: 1530-0293.

[35] Neel Agarwal et al. "Association of Pulse Pressure with Death, Myocardial Infarction, and Stroke among Cardiovascular Outcome Trial Participants". In: *American Journal of Preventive Cardiology* 17 (2023), p. 100623. ISSN: 2666-6677.

[36] Marijana Tadic et al. "The Importance of Pulse Pressure on Cardiovascular Risk and Total Mortality in the General Population: Is Sex Relevant?" In: *The Journal of Clinical Hypertension* 20.6 (2018), pp. 1001–1007. ISSN: 1524-6175.

[37] Sauradeep Sarkar, Sahib Singh, and Amit Rout. "Mean Arterial Pressure Goal in Critically Ill Patients: A Meta-Analysis of Randomized Controlled Trials". In: *Journal of Clinical Medicine Research* 14.5 (2022), pp. 196–201. ISSN: 1918-3003.

[38] Daniel DeMers and Daliah Wachs. "Physiology, Mean Arterial Pressure". In: *StatPearls*. Treasure Island (FL): StatPearls Publishing, 2025.

[39] Theodore G. Papaioannou et al. "Mean Arterial Pressure Values Calculated Using Seven Different Methods and Their Associations with Target Organ Deterioration in a Single-Center Study of 1878 Individuals". In: *Hypertension Research* 39.9 (2016), pp. 640–647. ISSN: 1348-4214.

[40] Patrick Segers et al. "Amplification of the Pressure Pulse in the Upper Limb in Healthy, Middle-Aged Men and Women". In: *Hypertension* 54.2 (2009), pp. 414–420.

[41] Tai Le et al. "Continuous Non-Invasive Blood Pressure Monitoring: A Methodological Review on Measurement Techniques". In: *IEEE Access* 8 (2020), pp. 212478–212498. ISSN: 2169-3536.

[42] Nishil Patel et al. "Physiology, Cardiac Index". In: *StatPearls*. Treasure Island (FL): StatPearls Publishing, 2025.

[43] Bart F. Geerts, Leon P. Aarts, and Jos R. Jansen. “Methods in Pharmacology: Measurement of Cardiac Output”. In: *British Journal of Clinical Pharmacology* 71.3 (2011), pp. 316–330. ISSN: 1365-2125.

[44] Lee S. Nguyen and Pierre Squara. “Non-Invasive Monitoring of Cardiac Output in Critical Care Medicine”. In: *Frontiers in Medicine* 4 (2017). ISSN: 2296-858X.

[45] Jacob E. Trammel and Amit Sapra. “Physiology, Systemic Vascular Resistance”. In: *StatPearls*. Treasure Island (FL): StatPearls Publishing, 2025.

[46] “Systemic Vascular Resistance”. In: *Essential Equations for Anaesthesia: Key Clinical Concepts for the FRCA and EDA*. Ed. by Edward T. Gilbert-Kawai and Marc D. Wittenberg. Cambridge: Cambridge University Press, 2014, pp. 102–103. ISBN: 978-1-107-63660-6.

[47] Olfa Hamzaoui and Jean-Louis Teboul. “Central Venous Pressure (CVP)”. In: *Intensive Care Medicine* 48.10 (2022), pp. 1498–1500. ISSN: 1432-1238.

[48] Max Ruge and Gregary D. Marhefka. “IVC Measurement for the Noninvasive Evaluation of Central Venous Pressure”. In: *Journal of Echocardiography* 20.3 (2022), pp. 133–143. ISSN: 1880-344X.

[49] David Sturgeon. “Blood Pressure”. In: *Introduction to Anatomy and Physiology for Healthcare Students*. Routledge, 2018. ISBN: 978-1-315-54429-8.

[50] Clyde W. Yancy et al. “2017 ACC/AHA/HFSA Focused Update of the 2013 ACCF/AHA Guideline for the Management of Heart Failure: A Report of the American College of Cardiology/American Heart Association Task Force on Clinical Practice Guidelines and the Heart Failure Society of America”. In: *Circulation* 136.6 (2017), e137–e161.

[51] Sean P. Murphy, Nasrien E. Ibrahim, and James L. Januzzi Jr. “Heart Failure With Reduced Ejection Fraction: A Review”. In: *JAMA* 324.5 (2020), pp. 488–504. ISSN: 0098-7484.

[52] Pirbhat Shams, Amandeep Goyal, and Amgad N. Makaryus. “Left Ventricular Ejection Fraction”. In: *StatPearls*. Treasure Island (FL): StatPearls Publishing, 2025.

[53] Samana Batool, Imtiaz Ahmad Taj, and Mubeen Ghafoor. “Ejection Fraction Estimation from Echocardiograms Using Optimal Left Ventricle Feature Extraction Based on Clinical Methods”. In: *Diagnostics* 13.13 (2023), p. 2155. ISSN: 2075-4418.

[54] Tahir Tak et al. “Measurement of Ejection Fraction by Cardiac Magnetic Resonance Imaging and Echocardiography to Monitor Doxorubicin-Induced Cardiotoxicity”. In: *The International Journal of Angiology : Official Publication of the International College of Angiology, Inc* 29.1 (2020), pp. 45–51. ISSN: 1061-1711.

[55] Nadish Garg et al. “Comparison of Left Ventricular Ejection Fraction Values Obtained Using Invasive Contrast Left Ventriculography, Two-Dimensional Echocardiography, and Gated Single-Photon Emission Computed Tomography”. In: *SAGE Open Medicine* 4 (2016), p. 2050312116655940. ISSN: 2050-3121.

[56] Johnny T. Ottesen et al. “2. Cardiovascular and Pulmonary Physiology and Anatomy”. In: *Applied Mathematical Models in Human Physiology*. Mathematical Modeling and Computation. Society for Industrial and Applied Mathematics, 2004, pp. 7–34. ISBN: 978-0-89871-539-2.

[57] Nicolaas Westerhof et al. “Wave Travel and Reflection”. In: *Snapshots of Hemodynamics: An Aid for Clinical Research and Graduate Education*. Ed. by Nicolaas Westerhof et al. Cham: Springer International Publishing, 2019, pp. 75–88. ISBN: 978-3-319-91932-4.

[58] Michael O’Rourke and Audrey Adji. “Arterial Pressure Waveform Analysis”. In: *McDonald’s Blood Flow in Arteries*. 7th ed. CRC Press, 2022. ISBN: 978-1-351-25376-5.

[59] Liam Y H Tien et al. “Optimal Calculation of Mean Pressure From Pulse Pressure”. In: *American Journal of Hypertension* 36.6 (2023), pp. 297–305. ISSN: 0895-7061.

[60] Frans N. Van De Vosse and Nikos Stergiopulos. “Pulse Wave Propagation in the Arterial Tree”. In: *Annual Review of Fluid Mechanics* 43 (2011), pp. 467–499. ISSN: 00664189.

[61] John E. Hall. *Guyton and Hall Textbook of Medical Physiology, Jordanian Edition E-Book*. Elsevier Health Sciences, 2016. ISBN: 978-0-7020-7409-7.

[62] Junichiro Hashimoto. “Pulse Pressure Amplification as a Hemodynamic Predictor of Cardiovascular Disease”. In: *Hypertension Research* 47.11 (2024), pp. 3270–3272. ISSN: 1348-4214.

[63] Nicolaas Westerhof et al. “Wave Travel and Pulse Wave Velocity”. In: *Snapshots of Hemodynamics: An Aid for Clinical Research and Graduate Education*. Ed. by Nicolaas Westerhof et al. Cham: Springer International Publishing, 2019, pp. 165–173. ISBN: 978-3-319-91932-4.

[64] Sofie Brouwers et al. “Arterial Hypertension”. In: *The Lancet* 398.10296 (2021), pp. 249–261. ISSN: 0140-6736, 1474-547X.

[65] Luc M. Van Bortel et al. “Expert Consensus Document on the Measurement of Aortic Stiffness in Daily Practice Using Carotid-Femoral Pulse Wave Velocity”. In: *Journal of Hypertension* 30.3 (2012), p. 445. ISSN: 0263-6352.

[66] Qi Zhong et al. “Carotid–Femoral Pulse Wave Velocity in the Prediction of Cardiovascular Events and Mortality: An Updated Systematic Review and Meta-Analysis”. In: *Angiology* 69.7 (2018), pp. 617–629. ISSN: 0003-3197.

[67] Laila Gbaoui et al. “Estimation of Central Blood Pressure Waveform from Femoral Blood Pressure Waveform by Blind Sources Separation”. In: *Frontiers in Cardiovascular Medicine* 10 (2023). ISSN: 2297-055X.

[68] Wilmer Nichols. “Properties of the Arterial Wall: Theory and Practice”. In: *McDonald’s Blood Flow in Arteries*. 7th ed. CRC Press, 2022.

[69] Michael O’Rourke and Audrey Adji. “Arterial Wave Reflections”. In: *McDonald’s Blood Flow in Arteries*. 7th ed. CRC Press, 2022. ISBN: 978-1-351-25376-5.

[70] Nicolaas Westerhof et al. “Resistance”. In: *Snapshots of Hemodynamics: An Aid for Clinical Research and Graduate Education*. Ed. by Nicolaas Westerhof et al. Cham: Springer International Publishing, 2019, pp. 33–41. ISBN: 978-3-319-91932-4.

[71] Christopher B. Overgaard and Vladimír Džavík. “Inotropes and Vasopressors”. In: *Circulation* 118.10 (2008), pp. 1047–1056.

[72] Michael F. O’Rourke and Michael G. Taylor. “Vascular Impedance of the Femoral Bed”. In: *Circulation Research* 18.2 (1966), pp. 126–139.

[73] Wilmer Nichols. “General Principles for Measuring Arterial Waves”. In: *McDonald’s Blood Flow in Arteries*. 7th ed. CRC Press, 2022. ISBN: 978-1-351-25376-5.

[74] Bernd Saugel et al. “How to Measure Blood Pressure Using an Arterial Catheter: A Systematic 5-Step Approach”. In: *Critical Care* 24 (2020), p. 172. ISSN: 1364-8535.

[75] Yenly Nguyen and Vaibhav Bora. “Arterial Pressure Monitoring”. In: *StatPearls*. Treasure Island (FL): StatPearls Publishing, 2025.

[76] Vivian L. Clark and James A. Kruse. “Arterial Catheterization”. In: *Critical Care Clinics* 8.4 (1992), pp. 687–697. ISSN: 0749-0704, 1557-8232.

[77] Jessica A. Schults et al. “Risk Factors for Arterial Catheter Failure and Complications during Critical Care Hospitalisation: A Secondary Analysis of a Multisite, Randomised Trial”. In: *Journal of Intensive Care* 12 (2024), p. 12. ISSN: 2052-0492.

[78] Michael F. O’Rourke. “Carotid Artery Tonometry: Pros and Cons”. In: *American Journal of Hypertension* 29.3 (2016), pp. 296–298. ISSN: 0895-7061.

[79] Kelly Rp. “Non-invasive registration of the arterial pulse waveform using high fidelity applanation tonometry”. In: *J Vasc Med Biol* 1 (1989), pp. 142–149.

[80] Anthony Laskovski. *Biomedical Engineering, Trends in Electronics: Communications and Software*. BoD – Books on Demand, 2011. ISBN: 978-953-307-475-7.

[81] J. Jilek and M. Stork. “The Contours of Arterial Pulsations in the Blood Pressure Cuff Are Hemodynamic Waveforms Rather than Oscillations”. In: *Proceedings of the 2nd International Conference on Circuits, Systems, Control, Signals*. CSCS ’11. Stevens Point, Wisconsin, USA: World Scientific and Engineering Academy and Society (WSEAS), Wrzesień 26, 2011, pp. 140–143. ISBN: 978-1-61804-035-0.

[82] Junyung Park et al. “Photoplethysmogram Analysis and Applications: An Integrative Review”. In: *Frontiers in Physiology* 12 (2022), p. 808451. ISSN: 1664-042X.

[83] Jiating Pan et al. “Robust Modelling of Arterial Blood Pressure Reconstruction from Photoplethysmography”. In: *Scientific Reports* 14.1 (2024), p. 30333. ISSN: 2045-2322.

[84] Te Ouyoung et al. “Machine-Learning Classification of Pulse Waveform Quality”. In: *Sensors* 22.22 (2022), p. 8607. ISSN: 1424-8220.

[85] Christoph Fischer et al. “An Algorithm for Real-Time Pulse Waveform Segmentation and Artifact Detection in Photoplethysmograms”. In: *IEEE Journal of Biomedical and Health Informatics* 21.2 (2017), pp. 372–381. ISSN: 2168-2208.

[86] J. Fortin et al. “Continuous Non-Invasive Blood Pressure Monitoring Using Concentrically Interlocking Control Loops”. In: *Computers in Biology and Medicine* 36.9 (2006), pp. 941–957. ISSN: 0010-4825.

[87] J. Penáz, A. Voigt, and W. Teichmann. “[Contribution to the continuous indirect blood pressure measurement]”. In: *Zeitschrift Fur Die Gesamte Innere Medizin Und Ihre Grenzgebiete* 31.24 (1976), pp. 1030–1033. ISSN: 0044-2542.

[88] Agnes S. Meidert and Bernd Saugel. “Techniques for Non-Invasive Monitoring of Arterial Blood Pressure”. In: *Frontiers in Medicine* 4 (2018). ISSN: 2296-858X.

[89] Michael F O'Rourke, Alfredo Pauca, and Xiong-Jing Jiang. "Pulse Wave Analysis". In: *British Journal of Clinical Pharmacology* 51.6 (2001), pp. 507–522. ISSN: 0306-5251.

[90] Joseph L. Izzo and Gary F. Mitchell. "Pitfalls of Pulse Wave Analysis and Oscillometric Blood Pressure Derivatives". In: *Hypertension* 78.2 (2021), pp. 372–375.

[91] Nicolaas Westerhof et al. "Transfer of Pressure". In: *Snapshots of Hemodynamics: An Aid for Clinical Research and Graduate Education*. Ed. by Nicolaas Westerhof et al. Cham: Springer International Publishing, 2019, pp. 225–230. ISBN: 978-3-319-91932-4.

[92] Bryan Williams et al. "Differential Impact of Blood Pressure–Lowering Drugs on Central Aortic Pressure and Clinical Outcomes". In: *Circulation* 113.9 (2006), pp. 1213–1225.

[93] Anastasios Kollias et al. "Association of Central Versus Brachial Blood Pressure With Target-Organ Damage". In: *Hypertension* 67.1 (2016), pp. 183–190.

[94] Rasmus K. Carlsen et al. "Estimated Aortic Blood Pressure Based on Radial Artery Tonometry Underestimates Directly Measured Aortic Blood Pressure in Patients with Advancing Chronic Kidney Disease Staging and Increasing Arterial Stiffness". In: *Kidney International* 90.4 (2016), pp. 869–877. ISSN: 0085-2538.

[95] Michael F. O'Rourke and Alfredo L. Pauca. "Augmentation of the Aortic and Central Arterial Pressure Waveform". In: *Blood Pressure Monitoring* 9.4 (2004), p. 179. ISSN: 1359-5237.

[96] Wilmer W. Nichols and Balkrishna M. Singh. "Augmentation Index as a Measure of Peripheral Vascular Disease State". In: *Current Opinion in Cardiology* 17.5 (2002), p. 543. ISSN: 0268-4705.

[97] Jens Nürnberger et al. "Augmentation Index Is Associated with Cardiovascular Risk". In: *Journal of Hypertension* 20.12 (2002), p. 2407. ISSN: 0263-6352.

[98] Gerald D. Buckberg et al. "Experimental Subendocardial Ischemia in Dogs with Normal Coronary Arteries". In: *Circulation Research* 30.1 (1972), pp. 67–81.

[99] Haotai Xie et al. "Research Progress and Clinical Value of Subendocardial Viability Ratio". In: *Journal of the American Heart Association* 13.6 (2024), e032614.

[100] G. B. John Mancini et al. "The Isovolumic Index: A New Noninvasive Approach to the Assessment of Left Ventricular Function in Man". In: *The American Journal of Cardiology* 50.6 (1982), pp. 1401–1408. ISSN: 0002-9149.

[101] Alia S. Alhakak et al. "The Significance of Left Ventricular Ejection Time in Heart Failure with Reduced Ejection Fraction". In: *European Journal of Heart Failure* 23.4 (2021), pp. 541–551. ISSN: 1879-0844.

[102] Tor Biering-Sørensen et al. "Left Ventricular Ejection Time Is an Independent Predictor of Incident Heart Failure in a Community-Based Cohort". In: *European Journal of Heart Failure* 20.7 (2018), pp. 1106–1114. ISSN: 1879-0844.

[103] Victor L. Streeter, W. Ford Keitzer, and David F. Bohr. "Pulsatile Pressure and Flow Through Distensible Vessels". In: *Circulation Research* 13.1 (1963), pp. 3–20.

[104] A. C. L. Barnard et al. “A Theory of Fluid Flow in Compliant Tubes”. In: *Biophysical Journal* 6.6 (1966), pp. 717–724. ISSN: 0006-3495, 1542-0086.

[105] N. Stergiopulos, D. F. Young, and T. R. Rogge. “Computer Simulation of Arterial Flow with Applications to Arterial and Aortic Stenoses”. In: *Journal of Biomechanics* 25.12 (1992), pp. 1477–1488. ISSN: 0021-9290.

[106] Mette S. Olufsen et al. “Numerical Simulation and Experimental Validation of Blood Flow in Arteries with Structured-Tree Outflow Conditions”. In: *Annals of Biomedical Engineering* 28.11 (2000), pp. 1281–1299. ISSN: 1573-9686.

[107] Jordi Alastruey, Kim Parker, and Spencer Sherwin. “Arterial Pulse Wave Haemodynamics”. In: *BHR Group - 11th International Conferences on Pressure Surges*. 2012, pp. 401–442. ISBN: 978-1-85598-133-1.

[108] Philippe Reymond et al. “Validation of a One-Dimensional Model of the Systemic Arterial Tree”. In: *Am J Physiol Heart Circ Physiol* 297 (2009), pp. 208–222.

[109] Huan Lei et al. “Blood Flow in Small Tubes: Quantifying the Transition to the Non-Continuum Regime”. In: *Journal of fluid mechanics* 722 (2013), 10.1017/jfm.2013.91. ISSN: 0022-1120.

[110] Nicolaas Westerhof et al. “Viscosity”. In: *Snapshots of Hemodynamics: An Aid for Clinical Research and Graduate Education*. Ed. by Nicolaas Westerhof et al. Cham: Springer International Publishing, 2019, pp. 3–8. ISBN: 978-3-319-91932-4.

[111] Luca Formaggia, Daniele Lamponi, and Alfio Quarteroni. “One-Dimensional Models for Blood Flow in Arteries”. In: *Journal of Engineering Mathematics* 47.3 (2003), pp. 251–276. ISSN: 1573-2703.

[112] Koen S. Matthys et al. “Pulse Wave Propagation in a Model Human Arterial Network: Assessment of 1-D Numerical Simulations against *in Vitro* Measurements”. In: *Journal of Biomechanics* 40.15 (2007), pp. 3476–3486. ISSN: 0021-9290.

[113] J. C. Stettler, P. Niederer, and M. Anliker. “Theoretical Analysis of Arterial Hemodynamics Including the Influence of Bifurcations”. In: *Annals of Biomedical Engineering* 9.2 (1981), pp. 145–164. ISSN: 1573-9686.

[114] Bernard W. Schaaf and Peter H. Abbrecht. “Digital Computer Simulation of Human Systemic Arterial Pulse Wave Transmission: A Nonlinear Model”. In: *Journal of Biomechanics* 5.4 (1972), pp. 345–364. ISSN: 00219290.

[115] N Westerhof, G Elzinga, and P Sipkema. “An Artificial Arterial System for Pumping Hearts.” In: *Journal of Applied Physiology* 31.5 (1971), pp. 776–781. ISSN: 8750-7587.

[116] Will Cousins and Pierre A. Gremaud. “Impedance Boundary Conditions for General Transient Hemodynamics”. In: *International Journal for Numerical Methods in Biomedical Engineering* 30.11 (2014), pp. 1294–1313. ISSN: 2040-7947.

[117] Tao Du, Dan Hu, and David Cai. “Outflow Boundary Conditions for Blood Flow in Arterial Trees”. In: *PLOS ONE* 10.5 (2015), e0128597. ISSN: 1932-6203.

[118] Annemette Sofie Olufsen. *Modeling the Arterial System with Reference to an Anesthesia Simulator*. Tekster Fra IMFUFA. Roskilde: Roskilde Universitet, 1998.

[119] Xiangdong Zhang et al. "Personalized Hemodynamic Modeling of the Human Cardiovascular System: A Reduced-Order Computing Model". In: *IEEE Transactions on Biomedical Engineering* 67.10 (2020), pp. 2754–2764. ISSN: 1558-2531.

[120] Peter H. Charlton et al. "Modeling Arterial Pulse Waves in Healthy Aging: A Database for in Silico Evaluation of Hemodynamics and Pulse Wave Indexes". In: *American Journal of Physiology-Heart and Circulatory Physiology* 317.5 (2019), H1062–H1085. ISSN: 0363-6135, 1522-1539.

[121] H. Suga and K. Sagawa. "Instantaneous Pressure-Volume Relationships and Their Ratio in the Excised, Supported Canine Left Ventricle". In: *Circulation Research* 35.1 (1974), pp. 117–126. ISSN: 0009-7330.

[122] Hiroyuki Suga, Kiichi Sagawa, and Artin A. Shoukas. "Load Independence of the Instantaneous Pressure-Volume Ratio of the Canine Left Ventricle and Effects of Epinephrine and Heart Rate on the Ratio". In: *Circulation Research* 32.3 (1973), pp. 314–322.

[123] Luca Formaggia et al. "Numerical Modeling of 1D Arterial Networks Coupled with a Lumped Parameters Description of the Heart". In: *Computer Methods in Biomechanics and Biomedical Engineering* 9.5 (2006), pp. 273–288. ISSN: 1025-5842.

[124] Johnny T. Ottesen et al. "6. A Cardiovascular Model". In: *Applied Mathematical Models in Human Physiology*. Mathematical Modeling and Computation. Society for Industrial and Applied Mathematics, 2004, pp. 137–155. ISBN: 978-0-89871-539-2.

[125] Lucas O. Müller and Eleuterio F. Toro. "A Global Multiscale Mathematical Model for the Human Circulation with Emphasis on the Venous System". In: *International Journal for Numerical Methods in Biomedical Engineering* 30.7 (2014), pp. 681–725. ISSN: 2040-7947.

[126] Xiancheng Zhang et al. "Gravitational Effects on Global Hemodynamics in Different Postures: A Closed-Loop Multiscale Mathematical Analysis". In: *Acta Mechanica Sinica* 33.3 (2017), pp. 595–618. ISSN: 1614-3116.

[127] Jan Poleszczuk et al. "Patient-Specific Pulse Wave Propagation Model Identifies Cardiovascular Risk Characteristics in Hemodialysis Patients". In: *PLOS Computational Biology* 14.9 (2018), e1006417. ISSN: 1553-7358.

[128] Jan Poleszczuk et al. "Subject-Specific Pulse Wave Propagation Modeling: Towards Enhancement of Cardiovascular Assessment Methods". In: *PLoS ONE* 13.1 (2018), e0190972. ISSN: 1932-6203.

[129] Philippe Reymond et al. "Validation of a Patient-Specific One-Dimensional Model of the Systemic Arterial Tree". In: *American Journal of Physiology-Heart and Circulatory Physiology* 301.3 (2011), H1173–H1182. ISSN: 0363-6135.

[130] Jaiyoung Ryu, Xiao Hu, and Shawn C. Shadden. "A Coupled Lumped-Parameter and Distributed Network Model for Cerebral Pulse-Wave Hemodynamics". In: *Journal of Biomechanical Engineering* 137.101009 (2015). ISSN: 0148-0731.

[131] Fuyou Liang et al. "A Computational Model of the Cardiovascular System Coupled with an Upper-Arm Oscillometric Cuff and Its Application to Studying the Suprasystolic Cuff Oscillation Wave, Concerning Its Value in Assessing Arterial Stiffness". In: *Computer Methods in Biomechanics and Biomedical Engineering* 16.2 (2013), pp. 141–157. ISSN: 1025-5842, 1476-8259.

[132] Liling Hao et al. “A Strategy to Personalize a 1D Pulse Wave Propagation Model for Estimating Subject-Specific Central Aortic Pressure Waveform”. In: *Computers in Biology and Medicine* 146 (2022), p. 105528. ISSN: 0010-4825.

[133] Jun Liu et al. “A Noninvasive Method of Estimating Patient-Specific Left Ventricular Pressure Waveform”. In: *Computer Methods and Programs in Biomedicine* 227 (2022), p. 107192. ISSN: 0169-2607.

[134] Qi Zhang et al. “A Personalized 0D-1D Model of Cardiovascular System for the Hemodynamic Simulation of Enhanced External Counterpulsation”. In: *Computer Methods and Programs in Biomedicine* 227 (2022), p. 107224. ISSN: 0169-2607.

[135] Xiangdong Zhang et al. “Early Diagnosis of Intracranial Internal Carotid Artery Stenosis Using Extracranial Hemodynamic Indices from Carotid Doppler Ultrasound”. In: *Bioengineering* 9.9 (2022), p. 422. ISSN: 2306-5354.

[136] Pascal Bogui et al. “The PhysioFlow Thoracic Impedancemeter Is Not Valid for the Measurements of Cardiac Hemodynamic Parameters in Chronic Anemic Patients”. In: *PLOS ONE* 8.10 (2013), e79086. ISSN: 1932-6203.

[137] Katherine Taylor et al. “Poor Accuracy of Noninvasive Cardiac Output Monitoring Using Bioimpedance Cardiography [PhysioFlow(R)] Compared to Magnetic Resonance Imaging in Pediatric Patients”. In: *Anesthesia and Analgesia* 114.4 (2012), pp. 771–775. ISSN: 1526-7598.

[138] Vasiliki Bikia et al. “Noninvasive Cardiac Output and Central Systolic Pressure From Cuff-Pressure and Pulse Wave Velocity”. In: *IEEE Journal of Biomedical and Health Informatics* 24.7 (2020), pp. 1968–1981. ISSN: 2168-2208.

[139] Blake Robbins et al. “Pharmacotherapy Adjuncts for Traumatic Brain Injury: A Narrative Review of Evidence and Considerations in the Emergency Department”. In: *The American Journal of Emergency Medicine* 89 (2025), pp. 78–84. ISSN: 0735-6757.

[140] J. Alastruey et al. “Modelling the Circle of Willis to Assess the Effects of Anatomical Variations and Occlusions on Cerebral Flows”. In: *Journal of Biomechanics* 40.8 (2007), pp. 1794–1805. ISSN: 0021-9290.

[141] I. M Sobol′. “Global Sensitivity Indices for Nonlinear Mathematical Models and Their Monte Carlo Estimates”. In: *Mathematics and Computers in Simulation*. The Second IMACS Seminar on Monte Carlo Methods 55.1 (2001), pp. 271–280. ISSN: 0378-4754.

[142] Andrea Saltelli et al. “Variance Based Sensitivity Analysis of Model Output. Design and Estimator for the Total Sensitivity Index”. In: *Computer Physics Communications* 181.2 (2010), pp. 259–270. ISSN: 0010-4655.

[143] Mette S. Olufsen and Johnny T. Ottesen. “A Practical Approach to Parameter Estimation Applied to Model Predicting Heart Rate Regulation”. In: *Journal of Mathematical Biology* 67.1 (2013), pp. 39–68. ISSN: 1432-1416.

[144] Jorge J. Moré. “The Levenberg-Marquardt Algorithm: Implementation and Theory”. In: *Numerical Analysis*. Ed. by G. A. Watson. Berlin, Heidelberg: Springer, 1978, pp. 105–116. ISBN: 978-3-540-35972-2.

[145] G. Drzewiecki, R. Hood, and H. Apple. “Theory of the Oscillometric Maximum and the Systolic and Diastolic Detection Ratios”. In: *Annals of Biomedical Engineering* 22.1 (1994), pp. 88–96. ISSN: 0090-6964.

[146] Max J. Hilz et al. “Valsalva Maneuver Unveils Central Baroreflex Dysfunction with Altered Blood Pressure Control in Persons with a History of Mild Traumatic Brain Injury”. In: *BMC Neurology* 16 (2016), p. 61. ISSN: 1471-2377.

[147] Agnieszka Uryga et al. “Association between Temporal Patterns of Baroreflex Sensitivity after Traumatic Brain Injury and Prognosis: A Preliminary Study”. In: *Neurological Sciences: Official Journal of the Italian Neurological Society and of the Italian Society of Clinical Neurophysiology* 44.5 (2023), pp. 1653–1663. ISSN: 1590-3478.

[148] Peter Toth et al. “Traumatic Brain Injury-Induced Autoregulatory Dysfunction and Spreading Depression-Related Neurovascular Uncoupling: Pathomechanisms, Perspectives, and Therapeutic Implications”. In: *American Journal of Physiology. Heart and Circulatory Physiology* 311.5 (2016), H1118–H1131. ISSN: 1522-1539.

[149] Vasiliki Bikia et al. “Determination of Aortic Characteristic Impedance and Total Arterial Compliance From Regional Pulse Wave Velocities Using Machine Learning: An in-Silico Study”. In: *Frontiers in Bioengineering and Biotechnology* 9 (2021), p. 649866. ISSN: 2296-4185.

[150] Vasiliki Bikia et al. “Estimation of Left Ventricular End-Systolic Elastance From Brachial Pressure Waveform via Deep Learning”. In: *Frontiers in Bioengineering and Biotechnology* 9 (2021). ISSN: 2296-4185.

[151] Tianqi Wang et al. “Machine Learning-Based Pulse Wave Analysis for Early Detection of Abdominal Aortic Aneurysms Using In Silico Pulse Waves”. In: *Symmetry* 13.5 (2021), p. 804. ISSN: 2073-8994.